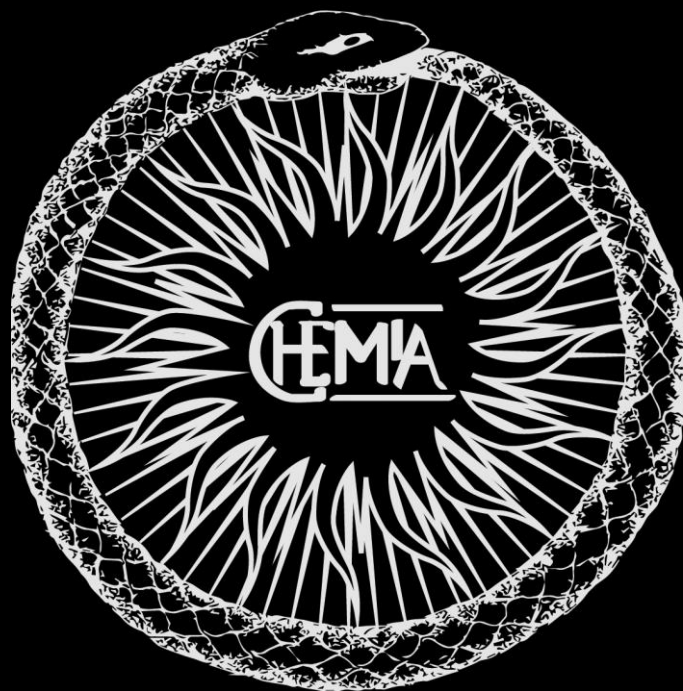




UNIVERSITAT
ROVIRA i VIRGILI

C-C and C-B Forming Strategies Driven by the Photoexcitation of Organocatalytic Intermediates

Daniele Mazzearella



DOCTORAL THESIS
2020

Daniele Mazzarella

C-C and C-B Bond Forming Strategies Driven by the Photoexcitation of Organocatalytic Intermediates

Doctoral Thesis

Supervised by Prof. Paolo Melchiorre

ICIQ – Institut Català d'Investigació Química



UNIVERSITAT
ROVIRA I VIRGILI



Tarragona

2020



UNIVERSITAT
ROVIRA i VIRGILI



Prof. Paolo Melchiorre, ICREA Research Professor & ICIQ Group Leader

I STATE that the present study, entitled “C-C and C-B Bond Forming Strategies Driven by the Photoexcitation of Organocatalytic Intermediates”, presented by Daniele Mazzarella for the award of the degree of Doctor, has been carried out under my supervision at the Institut Català d'Investigació Química (ICIQ).

Tarragona, June 23rd 2020

Doctoral Thesis Supervisor

Prof. Paolo Melchiorre

Acknowledgments

I would like to express my deepest gratitude to *Prof. Paolo Melchiorre*, for giving me the opportunity to be part of his research group, for his support and for guiding me through this process of self-growth as a scientist and as a person.

I am thankful to all the former and current members of the Melchiorre group for all the scientific and non-scientific moments shared together. It has been a real privilege to learn from and interact with such amazing people. In particular, I am grateful to the members of the laboratory 2.10 who have been like a family for the first two years of my PhD: *Charlie* for all the hardcore chemistry skills he taught me, *Nurty* for being my Phototrain buddy, *Luchino* for making me laugh a lot, *Bertie* for being Bertrawesome, *Maksim* for being the warrior of the light, *Tamal* for our war and peace, *Giacomo* for having shared so much time together and for having brought the beach volley trophy back home, *Matthew* for being always “enthusiastic” and *Dodino* for having admitted that Italian olive oil is better than the Spanish one. I am thankful to *Luca* and *Thomas* for having shared my short exile in the laboratory 1.12. I would like to thank also the members of the laboratory 1.7, my final destination in the Melchiorre group: *Pablo* for being my conference roommate and for the long discussions on whatever topic, mostly holding contrary opinions, *Giandomenico* for being a good friend and for the long chat about chemistry and life during our breaks, *Davide* for disrupting some boring days, *Sara* and *Ben* for the patience of having a loud individual as a desk-buddy and *Riccardo* and *Matteo* for making these post-lockdown months extremely happy. Moreover, I want to thank *Giulio*, the nicest guy I have probably ever met, *Eugenio* for having spent a lot of time under the red lights of the dark lab with me, *Cao*, *Alberto*, *Adriana* and *Giacomo Filippini*. I also want to thank *Eva* and *Laia* for having made my work much much easier. Special thanks to the proofreaders of this thesis, that hopefully helped me to avoid some mistakes: *Giandomenico*, *Giacomo*, *Giulio* and *Riccardo*.

I am also grateful to *Núria Planella*, *Dr. Lorna Piazzini* and *Maria Checa* for administrative support. I thank the research support units at ICIQ, in particular I am indebted to the NMR-staff, the photophysical unit, the spectroscopy unit and the chromatography unit.

I would like to thank all the people that welcomed me during my short stays. I am grateful to *Rob* and *Cris*, as well as all the people of the Dr. Reddy's Laboratories in Cambridge. In addition, I want to thank *Prof. Davide Bonifazi* for giving me the opportunity to join his research group and all the members of the *Bonifazi group* for making me feel at home also in Cardiff.

In these four years I have met really incredible people, I would like to thank *Marco*, for his sarcasm and for always being there when I needed him, *Carolina*, *Laura*, *Stefano*, *Jesus*, *Serena* and *Giulia*.

I am sure that without the people that I have met during my studies I would have never undertook any doctoral training. I would like to thank *Rosa*, *Edoardo*, *Gabriele*, *Giulia*,

Mauro, Laura, Pierpaolo, Federica, Lorenzo, Ruggero, Giulia, Riccardo, Adriano, Sabina, Andrea, Martina, Marco, Federica, Emilia and Elisabetta.

I am extremely thankful to *Prof. Pier Giorgio Cozzi* and *Dr. Andrea Gualandi* for having sparked my passion for catalysis and synthetic methodologies.

I am also thankful to my former co-workers at the Nippon Kayaku (*Sakai, Kaiho, Satake* and *Kogo*) and my “Japanese” friends: *Paolo, Andi e Mattias*.

I am extremely grateful to *Pier* who drew the cover of this thesis based on a very low quality image!

Voglio anche ringraziare i miei amici di una vita, la gente che mi ha visto crescere, anche se negli ultimi anni sempre di meno! Grazie a *Simone, Pier, Aldo, Yuri, Salva, Grazia, Gianluca, Nicola e Gianfranco*.

Grazie *Benedetta*, per essermi stata accanto in questi quattro anni. Sai che non sono molto bravo con le parole, però se dovessi pensare a quello che è successo in questi anni, sono sicuro che senza te al mio fianco non ce l'avrei fatta. Le difficoltà non sono finite, e lo sappiamo bene, però io credo che dopo aver superato questi anni insieme non c'è nulla che, se lo vogliamo entrambi, possa separarci.

Infine, voglio ringraziare le persone che mi hanno permesso di poter scegliere la mia strada senza pressioni, lasciandomi fare quello che mi rendeva e mi rende felice. Grazie a chi mi ha cresciuto e mi ha reso la persona che sono: grazie alla mia famiglia. Grazie *Mamma* per l'affetto e il supporto incondizionato, anche nei momenti più difficili della mia vita. Grazie *Papà* per avermi trasmesso la passione e l'etica lavorativa. Grazie *Alessia* per avermi sempre supportato in tutte le mie decisioni e per avermi sempre pazientemente aiutato (grazie anche a *Vaibhav!*). Grazie *Nonno* per essere stato il mio compagno di giochi prima e un riferimento dopo.

I would also like to acknowledge the financial support from the European Union's Horizon 2020 Research and Innovation Program under the Marie Skłodowska-Curie Actions H2020-MSCA-ITN-2016-722591 (PHOTOTRAIN) and from the Institute of Chemical Research of Catalonia (ICIQ).



PhotoTrain



List of publications

Some of the results presented in this thesis have been published:

- Mazzarella, D.; Crisenza, G. E. M.; H Melchiorre, P. “Asymmetric Photocatalytic C–H Functionalization of Toluene and Derivatives” *J. Am. Chem. Soc.* **2018**, *140*, 8439-8443.
- Mazzarella, D.; Magagnano, G.; Schweitzer-Chaput, B.; Melchiorre, P. “Photochemical Organocatalytic Borylation of Alkyl Chlorides, Bromides, and Sulfonates” *ACS Catal.* **2019**, *9*, 5876-5880.
- Crisenza G. E. M.; Mazzarella, D.; Melchiorre, P. “Synthetic Methods Driven by the Photoactivity of Electron Donor–Acceptor Complexes” *J. Am. Chem. Soc.* **2020**, *142*, 5461-5476.
- De Pedro Beato, E.; Mazzarella, D.; Balletti, M.; Melchiorre, P. “Photochemical generation of acyl and carbamoyl radicals using a nucleophilic organic catalyst: applications and mechanism thereof” *Chem. Sci.* **2020**, *11*, 6312-6324.

Al mio amico Simone

Table of Contents

1. General Overview	1
1.1. Photochemistry	1
1.2. Organocatalysis	5
1.3. Organocatalysis in the excited state	8
1.4. General Objectives and Summary	12
1.4.1. Asymmetric Photocatalytic C-H Functionalization of Toluene and Derivatives	13
1.4.2. Photochemical Organocatalytic Borylation of Alkyl Chlorides, Bromides, and Sulfonates	13
1.4.3. Photochemical Generation of Acyl and Carbamoyl Radicals	14
2. Asymmetric Photocatalytic C-H Functionalization of Toluene and Derivatives	17
2.1. Introduction	17
2.2. Iminium Ion Activation	19
2.2.1. Ground-state reactivity of iminium ions	19
2.2.2. Excited-state reactivity of iminium ions	21
2.3. Proton-Coupled Electron Transfer	24
2.4. Target of the Project	26
2.5. Results and Discussion	29
2.5.1. Preliminary results and optimization	29
2.5.2. Scope of the reaction	34
2.6. Mechanistic Investigation	37
2.6.1. Role of the acid co-catalyst, the aminocatalyst and light	37
2.6.2. Role of the iminium ion and its counteranion	39
2.6.3. Kinetic isotope effect	39
2.6.4. Mechanistic Proposal	40
2.7. Attempts to Expand the Scope	41
2.8. Conclusions	43
2.9. Experimental Section	44
2.9.1. General information	44
2.9.2. Substrate synthesis	45
2.9.3. General procedure for the photochemical C-H functionalization of toluene and derivatives	48
3. Photochemical Organocatalytic Borylation of Alkyl Chlorides, Bromides, and Sulfonates	71
3.1. Introduction	71
3.2. General Overview on Radical Generation Strategies	72
3.2.1. Methods based on the redox properties	72
3.2.2. Methods based on bond dissociation energies (BDE)	74
3.3. A New Photochemical Radical-Generating Strategy	76
3.4. Target of the Project	78
3.4.1. Methods for the synthesis of alkyl boronic derivatives	78

3.4.2. Design Plan	82
3.5. Results and Discussion	83
3.5.1. Reaction optimization	83
3.5.2. Scope of the reaction	85
3.5.3. Reaction limitations	87
3.6. Reaction Mechanism	88
3.6.1. Proposed mechanism	88
3.6.2. Other mechanistic scenarios	89
3.7. Three-component Variant	91
3.8. Conclusions	94
3.9. Experimental Section	95
3.9.1. General information	95
3.9.2. Experimental setup	96
3.9.3. General procedure for the photochemical organocatalytic borylation	97
3.9.4. General procedure for the three-component borylation	103
3.9.5. Cyclic voltammetry measurements	105
4. Photochemical generation of acyl and carbamoyl radicals using a nucleophilic organic catalyst	111
4.1. Introduction	111
4.2. Generation of Carbamoyl Radicals	113
4.2.1. Use of stoichiometric oxidants	113
4.2.2. Use of carbamoyl cobalt salophens and chalcogenes	114
4.2.3. Catalytic formation of carbamoyl radicals	116
4.3. Target of the Project	119
4.3.1 Design plan	119
4.4. Results and discussion	121
4.4.1. Optimization and scope of the intramolecular reaction	121
4.4.2. Optimization and scope of the intermolecular reaction	124
4.5. Acyl Derivatives	126
4.6. Mechanistic Studies	130
4.6.1. Nucleophilic acyl substitution and photochemical behavior of 30a	131
4.6.2. Fate and behavior of the xanthyl radical XIXd	133
4.6.3. Trap of the acyl radical and ensuing processes	137
4.6.4. Overall catalytic cycle	140
4.7. Conclusions	141
4.8. Experimental Section	141
4.8.1. General information	141
4.8.2. Substrate synthesis	143
4.8.3. Reaction of carbamoyl chlorides	149
4.8.4. Reaction of aromatic acyl chlorides	157
4.8.5. Reaction of aliphatic acyl chlorides	167
4.8.6. Reaction of carboxylic acids through acyl chloride formation	172
4.8.7. Reaction of carboxylic acids through anhydride formation	176
4.8.8. Mechanistic studies	177
5. General conclusion	197

Chapter I

General Overview

The work described in this thesis aims at combining two powerful strategies of molecule activation, namely *photochemistry* and *organocatalysis*, to develop new synthetic processes. This chapter provides a general overview of these two strategies for substrate activation while assessing the state-of-the-art regarding their synergistic combination.

1.1 Photochemistry

Photochemistry is the branch of chemistry concerned with the chemical effects of light.¹ In 1817, Theodore von Grotthuss established that “only the light absorbed by a molecule is effective in producing photochemical change”. Later on, between 1908 and 1914, Stark and Einstein independently formulated that “there should be a 1 : 1 equivalence between the number of molecules decomposed and the number of photons absorbed”. Although these statements might seem trivial and incomplete nowadays, they highlighted for the first time the importance of the interaction between light and matter.

The interaction between a molecule and one photon generally results in that the photonic energy promotes the transition of one electron from the highest occupied molecular orbital (HOMO, H in Figure 1.1a) to the lowest unoccupied molecular orbital (LUMO, L) of the substrate. This transition triggers the generation of an electronically excited state. In order to have a fruitful interaction between light and molecules, there has to be a correspondence between the energy of the photon ($h\nu$) and the difference in energy between the molecular orbitals involved, as described by the Bohr equation (1.1):

$$h\nu = E_f - E_i \quad (1.1)$$

where E_f and E_i are the energies of the excited state and the ground state, respectively, which are described by the corresponding wave functions Ψ_f and Ψ_i . In general, the energy required for these transitions lies between 9.95×10^{-19} and 1.99×10^{-19} J. This translates into a portion of the electromagnetic spectrum that includes near-UV, visible and, in a few cases, near infrared regions. Since during an electronic transition no change in nuclear position or nuclear kinetic energy occurs (Franck-Condon principle), electronic transition can be represented by a vertical arrow (Figure 1.1b).

¹ a) Balzani, V.; Ceroni, P.; Juris, A. "Photochemistry and Photophysics: Concepts, Research, Applications" **2014**, John Wiley & Sons. b) Turro, N. J.; Ramamurthy, V.; Scaiano, J. C. "Modern Molecular Photochemistry of Organic Molecules" **2010**, University Science Books.

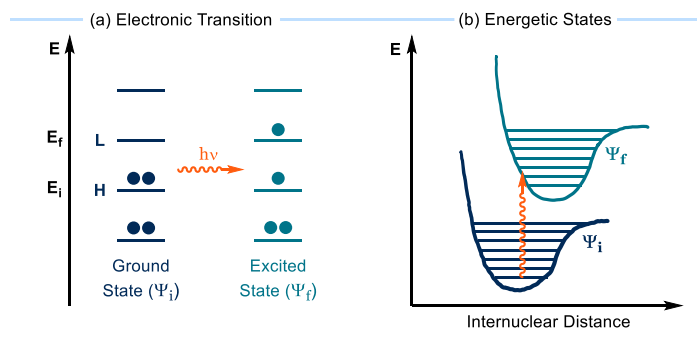


Figure 1.1: (a) Electronic transition from the HOMO (H) to the LUMO (L). (b) Vertical electronic transition from the ground state Ψ_i to the excited state Ψ_f .

Electronically excited-state molecules are completely different species compared to the corresponding ground-state analogues.² Indeed, they possess different electronic distribution, energy and lifetime. Having a higher energy content than in the ground state (between 150 and 600 kJ/mol higher), excited-state molecules have the tendency to rapidly lose it through different pathways. Deactivation can lead back to the ground state, mostly via emission (*photophysical process*), or can alter the chemical composition of the molecule (*photochemical process*) through a variety of uni- and bi-molecular processes. Among the unimolecular processes, the most prominent are *isomerization*, *fragmentation* and *rearrangement*, whereas different bi-molecular pathways are available, including *electron*, *energy* and *proton transfer*, and *photoadditions*.

These processes have been exploited in synthetic photochemistry since the beginning of the last century to access products not available through conventional thermal reactivity.³ As an example, Paternò⁴ and Büchi⁵ developed a photochemical process where aldehyde **1**, upon UV light absorption, reaches the excited state **1*** and subsequently reacts with olefin **2** to produce oxetane **3** in a photoaddition manifold (Figure 1.2).

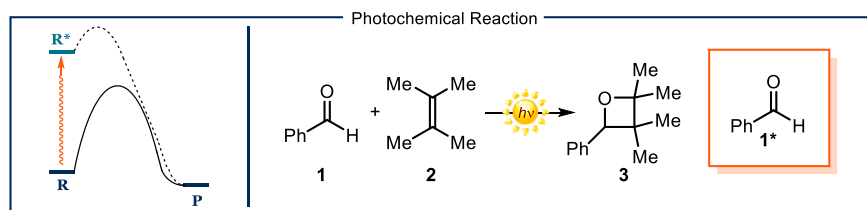


Figure 1.2: Direct photoexcitation of one of the reagents and application of this concept to afford oxetane **3**. R: reagent. P: product.

² Albini, A.; Fagnoni, M. "Photochemically generated intermediates in synthesis" **2013**, John Wiley & Sons.

³ Balzani, V.; Bergamini, G.; Ceroni, P. "Light: A Very Peculiar Reactant and Product" *Angew. Chem. Int. Ed.* **2015**, *54*, 11320-11337.

⁴ Paternò, E.; Cheffi, G.; "Sintesi in chimica organica per mezzo della luce. Nota II. Composti degli idrocarburi non saturi con aldeidi e chetoni" *Gazz. Chim. Ital.* **1909**, *39*, 341-361.

⁵ Büchi, G.; Inman, C. G.; Lipinsky, E. S. "Light-catalyzed Organic Reactions. I. The Reaction of Carbonyl Compounds with 2-Methyl-2-butene in the Presence of Ultraviolet Light" *J. Am. Chem. Soc.* **1954**, *76*, 4327-4331.

One of the main drawbacks of traditional synthetic photochemistry is that most of the organic molecules possess a large HOMO-LUMO gap, which is reflected into the need of hazardous, high-energy UV irradiation to access their excited states. Additionally, organic molecules are generally characterized by a low molar attenuation coefficient, which is a measurement of how strongly a substance absorbs light at a given wavelength, per molar concentration. In order to bypass this restriction and to broaden the number of reactions enabled by visible light, an alternative bimolecular strategy, called photocatalysis, has been developed. This approach employs transition-metal complexes and organic dyes, compounds that can absorb light in the visible range and possess high molar attenuation coefficients, as photo-mediators.⁶ These, upon light absorption, activate surrounding molecules through two mechanisms: energy-transfer⁷ or electron-transfer.⁸ In the energy-transfer manifold, the excited photomediator (or photosensitizer) dissipates the higher content in energy by transferring it to neighboring organic substrates. A pioneering example of this strategy was developed by Schenck to produce singlet oxygen from the excited-state of Rose Bengal, used as the photocatalyst (Figure 1.3).⁹

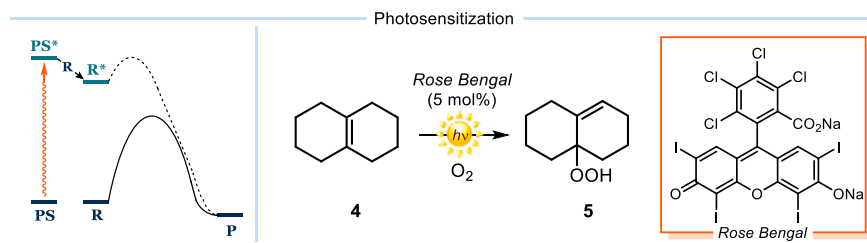


Figure 1.3: Use of a photosensitizer to absorb light and promote the energy transfer to produce an excited state of one of the reagents; application of this concept to singlet oxygen production. PS: photosensitizer. R: reagent. P: product.

Singlet oxygen is an extremely reactive species capable of undergoing an ene reaction with unactivated olefin **4**, producing peroxide **5**.

The electron-transfer approach exploits the enhanced redox properties of electronically excited photomediators. Indeed, the photochemical promotion of an electron from the HOMO to the LUMO lowers the ionization potential (IP) while increasing the electron affinity (EA) of the excited molecule. Thermodynamically, removing one electron from the half-filled LUMO of the excited state is less endothermic than removing it from the HOMO of the ground state. Conversely, adding one electron to the half-filled HOMO of the excited state is more exothermic than its addition into the LUMO of the ground state. In other words, light-excitation of the photoredox catalysts increases both their oxidative and reductive properties.

⁶ Yoon, T. P.; Ischay, M. A.; Du, J. "Visible Light Photocatalysis as a Greener Approach to Photochemical Synthesis" *Nat. Chem.* **2010**, *2*, 527-532.

⁷ Strieth-Kalthoff, F.; James, M. J.; Teders, M.; Pitzer, L.; Glorius, F. "Energy transfer catalysis mediated by visible light: principles, applications, directions" *Chem. Soc. Rev.* **2018**, *47*, 7190-7202.

⁸ Kavarnos, G. J. "Fundamentals of Photoinduced Electron Transfer" **1993**, VCH.

⁹ Schenck, G. O.; Schulte-Elte, K.-H. "Photosensibilisierte Synthese Tertiärer Allylhydroperoxyde Aus Symmetrisch Tetrasubstituierten Äthylenen" *Liebigs Ann. Chem.* **1958**, *618*, 185-193.

Thus, these photo-excited intermediates can be used to activate substrates via a single-electron transfer (SET) manifold, affording reactive open-shell intermediates under mild conditions.

One of the pioneering contributions in this field, called photoredox catalysis,¹⁰ has been reported in 1984 by Cano-Yelo and Deronzier (Figure 1.4).¹¹ In this process, the ruthenium-based catalyst $[\text{Ru}(\text{bpy})_3\text{Cl}_2]$, upon light absorption, becomes a good SET reductant, capable of transferring one electron to diazocompound **6**, affording, after nitrogen extrusion, an aryl radical which is trapped intramolecularly to generate product **7**.

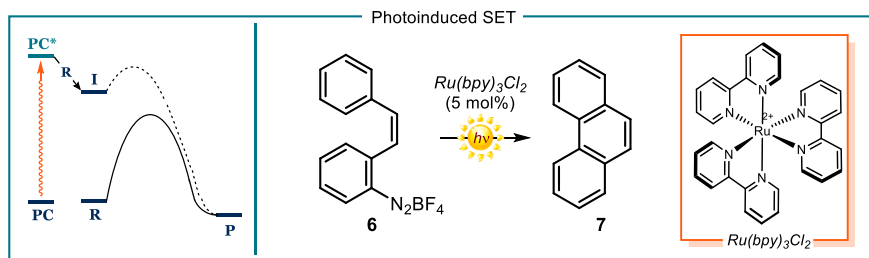


Figure 1.4: Use of a photocatalyst that absorbs light and promotes an electron transfer to produce a radical or a radical ion species; application of this concept to the formation of **7**. R: reagent. P: product. PC: photocatalyst. I: Intermediate.

Despite the synthetic potential of photoredox catalysis, this approach has been scarcely applied in chemical synthesis during the following 30 years. However, the recent technological developments, including light-emitting diodes (LEDs) and the synthesis of a huge family of visible-light absorbing transition-metal complexes and dyes, turned the niche field of photochemistry into a widely accessible synthetic tool for the chemical community. In particular, the pioneering works by Yoon,¹² MacMillan¹³ and Stephenson,¹⁴ published more than ten years ago, have spurred the renaissance of photoredox catalysis¹⁵ and, by extension, of the whole photochemistry field.

¹⁰ Shaw, M. H.; Twilton, J.; MacMillan, D. W. C. "Photoredox Catalysis in Organic Chemistry" *J. Org. Chem.* **2016**, *81*, 6898-6926.

¹¹ Cano-Yelo, H.; Deronzier, A. "Photocatalysis of the Pschorr reaction by tris-(2,2'-bipyridyl)ruthenium(II) in the phenanthrene series" *J. Chem. Soc. Perkin Trans. 2*, **1984**, 1093-1098.

¹² Ischay, M. A.; Anzovino, M. E.; Du, J.; Yoon, T. P., "Efficient visible light photocatalysis of [2+ 2] enone cycloadditions" *J. Am. Chem. Soc.* **2008**, *130*, 12886-12887.

¹³ Nicewicz, D. A.; MacMillan, D. W. C. "Merging photoredox catalysis with organocatalysis: the direct asymmetric alkylation of aldehydes" *Science* **2008**, *322*, 77-80.

¹⁴ Narayanam, J. M. R.; Tucker, J. W.; Stephenson, C. R. J. "Electron-Transfer Photoredox Catalysis: Development of a Tin-Free Reductive Dehalogenation Reaction" *J. Am. Chem. Soc.* **2009**, *131*, 8756-8757.

¹⁵ McAtee, R. C.; McClain, E. J.; Stephenson, C. R. J. "Illuminating Photoredox Catalysis" *Trends Chem.* **2019**, *1*, 111-125.

1.2 Organocatalysis

The term *organocatalysis* is the blend of the words *organic* and *catalysis* and, as implied by the name, exploits the ability of small organic molecules to act as catalysts.¹⁶ The low cost and toxicity along with the high stability of the organocatalysts bypass the need of advanced experimental setups (e.g. vacuum lines and glove boxes), which are typical of transition metal catalysis. In addition, the organocatalyzed reactions are usually performed under mild conditions and high concentrations, avoiding chemical waste. All these factors contributed to render organocatalysis an established tool for organic synthesis alongside biocatalysis and metal-based catalysis.

Although the words *organocatalysis* and *asymmetric* are closely linked in the chemical vocabulary, there are also numerous examples of non-enantioselective processes promoted by organocatalysts.¹⁷ Indeed, the first example of an organocatalyzed reaction is the non-enantioselective cyanide-catalyzed benzoin condensation, developed by Wöhler and Liebig in 1832 (Figure 1.5a).¹⁸ In 1912, Bredig and Fiske published the enantioselective hydrocyanation of benzaldehyde,¹⁹ which represented the first example of asymmetric organocatalytic reaction (Figure 1.5b).

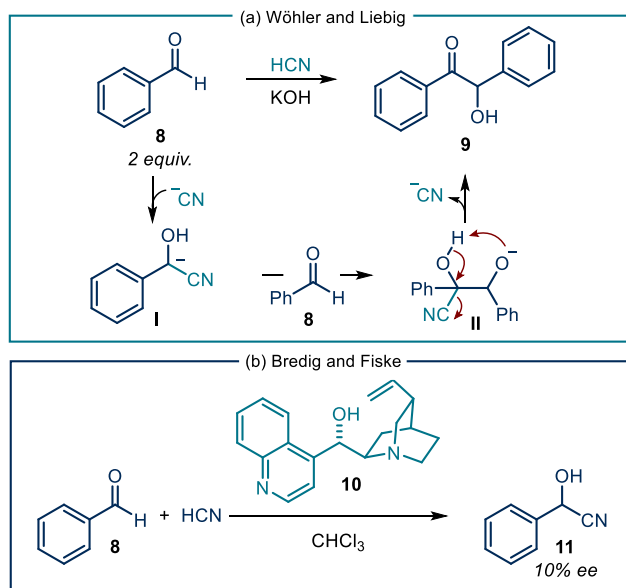


Figure 1.5: (a) First example of an organocatalytic reaction. (b) First example of an enantioselective organocatalytic process.

In general, organocatalysis enables the effective activation of a substrate through the interaction of a chiral catalyst with a key functional group, embedded within the

¹⁶ Dalco, P. I. "Comprehensive Enantioselective Organocatalysis: Catalysts, Reactions, and Applications" **2013**, Wiley-VCH.

¹⁷ Renzi, P.; Bella, M. "Non-asymmetric organocatalysis" *Chem. Commun.* **2012**, *48*, 6881-6896.

¹⁸ Wöhler, F.; Liebig, J. "Untersuchungen über das radikal der benzoessäure" *Ann. Der. Pharm.* **1832**, *3*, 249-282.

¹⁹ Bredig, G.; Fiske, P. S. "Asymmetric synthesis caused by catalysts" *Biochem. Z.* **1912**, *46*, 7-23.

substrate, in a specific and predictable manner.²⁰ Organocatalytic reactions can be classified on the basis of the mode of interaction between the catalyst and the substrate (Figure 1.6). The catalyst can interact through a covalent association, forming intermediates such as enamines **III** and iminium ions **IV**. Alternatively, non-covalent associations, elicited by hydrogen bonding or electrostatic interactions with substrates, can be responsible for the catalytic activity.

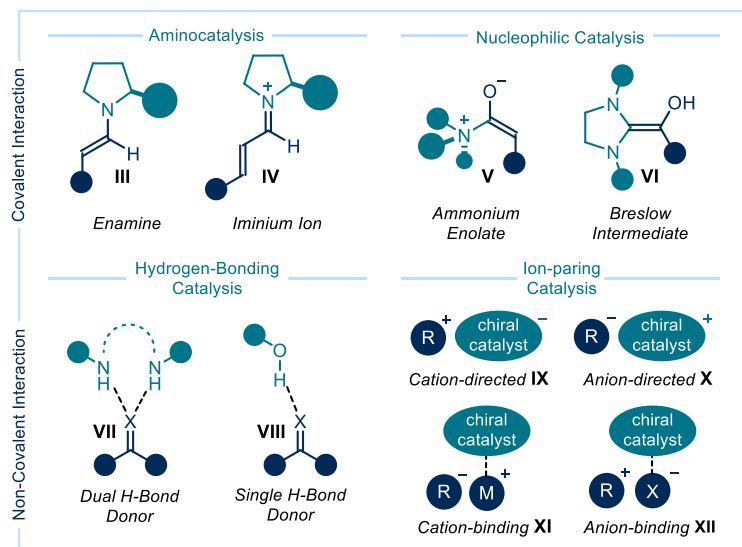


Figure 1.6: Reactive intermediates responsible for the enhanced activities in organocatalytic reactions. Green circles represent fragments on the chiral catalyst structure. For intermediates **VII** and **IX**, X: O, NR₂.

Among these organocatalytic modes of activation, aminocatalysis is perhaps the most employed. This approach relies on the generation, upon condensation of a primary or secondary amine catalyst with a carbonyl compound, of enamines **III** and iminium ions **IV**. In enamine-mediated reactions (Figure 1.7a), aminocatalyst **13** condenses with enolizable carbonyl compound **12**, generating the iminium ion **XIII** which contains a highly acidic α -proton. Its deprotonation leads to the formation of enamine **III**, an intermediate characterized by enhanced nucleophilic properties because of the increased energy of the HOMO with respect to the enol form of the native carbonyl compound **12**. Thus, the enamine intermediate **III** can readily react with several electrophiles at the α -carbon. In iminium ion-mediated reactions (Figure 1.7b), the

²⁰ For selected reviews on organocatalysis, see: (a) Melchiorre, P.; Marigo, M.; Carlone, A.; Bartoli, G. "Asymmetric Aminocatalysis-Gold Rush in Organic Chemistry" *Angew. Chem. Int. Ed.* **2008**, *47*, 6138–6171. (b) Beeson, T. D.; Mastracchio, A.; Hong, J.-B.; Ashton, K.; MacMillan, D. W. C. "Enantioselective Organocatalysis Using SOMO Activation" *Science*, **2007**, *316*, 582–585. (c) Gaunt, M. J.; Johansson, C. C. C.; "Recent Developments in the Use of Catalytic Asymmetric Ammonium Enolates in Chemical Synthesis" *Chem. Rev.* **2007**, *107*, 5596–5605. (d) Morrill, L. C.; Smith, A. D. "Organocatalytic Lewis Based Functionalization of Carboxylic Acids, Esters and Anhydrides via C1-Ammonium or Azolium Enolates" *Chem. Soc. Rev.* **2014**, *43*, 6214–6226. (e) Bugaut, X.; Glorius, F. "Organocatalytic Umpolung: N-heterocyclic Carbenes and Beyond" *Chem. Soc. Rev.* **2012**, *41*, 3511–3522. (f) Doyle, A. G.; Jacobsen, E. N. "Small-molecule H-bond Donors in Asymmetric Catalysis" *Chem. Rev.* **2007**, *107*, 5713–5743. (g) Brak, K.; Jacobsen, E. N. "Asymmetric Ion-Pairing Catalysis" *Angew. Chem. Int. Ed.* **2013**, *52*, 534–561.

condensation of aminocatalyst **13** with α,β -unsaturated carbonyl compound **14** produces the iminium ion **IV**. This intermediate is characterized by enhanced electrophilic properties, resulting from the reduced energy of the LUMO, hence **IV** reacts with several nucleophiles at the β -carbon.

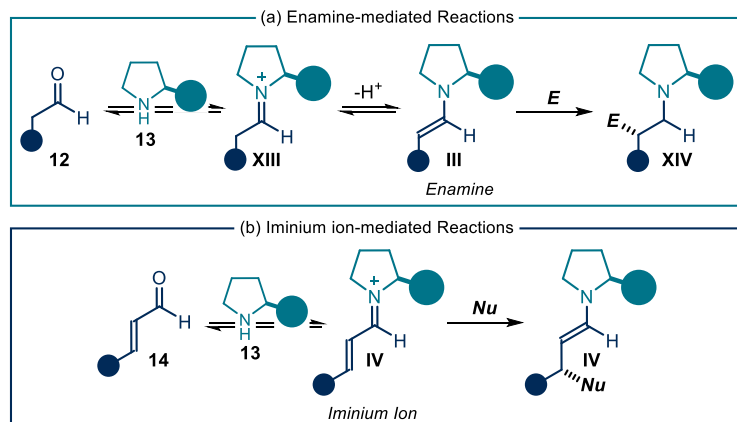


Figure 1.7: (a) Formation of enamines and their use in reactions involving electrophiles. (b) Formation of iminium ions and their use in reactions involving nucleophiles. Green circles represent bulky substituents on the chiral aminocatalyst structure. E: electrophile. Nu: nucleophile.

One of the most powerful features of organocatalysis is the high compatibility with other catalytic strategies of substrate activation. As an example, aminocatalysis has been extensively coupled with other organocatalytic manifolds²¹ and with metal catalysis.²² The propensity of enamine activation to function in synergy with other catalytic approaches has been exploited by MacMillan and Nicewicz¹² in a study which was seminal to the field of photoredox catalysis (Figure 1.8a). In this work, the elusive stereoselective α -alkylation of aldehydes **12** with electron-poor alkyl bromides **15** was developed via photo-excitation of $[\text{Ru}(\text{bpy})_3\text{Cl}_2]$. According to the first mechanism proposed by the authors (Figure 1.8b), the photoexcitation of $[\text{Ru}(\text{bpy})_3\text{Cl}_2]$ followed by single-electron transfer (SET) oxidation of a sacrificial amount of enamine **III** (not shown in Figure 1.8b), produces a strong reducing Ru(I) species, capable of transferring one electron to substrate **15**. This SET event, while regenerating the original Ru(II) complex, triggers the formation of the electrophilic radical **XV** after loss of the bromide anion. The latter is trapped by the transient electron-rich chiral enamine **III** in an enantioselective fashion, producing the α -amino radical **XVI**, which is oxidized by the photoexcited Ru(II) complex to form the iminium **XVII**. Finally, hydrolysis of the latter affords the desired enantioenriched product **16** and turns over the organocatalyst **13**.

²¹ Gu, J.; Du, W.; Chen, Y.-C. "Combined Asymmetric Aminocatalysis and Carbene Catalysis" *Synthesis* **2015**, 47, 3451-3459.

²² Afewerki, S.; Córdova, A. "Combinations of Aminocatalysts and Metal Catalysts: A Powerful Cooperative Approach in Selective Organic Synthesis" *Chem. Rev.* **2016**, 116, 13512-13570.

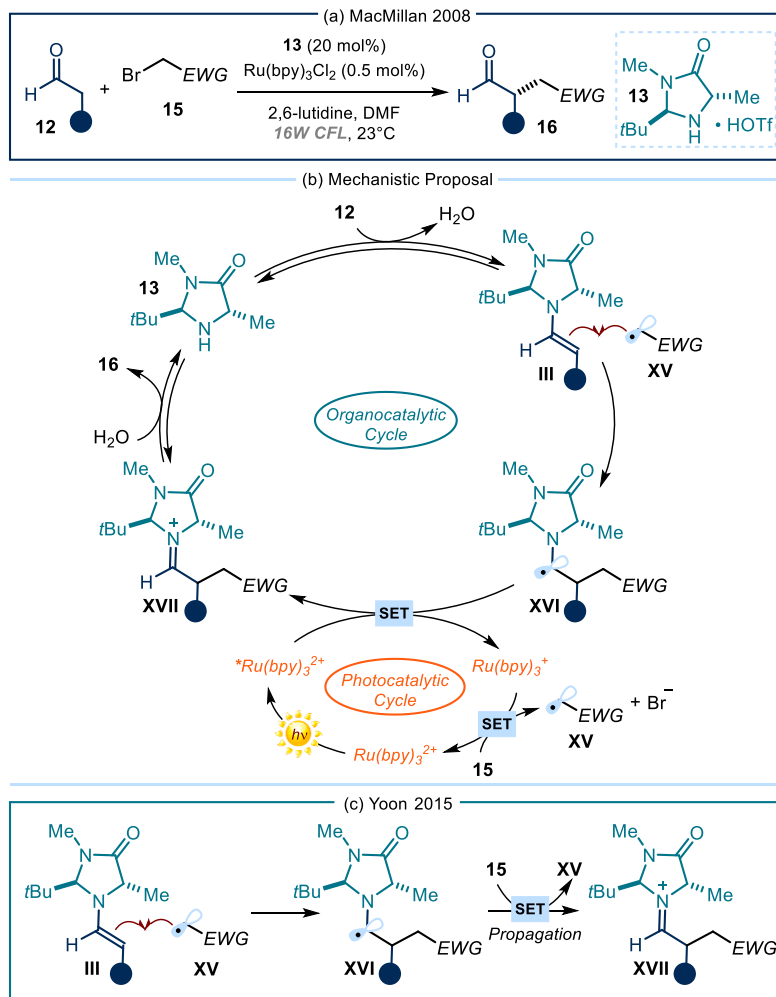


Figure 1.8: (a) Merger of organocatalysis with photoredox catalysis to promote the asymmetric α -alkylation of aldehydes. (b) Originally proposed mechanism. (c) Refined mechanistic picture proposed by Yoon and co-workers. EWG: electron-withdrawing group. DMF: dimethylformamide. CFL: compact fluorescent lamp.

Few years later, the group of Yoon²³ demonstrated that the mechanism of this process proceeds through a self-propagating radical chain manifold (Figure 1.8c). In this mechanistic picture, the photochemical activation acts as the initiation of the radical chain through the production of the electrophilic radical XV.

1.3 Organocatalysis in the Excited State

After the pioneering report of 2008, organocatalysis has been widely exploited, in conjunction with photoredox catalysis, for the synthesis of elusive enantioenriched

²³ Cismesia, M. A.; Yoon, T. P. "Characterizing Chain Processes in Visible Light Photoredox Catalysis" *Chem. Sci.* **2015**, *6*, 5426-5434.

chiral molecules.²⁴ In all these processes, the organocatalytic intermediates provide the chiral environment required to stereoselectively trap the open-shell intermediate generated by the photoredox catalyst. Nonetheless, the potential of organocatalysis to generate radicals is not restricted to the use of an external light-absorbing catalyst. Our research group recently found that some chiral organocatalytic intermediates can directly absorb light in the visible region, while the substrate does not. The organocatalytic intermediates can harvest the photonic energy to reach an excited state and unveil new catalytic functions.²⁵ The excited-state reactivity of organocatalytic intermediates can trigger the formation of radicals upon SET activation of the substrates. The radicals are then intercepted by the ground-state chiral organocatalytic intermediates in a stereocontrolled fashion. In this photochemical organocatalytic strategy (photo-organocatalysis), stereo-induction and photoactivation are combined in a single chiral organocatalytic intermediate (Figure 1.9).

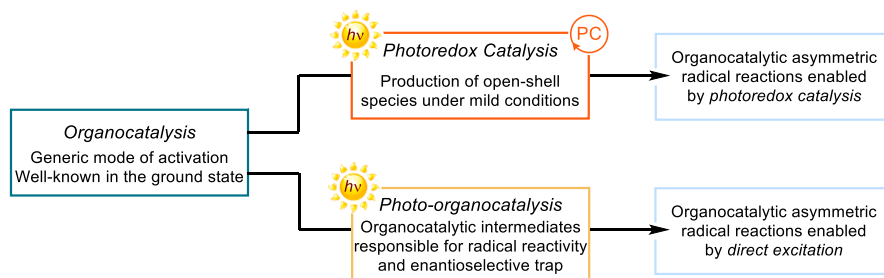


Figure 1.9: Two different approaches to combine photochemical activation and organocatalysis.

Specifically, our group demonstrated how electron rich chiral enamines **III**, generated via condensation of the aminocatalyst **13** with aldehyde **12** (Figure 1.10a), could interact with electron-poor benzyl bromides of type **15a**.²⁶ This aggregation brings about the formation of a new ground-state association, called electron donor-acceptor (EDA) complex **XVIII** (Figure 1.10b). This new bimolecular intermediate is able to absorb

²⁴ For selected examples please see: (a) Pirnot, M. T.; Rankic, D. A.; Martin, D. B. C.; MacMillan, D. W. C. "Photoredox Activation for the Direct β -Arylation of Ketones and Aldehydes" *Science* **2013**, *339*, 1593-1596. (b) DiRocco, D. A.; Rovis, T. "Catalytic asymmetric α -acylation of tertiary amines mediated by a dual catalysis mode: *N*-heterocyclic carbene and photoredox catalysis" *J. Am. Chem. Soc.* **2012**, *134*, 8094-8097. (c) Rono, L. J.; Yayla, H. G.; Wang, D. Y.; Armstrong, M. F.; Knowles, R. R. "Enantioselective photoredox catalysis enabled by proton-coupled electron transfer: development of an asymmetric aza-pinacol cyclization" *J. Am. Chem. Soc.* **2013**, *135*, 17735-17738. (d) Uraguchi, D.; Kinoshita, N.; Kizu, T.; Ooi, T. "Synergistic catalysis of ionic Brønsted acid and photosensitizer for a redox neutral asymmetric α -coupling of *N*-arylaminoethanes with aldimines" *J. Am. Chem. Soc.* **2015**, *137*, 13768-13771. (e) Murphy, J. J.; Bastida, D.; Paria, S.; Fagnoni, M.; Melchiorre, P. "Asymmetric catalytic formation of quaternary carbons by iminium ion trapping of radicals" *Nature* **2016**, *532*, 218-222. (f) Proctor, R. S. J.; Davis, H. J.; Phipps, R. J. "Catalytic enantioselective Minisci-type addition to heteroarenes" *Science*, **2018**, *360*, 419-422.

²⁵ Silvi, M.; Melchiorre, P. "Enhancing the potential of enantioselective organocatalysis with light" *Nature*, **2018**, *554*, 41-49.

²⁶ Arceo, E.; Jurberg, I. D.; Álvarez-Fernández, A.; Melchiorre, P. "Photochemical Activity of a Key Donor-Acceptor Complex Can Drive Stereoselective Catalytic α -alkylation of Aldehydes" *Nat. Chem.* **2013**, *5*, 750-756.

light in the visible region where the individual components cannot.²⁷ The selective photoexcitation of the EDA complex promotes an intra-complex SET, ultimately producing radical **XVa**, which is then trapped by a ground-state chiral enamine intermediate **III**.

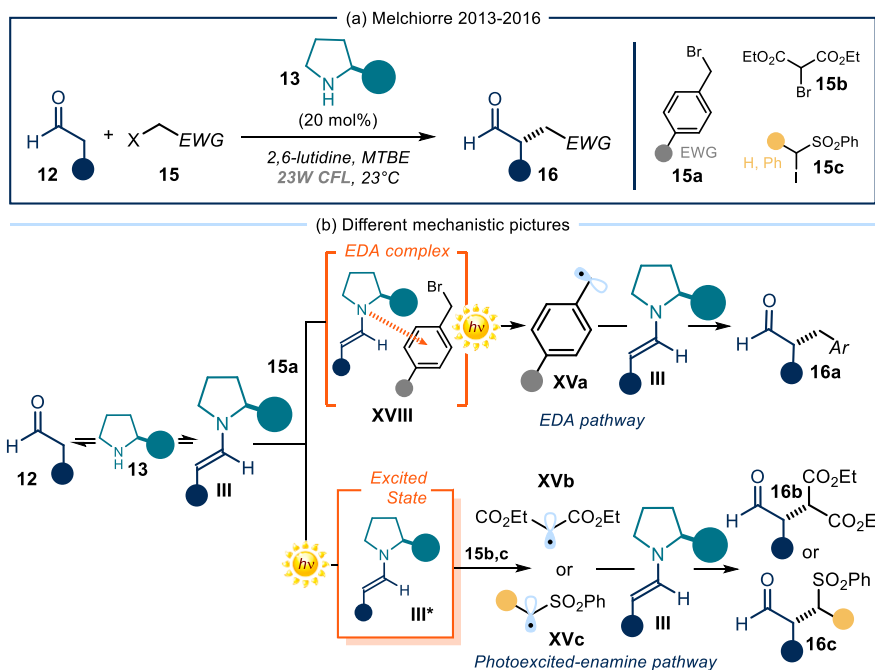


Figure 1.10: (a) Use of chiral enamines in photochemistry. (b) Photochemical activity enabled by EDA complex formation (EDA pathway), or by direct excitation (photoexcited-enamine pathway).

The rich photochemistry of enamines is not restricted to the EDA approach. Indeed, **III** can directly absorb light in the near-UV region, reaching an electronically excited state and acting as a strong SET reductant (Figure 1.10b). This photoexcited organocatalytic intermediate **III*** can activate bromomalonate **15b**²⁸ and α -iodo sulfone derivate **15c**²⁹ via SET reduction. The ensuing electrophilic alkyl radicals (**XVa** or **XVb**) are then stereoselectively trapped by the ground-state chiral enamine **III**. Mechanistic investigation by kinetic and photophysical means³⁰ suggested that, similarly to the aforementioned mechanism proposed by Yoon (Figure 1.8c),²³ a chain propagation manifold is operative in both the light-driven enamine processes.

²⁷ (a) Mulliken, R. S. "Molecular Compounds and their Spectra. II" *J. Am. Chem. Soc.* **1952**, *74*, 811-824. (b) Crisenza, G. E. M.; Mazzarella, D.; Melchiorre, P. "Synthetic Methods Driven by the Photoactivity of Electron Donor-Acceptor Complexes" *J. Am. Chem. Soc.* **2020**, *141*, 5461-5476.

²⁸ Silvi, M.; Arceo, E.; Jurberg, I. D.; Cassani, C.; Melchiorre, P. "Enantioselective Organocatalytic Alkylation of Aldehydes and Enals Driven by the Direct Photoexcitation of Enamines" *J. Am. Chem. Soc.* **2015**, *137*, 6120-6123.

²⁹ Filippini, G.; Silvi, M.; Melchiorre, P. "Enantioselective Formal α -Methylation and α -Benzoylation of Aldehydes by Means of Photo-organocatalysis" *Angew. Chem. Int. Ed.* **2017**, *56*, 4447-4451.

³⁰ Bahamonde, A.; Melchiorre, P. "Mechanism of the Stereoselective α -Alkylation of Aldehydes Driven by the Photochemical Activity of Enamines" *J. Am. Chem. Soc.* **2016**, *138*, 8019-8030.

The discovery that enamines could develop a strong reducing character upon photoexcitation motivated the quest for other organocatalytic intermediates capable of absorbing light and exhibit new catalytic properties. Our group demonstrated that also iminium ions **IV**, generated by the acid-promoted condensation of catalyst **13** with enals **14**, could absorb visible light (Figure 1.11a).³¹ In the excited state, iminium ions (**IV***, Figure 1.11b) act as strong oxidants, triggering the SET oxidation of benzylic trimethylsilanes **17**. Upon cleavage of the C-Si bond, the resulting benzyl radical **XIX** is intercepted by the ensuing chiral β -enaminy radical **XX** through an enantioselective radical coupling step. Hydrolysis of the resulting enamine furnishes the enantioenriched β -alkylated aldehyde **18**.

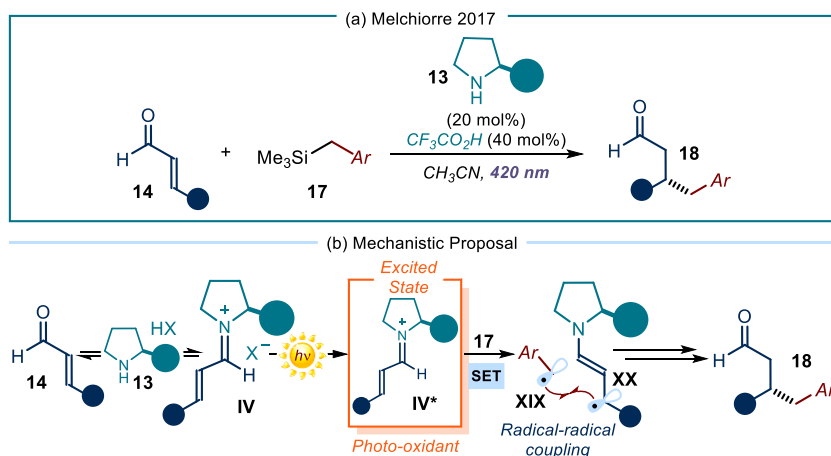


Figure 1.11: (a) Use of transiently generated iminium ions in photochemistry. (b) Photochemical activity enabled by direct excitation.

The synthetic potential of photo-organocatalysis is not restricted to the generation of strong reducing or oxidizing intermediates, which can generate radicals via SET mechanisms. In our laboratory, we recently developed a new organocatalytic methodology to produce radicals capitalizing upon the electrophilic properties of the substrates, and not on their redox abilities.³² This was achieved by shifting the stoichiometric xanthate transfer chemistry, developed by Barton³³ and Zard,³⁴ to a catalytic manifold. This shift was accomplished by designing a nucleophilic dithiocarbonyl catalyst (DTC catalyst **21**, Figure 1.12a) that could activate alkyl electrophiles **19** through a bimolecular nucleophilic substitution (S_N2) mechanism. The resulting photon-absorbing intermediate **XXI** (Figure 1.12b), upon irradiation by visible light, undergoes photolysis of the weak C-S bond, affording C(sp³)-centered

³¹ Silvi, M.; Verrier, C.; Rey, Y. P.; Buzzetti, L.; Melchiorre, P., "Visible-Light Excitation of Iminium Ions Enables the Enantioselective Catalytic β -Alkylation of Enals" *Nat. Chem.* **2017**, *9*, 868-873.

³² Schweitzer-Chaput, B.; Horwitz, M. A.; de Pedro Beato, E.; Melchiorre, P. "Photochemical generation of radicals from alkyl electrophiles using a nucleophilic organic catalyst" *Nat. Chem.* **2019**, *11*, 129-135.

³³ Barton, D. H. R.; McCombie, S. W. "A New Method for the Deoxygenation of Secondary Alcohols" *J. Chem. Soc. Perkin Trans. 1*, **1975**, 1574-1585.

³⁴ Zard, S. Z. "On the Trail of Xanthates: Some New Chemistry From an Old Functional Group" *Angew. Chem. Int. Ed.* **1997**, *36*, 672-685.

radicals **XXII**. These radicals are subsequently trapped by electron-poor olefins **20** to afford, after hydrogen atom transfer (HAT), products **22**. This catalytic S_N2 -based approach is solely relying on the electrophilic properties of the radical precursors **19** and grants access to open-shell intermediates from substrates usually inert to other catalytic radical-generating methods, which rely on SET or hydrogen atom abstraction (HAT) mechanisms.

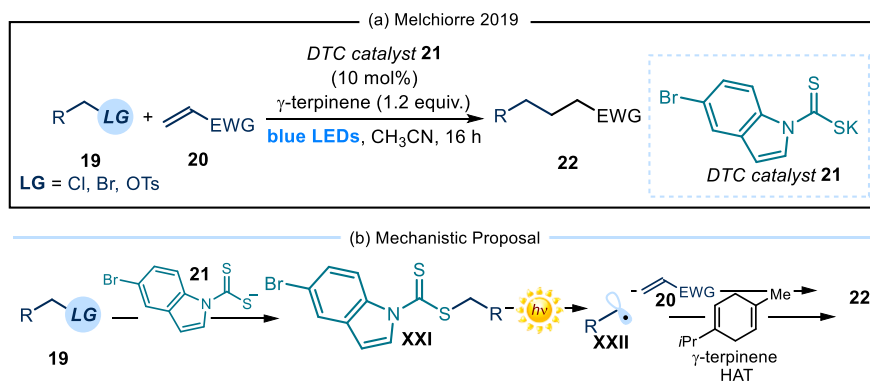


Figure 1.12: (a) Use of a nucleophilic dithiocarbonyl catalyst to promote radical formation from alkyl electrophiles. (b) Mechanistic proposal. LG: leaving group. HAT: hydrogen atom transfer.

Overall, the studies detailed in Figures 1.10 - 1.12 indicate that the excited-state reactivity of organocatalytic intermediates can produce open-shell intermediates through electron transfer or photolytic mechanisms. The research work developed during my doctoral thesis has used many of these photochemical activation concepts. The aim was to further advance and understand the potential of organocatalytic intermediates in the excited state and their utility in synthesis. Aims and objectives of the thesis are detailed in the next section.

1.4 General Objectives and Summary

The main scientific objective of this doctoral thesis was the investigation and understanding of the reactivity of organocatalytic intermediates in their excited states. We aimed at exploiting this excited-state reactivity to develop novel catalytic radical reactions, not possible through classical thermal pathways.

In the first project, discussed in Chapter II, we sought to expand the synthetic potential of excited-state chiral iminium ions to promote the enantioselective catalytic C-H functionalization of toluene derivatives. In the second part of the PhD endeavors, discussed in Chapters III and IV, we aimed at exploiting the photolysis of catalytically generated thiocarbonyl-based compounds to promote new C-B and C-C bond forming processes. Specifically, in Chapter III, we targeted the development of a photochemical organocatalytic method for the synthesis of alkyl boronic acid derivatives. Additionally, as detailed in Chapter IV, we aimed at expanding the potential of this photo-organocatalytic platform to include nucleophilic acyl substitution as a suitable manifold for the generation of acyl and carbamoyl radicals from the corresponding chlorides.

1.4.1 Asymmetric photocatalytic C-H functionalization of toluene and derivatives

Chapter II discusses the development of the asymmetric catalytic C-H functionalization of toluene and derivatives promoted by the visible-light excitation of chiral iminium ions. This transformation is achieved without the use of any external photocatalyst or transition-metal additive, since it relies solely on the excited-state properties of chiral iminium ion salts, transiently generated through acid-promoted condensation of the amine catalyst **13** with enal **14** (Figure 1.13).

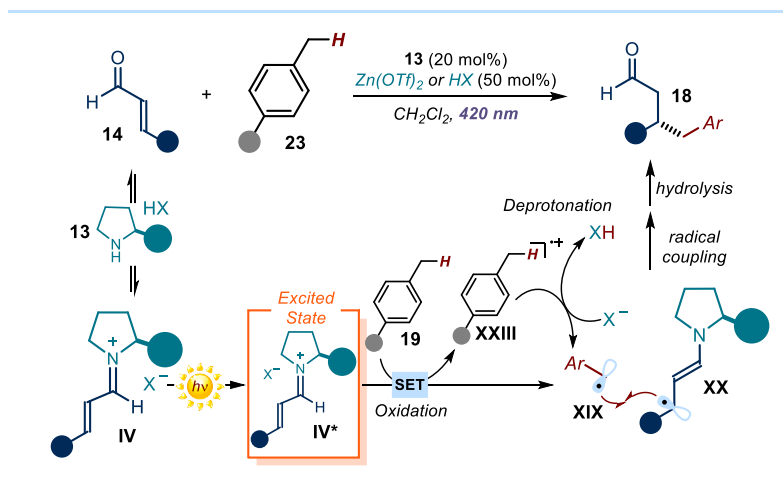


Figure 1.13: Asymmetric photocatalytic C-H functionalization of toluene and derivatives.

This reaction has been accomplished by combining the enhanced oxidative power of a chiral excited-state iminium ion **IV*** and the basic nature of its counter-anion. A sequential multisite PCET mechanism,³⁵ which implies oxidation of the substrate governed by the excited iminium ion **IV*** followed by a second deprotonation of the ensuing radical cation by the iminium ion counteranion, turns a toluene derivative **23** into the benzyl radical **XIX**. The latter intermediate reacts with the chiral radical intermediate **XX**, generated during the SET reduction of the iminium ion **IV**, to afford the enantioenriched β-alkylated aldehyde **18**. This study shows how readily available and inexpensive feedstock materials, generally used as solvents, can be used to produce chiral molecules.

1.4.2 Photochemical organocatalytic borylation of alkyl chlorides, bromides, and sulfonates

Chapter III details a new photochemical approach for the conversion of alkyl halides and sulfonates **19** into valuable boronic acid derivatives **25**. This methodology takes advantage of the nucleophilic properties of the dithiocarbonyl anion organocatalyst (DTC catalyst) **21**, which can activate alkyl electrophiles by means of a nucleophilic

³⁵ Weinberg, D. R.; Gagliardi, C. J.; Hull, J. F.; Murphy, C. F.; Kent, C. A.; Westlake, C. B.; Paul, A.; Ess, D. H.; Granville McCafferty, D.; Meyer, T. J. "Proton-Coupled Electron Transfer" *Chem. Rev.* **2012**, *112*, 4016-4093.

substitution manifold. The photolysis of the weak C-S bond within the resulting intermediate **XXI** (Figure 1.14) produces open-shell intermediates **XXII**, which are then intercepted by bis(catecholato)diboron **24** to afford the borylated products **25**.

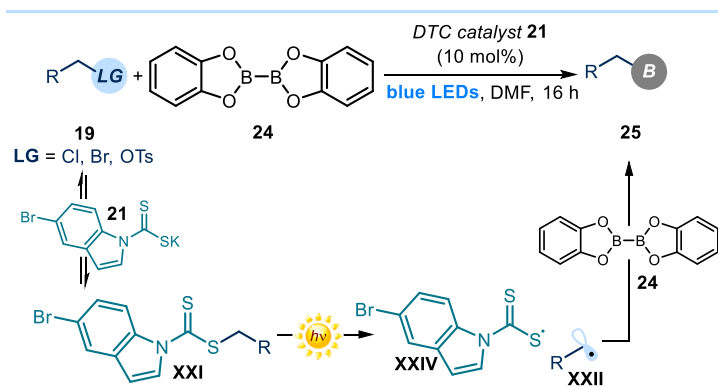


Figure 1.14: Photochemical organocatalytic borylation of alkyl chlorides, bromides and sulfonates.

This process has been further expanded to a three component variant. The key feature of this transformation is that the organic catalyst **21** can activate substrates exploiting their electrophilic nature, granting access to radicals that cannot be generated by classical strategies based on SET or HAT mechanisms. This feature enables the use of radical precursors that are inert to or unsuitable for previously reported metal-free borylation protocols.

1.4.3 Photochemical generation of acyl and carbamoyl radicals

In Chapter IV, the photolytic strategy based on the use of a nucleophilic DTC organocatalyst has been expanded to activate acyl and carbamoyl chlorides **26** (Figure 1.15) via a nucleophilic acyl substitution path. The photolysis of the resulting intermediate **XXV** affords nucleophilic radicals **XXVI** that are intercepted by a variety of electron-poor olefins **20** to give, after HAT, products **28**. Also in this case, we used substrates that, due to their high reduction potential, are not readily activated by redox-based radical generation methods.

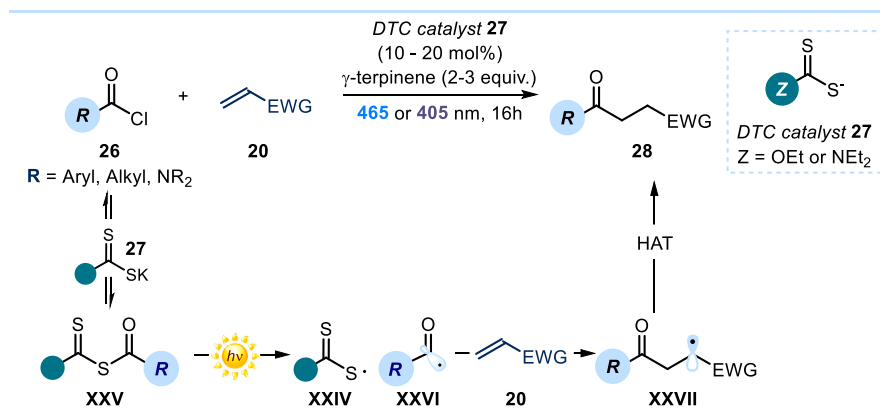


Figure 1.15: Photochemical generation of acyl and carbamoyl radicals using a nucleophilic organic catalyst.

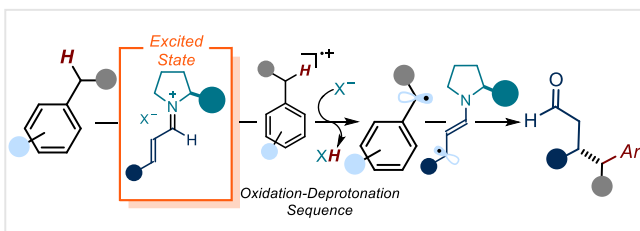
A detailed mechanistic investigation, based on spectroscopic and electrochemical analyses along with the characterization of key intermediates, identified a variety of off-the-cycle intermediates which control the overall concentrations of the reactive radicals. These regulated equilibria cooperate to control the overall concentrations of the radicals, contributing to the efficiency of the process.

Chapter II

Asymmetric Photocatalytic C-H Functionalization of Toluene and Derivatives

Target

Development of a photochemical organocatalytic method for the stereoselective C-H functionalization of toluene and its derivatives.



Tools

The excited-state oxidative properties of catalytically generated chiral iminium ions and the basicity of their counteranion.¹

2.1 Introduction

C-H functionalization reactions are defined as processes where an unactivated carbon-hydrogen bond is cleaved to promote the formation of a new chemical bond.² Since C-H bonds are ubiquitous in organic molecules, their direct functionalization is extremely valuable and can drastically streamline the installment of the desired functionality within a target molecule, circumventing routes requiring multistep functional group interconversions. Traditionally, C-H functionalization strategies rely on the use of a transition-metal catalyst to activate the inert C-H bond, thus forming a reactive organometallic species.³ Radical chemistry has also emerged as a useful strategy for the functionalization of C-H bonds.⁴ In this context, proton-coupled electron transfer (PCET)⁵ is a powerful approach to remove a hydrogen atom from the

¹ The project discussed in this Chapter has been conducted in collaboration with Dr. Giacomo Crisenza, who performed part of the reaction scope and part of the mechanistic investigation. I was mainly involved in the discovery of the reaction, its optimization, and evaluation of part of the scope, as well as on the mechanistic studies. This work has been published, see: Mazzarella, D.; Crisenza, G. E. M.; Melchiorre, P. "Asymmetric Photocatalytic C-H Functionalization of Toluene and Derivatives" *J. Am. Chem. Soc.* **2018**, *140* 8439-8443.

² (a) Abrams, D. J.; Provencher, P. A.; Sorensen, E. J. "Recent applications of C-H functionalization in complex natural product synthesis" *Chem. Soc. Rev.*, **2018**, *47*, 8925-8967. (b) Davies, H. M. L.; Du Bois, J.; Yu, J.-Q. "C-H Functionalization in organic synthesis" *Chem. Soc. Rev.* **2011**, *40*, 1855-1856 and related thematic issue.

³ Shilov, A. E.; Shul'pin, G. B. "Activation of C-H bonds by metal complexes" *Chem. Rev.* **1997**, *97*, 2879-2932.

⁴ Yi, H.; Zhang, G.; Wang, H.; Huang, Z.; Wang, J.; Singh, A. K.; Lei, A.; "Recent Advances in Radical C-H Activation/Radical Cross-Coupling" *Chem. Rev.* **2017**, *117*, 9016-9085.

⁵ Miller, D. C.; Tarantino, K. T.; Knowles, R.R. "Proton-Coupled Electron Transfer in Organic Synthesis: Fundamentals, Applications, and Opportunities" *Top. Curr. Chem.* **2016**, *374*, 30.

target substrate, affording a reactive radical which is subsequently used in bond forming processes. Despite the recent advances in radical-based methods for C-H functionalization, very limited asymmetric variants have been developed.⁶ Current methods for the enantioselective installment of functionalities from C-H bonds generally rely on asymmetric transition metal catalysis.⁷

Organocatalysis has stood out as an effective tool to control the stereochemical outcome of both polar⁸ and radical⁹ reactions. Moreover, specific organocatalytic intermediates, upon photoexcitation, can act as either strong oxidant or reductant and generate radical upon single-electron transfer (SET) mechanisms.⁹ In this context, our research group demonstrated that photoexcited chiral iminium ions can trigger the SET oxidation of benzyl silanes to then trap the ensuing benzyl radical in a stereoselective fashion.¹⁰

We envisioned to further expand the synthetic utility of the excited-state reactivity of chiral iminium ions **Ia*** (Figure 2.1) to develop an asymmetric radical C-H functionalization process. In particular, we sought to activate toluene derivatives **1** by means of an oxidation/deprotonation sequence assisted by a PCET manifold. The so-formed benzylic radical **III** would be then stereoselectively trapped by the chiral iminium ion, providing a fully organocatalytic asymmetric C-H functionalization strategy.

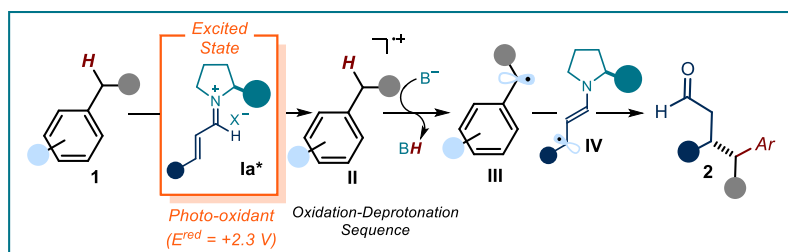


Figure 2.1: Use of PCET, enabled by the photo-excited iminium ion, to drive the enantioselective functionalization of toluene derivatives.

⁶ For selected examples please see: (a) Bauer, A.; Westkamper, F.; Grimme, S.; Bach, T. "Catalytic Enantioselective Reactions Driven by Photoinduced Electron Transfer" *Nature* **2005**, *436*, 1139-1140. (b) Uraguchi, D.; Kinoshita, N.; Kizu, T.; Ooi, T. "Synergistic Catalysis of Ionic Brønsted Acid and Photosensitizer for a Redox Neutral Asymmetric α -Coupling of N-Arylaminoethanes with Aldimines" *J. Am. Chem. Soc.* **2015**, *137*, 13768-13771. (c) Wang, C.; Qin, J.; Shen, X.; Riedel, R.; Harms, K.; Meggers, E. "Asymmetric Radical-Radical Cross-Coupling through Visible-Light Activated Iridium Catalysis" *Angew. Chem., Int. Ed.* **2016**, *55*, 685-688. (d) Murphy, J. J.; Bastida, D.; Paria, S.; Fagnoni, M.; Melchiorre, P. "Asymmetric catalytic formation of quaternary carbons by iminium ion trapping of radicals" *Nature*, **2016**, *532*, 218-222.

⁷ Newton, C. G.; Wang, S.-G.; Oliveira, C.; Cramer, N. "Catalytic Enantioselective Transformations Involving C-H Bond Cleavage by Transition-Metal Complexes" *Chem. Rev.* **2017**, *117*, 8908-8976.

⁸ Dalko, P. I. "Comprehensive Enantioselective Organocatalysis: Catalysts, Reactions, and Applications" **2013**, Wiley-VCH.

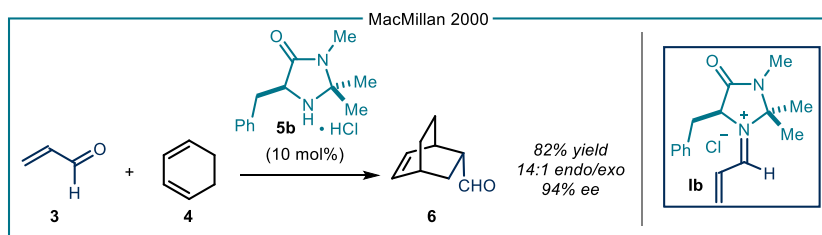
⁹ Silvi, M.; Melchiorre, P. "Enhancing the potential of enantioselective organocatalysis with light" *Nature*, **2018**, *554*, 41-49.

¹⁰ Silvi, M.; Verrier, C.; Rey, Y. P.; Buzzetti, L.; Melchiorre, P., "Visible-Light Excitation of Iminium Ions Enables the Enantioselective Catalytic β -Alkylation of Enals" *Nat. Chem.* **2017**, *9*, 868-873.

2.2 Iminium Ion Activation

2.2.1 Ground-state reactivity of iminium ions

Conjugated iminium ions (also known as eniminium ions) are electron-deficient intermediates arising from the reversible acid-promoted condensation of a chiral amine catalyst with α,β -unsaturated carbonyl compounds.¹¹ The lowest unoccupied molecular orbital (LUMO) of these organocatalytic intermediates have a lower energy than the parent unsaturated carbonyl compound. This makes iminium ions highly electrophilic π -systems. In 2000, iminium ion activation was first employed by the group of MacMillan to promote an organocatalytic asymmetric Diels-Alder reaction (Scheme 2.1).¹² Condensation of the chiral imidazolidinone catalyst **5b** with enal **3** generates the iminium ion intermediate **Ib**, which, acting as a chiral dienophile, undergoes a [4+2] cycloaddition with cyclohexadiene **4**. The overall process provides cycloadduct **6** with good levels of diastereo- and enantioselectivity.



Scheme 2.1: Iminium-ion-catalyzed asymmetric [4+2] cycloaddition.

Following this seminal example, countless transformations based on the enhanced electrophilicity of chiral iminium ions **I** have been developed (Figure 2.2a).¹³ The majority of these reactions involves attack of a soft nucleophile at the β -carbon of **I**, providing enantioenriched β -functionalized chiral aldehydes **7**. In parallel with the quest for new iminium-ion-mediated reactions, many efforts have been devoted to the development of new chiral aminocatalysts. Among these, imidazolidinone and proline derivatives **5b-e** displayed a wide applicability as chiral catalysts for iminium ion activation (Figure 2.2b). In particular, diarylprolinol silyl ethers **5c-d**, independently developed by Jørgensen¹⁴ and Hayashi,¹⁵ have been widely used for the functionalization of enals. The high efficiency of such chiral catalysts depends on their ability to *i*) condense with the enal substrate in a reversible manner, *ii*) control the geometry of the iminium ion and *iii*) discriminate the two prochiral π -faces of the

¹¹ Melchiorre, P.; Marigo, M.; Carlone, A.; Bartoli, G. "Asymmetric Aminocatalysis-Gold Rush in Organic Chemistry" *Angew. Chem. Int. Ed.* **2008**, *47*, 6138–6171.

¹² Ahrendt, K. A.; Borths, C. J.; MacMillan, D. W. C. "New Strategies for Organic Catalysis: The First Highly Enantioselective Organocatalytic Diels-Alder Reaction" *J. Am. Chem. Soc.* **2000**, *122*, 4243–4244.

¹³ Erkkilä, A.; Majander, I.; Pihko, P. M. "Iminium Catalysis" *Chem. Rev.* **2007**, *107*, 5416–5470.

¹⁴ Franzén, J.; Marigo, M.; Fielenbach, D.; Wabnitz, T. C.; Kjærsgaard, A.; Jørgensen, K. A., "A general organocatalyst for direct α -functionalization of aldehydes: stereoselective C–C, C–N, C–F, C–Br, and C–S bond-forming reactions. scope and mechanistic insights" *J. Am. Chem. Soc.* **2005**, *127*, 18296–18304.

¹⁵ Hayashi, Y.; Gotoh, H.; Hayashi, T.; Shoji, M., "Diphenylprolinol silyl ethers as efficient organocatalysts for the asymmetric Michael reaction of aldehydes and nitroalkenes" *Angew. Chem. Int. Ed.* **2005**, *44*, 4212–4215.

iminium ion thus inducing high stereocontrol in the nucleophilic attack at the β -carbon (Figure 2.1c).

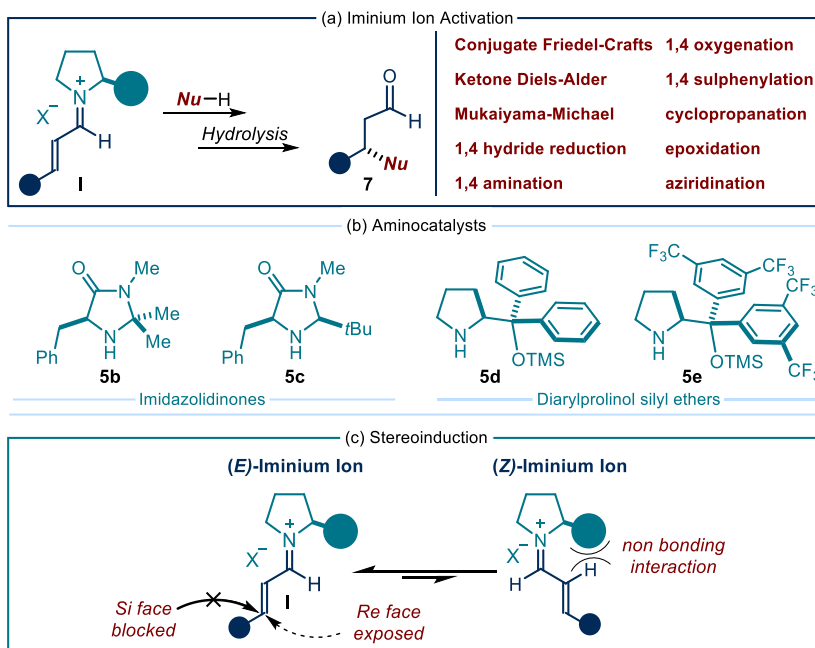


Figure 2.2: (a) The iminium ion activation strategy served to develop several asymmetric functionalizations of enals. (b) Most used chiral organocatalysts. (c) Chiral catalysts control the iminium ion geometry and discriminate between the two π -faces to secure high stereoselectivity. X^- represents the counteranion of **I**.

The structure of the chiral aminocatalyst is fundamental for the reactivity and the enantioselectivity of iminium-ion-mediated processes. Nevertheless, the counteranion of **I**, resulting from the acid-promoted condensation, can also influence the rate and the selectivity of the reaction. This was clearly demonstrated by Lakhdar and Mayr,¹⁶ who focused on the mechanism of a Friedel-Crafts reaction between pyrroles **9** and enals **8** (Figure 2.3a), originally reported by MacMillan.¹⁷

¹⁶ Lakhdar, S.; Mayr, H. "Counterion effects in iminium-activated electrophilic aromatic substitutions of pyrroles" *Chem. Commun.* **2011**, 47, 1866-1868.

¹⁷ Paras, N. A.; MacMillan D. W. C. "New Strategies in Organic Catalysis: The First Enantioselective Organocatalytic Friedel-Crafts Alkylation" *J. Am. Chem. Soc.* **2001**, 123, 4370-4371.

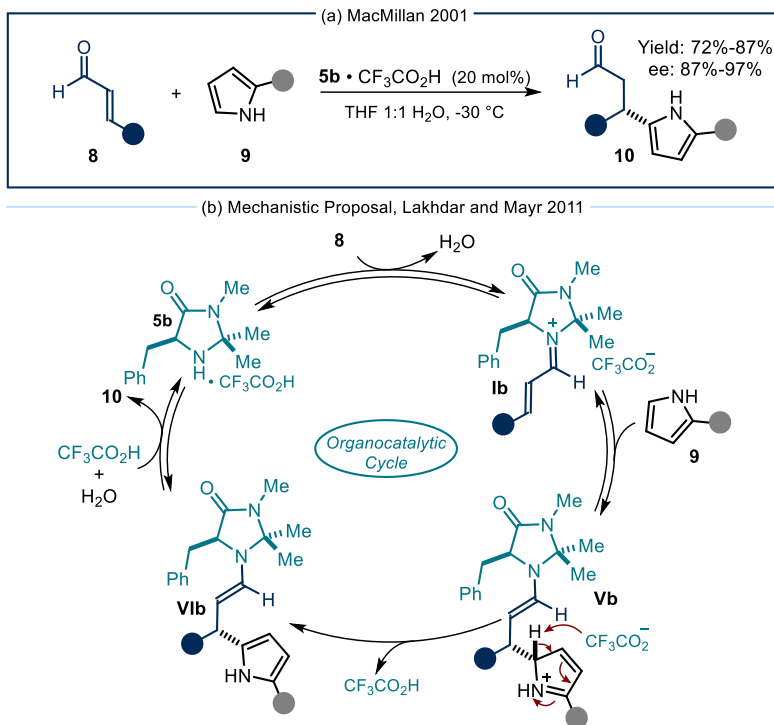


Figure 2.3: a) Asymmetric Friedel-Craft process reported by MacMillan. b) Rationalization of the mechanism and the influence of the counteranion by Lakhdar and Mayr.

They demonstrated that the use of trifluoroacetic acid as a promoter, which generates weakly basic trifluoroacetate counteranion, was necessary to obtain product **10** in good yields and selectivity. When a stronger acid was used, such as tosylic acid or triflic acid, a less basic counteranion was generated. Under this condition, the attack of pyrrole **9** onto the iminium ion **Ib** occurred reversibly, thus eroding both the yield and the enantioselectivity of the process. When using trifluoroacetate, the deprotonation-aromatization process within intermediate **Vb** was faster and intermediate **Vb** was formed rapidly, preventing the equilibrium between **Vb** and the iminium ion **Ib** to erode the efficiency of the overall process.

Overall, these examples highlight the synthetic power and the mechanistic requirements of ground-state iminium ion chemistry for promoting highly enantioselective reaction at the β -carbon of unsaturated carbonyl derivatives.

2.2.2 Excited-state reactivity of iminium ions

Besides their ground-state reactivity, iminium ions possess rich photochemical properties. These intermediates can efficiently absorb light within the UV-visible region, and undergo a $\pi \rightarrow \pi^*$ electronic transition, accessing moderately long-lived

singlet excited states.¹⁸ For instance, iminium ion photoisomerization plays a crucial role in biological systems, as exemplified by the photo-induced isomerization of 11-cis-retinal, which controls the mechanism of vision in higher organisms.¹⁹ Moreover, when in their excited state, iminium ions can act as strong oxidants. During the 1980s, studies by Patrick Mariano described the photochemical properties of preformed non-conjugated iminium ions.²⁰ These intermediates, when photoexcited, possess a very high redox potential, allowing for the SET oxidation of several organic molecules, such as unactivated alkenes (Figure 2.4).²¹ UV-light excitation of 2-phenyl-1-pyrrolinium perchlorate **11** produces the highly oxidizing species **11***, which takes one electron from isobutylene **12**, forming radical cation **VII** along with α -amino radical **VIII**. **VII** is electrophilic enough to undergo attack from methanol leading to **IX**. This intermediate is subsequently intercepted by **VIII** to yield the final product **13**.

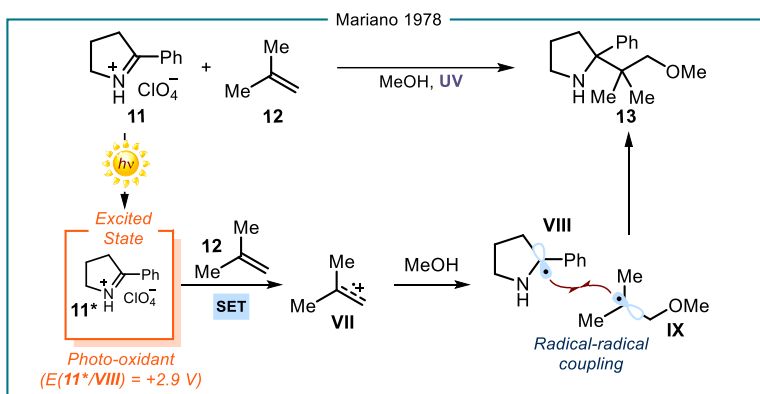


Figure 2.4: Photoexcitation of non-conjugated iminium ions by Mariano. SET: Single-electron transfer.

Recently, our research group demonstrated that catalytically generated chiral conjugated chiral iminium ions can absorb visible light and act as photo-oxidants to activate a selection of radical precursors (Figure 2.5).^{10,22} Specifically, acid promoted condensation of enal **8** with aminocatalyst **5a** generates the iminium ion **Ia**. Selective excitation of this intermediate furnishes the strong photo-oxidant **Ia*** ($E(Ia^*/IV) = +2.30$ V versus Ag/Ag^+ in CH_3CN),²³ which is able to activate organosilane **14** ($E(X/14) = +1.74$ V versus Ag/Ag^+ in CH_3CN) via an SET oxidation. This step produces the chiral β -enaminy radical **IV** along with benzyl radical **X**. The persistency of **IV**, which is both

¹⁸ Mariano, P. S. "The photochemistry of iminium salts and related heteroaromatic systems" *Tetrahedron* **1983**, *39*, 3845-3879.

¹⁹ Wald, G., "The molecular basis of visual excitation" *Nature* **1968**, *219*, 800-807.

²⁰ Mariano, P. S., "Electron-transfer mechanisms in photochemical transformations of iminium salts" *Acc. Chem. Res.* **1983**, *16*, 130-137.

²¹ Mariano, P. S.; Stavinoha, J. L.; Pepe, G.; Meyer Jr, E. F., "Novel photochemical addition reactions of iminium salts. Electron transfer initiated additions of olefins to 2-phenyl-1-pyrrolinium perchlorate" *J. Am. Chem. Soc.* **1978**, *100*, 7114-7116.

²² Verrier, C.; Alandini, N.; Pezzetta, C.; Moliterno, M.; Buzzetti, L.; Hepburn, H. B.; Vega-Peñaloza, A.; Silvi, M.; Melchiorre, P. "Direct Stereoselective Installation of Alkyl Fragments at the β -Carbon of Enals via Excited Iminium Ion Catalysis" *ACS Catal.* **2018**, *8*, 1062-1066.

²³ The reported potential has been estimated through a combination of spectroscopic and electrochemical analysis, following the Rehm-Weller theory. These studies were performed in the contribution in reference 10.

benzylic and allylic, allows the stereoselective radical coupling with **X**, forming the new C-C bond and the stereogenic center within the ensuing enamine **XII**. Hydrolysis of the latter furnishes the enantioenriched β -alkylated aldehyde **15**. This process does not work in the absence of light, since the benzyl silane is not nucleophilic enough to attack the ground-state electrophilic iminium ion.

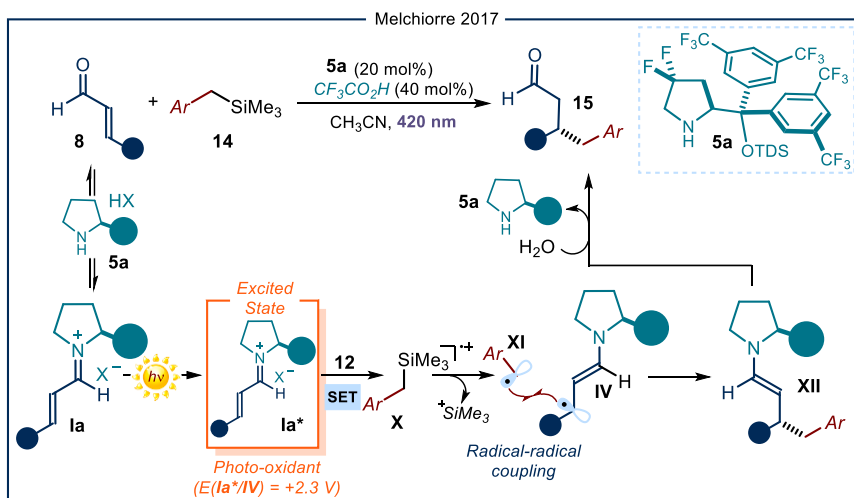


Figure 2.5: Photoexcitation of catalytically generated conjugated iminium ions and its use in asymmetric catalysis.

Three crucial parameters influence the efficiency and the selectivity of the overall process. The first one is the irradiation wavelength: the use of high-power light emitting diodes (LEDs) centered at 420 nm secures the selective excitation of iminium ion **1a** over the enal **8**, inhibiting possible racemic background reactions. Secondly, the use of the difluorinated diarylprolinol silyl ether catalyst **5a** is necessary to increase the aminocatalyst stability under oxidative conditions. Indeed, the SET oxidation and ensuing degradation of commonly used amine catalysts (*c.f.* Figure 2.1b) by **1a*** was observed during the optimization of the methodology. The presence of the two geminal fluorine atoms on the catalyst pyrrolidine backbone raises its oxidation potential ($E(\text{5a}^+/\text{5a}) = +2.20 \text{ V}$ versus Ag/Ag^+ in CH_3CN , compared to $E(\text{5e}^+/\text{5e}) = +1.57 \text{ V}$ versus Ag/Ag^+ in CH_3CN), while further increasing the excited-state oxidizing power of iminium ion **1a***. However, the addition of the two geminal fluorine substituents within **5a** also decreases the catalyst nucleophilicity, therefore hampering iminium ion formation. For this reason, as third requirement is necessary to use a strong acid co-catalyst, such as trifluoroacetic acid, to promote the catalyst condensation with enal **8**. These examples highlighted how transiently generated iminium ions could be used outside of the well-established two-electron thermal pathway. Their excited-state reactivity serves to promote reactions not available through polar mechanisms.

2.3 Proton-Coupled Electron Transfer

Proton-coupled electron transfer (PCET) processes are elementary steps in which a proton and an electron are transferred.²⁴ Based on the number of steps involved, as well as on the origin and destination of both the electron and the proton, these processes can be further classified as schematized in Figure 2.6. If the two entities are transferred in the same step, the process is defined as concerted PCET. Conversely, if the electron transfer precedes the proton transfer (ET-PT), or *vice versa* (PT-ET), the process is classified as sequential. Moreover, if both the proton and the electron are delivered to two distinct acceptors, or they have been transferred from diverse donors, the PCET event is defined as multisite (MS). Finally, when both the transferring electron and proton derive from the same bond, the process is called hydrogen atom transfer (HAT).

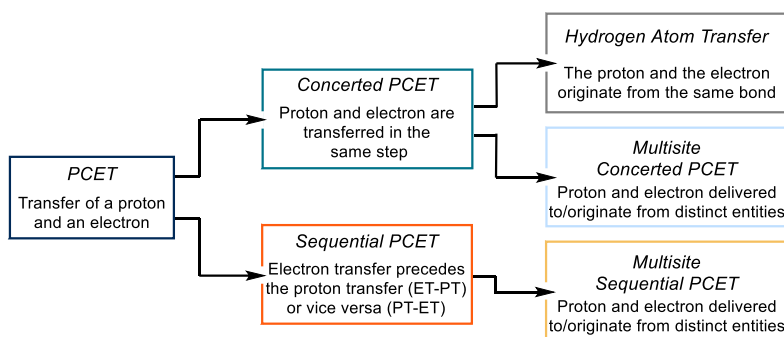


Figure 2.6 Classification of PCET processes.

These processes are ubiquitous in nature. For example, PCET plays a pivotal role in enzymatic C-H oxidations,²⁵ photosynthetic water oxidation,²⁶ and oxygen reduction by cytochrome C oxidase,²⁷ among others. At the same time, PCET has been exploited for CO₂ reduction²⁸ and oxygen evolution.²⁹ PCET has also been employed in organic synthesis.⁵ Among the several processes enabled by this strategy, the most used for synthetic purposes is undoubtedly HAT.³⁰ As an example, the iconic Hofmann-Löffler-

²⁴ Weinberg, D. R.; Gagliardi, C. J.; Hull, J. F.; Murphy, C. F.; Kent, C. A.; Westlake, C. B.; Paul, A.; Ess, D. H.; Granville McCafferty, D.; Meyer, T. J. "Proton-Coupled Electron Transfer" *Chem. Rev.* **2012**, *112*, 4016-4093.

²⁵ Hatcher, E.; Soudackov, A.; Hammes-Schiffer, S. "Proton-Coupled Electron Transfer in Soybean Lipoxygenase" *J. Am. Chem. Soc.* **2004**, *126*, 5763-5775.

²⁶ Meyer, T. J.; Huynh, M. H. V.; Thorp, H. H. "The Possible Role of Proton-Coupled Electron Transfer (PCET) in Water Oxidation by Photosystem II" *Angew. Chem. Int. Ed.* **2007**, *46*, 5284-5304.

²⁷ Kaila, V. R. I.; Verkhovsky, M. I.; Wikström, M. "Proton-Coupled Electron Transfer in Cytochrome Oxidase" *Chem. Rev.* **2010**, *110*, 7062-7081.

²⁸ Constantin, C.; Drouet, S.; Savéant, J.-M. "A Local Proton Source Enhances CO₂ Electroreduction to CO by a Molecular Fe Catalyst" *Science* **2012**, *338*, 90-94.

²⁹ Symes, M. D.; Surendranath, Y.; Lutterman, D. A.; Nocera, D. G. "Bidirectional and Unidirectional PCET in a Molecular Model of a Cobalt-Based Oxygen-Evolving Catalyst" *J. Am. Chem. Soc.* **2011**, *133*, 5174-5177.

³⁰ Costas, M.; Bietti, M. "Uncovering the Complexity of the Simplest Atom Transfer Reaction" *Acc. Chem. Res.* **2018**, *51*, 2601-2602 and related thematic issue.

Freytag reaction³¹ exploits the ability of nitrogen-centered radicals **XIV** (Figure 2.7), generated via photolysis of **XIII**, to promote a 1,5-HAT. This produces C-centered radicals of type **XV**. The latter react with a second molecule of **XIII**, feeding a radical chain propagation mechanism, while generating the alkyl halide **XVI**. This, upon intramolecular nucleophilic displacement, produces the pyrrolidine product **17**.

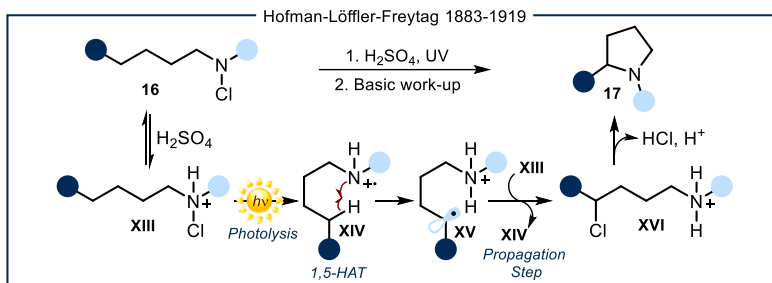


Figure 2.7: Use of HAT strategy to promote the distal functionalization of amines.

Within this context, MS concerted PCET has been used by the group of Knowles for the activation of N-H bonds in amides and sulfonamides.³² These bonds are difficult to be activated either via HAT, because of the high bond-dissociation energy of the N-H bond, or via ET-PT, due to the high oxidation potential of the amide moiety. However, the simultaneous action of an oxidant (e.g. photo-excited $[\text{Ir}(\text{dF}(\text{CF}_3)\text{ppy})_2(\text{bpy})]\text{PF}_6$) and a base (e.g. $\text{NBu}_4(\text{OBu})_2\text{PO}_2$), promotes the homolysis of N-H bond within **18** (Figure 2.8), furnishing amidyl radical **XVII**.³³ This is intramolecularly intercepted by the pendant olefin moiety to produce the alkyl radical **XVIII**, which is trapped by electrophilic acrylate **19** to generate **XIX**. The latter undergoes a SET reduction to afford, upon protonation, the carboamination product **20**.

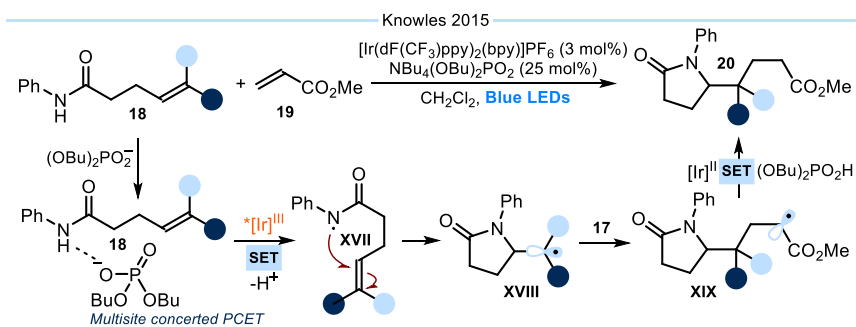


Figure 2.8: Use of MS concerted PCET to activate N-H bonds and drive the carboamination of olefins.

³¹ (a) Hofman, A. W.; "Ueber die Einwirkung des Broms in alkalischer Lösung auf die Amine" *Ber. Dtsch. Chem. Ges.* **1883**, *16*, 558-560. (b) Löffler, K.; Freytag, C.; "Über eine neue Bildungsweise von N-alkylierten Pyrrolidinen" *Ber. Dtsch. Chem. Ges.* **1909**, *42*, 3427-3431.

³² Gentry, E. C.; Knowles, R. R. "Synthetic Applications of Proton-Coupled Electron Transfer" *Acc. Chem. Res.* **2016**, *49*, 1546-1556.

³³ Choi, G. J.; Knowles, R. R. "Catalytic Alkene Carboaminations Enabled by Oxidative Proton-Coupled Electron Transfer" *J. Am. Chem. Soc.* **2015**, *137*, 9226-9229.

Sequential PCET has also been employed in organic synthesis. Nishibayashi exploited a photo-oxidant, $[\text{Ir}(\text{dtbbpy})(\text{ppy})_2]\text{BF}_4$, to promote the mono-electronic oxidation of amine **21** (Figure 2.9).³⁴ The resulting radical cation **XX** is around 25 orders of magnitude more acidic than the parent amine **21**,³⁵ and easily loses one proton to furnish the nucleophilic α -aminoradical **XXI**. The latter is later trapped by **20** to deliver, after SET reduction to give a carbanion (not shown in the Figure) and protonation, product **23**.

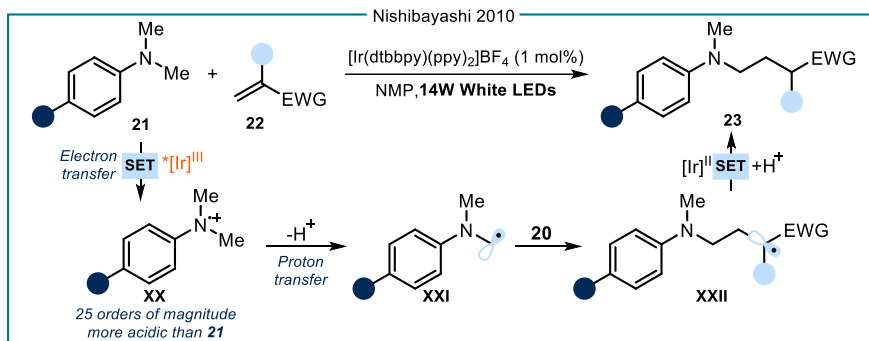


Figure 2.9: Use of sequential PCET to produce α -aminoradicals.

2.4 Target of the Project

The aim of this project was to expand the synthetic potential of excited-state chiral iminium ions (*c.f.* Figure 2.5) to enable the enantioselective C-H functionalization of feedstock materials, such as toluene and its derivatives.

Despite the invaluable synthetic solutions provided by transition metal-catalyzed C-H activation approaches, only few reports detail the selective oxidative insertion of a transition metal catalyst into primary benzylic $\text{C}(\text{sp}^3)\text{-H}$ bonds. On the one hand, this is due to the competing metal insertion into the more activated aromatic $\text{C}(\text{sp}^2)\text{-H}$,³⁶ especially in the absence of a directing group. On the other hand, this is complicated by the general low susceptibility of primary carbons to participate in C-H activation.³⁷ Sequential PCET can provide a solution to tackle this issue, since it offers a tool to selectively functionalize benzylic positions through radical manifolds. This strategy

³⁴ Miyake, Y.; Nakajima, K.; Nishibayashi, Y. "Visible-Light-Mediated Utilization of α -Aminoalkyl Radicals: Addition to Electron-Deficient Alkenes Using Photoredox Catalysts" *J. Am. Chem. Soc.* **2012**, *134*, 3338-3341.

³⁵ Beatty, J. W.; Stephenson, C. R. J. "Amine Functionalization via Oxidative Photoredox Catalysis: Methodology Development and Complex Molecule Synthesis" *Acc. Chem. Res.* **2015**, *48*, 1474-1484

³⁶ (a) Neufeldt, S. R.; Sanford, M. S. "Controlling Site Selectivity in Palladium-Catalyzed C-H Bond Functionalization" *Acc. Chem. Res.* **2012**, *45*, 936-946. (b) Davies, H. M. L.; Morton, D. "Guiding principles for site selective and stereoselective intermolecular C-H functionalization by donor/acceptor rhodium carbenes" *Chem. Soc. Rev.* **2011**, *40*, 1857-1869.

³⁷ Transition metal insertion into primary $\text{C}(\text{sp}^3)\text{-H}$ bonds generally requires the use of directing groups: (a) Baudoin, O. "Transition metal-catalyzed arylation of unactivated $\text{C}(\text{sp}^3)\text{-H}$ bonds" *Chem. Soc. Rev.* **2011**, *40*, 4902-4911. (b) Giri, R.; Shi, B.-F.; Engle, K. M.; Mangel, N.; Yu, J.-Q. "Transition metal-catalyzed C-H activation reactions: diastereoselectivity and enantioselectivity" *Chem. Soc. Rev.* **2009**, *38*, 3242-3272.

takes advantage of the increased acidity of the benzylic protons within the radical cation **II**, derived from the SET oxidation of toluene derivatives **1** (Figure 2.10).

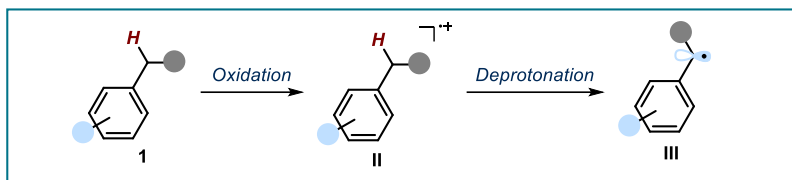


Figure 2.10: Use of sequential PCET to produce benzylic radicals.

However, oxidizing these stable substrates is far from easy, and a very strong oxidant is required (for toluene, $E(\text{II}/\text{I}) = +2.26$ V versus Ag/Ag^+ in CH_3CN).³⁸ The group of Fukuzumi³⁹ and, later, the group of Wu⁴⁰ both exploited the high oxidizing properties of methyl acridinium dyes Mes-AcrClO_4 in the excited state ($E(\text{Mes-Acr}^+/\text{Mes-Acr}^\bullet) = +2.06$ V vs. SCE in MeCN) to promote the SET oxidation of xylene **1a** (Figure 2.11). The ensuing radical cation **IIa** is characterized by extremely high acidic properties (pK_a of **IIa** estimated as -13 in CH_3CN).⁴¹ Deprotonation affords the corresponding benzyl radical **IIIa**. In the study by Fukuzumi, **IIIa** was trapped by molecular oxygen to yield benzaldehyde **24**, while Wu employed electron-poor olefins **22** to perform a Giese-type reaction, leading to product **25** after SET reduction from the reduced form of the photocatalyst (Mes-Acr^\bullet).

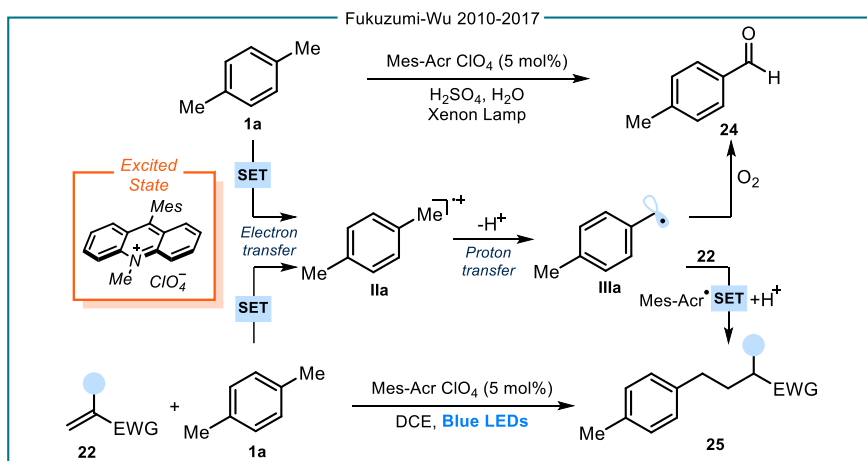


Figure 2.11: Use of sequential PCET to produce benzylic radicals.

³⁸ Merkel, P. B.; Luo, P.; Dinnocenzo, J. P.; Farid, S. "Accurate Oxidation Potentials of Benzene and Biphenyl Derivatives via Electron-Transfer Equilibria and Transient Kinetics" *J. Org. Chem.* **2009**, *74*, 5163-5173

³⁹ Ohkubo, K.; Mizushima, K.; Iwata, R.; Souma, K.; Suzuki, N.; Fukuzumi, S. "Simultaneous production of p-tolualdehyde and hydrogen peroxide in photocatalytic oxygenation of p-xylene and reduction of oxygen with 9-mesityl-10-methylacridinium ion derivatives" *Chem. Commun.* **2010**, *46*, 601-603.

⁴⁰ Zhou, R.; Liu, H.; Tao, H.; Yu, X.; Wu, J. "Metal-free direct alkylation of unfunctionalized allylic/benzylic sp^3 C-H bonds via photoredox induced radical cation deprotonation" *Chem. Sci.* **2017**, *8*, 4654-4659.

⁴¹ De Nicholas, A. M.; Arnold, D. A. "Thermochemical parameters for organic radicals and radical ions. Part 1. The estimation of the pK_a of radical cations based on thermochemical calculations" *Can. J. Chem.* **1982**, *60*, 2165-2179.

Despite the advance brought by these reports, the development of an asymmetric catalytic variant for the C-H functionalization of toluene derivatives remains largely underexplored. The group of Davies exploited the C-H insertion of a chiral rhodium-carbenoid⁴² to promote the enantioselective benzylic functionalization of toluene derivatives. Here, the use of reactive diazo compounds **26** (Figure 2.12), in the presence of a chiral rhodium-based catalyst, generated the corresponding rhodium carbenoids. These highly reactive organometallic intermediates can insert into the benzylic C-H bond and stereoselectively forge the C-C bond within the chiral product **27a**. These processes⁴³ worked smoothly for derivatives with a secondary benzylic position and for some functionalized toluene derivatives,^{43a} but were rather unselective when toluene was employed as substrate.^{43b} Indeed, the reaction delivered two different products: compounds **27b-c**, arising from a competitive cyclopropanation pathway, and the desired enantioenriched chiral C-H functionalized product **27a**, which was only a minor component of the complex mixture.

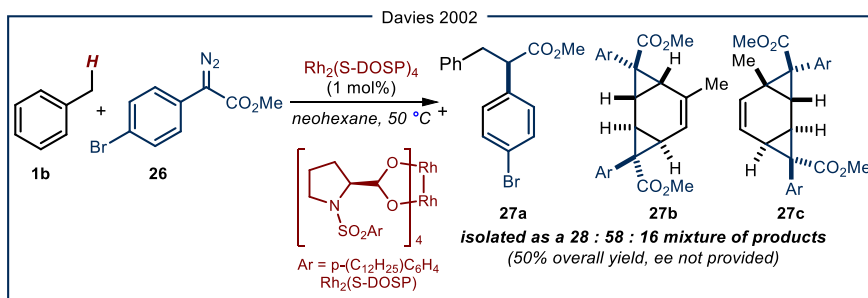


Figure 2.12: Attempts of using rhodium carbenoid to promote enantioselective functionalization of toluene.

In analogy with the SET oxidation mechanism used by Fukuzumi and Wu, we wondered whether a sequential PCET strategy could be employed for activating toluene derivatives (Figure 2.13). Specifically, the high oxidizing properties of the excited chiral iminium ions **Ia*** ($E(\text{Ia}^*/\text{IV}) = +2.30$ V versus Ag/Ag^+ in CH_3CN)¹⁰ should enable the oxidation of compounds **1** (for toluene, $E(\text{II}/\text{I}) = +2.26$ V versus Ag/Ag^+ in CH_3CN),³⁸ affording the corresponding radical cation **II**. Deprotonation by a base delivers the corresponding benzylic radical **III**. This step has to be faster than the unproductive back-electron transfer (BET), which would regenerate **Ia** and **I** (not shown in Figure 2.7). **III** would then be trapped stereoselectively by the chiral β -enaminyll radical **IV** to afford, upon hydrolysis of the resulting enamine intermediate, the enantioenriched chiral product **2**.

⁴² Davies, H. M. L.; Manning, J. R. "Catalytic C-H functionalization by metal carbenoid and nitrenoid insertion" *Nature* **2008**, *451*, 417-424.

⁴³ (a) Qin, C.; Davies, H. M. L. "Role of Sterically Demanding Chiral Dirhodium Catalysts in Site-Selective C-H Functionalization of Activated Primary C-H Bonds" *J. Am. Chem. Soc.* **2014**, *136*, 9792-9796. (b) Davies, H. M. L.; Jin, Q.; Ren, P.; Kovalevsky, A. Y. "Catalytic Asymmetric Benzylic C-H Activation by Means of Carbenoid-Induced C-H Insertions" *J. Org. Chem.* **2002**, *67*, 4165-4169.

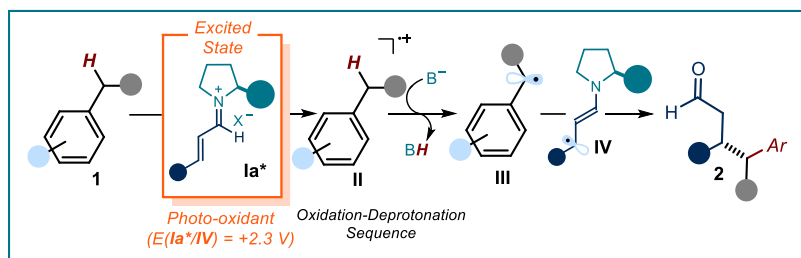


Figure 2.13: Use of sequential PCET, through photo-excited iminium ion chemistry, to drive the enantioselective functionalization of toluene derivatives.

If successful, this approach would enable the β -benzylation of enals using, as substrates, feedstock chemicals generally used as solvents, such as toluene and xylene derivatives.

2.5 Results and Discussion

2.5.1 Preliminary results and optimization

At the outset of our investigations, we envisioned two potential pitfalls for the good outcome of our design plan: i) the coexistence of an acid promoter, which is needed to foster the formation of the iminium ion **Ia**, with a basic additive, which is required to deprotonate the radical cation **II** (c.f. Figure 2.13), and ii) the akin redox potential showed by both aminocatalyst **5a** ($E(5a^+/5a) = +2.20$ V) and toluene, which would reflect in a competition for the SET step. The first issue would thwart the formation of iminium ion **Ia**, while the second would drive the degradation of the organic catalyst **5a**.

Aware of these potential problems, we tested the reaction of cinnamaldehyde **8a** and toluene, serving both as substrate and solvent, in the presence of catalyst **5a**, trifluoroacetic acid as an additive, and under irradiation at 420 nm by a single high-power light-emitting diode (HP single LED). This LED possesses a sharp emission profile, and can be connected to a power supplier to control the intensity of emission (irradiance, mW/cm^2). The LED was attached to an aluminum block (Figure 2.14), which secured its stability. Moreover, a 3D-printed vessel holder was mounted on the aluminum block to keep a fixed distance of 1 cm between the light source and the bottom of the reaction vessel. Alternatively, the 3D-printed vessel holder could be connected to a chiller in order to control the reaction temperature. Under normal conditions, the internal temperature of the reaction was detected to be ~ 35 °C, as measured with a thermometer.

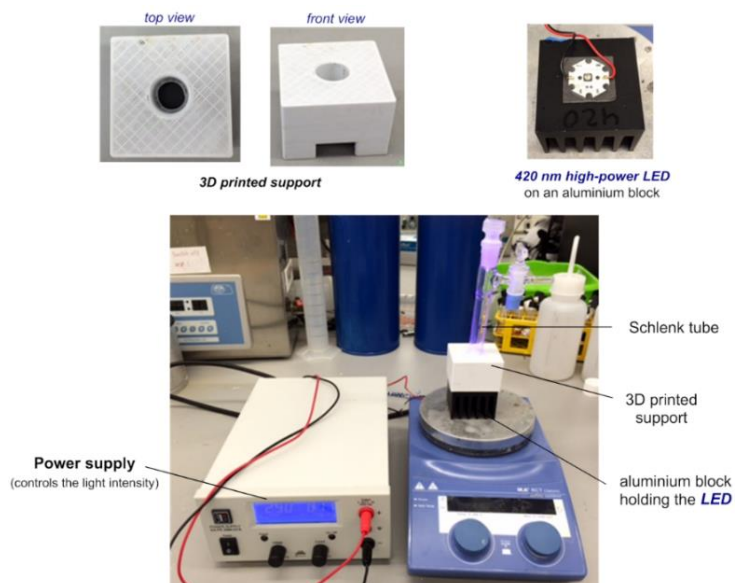
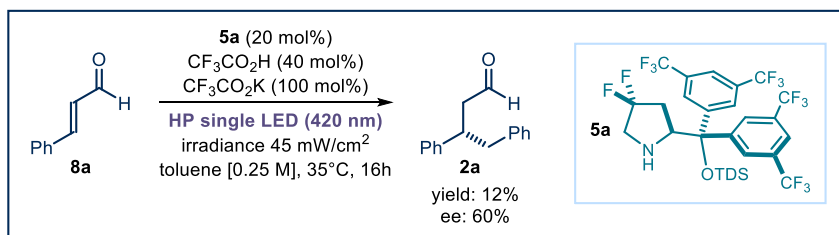


Figure 2.14: Detailed set-up and illumination system. The light source for illuminating the reaction vessel consisted of a 420 nm high-power single LED (OCU-440 UE420-X-T) purchased from OSA OPTO.

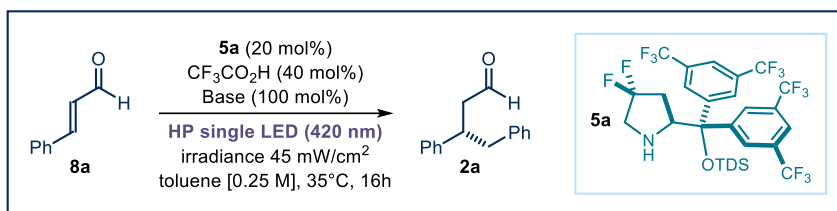
To address the first pitfall, we selected potassium trifluoroacetate as the base additive, in order to keep constant the amount of trifluoroacetic acid in the reaction medium. We also surmised that the used over-stoichiometric amount of toluene would prevent the competing oxidation of catalyst **5a** (pitfall 2).



Scheme 2.2: Preliminary results for the C-H functionalization of toluene. Reaction performed on a 0.1 mmol scale. Yield refers to the isolated product **2a** after chromatographic purification on silica gel. Enantiomeric excess of **2a** determined by HPLC analysis on a chiral stationary phase.

Under these catalytic conditions, the desired product **2a** was isolated in 12% yield and with 60% enantiomeric excess. With this result in hand, we started the optimization of the reaction conditions, aiming at improving both the chemical yield and the enantioselectivity of the process.

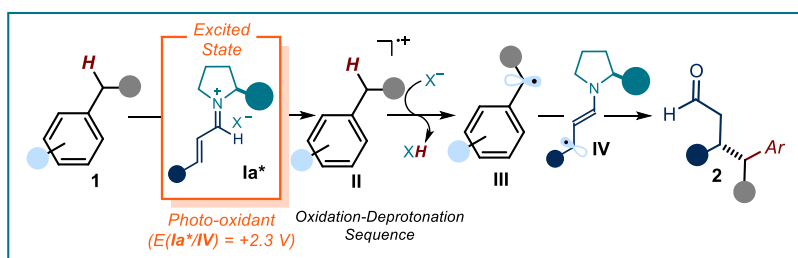
First, we evaluated the influence of the basic additive to the reactivity (Table 2.1).

Table 2.1: Effect of base additives on the C-H functionalization of toluene.^a

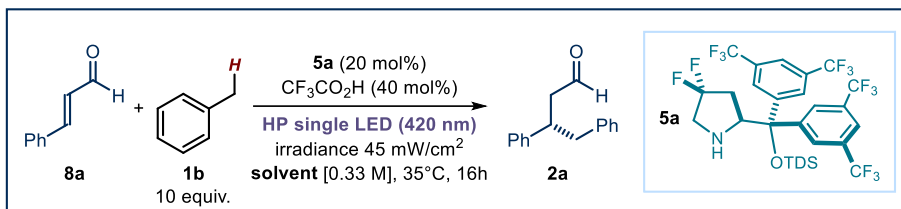
Entry	Base	Yield ^b	ee ^c
1	Cs ₂ CO ₃	10%	60%
2	2,6-lutidine	-	-
3	KOt-Bu	-	-
4	PhCO ₂ K	-	-
5	-	19%	60%

^aReaction performed on a 0.1 mmol scale. Yield refers to the isolated product **2a** after chromatographic purification on silica gel. ^cEnantiomeric excess of **2a** determined by HPLC analysis on a chiral stationary phase.

The reaction works with similar efficiency when Cs₂CO₃, insoluble in the reaction medium, was used (entry 1). When using more soluble bases (entries 2-4), no benzylated product was formed, and substrate **8a** was recovered almost unreacted. These findings corroborated our hypothesis of the problematic coexistence between a basic and an acidic additive. Interestingly, a control experiment performed in the absence of any base (entry 5) provided similar results to the ones highlighted in scheme 2.2. This initially surprising result suggested that there was no need for an external basic additive. To rationalize this observation, we hypothesized that the entity responsible of the deprotonation of the toluene radical cation **III** was the counteranion of the iminium ion (X^- in Figure 2.15).

**Figure 2.15:** The counteranion of the iminium ion can act as a base to promote the deprotonation of **II**.

We therefore continued the optimization in the absence of an external base. We focused on the influence of the reaction solvent. For these experiments, the amount of toluene was lowered to 10 equivalents (Table 2.2).

Table 2.2: Effect of the solvent on the C-H functionalization of toluene.^a

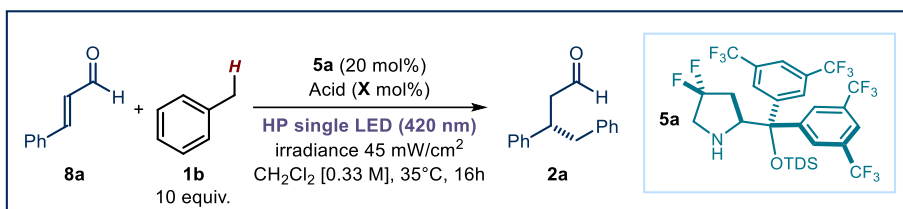
Entry	Solvent	Yield ^b	ee ^c
1	benzene	28%	68%
2	chlorobenzene	40%	68%
3	dichloroethane	30%	75%
4	dichloromethane	30%	75%
5	methyl <i>t</i> -butyl ether	-	-
6	acetonitrile	-	-
7	dimethylsulfoxide	-	-

^aReaction performed on a 0.1 mmol scale. Yield refers to the isolated product **2a** after chromatographic purification on silica gel. ^cEnantiomeric excess of **2a** determined by HPLC analysis on a chiral stationary phase.

The use of benzene (entry 1) afforded the desired product with increased yield and enantiomeric excess. A higher efficiency and selectivity were observed when using chlorobenzene (entry 2). This prompted us to evaluate other chlorinated solvents. Both dichloroethane (entry 3) and dichloromethane (entry 4) afforded **2a** with increased levels of enantioselectivity (75% ee). Conversely, the use of more polar solvents, such as methyl *tert*-butyl ether (entry 5), acetonitrile (entry 6) and dimethylsulfoxide (entry 7), completely inhibited the photochemical process. Having identified dichloromethane as the most suitable solvent, we screened other acid additives (Table 2.3). According to our hypothesis that the counteranion is responsible of the deprotonation, we expected the nature of the acid to greatly influence the reaction outcome.

The use of methanesulfonic acid provided similar results to trifluoroacetic acid (entry 1). The use of relatively weak acids, such as benzoic acid (entry 2) and diphenyl hydrogen phosphate (entry 3), completely inhibited the reaction, probably because of their inability to promote the catalyst condensation and form the iminium ion. However, also a stronger acid, such as trifluoromethanesulfonic acid (*p*K_a = -14 in dimethylsulfoxide),⁴⁴ failed to deliver the desired product (entry 4). These results suggested that a Brønsted acid suitable for promoting this photochemical process has to possess a *p*K_a value within a narrow window.

⁴⁴ Trummal, A.; Lipping, L.; Kaljurand, I.; Koppel, I. A.; Leito, I. "Acidity of Strong Acids in Water and Dimethyl Sulfoxide" *J. Phys. Chem. A* **2016**, *120*, 3663-3669.

Table 2.3: Influence of the acid additive on the C-H functionalization of toluene derivatives.^a

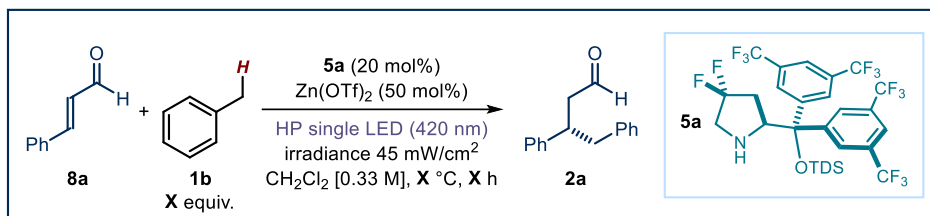
Entry	Acid	Yield ^b	ee ^c
1	CH ₃ SO ₃ H (40 mol%)	34%	78%
2	PhCO ₂ H (40 mol%)	-	-
3	(PhO) ₂ PO ₂ H (40 mol%)	-	-
4	CF ₃ SO ₃ H (40 mol%)	-	-
5	Zn(CF ₃ CO ₂) ₂ (40 mol%)	traces	-
6	Zn(ClO ₄) ₂ (40 mol%)	10%	n.d.
7	Zn(CF ₃ SO ₃) ₂ (40 mol%)	52%	83%
8	Zn(CF ₃ SO ₃) ₂ (50 mol%)	57%	83%
9	Zn(CF ₃ SO ₃) ₂ (60 mol%)	55%	83%
10	Zn(CF ₃ SO ₃) ₂ (70 mol%)	51%	83%
11	Mg(CF ₃ SO ₃) ₂ (50 mol%)	40%	80%
12	Ca(CF ₃ SO ₃) ₂ (50 mol%)	39%	78%

^aReaction performed on a 0.1 mmol scale. Yield refers to the isolated product **2a** after chromatographic purification on silica gel. ^cEnantiomeric excess of **2a** determined by HPLC analysis on a chiral stationary phase.

We wondered whether Lewis acids could be used to assist the formation of iminium ion **Ie**, while producing the basic counteranion needed for the PCET pathway.⁴⁵ Zinc(II) trifluoroacetate (entry 5) failed to promote the reaction, whereas zinc(II) perchlorate (entry 6) delivered product **2a** in low yield. Satisfyingly, zinc(II) triflate increased both the chemical yield and the enantioselectivity of the process (52% yield, 83% ee, entry 7). Further studies using zinc(II) triflate identified a 50 mol% loading as the optimal for the acid (entries 6-10). Other triflate sources, such as magnesium(II) triflate (entry 11) and calcium (II) triflate (entry 12), could promote the model reaction, albeit with worse results compared to the zinc analogue. These results indicated triflate as a suitable basic counteranion to promote the radical formation.

As a final cycle of optimization, we evaluated the effect of temperature, reaction time and equivalents of toluene **1b** on the reaction conducted in the presence of zinc(II) triflate (50 mol%, Table 2.4).

⁴⁵ For a discussion on the Zn(II) salt-mediated condensation of amines and aldehydes, see: Enthaler, S.; Wu, X.-F. "Zinc Catalysis: Applications in Organic Synthesis" **2015**, Wiley-VHC, 156–162.

Table 2.4: Final cycle of optimization for the C-H functionalization of toluene derivatives.

Entry	Temperature	Time	1b equiv.	Yield	ee
1	10 °C	16 h	10	25%	85%
2	45 °C	16 h	10	35%	80%
3	35 °C	48 h	10	63%	83%
4	35 °C	48 h	5	53%	82%
5	35 °C	48 h	1	28%	82%

^aReaction performed on a 0.1 mmol scale. Yield refers to the isolated product **2a** after chromatographic purification on silica gel. ^cEnantiomeric excess of **2a** determined by HPLC analysis on a chiral stationary phase.

The use of lower (entry 1) or higher temperature (entry 2) proved detrimental in terms of chemical yield. Increasing the reaction time from 16 to 48 hours afforded **2a** in 63% yield (entry 3). Additionally, after 48 hours, aldehyde **8a** was fully consumed, which facilitated the purification step. It was also possible to lower the amount of toluene to 5 equivalents (entry 4), although with slightly reduced chemical yield. On the other hand, the use of 1 equivalent of toluene (entry 5) heavily affected the efficiency of the reaction, and rapid consumption of the aminocatalyst **5a** was observed. This observation is coherent with a competing SET oxidation of toluene **1b** and amine **5a** from the photoexcited iminium ion **Ia**^{*}.

2.5.2 Scope of the reaction

Adopting the optimized conditions detailed in Table 2.4, entry 4, we set to demonstrate the generality of the β -benzylation of enals **8** using diverse toluene derivatives (Figure 2.16). Initially, we proved that the other enantiomer of catalyst **5a** (*ent-5a*) afforded the opposite enantiomer of product **2a** with comparable results. We then focused on the scope of the enals. Several aromatic enals **8**, decorated with both electron-donating and electron-withdrawing groups on the aromatic ring, could be used (compounds **2b-g**). Conversely, aliphatic enals, such as *tert*-butylacroleine or (*E*)-2-octenal, did not react under the optimized photochemical conditions. This lack of reactivity was already observed in our previous work with the excitation of iminium ions.^{10,22} There are two possible explanations for this observation: on one side, the absence of the aryl ring decreases the conjugation within the iminium ion, shifting its absorption profile to the UV-region. However, when employing a light centered at 365 nm, complete conversion of the enal was observed, but no product formation. This is probably due to the loss of persistency of the chiral radical intermediate **IV**, generated during the process, when replacing the aryl ring with a simple alkyl chain (see Figure 2.15 for details). This could prevent a stereoselective radical coupling leading to the formation of product **2**. Moreover, the presence of an enolizable position within octenal enables

the competitive formation of the more stable dienamine upon deprotonation of the γ -proton of the iminium ion, disabling the SET oxidation chemistry.

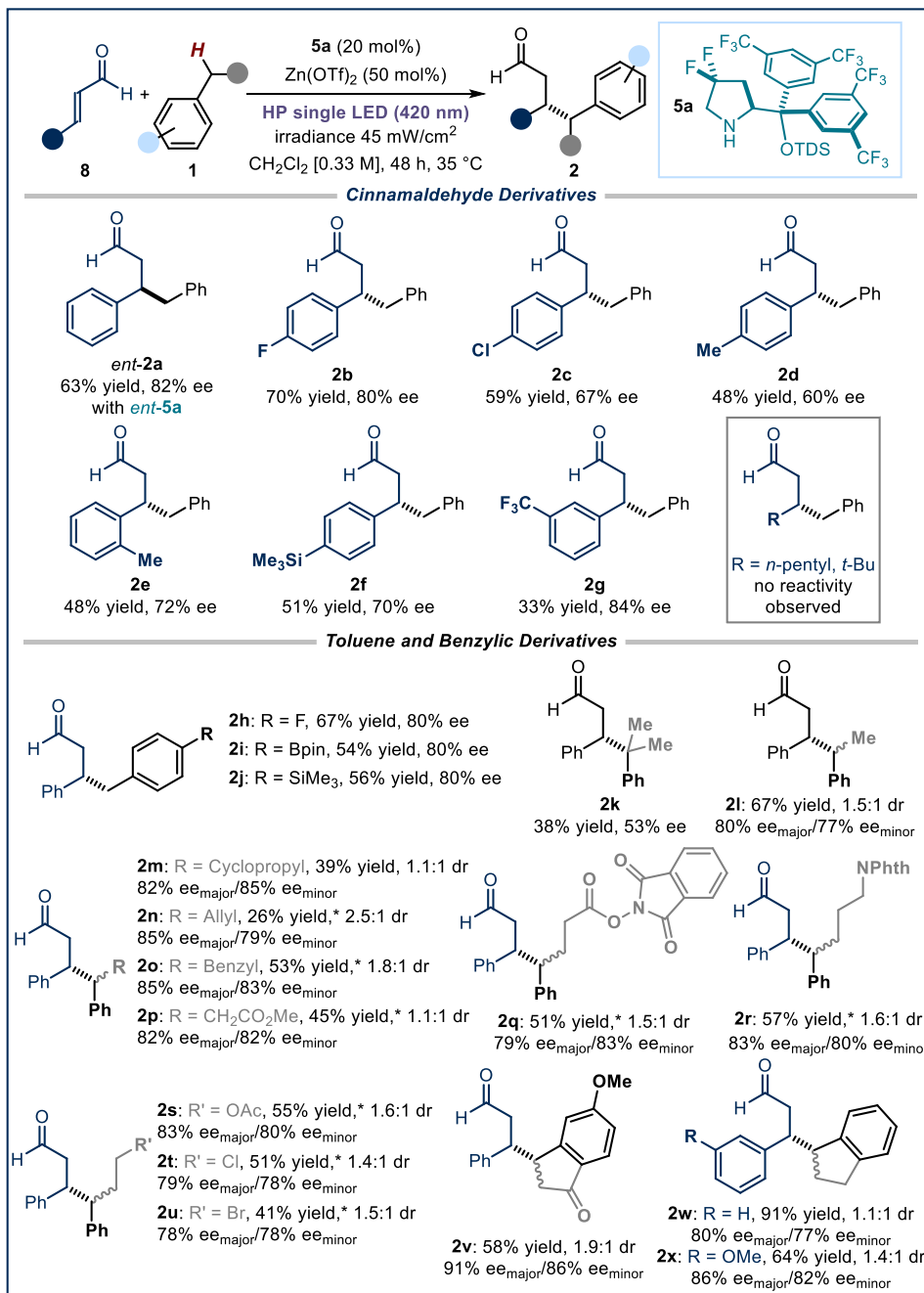


Figure 2.16: Survey of the enals **8** and toluene derivatives **1** that can participate in the reaction. Reactions performed on a 0.1 mmol scale using 10 equiv. of **1** in 0.3 mL of CH₂Cl₂. Yields and enantiomeric excesses of the isolated products are indicated below each entry (average of two runs per substrate). *Reaction run using 5 equiv. of benzylic derivatives. TDS: texyl-dimethylsilyl.

The protocol tolerates a plethora of toluene derivatives bearing several functional groups, both on the aryl ring and at the benzylic position. Fluorine, boron and silicon-based moieties all survive the reaction conditions, delivering the corresponding products **2h-j** in good yield and with high enantioselectivity. Tertiary benzylic positions can be functionalized but with moderate chemical yield and stereocontrol (**2k**). On the other hand, secondary benzylic derivatives readily react to furnish the corresponding products in good yields and enantioselectivity but limited control over the diastereoselectivity (**2l-x**). Oxidizable moieties, such as cyclopropyl (**2m**) or allyl (**2n**), survived the process, highlighting the chemoselectivity of the method. Furthermore, this strategy shows a good functional group tolerance, as substrates bearing moieties sensitive to polar or radical processes are selectively functionalized (**2p-v**). Specifically, the redox active moiety within **2q**, as well as the sensitive chloride and bromide moieties within **2t** and **2u**, all survived the reaction conditions. Moreover, this method enables the construction of dicarbonyl compounds with an umpolung 1,6-span (**2p,v**). Indane proved to be the most reactive substrate, and product **2w** was isolated in 91% yield. Unfortunately, electron-deficient toluene derivatives did not react under the photochemical conditions, due to their high oxidation potential. Conversely, when electron rich *p*-xylene was employed under the optimized conditions, the corresponding product was obtained only in 15% yield. We reasoned that electron-rich derivatives, after oxidation, would generate a more stable radical cation, which would require a stronger conjugate base for the deprotonation. The use of 100 mol% of trichloroacetic acid was found to be optimal for promoting both the iminium ion formation and the deprotonation of the radical cation of **1y**, delivering product **2y** in 63% yield and 83% ee. Under these modified conditions, the scope of the process was expanded to several xylene derivatives (**2y-ae**, Figure 2.17).

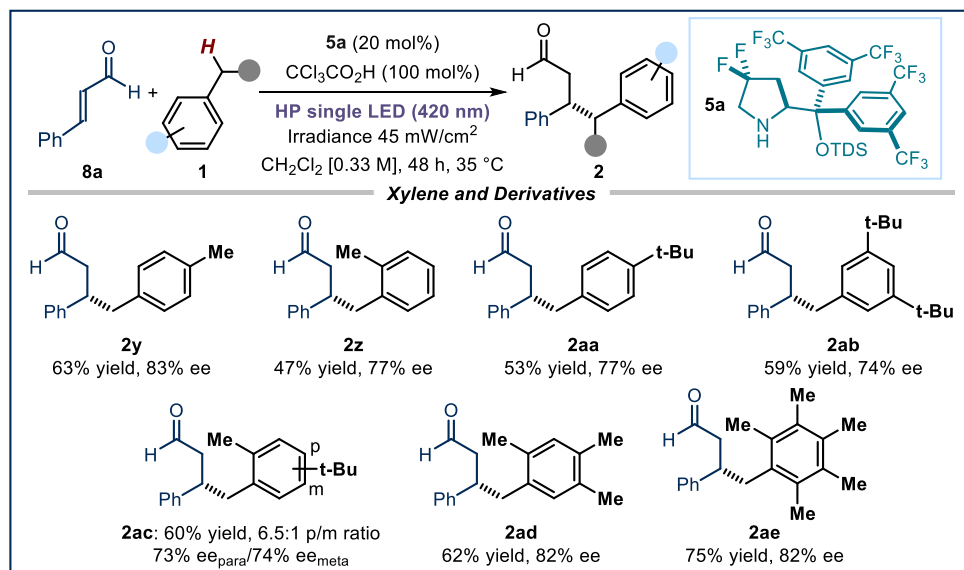
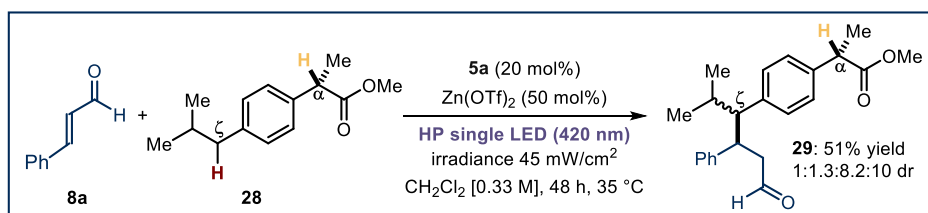


Figure 2.17: Survey of xylene derivatives that can participate in the reaction. Reactions performed on a 0.1 mmol scale using 10 equiv. of **1** in 0.3 mL of CH_2Cl_2 . Yields and enantiomeric excesses of the isolated products are indicated below each entry (average of two runs per substrate). TDS: tehyl-dimethylsilyl.

To evaluate the synthetic utility of this protocol, the benchmark reaction between cinnamaldehyde **8a** and toluene **1b** was scaled up to 1 mmol scale, obtaining the product **2a** in slightly reduced yield (52%) but preserved enantioselectivity (83%). Furthermore, we demonstrated that the method can serve as a C-H functionalization platform for relevant pharmaceutical agents. As depicted in Scheme 2.3, when the non-steroidal anti-inflammatory drug (NSAID) derivative (*S*)-ibuprofen methyl ester **28** was submitted to the reaction protocol with **8a**, the exclusive formation of the C- ζ -alkylated product **29** was observed, with moderate diastereoselectivity.



Scheme 2.3: Selective functionalization of the (*S*)-ibuprofen methyl ester **28**.

2.6 Mechanistic Investigation

At the outset of the mechanistic investigation, we decided to evaluate the feasibility of every single key step. To this end, we investigated the formation of the iminium ion **I**, its photo-excitation to form **I*** and the use of the enhanced oxidizing properties of **I*** in concert with the basic nature of its counteranion.

2.6.1 Role of the acid co-catalyst, the aminocatalyst and light

During the optimization studies (*c.f.* Table 2.1), we observed that weaker Brønsted acids than trifluoroacetic acid, such as $(\text{PhO})_2\text{PO}_2\text{H}$ or PhCO_2H , were ineffective for promoting the photochemical process. We reasoned that these additives were not acidic enough to promote the formation of the iminium ion **Ia**, thus inhibiting the reactivity. We performed nuclear magnetic resonance (NMR) studies to better clarify this aspect (Figure 2.18).

We analyzed mixtures of enal **8a** and aminocatalyst **5a** in the presence of either trifluoroacetic acid or diphenyl phosphate. When trifluoroacetic acid was used, the ¹H NMR analysis of the mixture showed the presence of a doublet at 8.73 ppm and a broad triplet at 4.43 ppm. These signals are diagnostic of the formation of the iminium ion **Ia**. In contrast, when $(\text{PhO})_2\text{PO}_2\text{H}$ was used, these signals were not observed. These findings indicate that $(\text{PhO})_2\text{PO}_2\text{H}$ is not acidic enough to promote the condensation step.

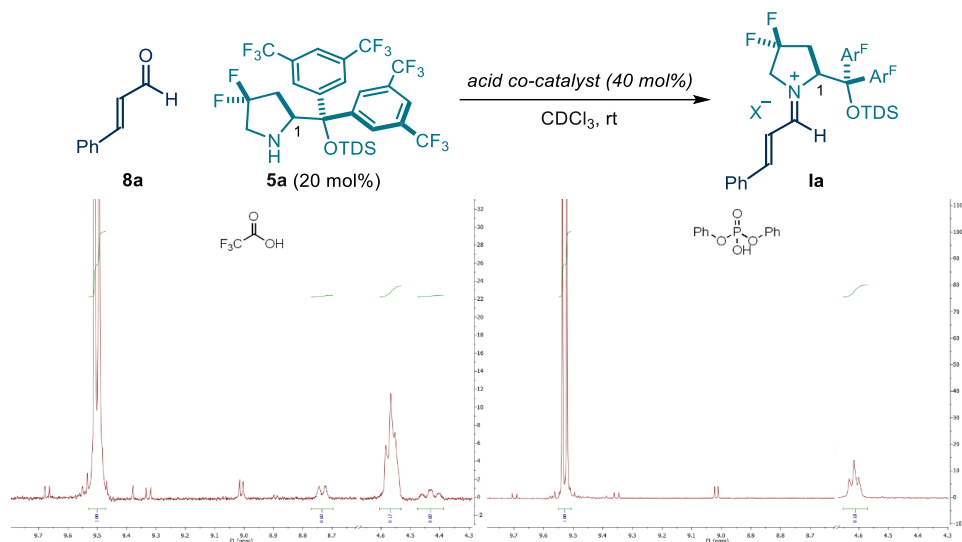


Figure 2.18: Evaluation of the ability of different Brønsted acids to promote the formation of **Ia**. Characteristic ^1H NMR signals of the species involved (400 MHz, CDCl_3): 9.50 (d, $J = 7.5$ Hz, CHO of **8a**), 8.73 (d, $J = 11.0$ Hz, CHN of **Ia**), 4.57 (t, $J = 8.0$ Hz, C1-H of **5a**), 4.43 (br. t, $J = 14.0$ Hz, C1-H of **Ia**).¹⁰ The spectrum on the left refers to the experiment performed with trifluoroacetic acid (TFA), while the spectrum on the right refers to the experiment performed with diphenyl phosphate (DPP) as acid co-catalyst.

Additional control experiments revealed that the exclusion of light or the absence of the amine catalyst **5a** completely suppressed the process. These findings highlight that the photo-excitation of iminium ion **Ia** is essential for the reaction in order to proceed. Furthermore, the ability of iminium ion **Ia** to absorb visible-light was corroborated by UV-Vis analysis (Figure 2.19).

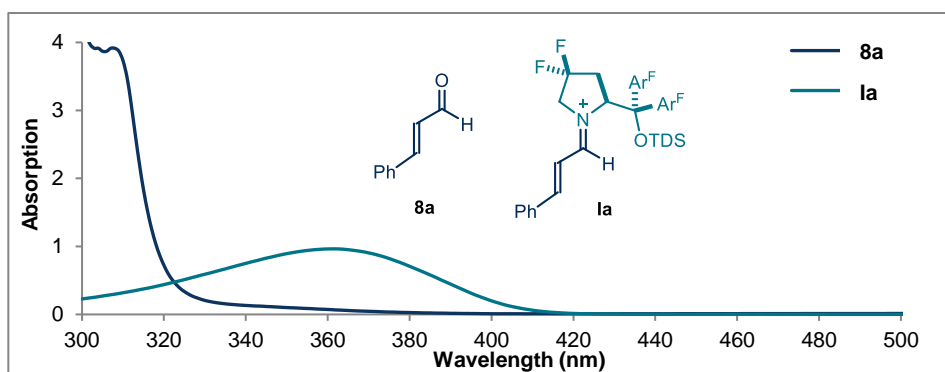
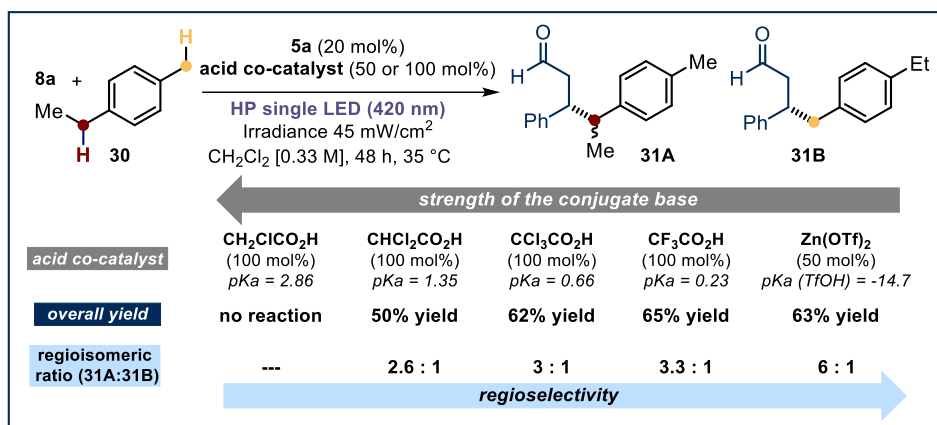


Figure 2.19: UV-Vis absorption spectra of cinnamaldehyde **6a** and iminium ion **Ie**.

Overall, these experiments highlight how the use of a strong acid, aminocatalyst **5a** and light are all required for the process to take place.

2.6.2 Role of the iminium ion and its counteranion

Previous work within our group established that the photoexcitation of the iminium ion **Ia** furnishes a very strong oxidant **Ia*** ($E(\text{Ia}^*/\text{IV}) = +2.30$ V versus Ag/Ag^+ in CH_3CN). At this point, the SET oxidation of toluene ($E(\text{II}/\text{I}) = +2.26$ V versus Ag/Ag^+ in CH_3CN) is thermodynamically feasible, producing the radical cation **II**. In order to gain evidence for the proposed role of the counteranion in the deprotonation of **II**, we performed a selectivity study. Specifically, we studied the photochemical reaction between enal **8a** and 4-ethyl toluene **30**, a substrate bearing both a primary and a secondary benzylic position, in the presence of different acid co-catalysts (Scheme 2.4). In each case, the process led to a mixture of two regioisomers: **31A** and **31B**. A correlation between the regioisomeric ratio and the nature of the conjugate base was observed: the weaker the acid, which in turn generates a stronger conjugate base, the lower is the regioisomeric ratio (**31A**/**31B**). This relationship implies that, upon SET oxidation and radical cation formation, an increased strength of the conjugate base lowers the ability to discriminate between the primary and the secondary benzylic position, which produces the thermodynamically more stable radical (BDEs for toluene and ethylbenzene are 368 kJ mol^{-1} and 357 kJ mol^{-1} , respectively).⁴⁶ Overall, these experiments are compliant with the counteranion of the iminium ion participating in the deprotonation of radical cation **II**.



Scheme 2.4: Selectivity studies highlights the role of the counteranion.

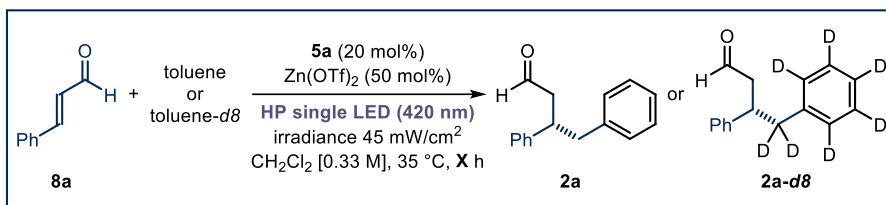
2.6.3 Kinetic isotope effect

To evaluate the irreversibility of the deprotonation step, we performed kinetic analyses to test the occurrence of a kinetic isotope effect (KIE). To this end, we carried out two series of parallel reactions between **8a** and either toluene or toluene-*d*8, which were stopped at different reaction times. The ratio between the two different rates ($k_{\text{H}}/k_{\text{D}}$) indicated the magnitude of the kinetic isotope effect, which was found to be 2.0 (Table 2.5). Since there is no difference in oxidation potential between toluene and toluene-

⁴⁶ Evans, S.; Smith, J. R. L. "The oxidation of ethylbenzene and other alkylaromatics by dioxygen catalysed by iron(III) tetrakis(pentafluorophenyl)porphyrin and related iron porphyrins" *Chem. Soc. Perkin. Trans. 2* **2000**, 1541-1552.

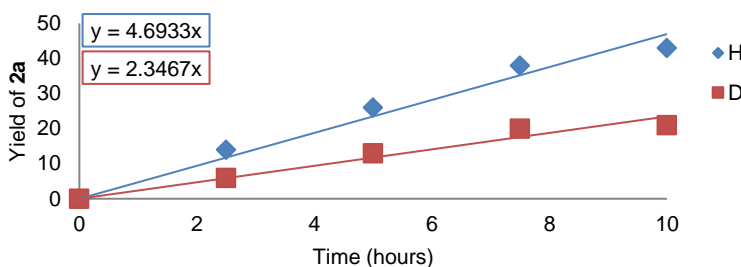
*d*8, such KIE value is in agreement with the deprotonation of the radical cation being the first irreversible step of the transformation.

Table 2.5: Kinetic isotope effect experiment



Time (h)	Toluene	Toluene- <i>d</i> 8
0	-	-
2.5	14	6
5	26	13
7.5	38	20
10	43	21

KIE Determination



2.6.4 Mechanistic proposal

Based on the aforementioned experiments (Sections 2.6.1-2.6.3) and on our previous report,¹⁰ we propose the mechanistic picture reported in Figure 2.20. The acid co-catalyst elicits the condensation of the achromatic enal **8** with aminocatalyst **5a**, forming the visible-light-absorbing iminium ion **Ia**. Selective irradiation of this colored intermediate produces the electronically excited state **Ia***. This intermediate is characterized by enhanced oxidizing properties and it is associated, via ion-pairing, to its basic counteranion. Because of these properties, **Ia*** can activate toluene derivatives through a multisite sequential PCET. Specifically, **Ia*** acts as a strong oxidant, subtracting one electron from toluene derivatives **1**, forming the radical cation **II**. **II** is irreversibly deprotonated by the counteranion of the iminium ion delivering radical **III**. Stereocontrolled radical coupling between **III** and **IV** forges the novel C-C bond. Ultimately, hydrolysis of the corresponding enamine intermediate generates product **2** while restoring the organocatalyst **5a**.

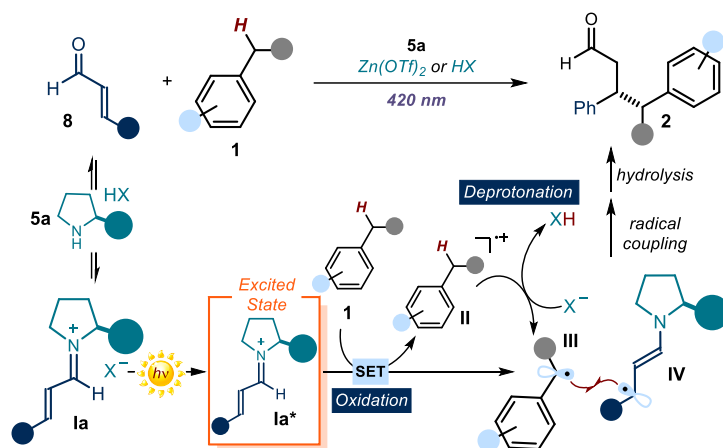
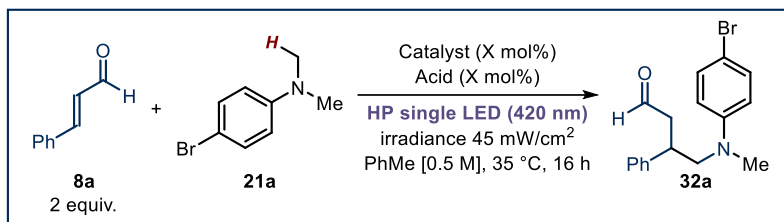


Figure 2.20: Asymmetric photocatalytic C-H functionalization of toluene and derivatives.

2.7 Attempts to Expand the Scope

We wondered whether this mode of activation could be expanded to other substrates amenable to SET oxidation and subsequent deprotonation. We first focused on anilines of type **21**, because of their low oxidation potential (for 4-bromo-*N,N*-dimethylaniline **21a**, $E(\mathbf{21a}^+/\mathbf{21a}) = +2.30$ V versus Ag/Ag^+ in CH_3CN vs SCE)⁴⁷ and the remarked acidity of the corresponding radical cation.³⁵ We started our optimization endeavors testing a benchmark photochemical reaction between cinnamaldehyde **8a** and 4-bromo-*N,N*-dimethylaniline **21a** (Table 2.6). The choice of the *para* substituent on the aryl ring was motivated by the need to avoid the tendency of unsubstituted anilines to undergo, in presence of iminium ions, Friedel-Crafts alkylation. The use of catalyst **5a** and $\text{Zn}(\text{OTf})_2$ as acid promoter proved ineffective and the desired product **32a**, which should arise from a PCET radical manifold, was not formed (entry 1). When trifluoroacetic acid was used (entry 2), **32a** was observed with promising level of chemical efficiency. However, when the enantiomeric excess was measured, we found that the product was completely racemic. Control experiments indicated that the reaction works better in the absence of either the acid co-catalyst (entry 3), the aminocatalyst (entry 4) or both of them (entry 5). Nevertheless, the reaction requires light irradiation, since a control experiment in the dark (entry 6) left the two starting materials completely untouched.

⁴⁷ Luo, P.; Feinberg, A. M.; Guirado, G.; Farid, S.; Dinnocenzo, J. P. "Accurate Oxidation Potentials of 40 Benzene and Biphenyl Derivatives with Heteroatom Substituents" *J. Org. Chem.* **2014**, *79*, 9297-9304.

Table 2.6: Preliminary results for the C-H functionalization of aniline derivatives.^a

Entry	Catalyst	Acid	Yield ^b	ee ^c
1	5a (20 mol%)	Zn(OTf) ₂ (40 mol%)	-	-
2	5a (20 mol%)	CF ₃ CO ₂ H (40 mol%)	20%	0
3	5a (20 mol%)	-	25%	0
4	-	CF ₃ CO ₂ H (40 mol%)	32%	0
5	-	-	37%	0
6 ^d	-	-	-	-

^aReaction performed on a 0.1 mmol scale. ^bYield of **32a** determined by ¹H NMR analysis of the crude mixture using trichloroethane as the internal standard. ^cEnantiomeric excess of **32a** determined by HPLC analysis on a chiral stationary phase. ^dReaction performed in the dark.

During the setup of the last two entries, we noticed that, upon simple mixing the two reagents, the color of the solution changed from colorless to light yellow. This color change is ascribable to the formation of an electron donor-acceptor (EDA) complex⁴⁸ between the electron-rich aniline **21a** and the electron-poor olefin **8a**. We believe that the visible light excitation of this aggregate could trigger the SET enabling the observed reactivity. UV-Vis analysis corroborated this hypothesis, as we detected the appearance of a new absorption band when preparing a fresh solution of **21a** and **8a**. This photochemical reactivity renders the development of an enantioselective reaction very difficult. Indeed, the EDA complex, responsible for the background reaction, absorbs light radiation until 480 nm, thus jeopardizing the selective irradiation of the chiral iminium ion **Ia**. Nonetheless, we started working on the development of a non-asymmetric variant. However, at the beginning of the optimization screening, Hsu and Sundén developed a very similar reaction involving dimethylanilines **21** and electron poor olefins.⁴⁹ Therefore, this line of research was abandoned.

Next, we decided to test whether unactivated substituted olefins of type **33a** could participate in our photochemical PCET strategy (Table 2.7). This idea was motivated by previous studies in our group demonstrating that **Ia**^{*} is able to perform SET oxidation on unactivated olefins.⁵⁰ In analogy to toluene derivatives, we envisioned

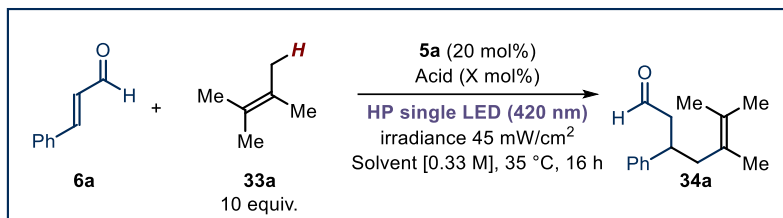
⁴⁸ (a) Mulliken, R. S. "Molecular Compounds and their Spectra. II" *J. Am. Chem. Soc.* **1952**, *74*, 811-824. (b) Crisenza, G. E. M.; Mazzarella, D.; Melchiorre, P. "Synthetic Methods Driven by the Photoactivity of Electron Donor-Acceptor Complexes" *J. Am. Chem. Soc.* **2020**, *142*, 5461-5476.

⁴⁹ Hsu, C.-W.; Sundén, H. "α-Aminoalkyl Radical Addition to Maleimides via Electron Donor-Acceptor Complexes" *Org. Lett.* **2018**, *20*, 2051-2054.

⁵⁰ Bonilla, P.; Rey, Y. P.; Holden, C. M.; Melchiorre, P. "Photo-Organocatalytic Enantioselective Radical Cascade Reactions of Unactivated Olefins" *Angew. Chem. Int. Ed.* **2018**, *57*, 12819-12823.

that oxidation of **33a** would afford an acidic radical cation that, upon deprotonation, would deliver an allylic radical intermediate. We started the optimization process by evaluating the reaction between 2,3-dimethyl-2-butene **33a** and cinnamaldehyde **8a**, in the presence of catalyst **5a**, an acid promoter and under light irradiation at 420 nm (Table 2.7).

Table 2.7: Preliminary results for the C-H functionalization of olefin derivatives.^a



Entry	Solvent	Acid	Yield ^b	ee
1	benzene	CF ₃ CO ₂ H (40 mol%)	-	-
2	CH ₃ CN	CF ₃ CO ₂ H (40 mol%)	-	-
3	C ₂ H ₄ Cl ₂	CF ₃ CO ₂ H (40 mol%)	traces	n.d.
4	C ₂ H ₄ Cl ₂	CF ₃ CO ₂ H (100 mol%)	7%	n.d.
5	C ₂ H ₄ Cl ₂	Zn(OTf) ₂ (40 mol%)	10%	n.d.
6	C ₂ H ₄ Cl ₂	Zn(OTf) ₂ (40 mol%)	11%	n.d.

^aReaction performed on a 0.1 mmol scale. ^bYield of **34a** determined by ¹H NMR analysis of the crude mixture using trichloroethane as the internal standard.

When either benzene (entry 1) or acetonitrile (entry 2) were employed as solvents and trifluoroacetic acid as acid additive, no product was observed. The use of chlorinated solvents, such as dichloroethane (entry 3), was beneficial for the reactivity, as compound **34a** was obtained, although in traces amount. Increasing the loading of the co-catalyst (entry 4) afforded the product in 7% yield, while the use of zinc(II) trifluoromethanesulfonate (entry 5) slightly increased the reaction efficiency. Increasing the reaction time to 48 hours (entry 6) was unsuccessful. Unfortunately, additional screening of acid co-catalysts, solvents, additives, and other standard reaction parameters, including light intensity, temperature and stoichiometry, did not lead to any improvement in the reaction outcome.

2.8 Conclusions

Our studies led to the development of the first organocatalytic strategy for the enantioselective C-H functionalization of toluene derivatives, selectively at their benzylic position. In particular, we demonstrated that the synergistic effect of the oxidizing properties of photoexcited chiral iminium ions and the basic character of their counteranions can be exploited to promote a sequential multisite PCET reaction. We employed this activation mode to drive the β -benzylation of enals, by employing unfunctionalized toluene derivatives. This photochemical process is operationally simple, conducted at ambient temperature with commercially available substrates, and using a 420 nm high power LED as the light source.

2.9 Experimental Section

2.9.1 General information

The NMR spectra and HPLC/UPC² traces are available in the published manuscript¹ and are not reported in the present dissertation.

The NMR spectra were recorded at 400 MHz and 500 MHz for ¹H, at 101 MHz and 125.8 MHz for ¹³C, at 376 MHz for ¹⁹F and at 47 MHz for ¹¹B. The chemical shifts (δ) for ¹H and ¹³C are given in ppm relative to residual signals of the solvents (CHCl₃ @ 7.26 ppm ¹H NMR, 77.00 ppm ¹³C NMR). Coupling constants are given in Hz and are quoted to the nearest 0.5 Hz. The following abbreviations are used to indicate the multiplicity: s, singlet; d, doublet; t, triplet; q, quartet; p, pentet; m, multiplet; br s, broad signal; app t, apparent triplet.

High-resolution mass spectra (HRMS) were obtained from the ICIQ High Resolution Mass Spectrometry Unit on MicroTOF Focus and Maxis Impact (Bruker Daltonics) with electrospray ionization. Optical rotations were measured on a Polarimeter Jasco P-1030 and are reported as follows: $[\alpha]_D$ ambient temperature (c in g per 100 mL, solvent).

General Procedures. All reactions were set up under an argon atmosphere in oven-dried glassware using standard Schlenk techniques, unless otherwise stated. Synthesis grade solvents were used as purchased. Anhydrous solvents were taken from a commercial SPS solvent dispenser. Chromatographic purification of products was accomplished using force-flow chromatography (FC) on silica gel (35-70 mesh). For thin layer chromatography (TLC) analysis throughout this work, Merck precoated TLC plates (silica gel 60 GF₂₅₄, 0.25 mm) were used, using UV light as the visualizing agent and either phosphomolybdic acid in EtOH or basic aqueous potassium permanganate (KMnO₄), and heat as developing agents. Organic solutions were concentrated under reduced pressure on a Büchi rotary evaporator (in vacuo at 40 °C, ~5 mbar).

Determination of Diastereomeric Ratio. The diastereomeric ratio was determined by ¹H NMR analysis of the crude reaction mixture through integration of diagnostic signals.

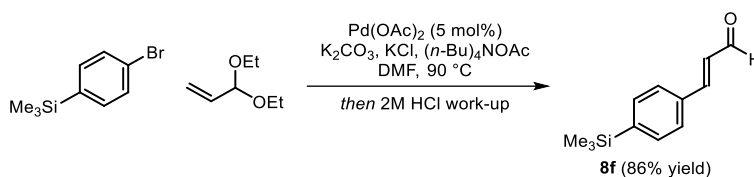
Determination of Enantiomeric Purity. HPLC analysis on chiral stationary phase was performed on an Agilent 1200 series HPLC, using a Daicel Chiralpak IC-3 column with *i*-PrOH:hexane as the eluent. UPC² analysis on chiral stationary phase was performed on a Waters Acquity instrument using a CEL1, ID3 or IE3 chiral columns. The exact conditions for the analyses are specified within the characterization section. HPLC/UPC² traces were compared to racemic samples prepared by running the reactions in the presence of a catalytic amount (20 mol%) of racemic catalyst **5a**. This was prepared by mixing equimolar amounts of amine catalysts **5a** and its enantiomer *ent*-**5a**, both synthesized according to literature procedures.^{10,22}

Materials: Commercial grade reagents and solvents were purchased at the highest commercial quality from Sigma Aldrich, Fluka, Acros Organics, Tokyo Chemical Industry, Fluorochem or Alfa Aesar and used as received, unless otherwise stated. Organic catalysts **5a** and *ent*-**5a** were synthesized according to previously reported

procedures.^{10,22} The majority of enals **8** and toluene derivatives are commercially available. Cinnamaldehyde **8a** was distilled prior to use. Enals **8d** and **8e** were prepared according to the literature procedure,²² whereas the synthetic procedures for compounds **8f**, **8g**, **28** and for the benzylic derivatives employed in the synthesis of products **2m**, **2q** and **2r** are here described.

2.9.2 Substrate synthesis

Synthesis of (*E*)-3-(4-(trimethylsilyl)phenyl)acrylaldehyde (**8f**):

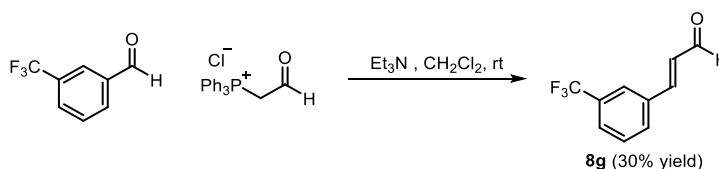


Compound **8f** was prepared according to a reported literature procedure.²² An oven-dried two-necked flask, fitted with a condenser, was charged with Pd(OAc)₂ (29.0 mg, 131 μmol), K₂CO₃ (905 mg, 6.54 mmol), KCl (325 mg, 4.36 mmol), (*n*-Bu)₄NOAc (2.63 g, 8.73 mmol), (4-bromophenyl)trimethylsilane (853 μL, 4.36 mmol) and 3,3-diethoxyprop-1-ene (2.00 mL, 13.1 mmol) in anhydrous DMF (45 mL). The resulting mixture was heated to 90 °C and stirred for 18 hours. The reaction was allowed to cool to room temperature and quenched by dropwise addition of 2M *aq.* HCl solution (30 mL). The resulting mixture was stirred at room temperature for further 15 minutes. Water (100 mL) was added and the crude mixture was extracted with Et₂O (3 x 150 mL). The organic phase were collected, dried over Na₂SO₄, filtered and concentrated *in vacuo*. Purification of the crude material by column chromatography on silica gel (gradient from 5% EtOAc in hexane to 10% EtOAc in hexane) gave product **8f** (766 mg, 86% yield) as an off-white solid.

¹H NMR (400 MHz, CDCl₃): δ 9.73 (d, *J* = 7.5 Hz, 1H), 7.65 – 7.43 (m, 5H), 6.76 (dd, *J* = 16.0, 7.5 Hz, 1H), 0.31 (s, 9H).

¹³C NMR (101 MHz, CDCl₃): δ 193.8, 152.9, 145.2, 134.2, 134.0, 128.7, 127.6, -1.3.

Synthesis of (*E*)-3-(3-(trifluoromethyl)phenyl)acrylaldehyde (**8g**):



Compound **8g** was prepared according to a reported literature procedure.²² To a solution of (formylmethyl)triphenylphosphonium chloride (3.55 g, 10.4 mmol) in anhydrous CH₂Cl₂ (50 mL) was added Et₃N (2.18 mL, 15.6 mmol) and, successively, 3-(trifluoromethyl)benzaldehyde (1.39 mL, 10.4 mmol) dropwise. The reaction was stirred for 48 hours at room temperature and, then, concentrated under reduced pressure. Purification of the crude material by column chromatography on silica gel (gradient from 5% EtOAc in hexane to 10% EtOAc in hexane) gave product **8g** (630 mg,

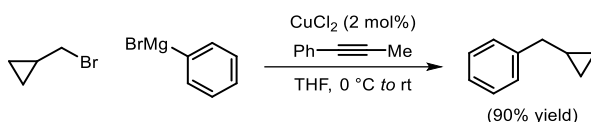
30% yield) as a yellow oil. The spectroscopic properties of this compound were consistent with the data available in the literature.⁵¹

¹H NMR (400 MHz, CDCl₃): δ 9.77 (d, *J* = 7.5 Hz, 1H), 7.83 (br. s, 1H), 7.78 (d, *J* = 7.5 Hz, 1H), 7.72 (d, *J* = 7.5 Hz, 1H), 7.60 (dd, *J* = 7.5 Hz, 1H), 7.53 (d, *J* = 16.0 Hz, 1H), 6.80 (dd, *J* = 16.0, 7.5 Hz, 1H).

¹³C NMR (101 MHz, CDCl₃): δ 193.1, 150.3, 134.8, 131.8 (q, ²*J*_{C-F} = 33.0 Hz), 131.2 (q, ⁴*J*_{C-F} = 1.5 Hz), 130.0, 129.7, 127.6 (q, ³*J*_{C-F} = 3.5 Hz), 125.2 (q, ³*J*_{C-F} = 4.0 Hz), 123.6 (q, ¹*J*_{C-F} = 272.5 Hz).

¹⁹F NMR (376 MHz, CDCl₃): δ -63.09 (s, 3F).

Synthesis of (cyclopropylmethyl)benzene:

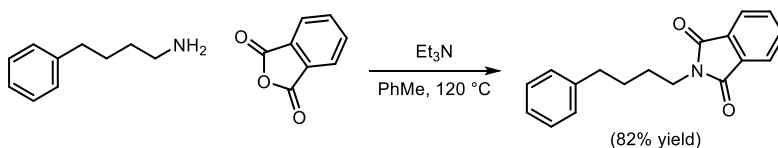


This compound was prepared according to a reported literature procedure.⁵² To a mixture of (bromomethyl)cyclopropane (1.94 mL, 20.0 mmol), CuCl₂ (54.0 mg, 0.40 mmol) and 1-phenyl-1-propyne (0.25 mL, 2.00 mmol) in anhydrous THF (25 mL) at 0 °C was added a 3M solution of phenylmagnesium bromide (10.0 mL, 30.0 mmol) in Et₂O. The mixture was stirred at 0 °C for 20 minutes, then, warmed up to room temperature and stirred overnight. The reaction was quenched by slow addition of 1M aq. HCl solution (25 mL) and sat. aq. NH₄Cl solution (25 mL). The resulting mixture was extracted with Et₂O (3 x 100 mL). The organic phase were collected, dried over Na₂SO₄ and the solvent was removed under reduced pressure to deliver the crude material. Purification by column chromatography on silica gel (hexane) provided the desired coupling product (2.38 g, 90% yield) as a colorless liquid. The spectroscopic properties of this compound were consistent with the data available in the literature.⁵³

¹H NMR (400 MHz, CDCl₃): δ 7.42 – 7.31 (m, 4H), 7.32 – 7.23 (m, 1H), 2.63 (d, *J* = 7.0 Hz, 2H), 1.14 – 1.01 (m, 1H), 0.63 – 0.58 (m, 2H), 0.38 – 0.21 (m, 2H).

¹³C NMR (101 MHz, CDCl₃): δ 142.2, 128.4, 128.3, 125.9, 40.4, 11.9, 4.7.

Synthesis of 2-(4-phenylbutyl)isoindoline-1,3-dione:



⁵¹ He, M.; Bode, J. W. "Catalytic Synthesis of γ -Lactams via Direct Annulations of Enals and N-Sulfonylimines" *Org. Lett.* **2005**, *7*, 3131-3134.

⁵² Terao, J.; Todo, H.; Begum, S. A.; Kuniyasu, H.; Kambe, N. "Copper-Catalyzed Cross-Coupling Reaction of Grignard Reagents with Primary-Alkyl Halides: Remarkable Effect of 1-Phenylpropyne" *Angew. Chem. Int. Ed.* **2007**, *46*, 2086-2089.

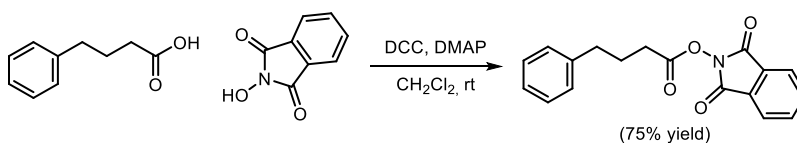
⁵³ Kumar, G. G. K. S. N.; Laali, K. K. "Facile coupling of propargylic, allylic and benzylic alcohols with allylsilane and alkenylsilane, and their deoxygenation with Et₃SiH, catalyzed by Bi(OTf)₃ in [BMIM][BF₄] ionic liquid (IL), with recycling and reuse of the IL" *Org. Biomol. Chem.* **2012**, *10*, 7347-7355.

A solution of 4-phenylbutylamine (0.79 mL, 5.00 mmol), phthalic anhydride (741 mg, 5.00 mmol) and triethylamine (2.79 mL, 20.0 mmol) in toluene (50 mL) was refluxed (120 °C) with a Dean–Stark apparatus for 16 hours. The reaction mixture was allowed to cool down to room temperature and concentrated under reduced pressure. The residue was re-dissolved in EtOAc (50 mL) and washed, first, with *sat. aq.* NaHCO₃ solution (2 x 25 mL) and, then, with water (25 mL). The organic phase were combined, dried over Na₂SO₄ and the solvent was removed *in vacuo*. Purification by column chromatography on silica gel support (*gradient from hexane to 20% EtOAc in hexane*) gave the desired amide (1.14 g, 82% yield) as a white solid. The spectroscopic properties of this compound were consistent with the data available in the literature.⁵⁴

¹H NMR (400 MHz, CDCl₃): δ 7.86 (dd, *J* = 5.5, 3.0 Hz, 2H), 7.72 (dd, *J* = 5.5, 3.0 Hz, 2H), 7.35 – 7.24 (m, 2H), 7.23 – 7.13 (m, 3H), 3.74 (t, *J* = 7.0 Hz, 2H), 2.68 (t, *J* = 7.5 Hz, 2H), 1.82 – 1.62 (m, 4H).

¹³C NMR (101 MHz, CDCl₃): δ 168.4, 142.0, 133.9, 132.2, 128.4, 128.3, 125.8, 123.2, 37.8, 35.4, 28.6, 28.2.

Synthesis of 1,3-dioxoisindolin-2-yl 4-phenylbutanoate:



This compound was prepared according to a reported literature procedure.⁵⁵ To a stirring solution of 4-phenylbutirric acid (1.07 g, 6.50 mmol), *N*-hydroxyphthalimide (1.17 g, 7.15 mmol) and DMAP (79.0 mg, 0.65 mmol) in CH₂Cl₂ (30 mL) was added DCC (1.48 g, 7.15 mmol). The reaction was stirred at room temperature for 6 hours and then placed in a freezer at -20 °C for 2 hours observing the precipitation of the urea by-product, which was filtered and rinsed with cold Et₂O. The filtrate was concentrated under reduced pressure to provide the crude material. Purification by column chromatography on silica gel (*gradient from hexane to 20% EtOAc in hexane*) gave the desired ester (1.50 g, 75% yield) as a white solid.

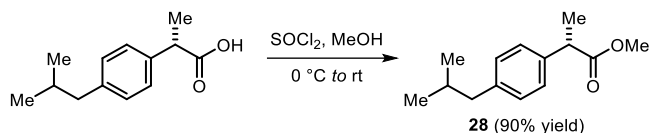
¹H NMR (400 MHz, CDCl₃): δ 7.96 – 7.87 (m, 2H), 7.86 – 7.77 (m, 2H), 7.37 – 7.30 (m, 2H), 7.31 – 7.20 (m, 3H), 2.80 (t, *J* = 7.5 Hz, 2H), 2.70 (t, *J* = 7.5 Hz, 2H), 2.14 (tt, *J* = 7.5 Hz, 2H).

¹³C NMR (101 MHz, CDCl₃): δ 169.4, 162.0, 140.7, 134.8, 129.0, 128.6, 128.5, 126.2, 124.0, 34.6, 30.2, 26.3.

⁵⁴ Li, X.; Che, X.; Chen, G.-H.; Zhang, J.; Yan, J.-L.; Zhang, Y.-F.; Zhang, L.-S.; Hsu, C.-P.; Gao, Y. Q.; Shi, Z.-J. "Direct Oxidation of Aliphatic C–H Bonds in Amino-Containing Molecules under Transition-Metal-Free Conditions" *Org. Lett.* **2016**, *18*, 1234-1237.

⁵⁵ Huang, L.; Olivares, A. M.; Weix, D. J. "Reductive Decarboxylative Alkynylation of *N*-Hydroxyphthalimide Esters with Bromoalkynes" *Angew. Chem. Int. Ed.* **2017**, *56*, 11901-11905.

Synthesis of methyl (*S*)-2-(4-isobutylphenyl)propanoate (**28**):

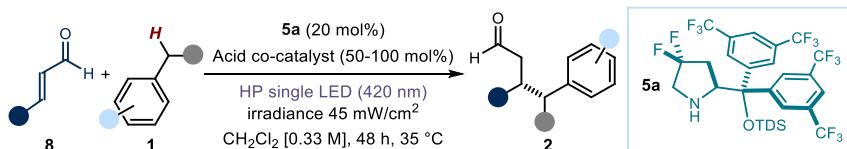


This compound was prepared according to a reported literature procedure.⁵⁶ To a solution of (*S*)-2-(4-isobutylphenyl)propanoic acid (0.775 g, 5.00 mmol) in MeOH (50 mL) at 0 °C was added dropwise thionyl chloride (2.4 g, 20.0 mmol). Completed the addition, the reaction was warmed to room temperature and stirred overnight. The solvent was removed under reduced pressure and the resulting residue was purified by column chromatography on silica gel (*gradient from hexane to 10% Et₂O in hexane*) to give ester **3** (0.828 g, 90% yield) as a colorless liquid. The spectroscopic properties of this compound were consistent with the data available in the literature.⁵⁶ $[\alpha]_D^{26} = +69.4$ ($c = 0.95$, CHCl₃); Lit: $[\alpha]_D^{26} = +64.6$ ($c = 1.00$, CHCl₃, for (*S*)-enantiomer).⁵⁷

¹H NMR (400 MHz, CDCl₃): δ 7.19 (d, $J = 8.0$ Hz, 2H), 7.09 (d, $J = 8.0$ Hz, 2H), 3.70 (q, $J = 7.0$ Hz, 1H), 3.66 (s, 3H), 2.44 (d, $J = 7.0$ Hz, 2H), 1.85 (dp, $J = 13.6, 7.0$ Hz, 1H), 1.49 (d, $J = 7.0$ Hz, 3H), 0.90 (d, $J = 7.0$ Hz, 6H);

¹³C NMR (101 MHz, CDCl₃): δ 175.4, 140.7, 137.9, 129.5, 127.3, 52.1, 45.2, 31.9, 30.3, 22.5, 18.8.

2.9.3 General procedure for the photochemical C-H functionalization of toluene and derivatives



General Procedure: A 15 mL Schlenk tube was charged with a mixture of amine catalyst **5a** (0.02 mmol, 20 mol%, 14 mg), acid co-catalyst (0.05-0.1 mmol, depending on the substrate) and enal **8** (0.1 mmol, 1 equiv.) in CH₂Cl₂ (300 μL). The corresponding toluene derivative **1** (1 mmol, 10 equiv.) was added to the reaction vessel. This was placed under an atmosphere of argon, cooled to -78 °C, degassed *via* vacuum evacuation (5 minutes), backfilled with argon and, ultimately, warmed to room temperature. The freeze-pump-thaw cycle was repeated four times, and then the Schlenk tube was sealed with Parafilm and placed into a 3D-printed plastic support mounted on an aluminum block fitted with a 420 nm high-power single LED ($\lambda = 420$ nm, irradiance = 45 mW/cm², as controlled by an external power supply; the setup is detailed in Figure 2.14). This setup secured a reliable irradiation while keeping a

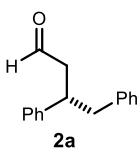
⁵⁶ Jiang, M. Y.; Dolphin, D. "Site-Specific Prodrug Release Using Visible Light" *J. Am. Chem. Soc.* **2008**, *130*, 4236-4237.

⁵⁷ Piccolo, O.; Spreafico, F.; Visentin, G.; Valoti, E. "Zinc salt catalyzed rearrangement of acetals of optically active aryl 1-chloroethyl ketones: synthesis of optically active 2-arylpropionic acids and esters" *J. Org. Chem.* **1987**, *52*, 10-14.

distance of 1 cm between the reaction vessel and the light source. The reaction was stirred at ambient temperature for 48 hours. The solvent was removed *in vacuo* and the crude mixture was purified by column chromatography on silica gel to give the corresponding product **2** in the stated yield and enantiomeric purity. If not otherwise stated, full consumption of the limiting enal (**8**) was observed by ¹H NMR analysis on the crude mixture at the end of the reaction.

In the case of the reactions delivering products **20-v** and **29**, it was possible to fully recover the unreacted starting material (~90% recovered yield), as the first eluting compound, after purification procedure via flash column chromatography.

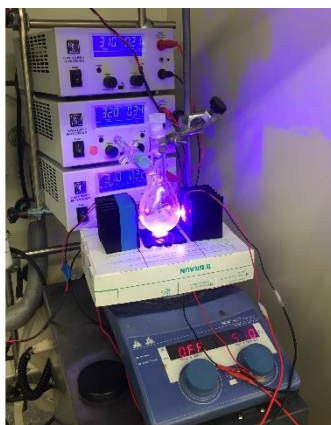
Characterization of Products **2**



(S)-3,4-diphenylbutanal (2a). Prepared according to the general procedure using enal **8a** (13.2 mg, 0.1 mmol), aminocatalyst **5a** (14.1 mg, 20 mol%), toluene (92.0 mg, 1 mmol), zinc(II) triflate (18.2 mg, 50 mol%) and dichloromethane (300 μ L). The crude mixture was purified by flash column chromatography (hexane/diethyl ether 92:8) to afford product **2a** (14.6 mg, 63% yield, 83% ee, average of two runs) as a colorless oil that displayed spectroscopic data consistent with those reported previously.¹⁰ The enantiomeric excess was determined to be 83% by HPLC analysis on a Daicel Chiralpak IC-3 column: 90:10 hexane/*i*-PrOH, flow rate 0.6 mL/min, $\lambda = 215$ nm: $\tau_{major} = 12.4$ min, $\tau_{minor} = 13.5$ min. $[\alpha]_D^{26} = -47.5$ ($c = 0.44$, CHCl₃, 83% ee); Lit: $[\alpha]_D^{26} = -45.8$ ($c = 0.49$, CHCl₃, 88% ee for (*S*)-enantiomer).¹⁰ The absolute configuration for compound **2a** was determined in comparison to the data available in the literature.¹⁰ Accordingly, the absolute configuration for all of the products **2** was assigned likewise.

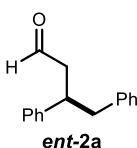
¹H NMR (500 MHz, CDCl₃): δ 9.59 (t, $J = 2.0$ Hz, 1H), 7.31 – 7.14 (m, 8H), 7.08 – 7.04 (app d, $J = 5.0$ Hz, 2H), 3.49 (p, $J = 7.5$ Hz, 1H), 2.96 (dd, $J = 13.5, 7.1$ Hz, 1H), 2.88 (dd, $J = 13.5, 7.9$ Hz, 1H), 2.81 – 2.70 (m, 2H);

¹³C NMR (125.8 MHz, CDCl₃): δ 201.7, 143.4, 139.4, 129.3, 128.7, 128.5, 127.7, 126.9, 126.5, 49.1, 43.5, 42.2.

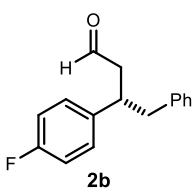


1 mmol scale reaction. The model reaction was repeated on a more synthetically useful scale using three high power single LEDs and a 50 mL round-bottom Schlenk flask to increase the surface-area-to-volume ratio, which secured

a more efficient irradiation of the reaction mixture (see pictures to the left). To a 50 mL round-bottom Schlenk flask containing aminocatalyst **5a** (0.2 mmol, 20 mol%, 141 mg), zinc(II) triflate (0.5 mmol, 181 mg) and **8a** (1 mmol, 1 equiv., 132 mg) in dichloromethane (3 mL) was added toluene (10 mmol, 921 mg). The reaction vessel was placed under an atmosphere of argon, cooled to $-78\text{ }^{\circ}\text{C}$, degassed via vacuum evacuation (5 min), backfilled with argon and, ultimately, warmed to room temperature. The freeze-pump-thaw cycle was repeated five times, and then three 420 nm high-power single LEDs ($\lambda = 420\text{ nm}$, irradiance = 45 mW/cm^2 , as controlled by an external power supply) were placed at 1 cm distance from the sides and the bottom of the Schlenk flask. The reaction was stirred under visible light irradiation at ambient temperature ($\sim 35\text{ }^{\circ}\text{C}$) for 60 hours. The solvent was removed under reduced pressure and the crude mixture was purified by column chromatography on silica gel (hexane/diethyl ether 92:8) to afford product **2a** as a pale yellow oil (111 mg, 51% yield, 83% ee).



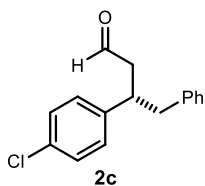
(R)-3,4-diphenylbutanal (ent-2a). Prepared according to the general procedure using enal **8a** (13.2 mg, 0.1 mmol), aminocatalyst **ent-5a** (14.1 mg, 20 mol%), toluene (92.0 mg, 1 mmol), zinc(II) triflate (18.2 mg, 50 mol%) and dichloromethane (300 μL). The crude mixture was purified by flash column chromatography (hexane/diethyl ether 92:8) to afford product **ent-2a** (14.6 mg, 63% yield, 82% ee, average of two runs) as a colorless oil that displayed spectroscopic data consistent with those reported previously.¹⁰ The enantiomeric excess was determined to be 82% by HPLC analysis on a Daicel Chiralpak IC-3 column: 90:10 hexane/*i*-PrOH, flow rate 0.6 mL/min, $\lambda = 215\text{ nm}$: $\tau_{\text{major}} = 13.5\text{ min}$, $\tau_{\text{minor}} = 12.4\text{ min}$. $[\alpha]_{\text{D}}^{26} = +55.3$ ($c = 0.067$, CHCl_3 , 82% ee).



(S)-3-(4-fluorophenyl)-4-phenylbutanal (2b). Prepared according to the general procedure using enal **8b** (15.0 mg, 0.1 mmol), aminocatalyst **5a** (14.1 mg, 20 mol%), toluene (92.0 mg, 1 mmol), zinc(II) triflate (18.2 mg, 50 mol%) and dichloromethane (300 μL). The crude mixture was purified by flash column chromatography (hexane/diethyl ether 92:8) to afford product **2b** (17.0 mg, 70% yield, 80% ee, average of two runs) as a colorless oil that displayed spectroscopic data consistent with those reported previously.¹⁰ The enantiomeric excess was determined to be 80% by UPC² analysis on a Daicel Chiralpak ID-3 column: gradient CO_2/MeCN from 100% CO_2 to 60:40 over 4 minutes, curve 6, flow rate 3 mL/min, $\lambda = 275\text{ nm}$: $\tau_{\text{major}} = 2.49\text{ min}$, $\tau_{\text{minor}} = 2.57\text{ min}$. $[\alpha]_{\text{D}}^{26} = -38.4$ ($c = 0.71$, CHCl_3 , 80% ee); Lit: $[\alpha]_{\text{D}}^{26} = -45.3$ ($c = 0.69$, CHCl_3 , 85% ee for (*S*)-enantiomer).¹⁰

¹H NMR (500 MHz, CDCl_3): δ 9.61 (t, $J = 2.0\text{ Hz}$, 1H), 7.25 – 7.21 (m, 2H), 7.20 – 7.15 (m, 1H), 7.12 – 7.07 (m, 2H), 7.04 – 7.01 (m, 2H), 6.96 (t, $J = 9.0\text{ Hz}$, 2H), 3.49 (p, $J = 7.5\text{ Hz}$, 1H), 2.89 (d, $J = 7.5\text{ Hz}$, 2H), 2.75 (dd, $J = 7.5, 2.0\text{ Hz}$, 2H);

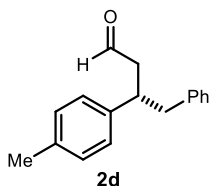
¹³C NMR (125.8 MHz, CDCl_3): δ 201.7, 161.7 (d, $^1J_{\text{C-F}} = 245.0\text{ Hz}$), 139.1, 139.0 (d, $^4J_{\text{C-F}} = 3.0\text{ Hz}$), 129.3, 129.1 (d, $^3J_{\text{C-F}} = 8.0\text{ Hz}$), 128.5, 126.6, 115.5 (d, $^2J_{\text{C-F}} = 21.0\text{ Hz}$), 49.3, 43.5, 41.3.



(S)-3-(4-Chlorophenyl)-4-phenylbutanal (2c). Prepared according to the general procedure using enal **8c** (16.7 mg, 0.1 mmol), aminocatalyst **5a** (14.1 mg, 20 mol%), toluene (92.0 mg, 1 mmol), zinc(II) triflate (18.2 mg, 50 mol%) and dichloromethane (300 μ L). The crude mixture was purified by flash column chromatography (hexane/diethyl ether 92:8) to afford product **2c** (15.3 mg, 59% yield, 67% ee, average of two runs) as a colorless oil that displayed spectroscopic data consistent with those reported previously.¹⁰ The enantiomeric excess was determined to be 67% by UPC² analysis on a Daicel Chiralpak IE-3 column: gradient CO₂/MeCN from 100% CO₂ to 60:40 over 4 minutes, curve 6, flow rate 3 mL/min, $\lambda = 220$ nm: $\tau_{\text{major}} = 4.2$ min, $\tau_{\text{minor}} = 4.41$ min. $[\alpha]_{\text{D}}^{26} = -46.5$ ($c = 0.49$, CHCl₃, 67% ee); Lit: $[\alpha]_{\text{D}}^{26} = -56.8$ ($c = 0.69$, CHCl₃, 86% ee for (S)-enantiomer).¹⁰

¹H NMR (400 MHz, CDCl₃): δ 9.61 (t, $J = 2.0$ Hz, 1H), 7.32 – 7.11 (m, 5H), 7.10 – 7.00 (m, 4H), 3.48 (p, $J = 7.5$ Hz, 1H), 2.89 (d, $J = 7.5$ Hz, 2H), 2.75 (dd, $J = 7.5, 2$ Hz, 2H);

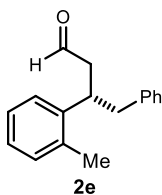
¹³C NMR (101 MHz, CDCl₃): δ 201.1, 141.8, 139.0, 132.6, 129.3, 128.9, 128.6, 126.6, 49.1, 43.3, 41.4.



(S)-4-phenyl-3-(p-tolyl)butanal (2d). Prepared according to the general procedure using enal **8d** (14.6 mg, 0.1 mmol), aminocatalyst **5a** (14.1 mg, 20 mol%), toluene (92 mg, 1 mmol), zinc(II) triflate (18.2 mg, 50 mol%) and dichloromethane (300 μ L). The crude mixture was purified by flash column chromatography (hexane/diethyl ether 92:8) to afford product **2d** (11.3 mg, 48% yield, 60% ee, average of two runs) as a colorless oil that displayed spectroscopic data consistent with those reported previously.¹⁰ The enantiomeric excess was determined to be 60% by UPC² analysis on a Daicel Chiralpak ID-3 column: gradient CO₂/MeCN from 100% CO₂ to 60:40 over 4 minutes, curve 6, flow rate 3 mL/min, $\lambda = 220$ nm: $\tau_{\text{major}} = 3.01$ min, $\tau_{\text{minor}} = 3.28$ min. $[\alpha]_{\text{D}}^{26} = -19.3$ ($c = 0.25$, CHCl₃, 60% ee); Lit: $[\alpha]_{\text{D}}^{26} = -42.5$ ($c = 0.50$, CHCl₃, 78% ee for (S)-enantiomer).¹⁰

¹H NMR (400 MHz, CDCl₃): δ 9.57 (t, $J = 2.0$ Hz, 1H), 7.28 – 7.15 (m, 3H), 7.11 – 7.02 (m, 6H), 3.45 (p, $J = 7.5$ Hz, 1H), 2.95 (dd, $J = 13.5, 7.0$ Hz, 1H), 2.85 (dd, $J = 13.5, 8.0$ Hz, 1H), 2.77 – 2.66 (m, 2H), 2.31 (s, 3H);

¹³C NMR (101 MHz, CDCl₃): δ 201.9, 140.3, 139.6, 136.4, 129.4, 128.5, 127.5, 126.5, 49.1, 43.5, 41.8, 21.2.

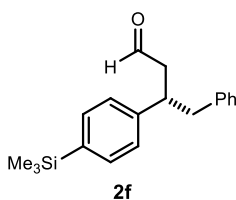


(S)-4-phenyl-3-(o-tolyl)butanal (2e). Prepared according to the general procedure using enal **8e** (14.6 mg, 0.1 mmol), aminocatalyst **5a** (14.1 mg, 20 mol%), toluene (92 mg, 1 mmol), zinc(II) triflate (18.2 mg, 50 mol%) and dichloromethane (300 μ L). The crude mixture was purified by flash column chromatography (hexane/diethyl ether 92:8) to afford product **2e** (11.5 mg, 48% yield, 72% ee, average of two runs) as a colorless oil that displayed spectroscopic data consistent with those reported

previously.¹⁰ The enantiomeric excess was determined to be 72% by UPC² analysis on a Daicel Chiralpak IE-3 column: gradient CO₂/MeCN from 100% CO₂ to 60:40 over 4 minutes, curve 6, flow rate 3 mL/min, $\lambda = 220$ nm: $\tau_{\text{major}} = 3.58$ min, $\tau_{\text{minor}} = 3.75$ min. $[\alpha]_{\text{D}}^{26} = -26.4$ ($c = 0.37$, CHCl₃, 72% ee).

¹H NMR (400 MHz, CDCl₃): δ 9.56 (t, $J = 2.0$ Hz, 1H), 7.25 – 7.14 (m, 5H), 7.12 – 7.07 (m, 2H), 7.04 (d, $J = 8.0$ Hz, 2H) 3.76 (p, $J = 7.5$ Hz, 1H), 2.91 (dd, $J = 13.5, 7.0$ Hz, 1H), 2.85 – 2.70 (m, 3H), 2.21 (s, 3H);

¹³C NMR (101 MHz, CDCl₃): δ 201.7, 141.6, 139.5, 136.0, 130.6, 129.3, 128.4, 126.51, 126.0, 49.0, 43.2, 36.9, 19.7.



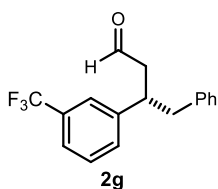
(S)-4-phenyl-3-(4-(trimethylsilyl)phenyl)butanal (2f).

Prepared according to the general procedure using enal **8f** (20.4 mg, 0.1 mmol), aminocatalyst **5a** (14.1 mg, 20 mol%), toluene (92 mg, 1 mmol), zinc(II) triflate (18.2 mg, 50 mol%) and dichloromethane (300 μ L). The crude mixture was purified by flash column chromatography (hexane/diethyl ether 92:8) to afford product **2f** (14.8 mg, 50% yield, 70% ee, average of two runs) as an off-white solid. The enantiomeric excess was determined to be 70% by UPC² analysis on a Daicel Chiralpak IE-3 column: gradient CO₂/MeCN from 100% CO₂ to 60:40 over 4 minutes, curve 6, flow rate 2 mL/min, $\lambda = 210$ nm: $\tau_{\text{major}} = 3.97$ min, $\tau_{\text{minor}} = 4.79$ min. $[\alpha]_{\text{D}}^{26} = -19.8$ ($c = 0.14$, CHCl₃, 70% ee).

¹H NMR (400 MHz, CDCl₃): δ 9.59 (t, $J = 2.0$ Hz, 1H), 7.47 (d, $J = 8.0$ Hz, 2H), 7.31 – 7.25 (m, 2H), 7.24 – 7.18 (m, 3H), 7.15 – 7.10 (m, 2H), 3.51 (tt, $J = 8.5, 6.5$ Hz, 1H), 3.03 (dd, $J = 13.5, 6.5$ Hz, 1H), 2.88 (dd, $J = 13.5, 8.5$ Hz, 1H), 2.82 – 2.69 (m, 2H), 0.28 (s, 9H).

¹³C NMR (101 MHz, CDCl₃): δ 201.6, 143.9, 139.3, 138.7, 133.7, 129.2, 128.4, 126.9, 126.4, 48.7, 43.2, 41.9, -1.10.

HRMS (ESI) Exact mass calculated for C₁₉H₂₄NaOSi [M+Na]⁺: 319.1489, found: 319.1488.



(S)-4-phenyl-3-(3-(trifluoromethyl)phenyl)butanal (2g).

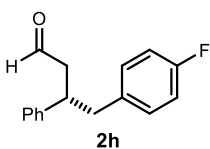
Prepared according to the general procedure using enal **8g** (20.0 mg, 0.1 mmol), aminocatalyst **5a** (14.1 mg, 20 mol%), toluene (92 mg, 1 mmol), zinc(II) triflate (18.2 mg, 50 mol%) and dichloromethane (300 μ L). The crude mixture was purified by flash column chromatography (hexane/diethyl ether 92:8) to afford product **2g** (9.6 mg, 33% yield, 84% ee, average of two runs) as a pale yellow oil. The enantiomeric excess was determined, upon sodium borohydride reduction of the isolated aldehyde to afford the corresponding alcohol, to be 84% by UPC² analysis on a Daicel Chiralpak IE-3 column: gradient CO₂/MeOH from 100% CO₂ to 80:20 over 4 minutes, curve 6, flow rate 2 mL/min, $\lambda = 215$ nm: $\tau_{\text{major}} = 3.97$ min, $\tau_{\text{minor}} = 4.06$ min. $[\alpha]_{\text{D}}^{26} = -25.8$ ($c = 0.21$, CHCl₃, 84% ee).

¹H NMR (400 MHz, CDCl₃): δ 9.64 (t, $J = 1.5$ Hz, 1H), 7.48 (d, $J = 7.5$ Hz, 1H), 7.44 – 7.37 (m, 2H), 7.34 (d, $J = 8.0$ Hz, 1H), 7.28 – 7.17 (m, 3H), 7.07 – 7.01 (m, 2H), 3.60 (tt, $J = 7.5$ Hz, 1H), 2.94 (d, $J = 7.5$ Hz, 2H), 2.83 (dd, $J = 7.5, 1.5$ Hz, 2H).

$^{13}\text{C NMR}$ (101 MHz, CDCl_3): δ 200.5, 144.3, 138.6, 131.13 (q, $^4J_{\text{C-F}} = 1.0$ Hz), 130.9 (q, $^2J_{\text{C-F}} = 32.0$ Hz), 129.2, 129.0, 128.4, 126.6, 124.2 (q, $^3J_{\text{C-F}} = 4.0$ Hz), 124.1 (q, $^1J_{\text{C-F}} = 272.5$ Hz), 123.6 (q, $^3J_{\text{C-F}} = 4.0$ Hz), 48.7, 43.0, 41.6.

$^{19}\text{F NMR}$ (376 MHz, CDCl_3): δ -62.70 (s, 3F).

HRMS (ESI) Exact mass calculated for $\text{C}_{18}\text{H}_{19}\text{F}_3\text{NaO}_2$ [$\text{M}+\text{CH}_3\text{OH}+\text{Na}$] $^+$: 347.1229, found: 347.1245.



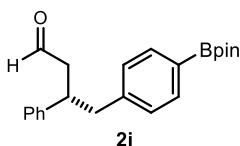
(S)-4-(4-fluorophenyl)-3-phenylbutanal (2h). Prepared according to the general procedure using enal **8a** (13.2 mg, 0.1 mmol), aminocatalyst **5a** (14.1 mg, 20 mol%), 4-fluorotoluene (110 mg, 1 mmol), zinc(II) triflate (18.2 mg, 50 mol%) and dichloromethane (300 μL). The crude mixture was purified by

flash column chromatography (hexane/diethyl ether 92:8) to afford product **2h** (16.2 mg, 67% yield, 80% ee, average of two runs) as a pale yellow oil that displayed spectroscopic data consistent with those reported previously.¹⁰ The enantiomeric excess was determined, upon sodium borohydride reduction of the isolated aldehyde to afford the corresponding alcohol, to be 80% by HPLC analysis on a Daicel Chiralpak IC-3 column: 90:10 hexane/*i*-PrOH, flow rate 0.5 mL/min, $\lambda = 215$ nm. $\tau_{\text{Major}} = 16.0$ min, $\tau_{\text{minor}} = 15.1$ min. $[\alpha]_{\text{D}}^{26} = -49.1$ ($c = 0.18$, CHCl_3); Lit: $[\alpha]_{\text{D}}^{26} = -46.0$ ($c = 0.63$, CHCl_3 , 92% ee for (S)-enantiomer).¹⁰

$^1\text{H NMR}$ (400 MHz, CDCl_3): δ 9.65 (t, $J = 2.0$ Hz, 1H), 7.33 – 7.26 (m, 2H), 7.26 – 7.19 (m, 1H), 7.18 – 7.11 (m, 2H), 7.03 – 6.96 (m, 2H), 6.96 – 6.88 (m, 2H), 3.47 (tt, $J = 7.5$ Hz, 1H), 2.92 (d, $J = 7.5$ Hz, 2H), 2.85 – 2.72 (m, 2H).

$^{13}\text{C NMR}$ (101 MHz, CDCl_3): δ 201.3, 161.5 (d, $^1J_{\text{C-F}} = 244.5$ Hz), 142.8, 134.9 (d, $^4J_{\text{C-F}} = 3.5$ Hz), 130.6 (d, $^3J_{\text{C-F}} = 8.0$ Hz), 128.6, 127.5, 126.8, 115.1 (d, $^2J_{\text{C-F}} = 21.0$ Hz), 49.0, 42.4, 42.0.

$^{19}\text{F NMR}$ (376 MHz, CDCl_3): δ -116.92 (tt, $^3J_{\text{H-F}} = 8.5$ Hz, $^4J_{\text{H-F}} = 5.5$ Hz, 1F).



(S)-3-phenyl-4-(4-(4,4,5,5-tetramethyl-1,3,2-dioxaborolan-yl)phenyl)but-

anal (2i). Prepared according to the general procedure using enal **8a** (13.2 mg, 0.1 mmol), aminocatalyst **5a** (14.1 mg, 20 mol%), 4,4,5,5-tetramethyl-2-(*p*-tolyl)-1,3,2-dioxaborolane (218

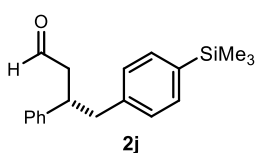
mg, 1 mmol), zinc(II) triflate (18.2 mg, 0.05 mmol) and dichloromethane (300 μL). The crude mixture was purified by flash column chromatography (hexane/diethyl ether 92:8) to afford product **2i** (19.0 mg, 54% yield, 80% ee, average of two runs) as a pale yellow oil. The enantiomeric excess was determined to be 80% by UPC² analysis on a Daicel Chiralpak IE-3 column: gradient CO_2/MeCN from 100% CO_2 to 60:40 over 4 minutes, curve 6, flow rate 2 mL/min, $\lambda = 229$ nm: $\tau_{\text{major}} = 1.74$ min, $\tau_{\text{minor}} = 2.00$ min. $[\alpha]_{\text{D}}^{26} = -29.7$ ($c = 0.37$, CHCl_3 , 80% ee).

$^1\text{H NMR}$ (400 MHz, CDCl_3) δ 9.59 (t, $J = 1.9$ Hz, 1H), 7.67 (d, $J = 7.9$ Hz, 1H), 7.30 – 7.24 (m, 3H), 7.22 – 7.13 (m, 3H), 7.06 (d, $J = 7.9$ Hz, 2H), 3.50 (p, $J = 7.5$ Hz, 1H), 2.93 (qd, $J = 13.5$, 7.5 Hz, 2H), 2.82 – 2.67 (m, 2H), 1.33 (s, 1H);

$^{13}\text{C NMR}$ (101 MHz, CDCl_3) δ 201.6, 143.2, 142.7, 135.0, 128.8, 128.8, 128.7, 127.7, 126.9, 83.9, 49.1, 43.6, 42.0, 29.9, 25.0;

$^{11}\text{B NMR}$ (47 MHz, CDCl_3) δ 30.8;

HRMS (ESI) Exact mass calculated for $\text{C}_{22}\text{H}_{27}\text{NaO}_3\text{B}$ $[\text{M}+\text{Na}]^+$: 372.1982, found: 372.1973.



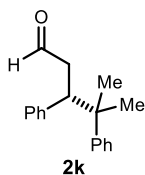
(S)-3-phenyl-4-(4-(trimethylsilyl)phenyl)butanal (2j).

Prepared according to the general procedure using enal **8a** (13.2 mg, 0.1 mmol), aminocatalyst **5a** (14.1 mg, 20 mol%), trimethyl(*p*-tolyl)silane (164 mg, 1 mmol), zinc(II) triflate (18.2 mg, 50 mol%) and dichloromethane (300 μL). The crude mixture was purified by flash column chromatography (hexane/diethyl ether 92:8) to afford product **2j** (16.5 mg, 56% yield, 80% ee, average of two runs) as a colorless oil. The enantiomeric excess was determined, upon sodium borohydride reduction of the isolated aldehyde to afford the corresponding alcohol, to be 80% by HPLC analysis on a Daicel Chiralpak IC-3 column: 90:10 hexane/*i*-PrOH, flow rate 0.6 mL/min, $\lambda = 215$ nm: $\tau_{\text{Major}} = 10.0$ min, $\tau_{\text{minor}} = 11.0$ min. $[\alpha]_{\text{D}}^{26} = -40.1$ ($c = 0.67$, CHCl_3 , 80% ee).

$^1\text{H NMR}$ (400 MHz, CDCl_3): δ 9.58 (t, $J = 2.0$ Hz, 1H), 7.40 (d, $J = 7.9$ Hz, 2H), 7.32 – 7.27 (m, 2H), 7.24 – 7.17 (m, 3H), 7.07 (d, $J = 7.9$ Hz, 2H), 3.55–3.44 (m, 1H), 2.99 (dd, $J = 13.5$, 6.7 Hz, 1H), 2.85 (dd, $J = 13.6$, 8.3 Hz, 1H), 2.80 – 2.67 (m, 2H), 0.24 (s, 9H);

$^{13}\text{C NMR}$ (101 MHz, CDCl_3): δ 201.8, 143.5, 140.0, 138.3, 133.6, 128.8 (2 signals), 127.7, 126.9, 49.0, 43.4, 42.0, -0.9.

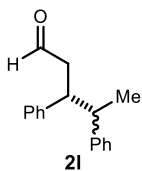
HRMS (ESI) Exact mass calculated for $\text{C}_{19}\text{H}_{24}\text{NaOSi}$ $[\text{M}+\text{Na}]^+$: 319.1484, found: 319.1489.



(S)-4-methyl-3,4-diphenylpentanal (2k). Prepared according to the general procedure using enal **8a** (13.2 mg, 0.1 mmol), aminocatalyst (*S*)-**A** (14.1 mg, 20 mol%), cumene (120 mg, 1 mmol), zinc(II) triflate (18.2 mg, 50 mol%) and dichloromethane (300 μL). The crude mixture was purified by flash column chromatography (hexane/diethyl ether 92:8) to afford product **2k** (9.6 mg, 38% yield, 53% ee, average of two runs) as a pale yellow oil that displayed spectroscopic data consistent with those reported previously.¹⁰ The enantiomeric excess was determined to be 53% by HPLC analysis on a Daicel Chiralpak IC-3 column: 90:10 hexane/*i*-PrOH, flow rate 1.0 mL/min, $\lambda = 215$ nm: $\tau_{\text{Major}} = 8.4$ min, $\tau_{\text{minor}} = 12.2$ min. $[\alpha]_{\text{D}}^{26} = -35.2$ ($c = 0.11$, CHCl_3 , 53% ee); Lit: $[\alpha]_{\text{D}}^{26} = -33.0$ ($c = 0.37$, CHCl_3 , 71% ee for (*S*)-enantiomer).¹⁰

$^1\text{H NMR}$ (400 MHz, CDCl_3): δ 9.34 (dd, $J = 3.0$, 1.5 Hz, 1H), 7.41 – 7.31 (m, 4H), 7.31 – 7.21 (m, 4H), 7.15 – 7.09 (m, 2H), 3.53 (dd, $J = 11.0$, 4.0 Hz, 1H), 2.81 (ddd, $J = 16.5$, 11.0, 3.0 Hz, 1H), 2.46 (ddd, $J = 16.5$, 4.0, 1.5 Hz, 1H), 1.33 (s, 3H), 1.24 (s, 3H).

$^{13}\text{C NMR}$ (101 MHz, CDCl_3): δ 202.0, 147.9, 140.2, 130.0, 128.3, 128.0, 127.0, 126.6, 126.3, 51.2, 45.0, 41.2, 28.8, 23.2.



(3R)-3,4-diphenylpentanal (2l). Prepared according to the general procedure using enal **8a** (13.2 mg, 0.1 mmol), aminocatalyst **5a** (14.1 mg, 20 mol%), ethylbenzene (106 mg, 1 mmol), zinc(II) triflate (18.2 mg, 50 mol%) and dichloromethane (300 μ L). The d.r. was determined to be 1.5:1 by ^1H NMR analysis of the crude mixture, which was purified by flash column chromatography (hexane/diethyl ether 92:8) to afford product **2l** (15.9 mg, 67% yield, average of two runs) as an off-white solid that displayed spectroscopic data consistent with those reported previously.¹⁰ The enantiomeric excess of both diastereoisomers was determined, upon sodium borohydride reduction of the isolated aldehydes to afford the corresponding alcohols, by HPLC analysis on a Daicel Chiralpak IC-3 column, 97:3 hexane/*i*-PrOH, flow rate 1.2 mL/min, $\lambda = 215$ nm. *Major diastereomer*: $\tau_{\text{Major}} = 24.9$ min, $\tau_{\text{minor}} = 20.4$ min. *Minor diastereomer*: $\tau_{\text{Major}} = 18.0$ min, $\tau_{\text{minor}} = 19.1$ min. $[\alpha]_{\text{D}}^{26} = -19.4$ ($c = 0.087$, CHCl_3 , 1.5:1 d.r., 80% ee_{major} , 77% ee_{minor}); Lit: $[\alpha]_{\text{D}}^{26} = -40.4$ ($c = 0.42$, CHCl_3 , 1.2:1 d.r., 92% ee_{major} , 92% ee_{minor} for (3R)-enantiomer).¹⁰

Spectroscopic data for major diastereoisomer:

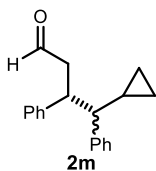
^1H NMR (400 MHz, CDCl_3) δ 9.38 (dd, $J = 2.5, 1.5$ Hz, 1H), 7.43 – 7.12 (m, 8H), 7.05 – 6.97 (m, 2H), 3.33 (td, $J = 10.5, 4.5$ Hz, 1H), 2.92 (dq, $J = 10.5, 7.0$ Hz, 1H, A), 2.65 (ddd, $J = 16.5, 10.5, 2.5$ Hz, 1H), 2.49 (ddd, $J = 16.5, 4.5, 1.5$ Hz, 1H), 1.07 (d, $J = 7.0$ Hz, 3H).

^{13}C NMR (125.8 MHz, CDCl_3) δ 201.6, 145.1, 142.6, 128.7, 128.7, 128.1, 127.6, 126.8, 126.7, 49.0, 47.5, 46.0, 20.5.

Spectroscopic data for minor diastereoisomer:

^1H NMR (400 MHz, CDCl_3) δ 9.60 (t, $J = 2.0$ Hz, 1H), 7.43 – 7.12 (m, 8H), 7.05 – 6.97 (m, 2H), 3.49 (td, $J = 7.5, 7.5$ Hz, 1H), 3.09 (dq, $J = 7.0, 7.0$ Hz, 1H), 2.83 (dd, $J = 7.5, 2.0$ Hz, 2H), 1.31 (d, $J = 7.0$ Hz, 3H).

^{13}C NMR (125.8 MHz, CDCl_3) δ 202.0, 143.8, 141.5, 128.5, 128.1 (2 signals), 128.0, 126.6, 126.3, 46.6, 46.1, 45.0, 18.0.



(3R)-4-cyclopropyl-3,4-diphenylbutanal (2m). Prepared according to the general procedure using enal **8a** (13.2 mg, 0.1 mmol), aminocatalyst **5a** (14.1 mg, 20 mol%), (cyclopropylmethyl)benzene (132 mg, 1 mmol), zinc(II) triflate (18.2 mg, 50 mol%) and dichloromethane (300 μ L). The d.r. was determined to be 1:1 by ^1H NMR analysis of the crude mixture, which was purified by flash column chromatography (hexane/diethyl ether 92:8) to afford product **2m** (10.3 mg, 39% yield, average of two runs) as an off-white solid. The enantiomeric excess of both diastereoisomers was determined, upon sodium borohydride reduction of the isolated aldehydes to afford the corresponding alcohols, by UPC² analysis on a Daicel Chiralpak CEL-1 column: gradient CO_2 /*i*-PrOH from 100% CO_2 to 60:40 over 4 minutes, curve 6, flow rate 3 mL/min, $\lambda = 220$ nm. *Diastereomer A*: $\tau_{\text{Major}} = 4.07$ min, $\tau_{\text{minor}} = 3.96$ min. *Diastereomer B*: $\tau_{\text{Major}} = 4.42$ min, $\tau_{\text{minor}} = 4.13$ min. $[\alpha]_{\text{D}}^{26} = -15.4$ ($c = 0.15$, CHCl_3 , 1:1 d.r., 82% ee_{A} , 85% ee_{B}).

Spectroscopic data for diastereoisomer A:

¹H NMR (400 MHz, CDCl₃): δ 9.69 (t, *J* = 2.0 Hz, 1H), 7.38 – 7.11 (m, 10H), 3.71 (ddd, *J* = 9.0, 8.0, 6.0 Hz, 1H), 3.10 (ddd, *J* = 17.0, 6.0, 2.0 Hz, 1H), 2.84 (ddd, *J* = 17.0, 9.0, 2.0 Hz, 1H), 2.01 (dd, *J* = 10.5, 8.0 Hz, 1H), 1.07 (dddd, *J* = 13.0, 10.5, 8.0, 5.0 Hz, 1H), 0.76 (dddd, *J* = 9.0, 7.5, 6.0, 4.5 Hz, 1H), 0.44 (dddd, *J* = 9.0, 8.0, 5.5, 4.5 Hz, 1H), 0.34 (ddd, *J* = 10.5, 9.0, 5.0 Hz, 1H), 0.03 (ddd, *J* = 9.0, 5.5, 4.5 Hz, 1H).

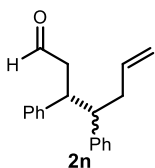
¹³C NMR (101 MHz, CDCl₃, aromatic C-H signals were not assigned and reported for both diastereoisomers): δ 201.7, 142.8, 141.5, 128.6 (C_{Ar}-H), 128.5 (2 signals, C_{Ar}-H), 128.4 (C_{Ar}-H), 128.3 (C_{Ar}-H), 128.2 (C_{Ar}-H), 128.0 (C_{Ar}-H), 127.8 (C_{Ar}-H), 56.9, 47.4, 46.3, 14.9, 7.7, 1.0.

Spectroscopic data for diastereoisomer B:

¹H NMR (400 MHz, CDCl₃): δ 9.46 (dd, *J* = 2.5, 1.5 Hz, 1H), 7.38 – 7.11 (m, 6H), 7.00 – 6.96 (m, 2H), 6.95 – 6.92 (m, 2H), 3.62 (ddd, *J* = 9.5, 9.5, 5.0 Hz, 1H), 2.75 (ddd, *J* = 17.0, 9.5, 2.5 Hz, 1H), 2.61 (ddd, *J* = 17.0, 5.0, 1.5 Hz, 1H), 2.09 (dd, *J* = 9.5, 9.5 Hz, 1H), 0.98 – 0.88 (m, 1H), 0.31 – 0.21 (m, 2H), -0.08 – -0.15 (m, 1H), -0.21 – -0.27 (m, 1H).

¹³C NMR (101 MHz, CDCl₃, aromatic C-H signals were not assigned and reported for both diastereoisomers): δ 202.1, 143.4, 142.3, 128.6 (C_{Ar}-H), 128.5 (2 signals, C_{Ar}-H), 128.4 (C_{Ar}-H), 128.3 (C_{Ar}-H), 128.2 (C_{Ar}-H), 128.0 (C_{Ar}-H), 127.8 (C_{Ar}-H), 56.7, 48.2, 46.7, 15.3, 7.2, 2.8.

HRMS (ESI) Exact mass calculated for C₁₉H₂₀NaO [M+Na]⁺: 287.1406, found: 287.1403.



(3R)-3,4-diphenylhept-6-enal (2n). Prepared according to the general procedure using enal **8a** (13.2 mg, 0.1 mmol), aminocatalyst **5a** (14.1 mg, 20 mol%), 4-phenyl-1-butene (66.1 mg, 0.5 mmol), zinc(II) triflate (18.2 mg, 50 mol%) and CH₂Cl₂ (300 μL). The d.r. was determined to be 2.5:1 by ¹H NMR analysis of the crude mixture, which was purified by flash column chromatography (hexane/diethyl ether

92:8) to afford product **2n** (6.8 mg, 26% yield, average of two runs) as a white solid that displayed spectroscopic data consistent with those reported previously.¹⁰ The enantiomeric excess was determined by HPLC analysis on a Daicel Chiralpak IC-3 column: 95:5 hexane/*i*-PrOH, flow rate 0.5 mL/min, λ = 215 nm. *Major diastereomer*: τ_{Major} = 19.9 min, τ_{minor} = 26.4 min. *Minor diastereomer*: τ_{Major} = 15.9 min, τ_{minor} = 16.7 min. [α]_D²⁶ = -1.3 (c = 0.11, CHCl₃, 4:1 d.r., 86% ee_{major}, 79% ee_{minor}); Lit: [α]_D²⁶ = -1.7 (c = 0.48, CHCl₃, 1.5:1 d.r., 92% ee_{major}, 90% ee_{minor} for (3R)-enantiomer).¹⁰

Spectroscopic data for major diastereoisomer:

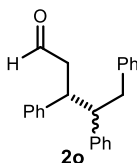
¹H NMR (400 MHz, CDCl₃): δ 9.36 (dd, *J* = 2.5, 1.5 Hz, 1H), 7.41 – 7.16 (m, 10H), 5.43 (ddt, *J* = 17.0, 10.5, 7.0 Hz, 1H), 4.84 – 4.69 (m, 2H), 3.42 (td, *J* = 10.5, 4.5 Hz, 1H), 2.93 – 2.75 (m, 1H), 2.62 (ddd, *J* = 17.0, 10.5, 2.5 Hz, 1H), 2.57 – 2.37 (m, 1H), 2.27 – 2.14 (m, 2H).

¹³C NMR (101 MHz, CDCl₃): δ 201.5, 142.7, 142.4, 136.5, 128.9, 128.8, 128.6, 128.3, 127.1, 127.0, 116.2, 52.1, 49.0, 46.3, 38.5.

Spectroscopic data for minor diastereoisomer:

$^1\text{H NMR}$ (400 MHz, CDCl_3): δ 9.64 (t, $J = 2.0$ Hz, 1H), 7.41 – 7.16 (m, 8H), 6.95 – 6.85 (m, 2H), 5.64 (ddt, $J = 17.0, 10.0, 6.5$ Hz, 1H), 5.08 – 4.92 (m, 2H), 3.61 (dt, $J = 9.0, 6.0$ Hz, 1H), 3.01 (dt, $J = 9.6, 6.0$ Hz, 1H), 2.93 – 2.75 (m, 2H), 2.57 – 2.37 (m, 2H).

$^{13}\text{C NMR}$ (101 MHz, CDCl_3): δ 202.0, 142.8, 142.4, 136.8, 129.4, 129.1, 128.1, 127.9, 126.8, 126.6, 116.7, 50.6, 47.2, 44.5, 37.0.



(3R)-3,4,5-triphenylpentanal (20). Prepared according to the general procedure using enal **8a** (13.2 mg, 0.1 mmol), aminocatalyst **5a** (14.1 mg, 20 mol%), 1,2-diphenylethane (91 mg, 0.5 mmol), zinc(II) triflate (18.2 mg, 50 mol%) and dichloromethane (300 μL). The d.r. was determined to be 1.8:1 by $^1\text{H NMR}$ analysis of the crude mixture, which was purified by flash column chromatography (hexane/diethyl ether 97:3) to afford product **20** (16.7 mg, 53% yield, average of two runs) as an off-white solid. The enantiomeric excess of both diastereoisomers was determined, upon sodium borohydride reduction of the isolated aldehydes to afford the corresponding alcohols, by UPC² analysis on a Daicel Chiralpak CEL-1 column: gradient CO_2/MeOH from 100% CO_2 to 60:40 over 4 minutes, curve 6, flow rate 3 mL/min, $\lambda = 210$ nm. *Major diastereomer*: $\tau_{\text{Major}} = 4.13$ min, $\tau_{\text{minor}} = 4.00$ min. *Minor diastereomer*: $\tau_{\text{Major}} = 4.41$ min, $\tau_{\text{minor}} = 4.27$ min. $[\alpha]_{\text{D}}^{26} = -20.4$ ($c = 0.11$, CHCl_3 , 1.8:1 d.r., 85% ee_{major} , 83% ee_{minor}).

Spectroscopic data for major diastereoisomer:

$^1\text{H NMR}$ (400 MHz, CDCl_3): δ 9.39 (dd, $J = 2.5, 1.5$ Hz, 1H), 7.46 – 6.82 (m, 13H), 6.70 (dd, $J = 7.5, 2.0$ Hz, 2H), 3.54 (td, $J = 10.5, 4.5$ Hz, 1H), 3.15 – 2.99 (m, 1H), 2.97 – 2.87 (m, 1H), 2.87 – 2.74 (m, 1H), 2.71 – 2.54 (m, 1H), 2.49 (ddd, $J = 17.0, 4.5, 1.5$ Hz, 1H).

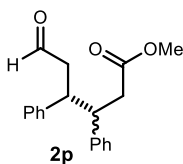
$^{13}\text{C NMR}$ (101 MHz, CDCl_3): δ 201.3, 142.8, 142.0, 140.2, 128.9, 128.8, 128.6, 128.5, 128.2, 127.8, 127.1, 126.8, 125.6, 54.5, 49.0, 46.2, 40.7.

Spectroscopic data for minor diastereoisomer:

$^1\text{H NMR}$ (400 MHz, CDCl_3): δ 9.62 (t, $J = 2.0$ Hz, 1H), 7.46 – 6.82 (m, 15H), 3.65 (dt, $J = 9.0, 6.0$ Hz, 1H), 3.30 (dt, $J = 9.0, 6.0$ Hz, 1H), 3.15 – 2.99 (m, 1H), 2.87 – 2.74 (m, 1H), 2.71 – 2.54 (m, 2H).

$^{13}\text{C NMR}$ (101 MHz, CDCl_3): δ 201.8, 140.5, 140.4, 140.0, 129.3, 129.1, 129.0, 128.2, 128.0, 127.7, 126.7, 126.5, 125.9, 52.2, 47.4, 44.3, 38.9.

HRMS (ESI) Exact mass calculated for $\text{C}_{24}\text{H}_{26}\text{NaO}_2$ $[\text{M}+\text{CH}_3\text{OH}+\text{Na}]^+$: 369.1825, found: 369.1841.



methyl (4R)-6-oxo-3,4-diphenylhexanoate (2p). Prepared according to the general procedure using enal **8a** (13.2 mg, 0.1 mmol), aminocatalyst **5a** (14.1 mg, 20 mol%), methyl 3-phenylpropionate (82 mg, 0.5 mmol), zinc(II) triflate (18.2 mg, 50 mol%) and dichloromethane (300 μL). The d.r. was determined to be 1.1:1 by $^1\text{H NMR}$ analysis of the crude mixture, which was purified by flash column chromatography (gradient from hexane/diethyl ether 95:5 to hexane/diethyl ether

75:25) to afford the *major diastereoisomer* of product **2p** (7.3 mg) as a colorless solid. Continued elution delivered the *minor diastereoisomer* of **2p** (5.9 mg) as a colorless oil (45% overall yield, average of two runs). The enantiomeric excess of both diastereoisomers was determined by HPLC analysis on a Daicel Chiralpak IC-3 column: 80:20 hexane/*i*-PrOH, flow rate 1.0 mL/min, $\lambda = 215$ nm. *Major diastereomer*: $\tau_{Major} = 11.1$ min, $\tau_{minor} = 14.3$ min. *Minor diastereomer*: $\tau_{Major} = 16.0$ min, $\tau_{minor} = 14.4$ min.

Characterization for major diastereoisomer:

$[\alpha]_D^{26} = +18.3$ ($c = 0.04$, CHCl_3 , 82% *ee*).

$^1\text{H NMR}$ (400 MHz, CDCl_3): δ 9.35 (dd, $J = 2.5, 1.5$ Hz, 1H), 7.41 – 7.24 (m, 10H), 3.46 – 3.31 (m, 2H), 3.40 (s, 3H), 2.67 (ddd, $J = 17.0, 9.5, 2.5$ Hz, 1H), 2.55 – 2.38 (m, 3H).

$^{13}\text{C NMR}$ (101 MHz, CDCl_3): δ 200.8, 172.3, 141.7, 141.6, 129.0, 128.8, 128.2, 128.1, 127.3 (2 signals), 51.3, 48.7, 47.9, 45.9, 39.5.

HRMS (ESI) Exact mass calculated for $\text{C}_{19}\text{H}_{20}\text{NaO}_3$ $[\text{M}+\text{Na}]^+$: 319.1305, found: 319.1307.

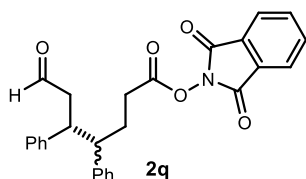
Characterization for minor diastereoisomer:

$[\alpha]_D^{26} = +18.3$ ($c = 0.07$, CHCl_3 , 82% *ee*).

$^1\text{H NMR}$ (400 MHz, CDCl_3): δ 9.61 (t, $J = 2.0$ Hz, 1H), 7.26 – 7.16 (m, 6H), 6.95 – 6.87 (m, 4H), 3.66 – 3.59 (m, 1H), 3.59 (s, 3H), 3.56 – 3.51 (m, 1H), 2.83 – 2.79 (m, 2H), 2.76 (dd, $J = 16.0, 6.5$ Hz, 1H), 2.65 (dd, $J = 16.0, 8.5$ Hz, 1H).

$^{13}\text{C NMR}$ (101 MHz, CDCl_3): δ 201.3, 172.5, 139.9, 139.7, 128.9, 128.7, 128.1, 128.0, 127.0, 126.9, 51.7, 46.5, 46.5, 44.2, 37.4.

HRMS (ESI) Exact mass calculated for $\text{C}_{19}\text{H}_{20}\text{NaO}_3$ $[\text{M}+\text{Na}]^+$: 319.1305, found: 319.1295.



1,3-dioxoisindolin-2-yl (5R)-7-oxo-4,5-diphenylheptanoate (2q). Prepared according to the general procedure using enal **8a** (13.2 mg, 0.1 mmol), aminocatalyst **5a** (14.1 mg, 20 mol%), 1,3-dioxoisindolin-2-yl 4-phenylbutanoate (155 mg, 0.5 mmol), zinc(II) triflate (18.2 mg, 50 mol%) and dichloromethane (300 μL).

The d.r. was determined to be 1.5:1 by $^1\text{H NMR}$ analysis of the crude mixture, which was purified by flash column chromatography on *neutral* silica gel support in order to prevent hydrolysis of the product (*gradient from* hexane/diethyl ether 90:10 *to* hexane/diethyl ether 40:60) to afford the *major diastereoisomer* of product **2q** (14.3 mg) as an off-white solid. Continued elution delivered the *minor diastereoisomer* of **2q** (8.3 mg) as an amber wax (51% overall yield, average of two runs). The enantiomeric excess for both diastereoisomer was determined, upon sodium borohydride reduction of the isolated aldehydes to afford the corresponding diols, by UPC² analysis on a Daicel Chiralpak CEL-1 column: gradient CO_2/EtOH from 100% CO_2 to 60:40 over 4 minutes, curve 6, flow rate 3 mL/min, $\lambda = 215$ nm: *Major diastereomer*: $\tau_{major} = 4.42$ min, $\tau_{minor} = 4.28$ min; *Minor diastereomer*: $\tau_{major} = 4.43$ min, $\tau_{minor} = 4.34$ min.

Characterization for major diastereoisomer:

$[\alpha]_D^{26} = -11.2$ ($c = 0.12$, CHCl_3 , 79% *ee_{major}*).

¹H NMR (400 MHz, CDCl₃): δ 9.32 (dd, *J* = 2.5, 1.5 Hz, 1H), 7.86 (dd, *J* = 5.5, 3.0 Hz, 2H), 7.77 (dd, *J* = 5.5, 3.0 Hz, 2H), 7.38 (dd, *J* = 8.5, 6.5 Hz, 2H), 7.34 – 7.26 (m, 7H), 7.24 – 7.20 (m, 1H), 3.38 (td, *J* = 11.0, 4.5 Hz, 1H), 2.95 (td, *J* = 11.0, 3.5 Hz, 1H), 2.65 – 2.58 (m, 2H), 2.42 (ddd, *J* = 17.0, 4.5, 1.5 Hz, 1H), 2.34 (ddd, *J* = 16.5, 8.0, 5.0 Hz, 1H), 2.25 – 2.18 (m, 1H), 1.94 – 1.84 (m, 1H), 1.81 – 1.72 (m, 1H).

¹³C NMR (101 MHz, CDCl₃): δ 201.5, 169.5, 162.3, 142.4, 141.7, 135.1, 129.5, 129.3, 128.7, 128.4, 127.9, 127.5, 125.9, 124.3, 50.6, 49.7, 47.0, 29.4, 29.2.

HRMS (ESI) Exact mass calculated for C₂₇H₂₃NNaO₅ [M+Na]⁺: 464.1468, found: 464.1481.

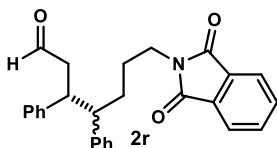
Characterization for *minor diastereoisomer*:

[α]_D²⁶ = +10.2 (*c* = 0.09, CHCl₃, 83% *ee*_{minor}).

¹H NMR (400 MHz, CDCl₃): δ 9.62 (t, *J* = 2.0 Hz, 1H), 7.88 (dd, *J* = 5.5, 3.0 Hz, 2H), 7.78 (dd, *J* = 5.5, 3.0 Hz, 2H), 7.21 – 7.09 (m, 6H), 6.95 – 6.88 (m, 4H), 3.57 – 3.51 (m, 1H), 3.03 (ddd, *J* = 11.0, 7.0, 3.5 Hz, 1H), 2.93 (ddd, *J* = 17.0, 6.0, 2.0 Hz, 1H), 2.82 (ddd, *J* = 17.0, 9.0, 2.0 Hz, 1H), 2.54 – 2.45 (m, 1H), 2.41 – 2.25 (m, 3H), 2.08 – 1.98 (m, 1H).

¹³C NMR (101 MHz, CDCl₃): δ 201.5, 169.4, 161.9, 140.7, 139.6, 134.8, 128.9 (2 signals), 128.7, 128.3, 128.1, 126.9, 126.7, 124.0, 49.9, 47.3, 45.2, 29.3, 28.1.

HRMS (ESI) Exact mass calculated for C₂₇H₂₃NNaO₅ [M+Na]⁺: 464.1468, found: 464.1464.



(*R*)-7-(1,3-dioxoisindolin-2-yl)-3,4-diphenylheptanal (**2r**). Prepared according to the general procedure using enal **8a** (13.2 mg, 0.1 mmol), aminocatalyst **5a** (14.1 mg, 20 mol%), 2-(4-phenylbutyl)isindoline-1,3-dione (140 mg, 0.5 mmol), zinc(II) triflate (18.2 mg, 50 mol%) and dichloromethane (300 μL). The d.r. was determined to be 1.6:1 by ¹H NMR analysis of the crude mixture, which was purified by flash column chromatography on silica gel support (*gradient from hexane/diethyl ether 95:5 to hexane/diethyl ether 70:30*) to afford the *major diastereoisomer* of product **2r** (15.0 mg) as an off-white solid. Continued elution delivered the *minor diastereoisomer* of **2r** (8.7 mg) as a pale yellow solid (57% overall yield, average of two runs). The enantiomeric excess for both diastereoisomer was determined by UPC² analysis on a Daicel Chiralpak IC-3 column: *gradient CO₂/i-PrOH from 100% CO₂ to 60:40 over 4 minutes, curve 6, flow rate 3 mL/min, λ = 210 nm*: *Major diastereomer*: τ_{major} = 3.92 min, τ_{minor} = 4.04 min; *Minor diastereomer*: τ_{major} = 4.13 min, τ_{minor} = 4.23 min.

Characterization for *major diastereoisomer*:

[α]_D²⁶ = -191.0 (*c* = 0.18, CHCl₃, 83% *ee*_{major}).

¹H NMR (400 MHz, CDCl₃): δ 9.33 (dd, *J* = 2.5, 1.5 Hz, 1H), 7.78 (dd, *J* = 5.5, 3.0 Hz, 2H), 7.70 (dd, *J* = 5.5, 3.0 Hz, 2H), 7.34 (ddd, *J* = 7.0, 7.0, 1.0 Hz, 2H), 7.28 – 7.20 (m, 7H), 7.16 – 7.08 (m, 1H), 3.52 – 3.39 (m, 2H), 3.34 (ddd, *J* = 10.5, 10.0, 4.5 Hz, 1H), 2.79 (ddd, *J* = 10.5, 10.5, 2.5 Hz, 1H), 2.59 (ddd, *J* = 17.0, 10.0, 2.5 Hz, 1H), 2.41 (ddd, *J* = 17.0, 4.5, 1.5 Hz, 1H), 1.54 – 1.43 (m, 2H), 1.41 – 1.33 (m, 2H).

¹³C NMR (101 MHz, CDCl₃): δ 201.4, 168.2, 142.5, 142.3, 133.8, 132.0, 128.8, 128.6, 128.2, 128.0, 127.0, 126.8, 123.1, 51.2, 49.0, 46.6, 37.4, 30.7, 26.1.

HRMS (ESI) Exact mass calculated for C₂₇H₂₃NNaO₅ [M+Na]⁺: 464.1468, found: 464.1481.

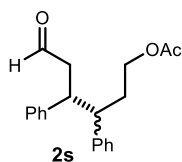
Characterization for *minor diastereoisomer*:

[α]_D²⁶ = +62.7 (c = 0.21, CHCl₃, 80% *ee*_{minor}).

¹H NMR (400 MHz, CDCl₃): δ 9.61 (t, *J* = 2.0 Hz, 1H), 7.84 (dd, *J* = 5.5, 3.0 Hz, 2H), 7.72 (dd, *J* = 5.5, 3.0 Hz, 2H), 7.21 – 7.10 (m, 6H), 6.94 – 6.83 (m, 4H), 3.70 – 3.56 (m, 2H), 3.50 (ddd, *J* = 9.0, 6.5, 6.0 Hz, 1H), 2.94 (ddd, *J* = 11.0, 6.5, 4.5 Hz, 1H), 2.86 (ddd, *J* = 17.0, 6.0, 2.0 Hz, 1H), 2.77 (ddd, *J* = 17.0, 9.0, 2.0 Hz, 1H), 1.85 – 1.75 (m, 1H), 1.75 – 1.65 (m, 1H), 1.58 – 1.47 (m, 2H).

¹³C NMR (101 MHz, CDCl₃): δ 201.9, 168.4, 140.8, 140.7, 133.9, 132.1, 128.9, 128.8, 128.0 (2 signals), 126.6, 126.5, 123.2, 50.5, 47.0, 45.4, 37.7, 29.6, 26.7.

HRMS (ESI) Exact mass calculated for C₂₇H₂₃NNaO₅ [M+Na]⁺: 464.1468, found: 464.1464.



(4*R*)-6-oxo-3,4-diphenylhexyl acetate (2s). Prepared according to the general procedure using enal **8a** (13.2 mg, 0.1 mmol), aminocatalyst **5a** (14.1 mg, 20 mol%), 3-phenylpropyl acetate (89 mg, 0.5 mmol), zinc(II) triflate (18.2 mg, 50 mol%) and dichloromethane (300 μL). The d.r. was determined to be 1.6:1 by ¹H NMR analysis of

the crude mixture, which was purified by flash column chromatography (*gradient from hexane/diethyl ether 90:10 to hexane/diethyl ether 50:50*) to afford the *major diastereoisomer* of product **2s** (10.4 mg) as a pale yellow oil. Continued elution delivered the *minor diastereoisomer* of **2s** (6.9 mg) as a yellow oil (55% overall yield, average of two runs). The enantiomeric excess of both diastereoisomers was determined, upon sodium borohydride reduction of the isolated aldehydes to afford the corresponding alcohols, by HPLC analysis on a Daicel Chiralpak IC-3 column: 90:10 hexane/*i*-PrOH, flow rate 1.2 mL/min, λ = 215 nm. *Major diastereomer*: τ_{Major} = 26.4 min, τ_{minor} = 32.0 min. *Minor diastereomer*: τ_{Major} = 24.8 min, τ_{minor} = 26.9 min.

Characterization for *major diastereoisomer*:

[α]_D²⁶ = -8.8 (c = 0.15, CHCl₃, 83% *ee*_{major}).

¹H NMR (400 MHz, CDCl₃): δ 9.35 (dd, *J* = 2.5, 1.5 Hz, 1H), 7.41 – 7.33 (m, 4H), 7.32 – 7.22 (m, 6H), 3.78 (ddd, *J* = 11.0, 7.0, 5.5 Hz, 1H), 3.64 (dt, *J* = 11.0, 7.5 Hz, 1H), 3.39 (ddd, *J* = 10.5, 10.5, 4.5 Hz, 1H), 2.89 (ddd, *J* = 10.5, 10.5, 5.0 Hz, 1H), 2.62 (ddd, *J* = 17.0, 10.5, 2.5 Hz, 1H), 2.44 (ddd, *J* = 17.0, 4.5, 1.5 Hz, 1H), 1.90 (s, 3H), 1.82 – 1.70 (m, 2H).

¹³C NMR (101 MHz, CDCl₃): δ 201.1, 170.8, 142.3, 141.8, 129.0, 128.9, 128.2, 128.1, 127.2, 127.1, 62.8, 49.0, 48.7, 46.6, 32.8, 20.8.

HRMS (ESI) Exact mass calculated for C₂₀H₂₂NaO₃ [M+Na]⁺: 333.1461, found: 333.1461.

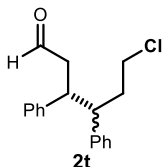
Characterization for *minor diastereoisomer*:

[α]_D²⁶ = +6.2 (c = 0.26, CHCl₃, 80% *ee*_{minor}).

¹H NMR (400 MHz, CDCl₃): δ 9.64 (t, *J* = 2.0 Hz, 1H), 7.24 – 7.14 (m, 6H), 6.95 – 6.91 (m, 2H), 6.91 – 6.86 (m, 2H), 3.96 (ddd, *J* = 11.0, 7.5, 5.0 Hz, 1H), 3.81 (dt, *J* = 11.0, 7.5 Hz, 1H), 3.55 (ddd, *J* = 9.0, 6.5, 6.5 Hz, 1H), 3.03 (ddd, *J* = 11.0, 6.5, 4.0 Hz, 1H), 2.88 (ddd, *J* = 17.0, 6.5, 2.0 Hz, 1H), 2.79 (ddd, *J* = 17.0, 9.0, 2.0 Hz, 1H), 2.19 – 2.06 (m, 1H), 2.05 – 1.90 (m, 4H).

¹³C NMR (101 MHz, CDCl₃): δ 201.5, 170.9, 140.5, 139.9, 128.9, 128.8, 128.1, 128.0, 126.8, 126.8, 62.9, 47.5, 46.9, 45.1, 31.6, 20.9.

HRMS (ESI) Exact mass calculated for C₂₀H₂₂NaO₃ [M+Na]⁺: 333.1461, found: 333.1473.



(R)-6-chloro-3,4-diphenylhexanal (2t). Prepared according to the general procedure using enal **8a** (13.2 mg, 0.1 mmol), aminocatalyst **5a** (14.1 mg, 20 mol%), (3-chloropropyl)benzene (77 mg, 0.5 mmol), zinc(II) triflate (18.2 mg, 50 mol%) and dichloromethane (300 μL). The d.r. was determined to be 1.4:1 by ¹H NMR analysis of the crude mixture, which was purified by flash column chromatography

(hexane/diethyl ether 97:3) to afford product **2t** (14.5 mg, 51% yield, average of two runs) as an off-white solid. The enantiomeric excess of both diastereoisomers was determined, upon sodium borohydride reduction of the isolated aldehydes to afford the corresponding alcohols, by UPC² analysis on a Daicel Chiralpak CEL-1 column: gradient CO₂/MeOH from 100% CO₂ to 60:40 over 4 minutes, curve 6, flow rate 3 mL/min, λ = 210 nm. *Major diastereomer*: τ_{Major} = 4.33 min, τ_{minor} = 4.13 min. *Minor diastereomer*: τ_{Major} = 4.22 min, τ_{minor} = 4.07 min. [α]_D²⁶ = -64.7 (c = 0.43, CHCl₃, 1.4:1 d.r., 79% ee_{major}, 78% ee_{minor}).

Spectroscopic data for major diastereoisomer:

¹H NMR (400 MHz, CDCl₃): δ 9.63 (t, *J* = 2.0 Hz, 1H), 7.42 – 7.35 (m, 2H), 7.33 – 7.25 (m, 5H), 7.24 – 7.15 (m, 2H), 6.92 (ddd, *J* = 14.0, 8.0, 2.0 Hz, 1H), 3.47 – 3.37 (m, 1H), 3.30 – 3.13 (m, 1H), 3.12 – 2.97 (m, 2H), 2.64 (ddd, *J* = 17.0, 10.0, 2.5 Hz, 1H), 2.44 (ddd, *J* = 17.0, 4.5, 1.5 Hz, 1H), 1.93 – 1.77 (m, 2H).

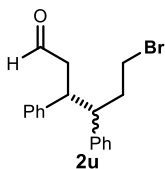
¹³C NMR (101 MHz, CDCl₃): δ 201.2, 142.3, 141.4, 129.2, 129.1, 128.2, 128.2, 127.5, 127.3, 49.4, 48.8, 46.6, 43.2, 36.9.

Spectroscopic data for minor diastereoisomer:

¹H NMR (400 MHz, CDCl₃): δ 9.33 (dd, *J* = 2.5, 1.5 Hz, 1H), 7.42 – 7.35 (m, 2H), 7.33 – 7.25 (m, 5H), 7.24 – 7.15 (m, 2H), 6.92 (ddd, *J* = 14.0, 8.0, 2.0 Hz, 1H), 3.60 – 3.51 (m, 1H), 3.47 – 3.37 (m, 1H), 3.30 – 3.13 (m, 2H), 2.95 – 2.74 (m, 2H), 2.28 – 2.06 (m, 2H).

¹³C NMR (101 MHz, CDCl₃): δ 201.6, 140.7, 139.6, 129.1, 128.9, 128.4, 128.3, 127.0, 126.9, 48.1, 47.3, 46.4, 36.0, 29.8.

HRMS (ESI) Exact mass calculated for C₁₉H₂₃ClNaO₂ [M+CH₃OH+Na]⁺: 341.1279, found: 341.1268.



(R)-6-bromo-3,4-diphenylhexanal (2u). Prepared according to the general procedure using enal **8a** (13.2 mg, 0.1 mmol), aminocatalyst **5a** (14.1 mg, 20 mol%), (3-bromopropyl)benzene (100 mg, 0.5 mmol), zinc(II) triflate (18.2 mg, 50 mol%) and dichloromethane (300 μ L). The d.r. was determined to be 1.5:1 by ^1H NMR analysis of the crude mixture, which was purified by flash column chromatography (hexane/diethyl ether 97:3) to afford product **2u** (13.5 mg, 41% yield, average of two runs) as an off-white solid. The enantiomeric excess of both diastereoisomers was determined, upon sodium borohydride reduction of the isolated aldehydes to afford the corresponding alcohols, by UPC² analysis on a Daicel Chiralpak CEL-1 column: gradient CO_2/MeOH from 100% CO_2 to 60:40 over 4 minutes, curve 6, flow rate 3 mL/min, $\lambda = 210$ nm. *Major diastereomer*: $\tau_{\text{Major}} = 4.47$ min, $\tau_{\text{minor}} = 4.26$ min. *Minor diastereomer*: $\tau_{\text{Major}} = 4.34$ min, $\tau_{\text{minor}} = 4.20$ min. $[\alpha]_{\text{D}}^{26} = -38.8$ ($c = 0.49$, CHCl_3 , 1.5:1 d.r., 78% ee_{major} , 78% ee_{minor}).

Spectroscopic data for major diastereoisomer:

^1H NMR (400 MHz, CDCl_3): δ 9.35 (dd, $J = 2.5, 1.5$ Hz, 1H), 7.43 – 7.34 (m, 2H), 7.34 – 7.25 (m, 5H), 7.24 – 7.13 (m, 2H), 6.92 (ddd, $J = 12.0, 8.0, 2.0$ Hz, 1H), 3.42 (td, $J = 10.5, 4.5$ Hz, 1H), 3.20 – 2.98 (m, 2H), 2.95 – 2.76 (m, 1H), 2.64 (ddd, $J = 17.0, 10.0, 2.5$ Hz, 1H), 2.44 (ddd, $J = 17.0, 4.5, 1.5$ Hz, 1H), 2.03 – 1.83 (m, 2H).

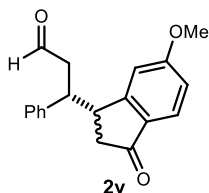
^{13}C NMR (101 MHz, CDCl_3): δ 201.2, 142.2, 141.3, 129.2, 129.0, 128.2, 128.2, 127.5, 127.3, 49.8, 49.4, 46.3, 36.9, 32.1.

Spectroscopic data for minor diastereoisomer:

^1H NMR (400 MHz, CDCl_3): δ 9.65 (t, $J = 2.0$ Hz, 1H), 7.43 – 7.34 (m, 2H), 7.34 – 7.25 (m, 5H), 7.24 – 7.13 (m, 2H), 6.92 (ddd, $J = 12.0, 8.0, 2.0$ Hz, 1H), 3.60 – 3.51 (m, 1H), 3.34 – 3.26 (m, 1H), 3.20 – 2.98 (m, 2H), 2.95 – 2.76 (m, 2H), 2.35 – 2.15 (m, 2H).

^{13}C NMR (101 MHz, CDCl_3): δ 201.5, 140.7, 139.4, 129.1, 128.9, 128.4, 128.3, 127.0, 126.9, 49.4, 47.3, 45.0, 36.1, 31.9.

HRMS (ESI) Exact mass calculated for $\text{C}_{19}\text{H}_{23}\text{BrNaO}_2$ $[\text{M}+\text{CH}_3\text{OH}+\text{Na}]^+$: 385.0774, found: 385.0768.



(R)-3-(6-methoxy-3-oxo-2,3-dihydro-1H-inden-1-yl)-3-phenylpropanal (2v) Prepared according to the general procedure using enal **8a** (13.2 mg, 0.1 mmol), aminocatalyst **5a** (14.1 mg, 20 mol%), 5-methoxy-2,3-dihydro-1H-inden-1-one (162 mg, 1 mmol), zinc(II) triflate (18.2 mg, 50 mol%) and dichloromethane (300 μ L). The d.r. was determined to be 1.9:1 by ^1H NMR analysis of the crude mixture, which was purified by flash column chromatography (gradient from hexane/diethyl ether 90:10 to hexane/diethyl ether 80:20, two consecutive purifications) to afford the *minor diastereoisomer* of product **2v** (7.6 mg) as an off-white solid. Continued elution delivered the *major diastereoisomer* of **2v** (9.4 mg) as an off-white solid (58% overall yield, average of two runs). The enantiomeric excess was determined UPC² analysis on a Daicel Chiralpak IC-3 column:

gradient CO₂/*i*-PrOH from 100% CO₂ to 60:40 over 4 minutes, curve 6, flow rate 3 mL/min, $\lambda = 220$ nm. *Major diastereomer*: $\tau_{major} = 4.67$ min, $\tau_{minor} = 4.82$ min. *Minor diastereomer*: $\tau_{major} = 4.58$ min, $\tau_{minor} = 4.42$ min. UPC² (Daicel Chiralpak IC-3 column, 20 °C, gradient CO₂/*i*-PrOH from 100% CO₂ to 60:40 over 4 minutes, curve 6, flow rate 3 mL/min, $\lambda = 220$ nm).

Characterization for major diastereoisomer:

$[\alpha]_D^{26} = -5.41$ ($c = 0.21$ CHCl₃, 91% ee_{major}).

¹H NMR (500 MHz, CDCl₃) δ 9.70 (dd, $J = 2.0, 1.5$ Hz, 1H), 7.65 (d, $J = 8.5$ Hz, 1H), 7.31 – 7.17 (m, 5H), 6.87 (dd, $J = 8.5, 2.0$ Hz, 1H), 6.74 (d, $J = 2.0$ Hz, 1H), 3.83 (s, 3H), 3.62 – 3.69 (m, 1H), 3.56 (ddd, $J = 17.5, 5.5, 1.5$ Hz, 1H), 3.04 – 2.91 (m, 3H), 2.69 (d, $J = 13.5$ Hz, 1H);

¹³C NMR (128 MHz, CDCl₃) δ 205.1, 200.1, 165.5, 156.0, 141.9, 130.0, 128.7, 128.2, 127.0, 125.7, 115.5, 109.4, 55.6, 51.2, 48.2, 41.0, 29.7;

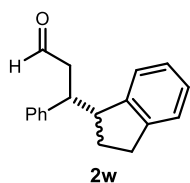
Characterization data for minor diastereoisomer

$[\alpha]_D^{26} = -23.85$ ($c = 0.08$, CHCl₃, 86% ee_{minor}).

¹H NMR (500 MHz, CDCl₃) δ 9.71 (dd, $J = 2.5, 1.5$ Hz, 1H), 7.66 (d, $J = 8.5$ Hz, 1H), 7.30 – 7.14 (m, 5H), 6.87 (dd, $J = 8.5, 2.5$ Hz, 1H), 6.79 (bs, 1H), 3.97 (ddd, $J = 9.5, 6.0, 4.0$ Hz, 1H), 3.85 (s, 3H), 3.08 (qd, $J = 8.0, 4.5$ Hz, 2H), 3.03 – 2.87 (m, 3H);

¹³C NMR (128 MHz, CDCl₃) δ 205.4, 201.5, 165.6, 156.6, 141.2, 130.8, 128.8, 128.2, 127.2, 125.7, 115.7, 109.6, 55.8, 51.2, 44.8, 40.1, 29.8;

HRMS (ESI) Exact mass calculated for C₁₉H₁₈NaO₃ [M+ Na]⁺: 317.1148, found: 317.1148.



(3R)-3-(2,3-dihydro-1H-inden-1-yl)-3-phenylpropanal (2w).

Prepared according to the general procedure using enal **8a** (13.2 mg, 0.1 mmol), aminocatalyst **5a** (14.1 mg, 20 mol%), indane (118 mg, 1 mmol), zinc(II) triflate (18.2 mg, 50 mol%) and dichloromethane (300 μ L). The d.r. was determined to be 1.1:1 by ¹H NMR analysis of the crude mixture, which was purified by flash

column chromatography (hexane/diethyl ether 95:5) to afford product **2w** (23.7 mg, 91% yield, 1.1:1 mixture of diastereoisomers, average of two runs) as a pale yellow oil. The enantiomeric excess of both diastereoisomers was determined, upon sodium borohydride reduction of the isolated aldehydes to afford the corresponding alcohols, by HPLC analysis on a Daicel Chiralpak IC-3 column, 98.5:1.5 hexane/*i*-PrOH, flow rate 1.2 mL/min, T = 30 °C, $\lambda = 215$ nm. *Major diastereomer*: $\tau_{minor} = 45.9$ min, $\tau_{major} = 62.2$ min. *Minor diastereomer*: $\tau_{major} = 43.7$ min, $\tau_{minor} = 52.1$ min. $[\alpha]_D^{26} = -28.8$ ($c = 0.80$, CHCl₃, 1.1:1 d.r., 80% ee_{major} , 77% ee_{minor}).

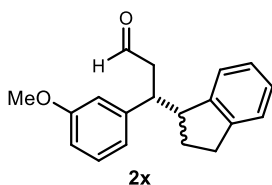
The spectroscopic data for compound 2w were not assigned and are reported as a mixture of diastereoisomers:

¹H NMR (400 MHz, CDCl₃, isolated as a 1.1:1 mixture of diastereoisomers) δ 9.60 (dd, $J = 2.5, 1.7$ Hz, 1H), 9.57 (t, $J = 2.1$ Hz, 1H), 7.33 – 7.11 (m, 16H), 7.07 (app t, $J = 7.2$ Hz, 1H), 6.88 (d, $J = 7.5$ Hz, 1H), 3.65 – 3.58 (m, 1H), 3.53 (q, $J = 6.4$ Hz, 1H), 3.43 – 3.35 (m, 2H),

2.96 – 2.83 (m, 3H), 2.80 – 2.60 (m, 5H), 2.20 – 2.11 (m, 1H), 2.10 – 1.99 (m, 1H), 1.97 – 1.88 (m, 1H), 1.87 – 1.79 (m, 1H);

¹³C NMR (101 MHz, CDCl₃) δ 201.9, 201.8, 144.9, 144.8, 144.7, 144.3, 142.4, 142.0, 128.5, 128.4, 128.3, 128.2, 127.0, 126.9, 126.8, 126.7, 126.0, 125.9, 125.3, 124.8, 124.6, 124.5, 50.4, 47.6, 46.1, 43.8, 43.6, 31.2, 30.7, 29.3, 29.1;

HRMS (ESI) Exact mass calculated for C₁₉H₂₂NaO₂ [M+CH₃OH+Na]⁺: 305.1512, found: 305.1516.



(3R)-3-(2,3-dihydro-1H-inden-1-yl)-3-(3-methoxyphenyl)propanal (2x). Prepared according to the general procedure using enal **8u** (16.2 mg, 0.1 mmol), aminocatalyst **5a** (14.1 mg, 20 mol%), indane (118 mg, 1 mmol), zinc(II) triflate (18.2 mg, 50 mol%) and dichloromethane (300 μL). The d.r. was determined to be

1.4:1 by ¹H NMR analysis of the crude mixture, was purified by flash column chromatography (hexane/diethyl ether 95:5) to afford product **2x** (18.0 mg, 64% yield, 1.4:1 mixture of diastereoisomers, average of two runs) as a pale yellow oil. The enantiomeric excess of both diastereoisomers was determined, upon sodium borohydride reduction of the isolated aldehydes to afford the corresponding alcohols, by UPC² analysis on a Daicel Chiralpak ID-3 column: gradient CO₂/iPrOH from 100% CO₂ to 60:40 over 4 minutes, curve 6, flow rate 3 mL/min, λ = 273 nm: *Minor diastereomer*: τ_{major} = 3.35 min, τ_{minor} = 3.48 min; *Major diastereomer*: τ_{major} = 3.40 min, τ_{minor} = 3.67 min. [α]_D²⁶ = -24.0 (c = 0.55, CHCl₃, 1.4:1 d.r., 86% ee_{Major}, 82% ee_{minor}).

Spectroscopic data for major diastereoisomer:

¹H NMR (400 MHz, CDCl₃) δ 9.60 (dd, J = 2.5, 1.5 Hz, 1H, A), 7.30 – 7.25 (m, 1H), 7.23 – 7.12 (m, 3H), 7.11 – 7.04 (m, 1H), 6.81 – 6.73 (m, 2H), 6.66 (t, J = 2.0 Hz, 1H), 3.74 (s, 3H), 3.63 – 3.47 (m, 1H), 3.41 – 3.32 (m, 1H), 2.93 – 2.60 (m, 4H), 2.23 – 1.99 (m, 1H), 1.97 – 1.90 (m, 1H);

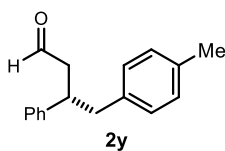
Spectroscopic data for minor diastereoisomer:

¹H NMR (400 MHz, CDCl₃) δ 9.58 (t, J = 2.0 Hz, 1H), 7.30 – 7.25 (m, 1H), 7.23 – 7.12 (m, 3H), 7.11 – 6.93 (d, 7.07 J = 7.5 Hz, 1H), 6.81 – 6.73 (m, 2H), 6.62 (t, J = 2.0 Hz, 1H), 3.72 (s, 3H), 3.63 – 3.47 (m, 1H), 3.41 – 3.32 (m, 1H), 2.93 – 2.60 (m, 4H), 2.23 – 1.99 (m, 1H), 1.97 – 1.90 (m, 1H);

The signals relative to ¹³C NMR analysis were not assigned and are reported as a mixture of diastereoisomers:

¹³C NMR (101 MHz, CDCl₃) δ 202.0, 202.0, 159.8, 159.6, 145.1, 145.0, 144.9, 144.4, 144.1, 143.7, 129.6, 129.5, 127.2, 127.1, 126.2, 126.0, 125.4, 125.0, 124.7, 124.7, 120.8, 120.6, 114.4, 114.1, 112.3, 112.1, 55.3, 50.4, 47.7, 46.2, 44.0, 43.7, 31.7, 30.9, 29.3.

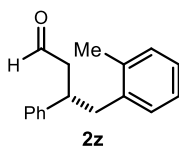
HRMS (ESI) Exact mass calculated for C₁₉H₂₀NaO₂ [M+Na]⁺: 303.1356, found: 303.1368.



(S)-3-phenyl-4-(p-tolyl)butanal (2y). Prepared according to the general procedure using enal **8a** (13.2 mg, 0.1 mmol), aminocatalyst **5a** (14.1 mg, 20 mol%), *p*-xylene (134 mg, 1 mmol), trichloroacetic acid (16.3 mg, 100 mol%) and dichloromethane (300 μ L). The crude mixture was purified by flash column chromatography (hexane/diethyl ether 92:8) to afford product **2y** (15.0 mg, 63% yield, 83% ee, average of two runs) as a colorless oil that displayed spectroscopic data consistent with those reported previously.¹⁰ The enantiomeric excess was determined to be 83% by HPLC analysis on a Daicel Chiralpak IC-3 column: 96:4 hexane/*i*-PrOH, flow rate 0.8 mL/min, $\lambda = 215$ nm: $\tau_{major} = 12.1$ min, $\tau_{minor} = 13.1$ min. $[\alpha]_{D^{26}} = -17.3$ ($c = 0.45$, CHCl_3 , 83% ee); Lit: $[\alpha]_{D^{26}} = -50.8$ ($c = 0.69$, CHCl_3 , 91% ee for (*S*)-enantiomer).¹⁰

¹H NMR (500 MHz, CDCl_3): δ 9.58 (t, $J = 2.0$ Hz, 1H), 7.31–7.26 (m, 2H), 7.04 (d, $J = 8.0$ Hz, 2H), 6.95 (d, $J = 8.0$ Hz, 2H), 3.46 (p, 7.04 (d, $J = 7.5$ Hz, 1H) 2.94 (dd, $J = 13.5$, 7.0 Hz, 1H), 2.83 (dd, $J = 13.5$, 8.0 Hz, 1H), 2.78 – 2.68 (m, 2H), 2.29 (s, 3H);

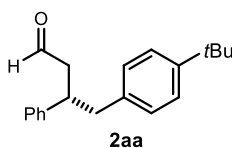
¹³C NMR (125.8 MHz, CDCl_3): δ 201.8, 143.5, 136.3, 136.0, 129.2, 129.2, 128.7, 127.7, 126.8, 49.1, 43.0, 42.2, 21.2.



(S)-3-phenyl-4-(o-tolyl)butanal (2z). Prepared according to the general procedure using enal **8a** (13.2 mg, 0.1 mmol), aminocatalyst **5a** (14.1 mg, 20 mol%), *o*-xylene (134 mg, 1 mmol), trichloroacetic acid (16.3 mg, 100 mol%) and dichloromethane (300 μ L). The crude mixture was purified by flash column chromatography (hexane/diethyl ether 92:8) to afford product **2z** (11.0 mg, 47% yield, 77% ee, average of two runs) as a colorless oil that displayed spectroscopic data consistent with those reported previously.¹⁰ The enantiomeric excess was determined to be 77% by HPLC analysis on a Daicel Chiralpak IC-3 column: 90:10 hexane/*i*-PrOH, flow rate 0.7 mL/min, $\lambda = 215$ nm: $\tau_{major} = 10.5$ min, $\tau_{minor} = 11.9$ min. $[\alpha]_{D^{26}} = -40.7$ ($c = 0.23$, CHCl_3 , 77% ee); Lit: $[\alpha]_{D^{26}} = -22.2$ ($c = 0.59$, CHCl_3 , 90% ee for (*S*)-enantiomer).¹⁰

¹H NMR (400 MHz, CDCl_3): δ 9.57 (t, $J = 1.9$ Hz, 1H), 7.32–7.25 (m, 2H), 7.23–7.03 (m, 6H), 6.97 (d, $J = 7.0$ Hz, 1H), 6.78 (s, 1H), 3.47 (p, $J = 7.4$ Hz, 1H), 2.97 – 2.86 (m, 2H), 2.85 – 2.72 (m, 2H), 2.26 (s, 3H);

¹³C NMR (101 MHz, CDCl_3): δ 201.7, 143.6, 137.7, 136.5, 130.6, 130.3, 128.8, 127.6, 126.9, 126.7, 125.9, 49.0, 41.0, 19.6.



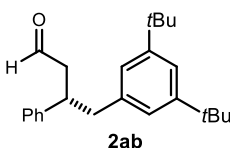
(S)-4-(4-(tert-butyl)phenyl)-3-phenylbutanal (2aa). Prepared according to the general procedure using enal **8a** (13.2 mg, 0.1 mmol), aminocatalyst **5a** (14.1 mg, 20 mol%), 1-(*t*-butyl)-4-methylbenzene (148 mg, 1 mmol), trichloroacetic acid (16.3 mg, 100 mol%) and dichloromethane (300 μ L). The crude mixture was purified by flash column chromatography (hexane/diethyl ether 92:8) to afford product **2aa** (15.0 mg, 53% yield, 77% ee, average of two runs) as a colorless oil. The enantiomeric excess was determined, upon sodium borohydride reduction of the isolated aldehyde to afford the corresponding alcohol, to be 77% by HPLC analysis on

a Daicel Chiralpak IC-3 column: 90:10 hexane/*i*-PrOH, flow rate 0.6 mL/min, $\lambda = 215$ nm: $\tau_{Major} = 10.9$ min, $\tau_{minor} = 12.2$ min. $[\alpha]_{D^{26}} = -33.4$ ($c = 0.63$, $CHCl_3$, 78% ee).

1H NMR (500 MHz, $CDCl_3$): δ 9.57 (t, $J = 2.0$ Hz, 1H), 7.33–7.22 (m, 4H), 7.24–7.18 (m, 3H), 7.02 (d, $J = 8.2$ Hz, 2H), 3.54–3.47 (m, 1H), 3.00 (dd, $J = 13.6, 6.4$ Hz, 1H), 2.85 (dd, $J = 13.6, 8.6$ Hz, 1H) 2.81–2.69 (m, 2H), 1.32 (s, 9H);

^{13}C NMR (125.8 MHz, $CDCl_3$): δ 202.0, 149.4, 143.7, 136.3, 129.0, 128.8, 127.6, 126.9, 125.4, 48.9, 42.9, 42.1, 34.5, 31.5.

HRMS (ESI) Exact mass calculated for $C_{21}H_{28}NaO_2$ $[M+CH_3OH+Na]^+$: 335.1980, found: 335.1982.



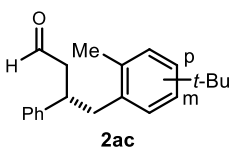
(S)-4-(3,5-di-tert-butylphenyl)-3-phenylbutanal (2ab).

Prepared according to the general procedure using enal **8a** (13.2 mg, 0.1 mmol), aminocatalyst **5a** (14.1 mg, 20 mol%), 1,3-di-*t*-butyl-5-methylbenzene (204 mg, 1 mmol), trichloroacetic acid (16.3 mg, 100 mol%) and dichloromethane (300 μ L). The crude mixture was purified by flash column chromatography (hexane/diethyl ether 92:8) to afford product **2ab** (20.0 mg, 59% yield, 74% ee, average of two runs) as a colorless oil. The enantiomeric excess was determined to be 74% by HPLC analysis on a Daicel Chiralpak IC-3 column: 98:2 hexane/*i*-PrOH, flow rate 0.6 mL/min, $\lambda = 215$ nm: $\tau_{Major} = 10.9$ min, $\tau_{minor} = 12.2$ min. $[\alpha]_{D^{26}} = -19.1$ ($c = 0.73$, $CHCl_3$, 74% ee).

1H NMR (500 MHz, $CDCl_3$): δ 9.59 (t, $J = 2.0$ Hz, 1H), 7.30–7.25 (m, 2H), 7.23–7.17 (m, 2H), 7.14 (d, $J = 6.8$ Hz, 2H), 6.82 (d, $J = 1.8$ Hz, 2H), 3.45 (p, $J = 7.4$ Hz, 1H), 2.95 (dd, $J = 13.4, 7.2$ Hz, 1H), 2.87 (dd, $J = 13.4, 7.6$ Hz, 1H) 2.81–2.72 (m, 2H), 1.26 (s, 18H);

^{13}C NMR (125.8 MHz, $CDCl_3$): δ 202.0, 150.7, 143.5, 138.2, 128.7, 127.8, 126.8, 123.7, 120.2, 49.0, 44.1, 42.4, 34.8, 31.5.

HRMS (ESI) Exact mass calculated for $C_{24}H_{32}NaO$ $[M+Na]^+$: 359.2348, found: 359.2345.



(S)-4-(4-(tert-butyl)-2-methylphenyl)-3-phenylbutanal and (S)-4-(5-(tert-butyl)-2-methylphenyl)-3-phenylbutanal (2ac).

Prepared according to the general procedure using enal **8a** (13.2 mg, 0.1 mmol), aminocatalyst **5a** (14.1 mg, 20 mol%), 4-(*t*-butyl)-1,2-dimethylbenzene (134 mg, 1 mmol), trichloroacetic acid (16.3 mg, 100 mol%) and dichloromethane (300 μ L). The regioisomeric ratio was determined to be 6.5:1 by 1H NMR analysis of the crude mixture, which was purified by flash column chromatography (hexane/diethyl ether 92:8) to afford product **2ac** (18.0 mg, 60% yield, average of two runs) as a colorless oil. The enantiomeric excess was determined, upon sodium borohydride reduction of the isolated aldehyde to afford the corresponding alcohol, to be 73% for the major regioisomer and 74% for the minor by UPC² analysis on CEL1 chiral column: 95:5 CO_2 /EtOH, curve 6, flow rate 3 mL/min, $\lambda = 203$ nm. *Minor regioisomer*: $\tau_{minor} = 1.51$ min, $\tau_{major} = 1.85$ min; *major regioisomer*: $\tau_{minor} = 1.63$ min, $\tau_{major} = 1.97$ min. $[\alpha]_{D^{26}} = -15.6$ ($c = 0.25$, $CHCl_3$, 6.5:1 regioisomeric ratio, 73% ee_{major} , 74% ee_{minor}).

Spectroscopic data for major regioisomer (2ac-p):

¹H NMR (400 MHz, CDCl₃): δ 9.55 (t, *J* = 2.0 Hz, 1H), 7.33–7.26 (m, 2H), 7.24–7.18 (m, 3H), 7.16–7.04 (m, 2H), 6.90 (d, *J* = 8.0 Hz, 1H), 3.50–3.41 (m, 1H), 2.94 (dd, *J* = 14.0, 6.0 Hz, 1H), 2.90–2.60 (m, 3H), 2.28 (s, 3H), 1.29 (s, 9H);

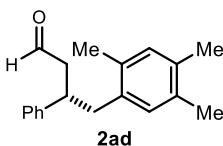
¹³C NMR (101 MHz, CDCl₃): δ 202.0, 149.5, 143.9, 143.6, 135.9, 134.6, 129.9, 128.8, 127.5, 126.9, 122.9, 48.8, 40.9, 40.6, 34.4, 31.5, 19.9.

Spectroscopic data for minor regioisomer (2ac-m):

¹H NMR (400 MHz, CDCl₃): δ 9.60 (t, *J* = 2.0 Hz, 1H), 7.33–7.26 (m, 2H), 7.24–7.18 (m, 3H), 7.16–7.04 (m, 2H), 6.82 (d, *J* = 2.0 Hz, 1H), 3.50–3.41 (m, 1H), 2.94 (dd, *J* = 14.0, 6.0 Hz, 1H), 2.90–2.60 (m, 3H), 2.27 (s, 3H), 1.19 (s, 9H);

¹³C NMR (101 MHz, CDCl₃): δ 201.8, 148.6, 137.0, 133.3, 130.2, 128.7, 127.7, 126.8, 123.4, 49.2, 41.4, 40.9, 34.2, 31.4, 19.0.

HRMS (ESI) Exact mass calculated for C₂₂H₃₀NaO₂ [M+CH₃OH+Na]⁺: 349.2154, found: 349.2138.



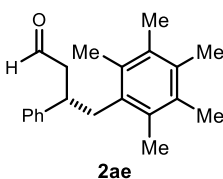
(S)-3-phenyl-4-(2,4,5-trimethylphenyl)butanal (2ad).

Prepared according to the general procedure using enal **8a** (13.2 mg, 0.1 mmol), aminocatalyst **5a** (14.1 mg, 20 mol%), 1,2,4,5-tetramethylbenzene (134 mg, 1 mmol), trichloroacetic acid (16.3 mg, 100 mol%) and dichloromethane (300 μL). The crude mixture was purified by flash column chromatography (hexane/diethyl ether 92:8) to afford product **2ad** (18.0 mg, 68% yield, 82% ee, average of two runs) as a colorless oil. The enantiomeric excess was determined by HPLC analysis on a Daicel Chiralpak IC-3 column: 90:10 hexane/*i*-PrOH, flow rate 0.6 mL/min, λ = 215 nm: τ_{Major} = 11.1 min, τ_{minor} = 12.0 min. [α]_D²⁶ = -32.7 (c = 0.50, CHCl₃, 82% ee).

¹H NMR (500 MHz, CDCl₃): δ 9.54 (t, *J* = 2.0 Hz, 1H), 7.32–7.27 (m, 2H), 7.23–7.18 (m, 3H), 6.90 (s, 1H), 6.78 (s, 1H), 3.47–3.40 (m, 1H), 2.89 (dd, *J* = 13.7, 6.2 Hz, 1H), 2.82–2.71 (m, 3H), 2.19 (s, 6H), 2.17 (s, 6H);

¹³C NMR (125.8 MHz, CDCl₃): δ 202.0, 144.0, 134.9, 134.7, 133.9, 133.6, 131.9, 131.6, 128.8, 127.5, 126.8, 48.8, 41.2, 40.6, 19.3, 19.0.

HRMS (ESI) Exact mass calculated for C₂₀H₂₆NaO₂ [M+CH₃OH+Na]⁺: 321.1828, found: 321.1825.



(S)-4-(2,3,4,5,6-pentamethylphenyl)-3-phenylbutanal (2ae).

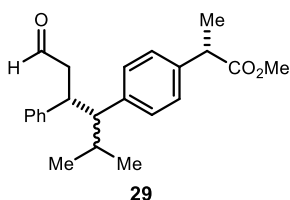
Prepared according to the general procedure using enal **8a** (13.2 mg, 0.1 mmol), aminocatalyst **5a** (14.1 mg, 20 mol%), hexamethylbenzene (162 mg, 1 mmol), trichloroacetic acid (16.3 mg, 100 mol%) and dichloromethane (300 μL). The crude mixture was purified by flash column chromatography (hexane/diethyl ether 92:8) to afford product **2ae** (22.2 mg, 75% yield, 82% ee, average of two runs) as off-white solid. The enantiomeric excess was determined by HPLC analysis on a Daicel Chiralpak IC-3 column: 90:10 hexane/*i*-PrOH, flow rate 0.6

mL/min, $\lambda = 215$ nm: $\tau_{major} = 11.1$ min, $\tau_{minor} = 14.7$ min. $[\alpha]_D^{26} = -23.6$ ($c = 0.50$, CHCl_3 , 82% ee).

$^1\text{H NMR}$ (400 MHz, CDCl_3): δ 9.47 (dd, $J = 2.5, 1.5$ Hz, 1H), 7.35–7.30 (m, 2H), 7.30–7.20 (m, 3H), 3.42 (tt, $J = 10.0, 5.5$ Hz, 1H), 3.11 (dd, $J = 14.5, 9.5$ Hz, 1H), 3.00 (dd, $J = 14.5, 5.5$ Hz, 1H), 2.86 (ddd, $J = 16.5, 10.0, 2.5$ Hz, 1H), (ddd, $J = 16.5, 5.0, 2.0$ Hz, 1H), 2.26 (s, 3H), 2.23 (s, 12H);

$^{13}\text{C NMR}$ (101 MHz, CDCl_3): δ 202.2, 144.1, 133.4, 133.3, 132.9, 132.4, 128.8, 127.4, 126.9, 47.9, 41.3, 37.9, 17.3, 17.1, 17.1.

HRMS (ESI) Exact mass calculated for $\text{C}_{22}\text{H}_{30}\text{NaO}_2$ $[\text{M}+\text{CH}_3\text{OH}+\text{Na}]^+$: 349.2138, found: 349.2139



methyl (S)-2-(4-((R)-6-methyl-1-oxo-3-phenylheptan-4-yl)phenyl)

propanoate (29). Prepared according to the general procedure using enal **8a** (13.2 mg, 0.1 mmol), aminocatalyst **5a** (14.1 mg, 20 mol%), **28** (110 mg, 0.5 mmol), zinc(II) triflate (18.2 mg, 50 mol%) and dichloromethane (300 μL).

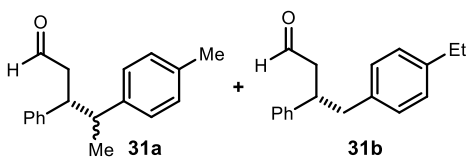
The crude mixture, which was purified by flash column chromatography (hexane/diethyl ether 92:8) to afford product **29** (34.5 mg, 50% yield) as a colorless oil. Due to the overlap of diagnostic signals in the $^1\text{H NMR}$ spectrum, the diastereomeric ratio of the product mixture was determined, upon sodium borohydride reduction of the isolated aldehydes to afford the corresponding alcohols, *via* UPC² analysis to be 1:1.3:8.2:10. $[\alpha]_D^{26} = 42.4$ ($c = 0.99$, CHCl_3 , 1:1.3:8.2:10 *d.r.*).

The spectroscopic data for compound **28** were not assigned and are reported as a mixture of diastereoisomers:

$^1\text{H NMR}$ (400 MHz, CDCl_3 , isolated as a 1.2:1 mixture of diastereoisomers): δ 9.64 (t, $J = 2.0$, Hz, 1H), 9.41 (dd, $J = 2.5, 1.0$ Hz, 1H), 7.35–7.28 (m, 2H), 7.26–7.19 (m, 4H), 7.14–7.08 (m, 6H), 7.04 (d, $J = 8.0$ Hz, 2H), 6.89–6.84 (m, 2H), 6.67 (d, $J = 8.0$ Hz, 2H), 3.85 (dt, $J = 8.5, 6.0$ Hz, 1H), 3.76 – 3.61 (m, 9H), 2.84 – 2.74 (m, 2H), 2.67 (ddd, $J = 16.5, 8.5, 2.0$ Hz, 1H), 2.61 – 2.52 (m, 2H), 2.44 (ddd, $J = 17.0, 4.0, 1.5$ Hz, 1H), 2.04 – 1.93 (m, 1H), 1.69 – 1.59 (m, 1H), 1.51 (d, $J = 7.0$ Hz, 3H), 1.44 (d, $J = 7.0$ Hz, 3H), 1.13 (d, $J = 6.5$ Hz, 3H), 0.74 (d, $J = 7.0$ Hz, 3H), 0.71 (d, $J = 6.5$ Hz, 2H), 0.65 (d, $J = 7.0$ Hz, 3H);

$^{13}\text{C NMR}$ (101 MHz, CDCl_3): δ 202.3, 202.1, 175.3, 175.3, 143.0, 140.8, 138.9, 138.4, 138.3, 138.2, 130.7, 129.3, 128.9, 128.2, 127.9, 127.2, 126.9, 126.6, 126.4, 57.6, 57.0, 52.2, 52.1, 49.5, 48.4, 45.1, 45.1, 42.3, 40.6, 28.8, 28.4, 22.3, 20.1, 18.8, 16.6;

HRMS (ESI) Exact mass calculated for $\text{C}_{23}\text{H}_{28}\text{NaO}_3$ $[\text{M}+\text{Na}]^+$: 375.1923, found: 375.1931.



(3R)-3-phenyl-4-(p-tolyl)pentanal (31a)
and
(S)-4-(4-ethylphenyl)-3-phenylbutanal (31b).

Prepared according to the general procedure using enal **8a** (13.2 mg, 0.1 mmol), aminocatalyst **5a** (14.1 mg, 20 mol%), methyl 4-ethyltoluene (120 mg, 1

mmol), zinc(II) triflate (18.2 mg, 50 mol%) and dichloromethane (300 μ L). The crude mixture was purified by flash column chromatography (hexane/diethyl ether 92:8) to afford products **31** [16.0 mg, 63% yield, 6:1 mixture of regioisomers **31a** (1.7:1 d.r., 76% *ee*_{major}, 75% *ee*_{minor}) and **31b** (77% *ee*)] as a pale yellow oil. The enantiomeric excess of both regioisomers, and corresponding diastereoisomers for **31a**, was determined, upon sodium borohydride reduction of the isolated aldehydes to afford the corresponding alcohols, by UPC² analysis on a Daicel Chiralpak CEL-1 column: CO₂/MeOH 95:5, flow rate 3 mL/min, λ = 210 nm. For compound **31a**, *Major diastereomer*: τ_{Major} = 3.27 min, τ_{minor} = 2.59 min. *Minor diastereomer*: τ_{Major} = 3.47 min, τ_{minor} = 3.02 min. For compound **31b**: τ_{Major} = 4.46 min, τ_{minor} = 3.70 min.

Spectroscopic data for compound 31a, major diastereoisomer:

¹H NMR (400 MHz, CDCl₃): δ 9.47 (dd, *J* = 2.5, 1.5 Hz, 1H), 7.48 – 7.23 (m, 7H), 7.16 – 7.10 (m, 2H), 3.40 (ddd, *J* = 10.0, 10.0, 4.5 Hz, 1H), 3.02 – 2.93 (m, 1H), 2.76 – 2.69 (m, 1H), 2.60 (ddd, *J* = 16.5, 4.5, 1.5 Hz, 1H), 2.47 (s, 3H), 1.15 (d, *J* = 7.0 Hz, 3H).

¹³C NMR (101 MHz, CDCl₃): δ 201.8, 142.9, 142.2, 136.4, 129.5, 128.8, 128.3, 127.6, 126.9, 49.2, 47.7, 45.8, 21.2, 20.8.

Spectroscopic data for compound 31a, minor diastereoisomer:

¹H NMR (400 MHz, CDCl₃): δ 9.68 (t, *J* = 2.0 Hz, 1H), 7.48 – 7.23 (m, 7H), 7.03 – 6.99 (m, 2H), 3.64 – 3.57 (m, 1H), 3.17 (qd, *J* = 7.0, 7.0 Hz, 1H), 2.93 – 2.89 (m, 2H), 2.41 (s, 3H), 1.38 (d, *J* = 7.0 Hz, 3H).

¹³C NMR (101 MHz, CDCl₃): δ 202.3, 141.7, 140.8, 135.9, 128.8, 128.7, 128.2, 128.1, 126.7, 46.6, 46.1, 44.6, 21.1, 18.0.

Spectroscopic data for compound 31b:

¹H NMR (400 MHz, CDCl₃): δ 9.70 (t, *J* = 2.0 Hz, 1H), 7.48 – 7.23 (m, 5H), 7.20 (d, *J* = 8.0 Hz, 2H), 7.14 – 7.10 (m, 2H), 3.61 – 3.55 (m, 1H), 3.08 (dd, *J* = 13.5, 6.5 Hz, 1H), 3.01 – 2.93 (m, 1H), 2.88 – 2.84 (m, 2H), 2.76 – 2.69 (m, 2H), 1.34 (t, *J* = 7.5 Hz, 3H).

¹³C NMR (101 MHz, CDCl₃): δ 201.9, 143.6, 142.4, 136.5, 129.3, 128.7, 128.0, 127.7, 126.8, 49.0, 43.1, 42.2, 28.6, 15.7.

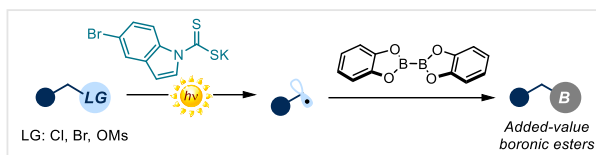
HRMS (ESI) Exact mass calculated for C₁₉H₂₄NaO₂ [M+CH₃OH+Na]⁺: 307.1669, found: 307.1665.

Chapter III

Photochemical Organocatalytic Borylation of Alkyl Chlorides, Bromides and Sulfonates

Target

Development of a photochemical organocatalytic method for the borylation of alkyl electrophiles.



Tool

Exploit the nucleophilic properties of dithiocarbamate catalysts to displace suitable leaving groups within alkyl electrophiles and generate a photolabile intermediate that produces radicals, which are then intercepted by a boron reagent.¹

3.1 Introduction

Boronic acids and esters are versatile compounds used in chemosensing,² medicinal chemistry³ and in material science.⁴ They are also of paramount importance in synthetic chemistry. For example, aromatic boronic acids and esters are extensively used to construct a variety of C-C bonds via the Suzuki-Miyaura⁵ and the Chan-Evans-Lam reaction.⁶ Additionally, boronic acids and esters can be readily converted into a variety of functional groups.⁷ As a consequence, the synthesis of these versatile aromatic boron derivatives has been widely explored.

¹ The project discussed in this Chapter has been conducted in collaboration with Dr Giandomenico Magagnano, who performed part of the optimization studies, part of the scope and the mechanistic investigation, and Dr. Bertrand Schweitzer-Chaput, who designed the organic catalyst. I was mainly involved in the discovery of the reaction, its optimization, and evaluation of part of the scope. This work has been published, see: Mazzarella, D.; Magagnano, G.; Schweitzer-Chaput, B.; Melchiorre, P. "Photochemical Organocatalytic Borylation of Alkyl Chlorides, Bromides, and Sulfonates" *ACS Catal.* **2019**, *9*, 5876-5880.

² Bull, S. D.; Davidson, M. G.; Van den Elsen, J. M. H.; Fossey, J. S.; Jenkins, A. T. A.; Jiang, Y.-B.; Marken, F.; Sakurai, K.; Zhao, J.; James, T. D. "Exploiting the Reversible Covalent Bonding of Boronic Acids: Recognition, Sensing, and Assembly" *Acc. Chem. Res.* **2013**, *46*, 312-326.

³ (a) Trippier, P. C.; McGuigan, C. "Boronic Acids in Medicinal Chemistry: Anticancer, Antibacterial and Antiviral Applications" *Med. Chem. Commun.* **2010**, *1*, 183-198. (b) Smoum, R.; Rubinstein, A.; Dembitsky, V. M.; Srebnik, M. "Boron Containing Compounds as Protease Inhibitors" *Chem. Rev.* **2012**, *112*, 4156-4220

⁴ Brooks, W. L. A.; Sumerline, B. S. "Synthesis and Applications of Boronic Acid-Containing Polymers: From Materials to Medicine" *Chem. Rev.* **2016**, *116*, 1375-1397.

⁵ (a) Miyaura, N.; Suzuki, A. "Palladium-Catalyzed Cross-Coupling Reactions of Organoboron Compounds" *Chem. Rev.* **1995**, *95*, 2457-2483. (b) Lennox, A. J. J.; Lloyd-Jones, G. C. "Selection of Boron Reagents for Suzuki-Miyaura Coupling" *Chem. Soc. Rev.* **2013**, *43*, 412-443.

⁶ Munir, I.; Zahoor, A. F.; Rasool, N.; Naqvi, S. A. R.; Zia, K. M.; Ahmad, R. "Synthetic applications and methodology development of Chan-Lam coupling: a review" *Mol. Div.* **2019**, *23*, 215-259.

⁷ Fyfe, J. W. B.; Watson, A. J. B. "Recent Developments in Organoboron Chemistry: Old Dogs, New Trick" *Chem* **2017**, *3*, 31-55.

Alkyl boronic acids and esters are also highly useful intermediates, which justifies the recent interest in developing effective methods for their preparation. Several transition-metal-catalyzed procedures for the borylation of alkyl electrophiles through the use of diboron compounds have been disclosed. These methods mainly rely on alkyl iodides and bromides, in combination with metals such as iron, nickel, copper and palladium, among others.⁸

Recently, metal-free methodologies have also been developed. In this context, radical-mediated processes, in which alkyl radicals are borylated with diboranes, have become increasingly important.⁹ However these strategies usually rely on the use of pendant redox-active auxiliaries, usually preinstalled within the substrates, to drive the formation of the alkyl radicals. In this vein, the development of an organocatalytic system for the borylation of readily available alkyl electrophiles, such as chlorides, bromides or sulfonates, which avoids the need for tailored substrates, would be synthetically appealing. This requires the development of a new radical generation approach, which does not require preinstalled redox-active moieties on the substrates. An overview of the different strategies available for effectively making radicals is discussed in the next section.

3.2 General Overview on Radical Generation Strategies

Free-radical chemistry is a powerful tool in synthetic organic chemistry. Radical strategies offer ways to synthesize molecules that are often complementary to the ionic pathways.¹⁰ Advances within this field have been stimulated by the identification of mild and practical radical-generating approaches. Classically, these strategies exploit two properties of the radical precursor: the redox properties and the bond dissociation energies (BDE).¹¹

3.2.1 Methods based on the redox properties

The ability of a given substrate to undergo a redox process is dependent on its electron affinity and ionization potential, thus on its ability to accept or donate one electron, respectively. Traditionally, redox processes were promoted either by stoichiometric reductants/oxidants or electrochemically (Figure 3.1).¹² The radical ion intermediate emerging from the single-electron transfer (SET) event then fragments to produce the desired radical **I**. Generally, these strategies require harsh conditions, such as high temperatures and hazardous reagents in usually superstoichiometric amounts.

⁸ Kubota, K.; Iwamoto, H.; Ito, H. "Formal Nucleophilic Borylation and Borylative Cyclization of Organic Halides" *Org. Biomol. Chem.* **2017**, *15*, 285-300.

⁹ Friese, F. W.; Studer, A. "New avenues for C–B bond formation *via* radical intermediates" *Chem. Sci.* **2019**, *10*, 8503-8518.

¹⁰ Renaud, P.; Sibi, M. P. "Radicals in Organic Synthesis" **2001**, Wiley-VCH.

¹¹ Lalevée, J.; Fouassier, J. P. "Encyclopedia of Radicals in Chemistry, Biology and Materials, Vol 1." **2012**, John Wiley & Sons.

¹² Kingston, C.; Palkowitz, M. D.; Takahira, Y.; Vantourout, J. C.; Peters, B. K.; Kawamata, Y.; Phil S. Baran "A Survival Guide for the "Electro-curious"" *Acc. Chem. Res.* **2020**, *53*, 72-83.

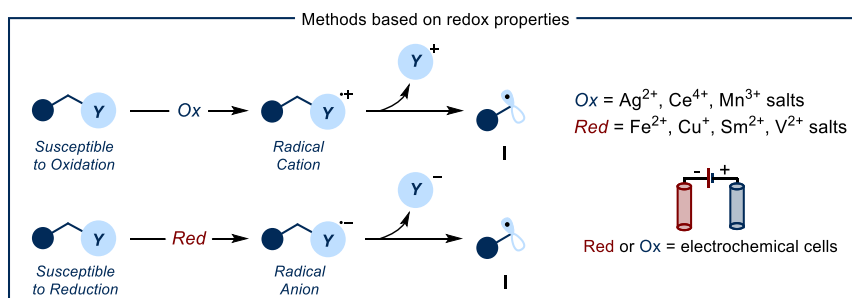


Figure 3.1: Formation of radicals exploiting the redox properties of suitable precursors. Ox: Oxidant. Red: Reductant.

Photoredox catalysis has recently provided a strategy to mitigate many of these limitations, since it can catalytically generate radicals under mild conditions and under visible light irradiation.¹³ This photochemical approach uses a photocatalyst (PC, Figure 3.2), that can absorb light in the visible range to access an electronically excited state (PC^*). The excited intermediate can activate redox-active substrates via an SET manifold, ultimately producing the desired radical **I** and the oxidized or reduced form of the photocatalyst (PC^{I}). A second SET event turns over PC^{I} to form the original catalyst PC, enabling its use as a catalyst.

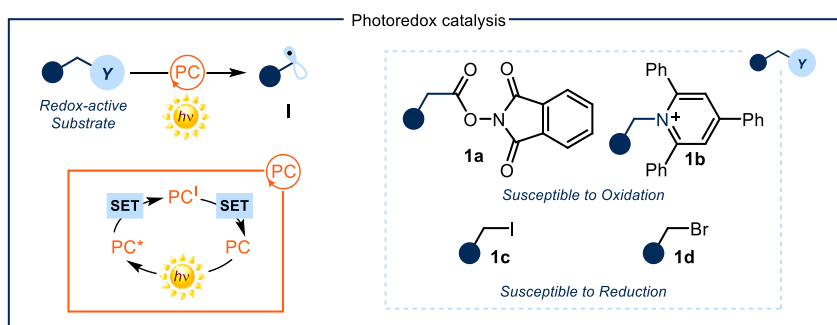


Figure 3.2: Formation of radicals through photoredox catalysis and the use of redox-active substrates. PC: Photocatalyst. SET: Single-electron transfer.

The mild experiment conditions, along with the well-studied redox properties of both photocatalysts and radical precursors,¹⁴ have quickly established photoredox catalysis as an effective and flexible radical generation strategy. However, because of its mechanism, this strategy is inextricably linked with the redox properties of the substrate. This means that purposely designed substrates, adorned with redox-active moieties, such as *N*-(acyloxy)phthalimides **1a** (Figure 3.2) and Katritzky *N*-

¹³ (a) Shaw, M. H.; Twilton, J.; MacMillan, D. W. C. "Photoredox Catalysis in Organic Chemistry" *J. Org. Chem.* **2016**, *81*, 6898-6926. (b) Matsui, J. K.; Lang, S. B.; Heitz, D. R.; Molander, G. A. "Photoredoxmediated Routes to Radicals: the Value of Catalytic Radical Generation in Synthetic Methods Development" *ACS Catal.* **2017**, *7*, 2563-2575.

¹⁴ (a) Pitre, S. P.; McTiernan, C. D.; Scaiano, J. C. "Library of Cationic Organic Dyes for Visible-Light-Driven Photoredox Transformations" *ACS Omega* **2016**, *1*, 66-76. (b) Roth, H. G.; Romero, N. A.; Nicewicz, D. A. "Experimental and Calculated Electrochemical Potentials of Common Organic Molecules for Applications to Single-Electron Redox Chemistry" *Synlett.* **2016**, *27*, 714-723.

alkylpyridinium salts **1b**, or easily reducible organic iodides **1c** or bromides **1d** are necessary to favor the SET event and the subsequent radical formation.

3.2.2 Methods based on bond dissociation energies (BDE)

In an alternative strategy, the generation of an open-shell intermediate can be elicited exploiting the BDE of a given bond within the radical precursor. Traditionally, this approach has used stoichiometric amounts of initiators (In-In, Figure 3.3),^{11,15} which are high-energy compounds containing at least one weak bond. Homolysis of this weak bond, promoted by either high temperatures or UV-light irradiation, generates radical intermediate In· that interacts with the substrate through hydrogen or halogen atom abstraction, furnishing the desired radical **I**.

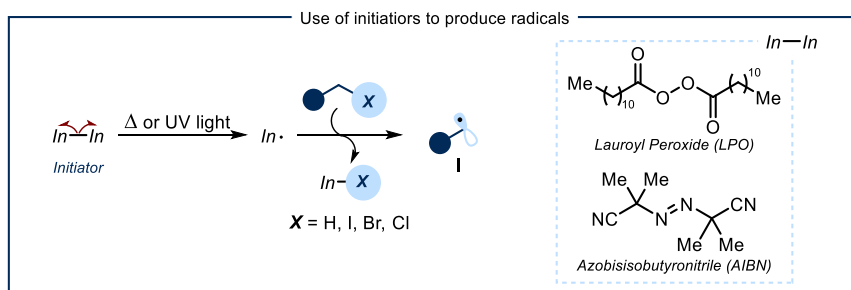


Figure 3.3: Formation of radicals from precursors with appropriate bond dissociation energies using initiators (In-In).

In the 1980s, Barton developed an effective approach¹⁶ based on thiocarbonyl-based reagents **4** (Figure 3.4). These substrates are readily available through the condensation of carboxylic acids **2** with *N*-hydroxy-2-thiopyridone **3**. The versatility of substrates **4**, also known as Barton esters, allows the generation of radicals not only through exogenous initiators, but also upon direct thermolysis or photolysis. Radicals are therefore generated by the cleavage of the labile N-O bond within **4**. When using an initiator, the resulting In· adds on the sulfur atom within **4** to trigger a sequence of bond breaking/forming event, ultimately leading to **5** and the acyloxy radical **II**. The latter rapidly undergoes decarboxylation to yield the target radical **I**.

¹⁵ Denisov, E. T.; Denisova, T. G.; Pokidova, T. S. "Handbook of Free Radical Initiators" 2005, John Wiley & Sons.

¹⁶ (a) Barton, D. H. R.; Crich, D.; Motherwell, W. B. "New and Improved Methods for the Radical Decarboxylation of Acids" *J. Chem. Soc., Chem. Commun.* **1983**, 939-941. (b) Barton, D. H. R.; Hervé, Y.; Potier, P.; Thierry, J. "Reductive Radical Decarboxylation of Amino-Acids and Peptides" *J. Chem. Soc., Chem. Commun.* **1984**, 1298-1299. (c) Barton, D. H. R.; Crich, D.; Motherwell, W. B. "The Invention of New Radical Chain Reactions. Part VII. Radical Chemistry of Thiohydroxamic Esters: A New Method for the Generation of Carbon Radicals from Carboxylic Acids" *Tetrahedron* **1985**, *41*, 3901-3924.

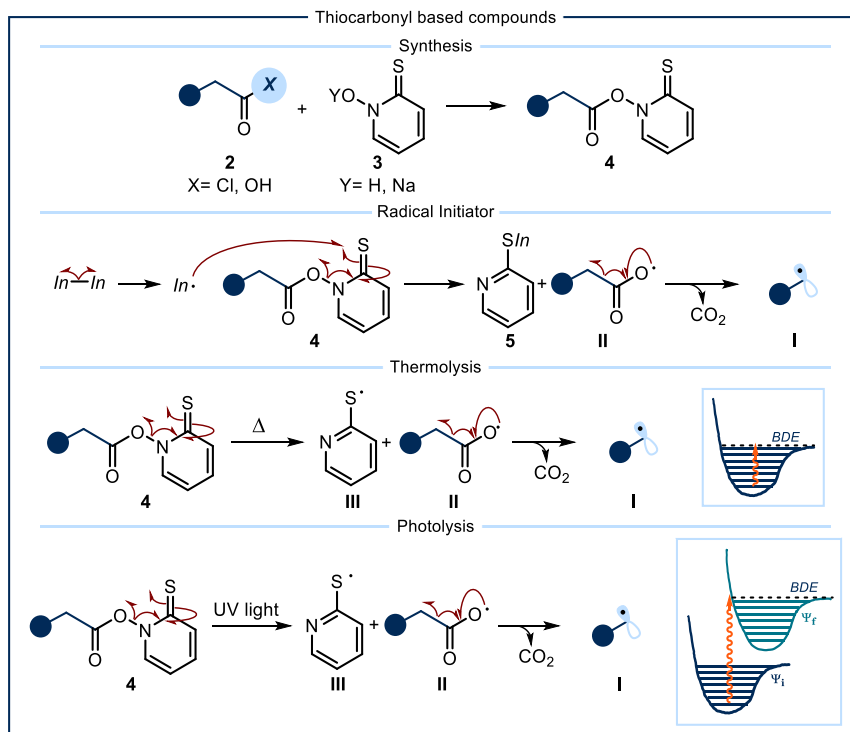


Figure 3.4: Synthesis and use of Barton esters for the generation of radicals through the use of stoichiometric initiators, thermolysis and photolysis. In: Initiator. BDE: Bond dissociation energy.

The labile N-O bond in **4** is so weak that can be cleaved through thermolysis. The computed BDE of the N-O bond in **4** is ~ 28 Kcal/mol,¹⁷ thus the fragmentation can be readily promoted using temperatures higher than 62 °C. Moreover, the *N*-hydroxy-2-thiopyridone chromophore within **4** possesses an absorption maximum at ~ 365 nm.¹⁸ The energy corresponding to this wavelength is ~ 78 Kcal/mol, more than enough to induce the fragmentation of the N-O bond within **4** upon excitation.

Another class of thiocarbonyl compounds useful for the generation of radical intermediates are xanthates and dithiocarbamates **8** (Figure 3.5), developed by Zard.¹⁹ These compounds can be readily synthesized by reacting electrophiles **6** bearing a suitable leaving group with a sulfur anion salt **7**. As a consequence, alkyl halides can be activated and employed to form radical intermediates.

¹⁷ For computational details, see: Allonas, X.; Dietlin, C.; Fouassier, J.-P.; Casiraghi, A.; Visconti, M.; Norcini, G.; Bassi, G. "Barton Esters as New Radical Photoinitiators for Flat Panel Display Applications" *J. Photopolym. Sci. Technol.* **2008**, *21*, 505-509.

¹⁸ (a) Barton, D. H. R.; Blundell, P.; Jaszberenyi, J. C. Quantum Yields in the Photochemically Induced Radical Chemistry of Acyl Derivatives of Thiohydroxamic Acids. *J. Am. Chem. Soc.* **1991**, *113*, 6937-6942. (b) Barton, D. H. R.; Jaszberenyi, J. C.; Tang, D. Photolytic Generation of Carbon Radicals from Barton Esters: Recent Developments. *Tetrahedron Lett.* **1993**, *34*, 3381-3384.

¹⁹ (a) Zard, S. Z. "On the Trail of Xanthates: Some New Chemistry from an Old Functional Group" *Angew. Chem. Int. Ed.* **1997**, *36*, 672-685. (b) Quiclet-Sire, B.; Zard, S. Z. "Powerful Carbon-Carbon Bond Forming Reactions Based on a Novel Radical Exchange Process" *Chem. Eur. J.* **2006**, *12*, 6002-6016.

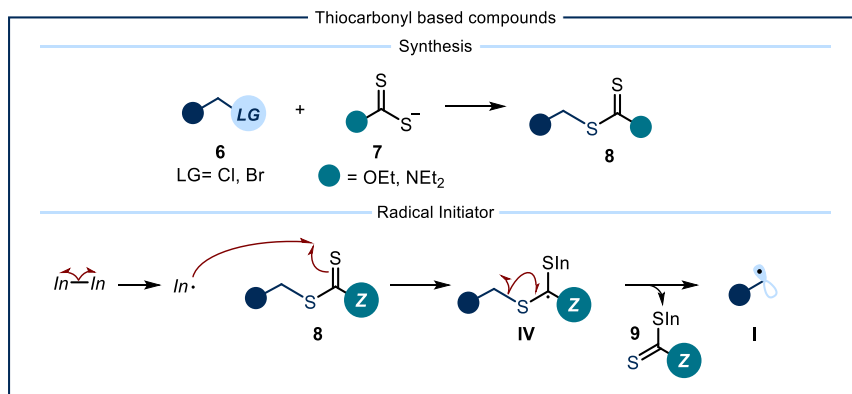


Figure 3.5: Synthesis and use of xanthates for the generation of radicals through the use of initiators. LG: Leaving group. In: Initiator.

Analogously to the Barton esters **4** (Figure 3.4), xanthates and dithiocarbamates **8** possess a weak C-S bond²⁰ that can be homolytically cleaved using a radical initiator or by direct thermolysis or photolysis. When using radical initiators, $\text{In}\cdot$ adds onto the sulphur atom within **8**, leading to radical **IV** which collapses to produce **9** and the target radical **I**. The photolysis of intermediates **8** is also a viable option for radical generation (Figure 3.6). To ensure a more efficient absorption, the xanthate derivative is generally adorned with a better chromophoric unit. For example, carbazole derivative **8c** can undergo homolytic cleavage to form radical **I** upon light irradiation.²⁰

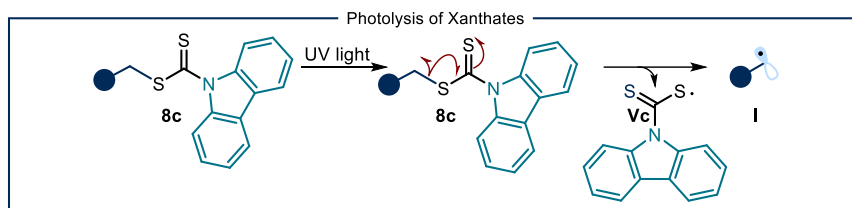


Figure 3.6: Photolysis of the C-S bond within **8c** facilitated by the employment of the carbazole chromophore.

Despite their undoubted synthetic value, all the aforementioned methods rely on the use of purposely designed stoichiometric substrates, which require at least one additional step to install the fragmenting unit within **4** or **8**.

3.3 A New Photochemical Radical-Generating Strategy

The radical-generating approaches reported so far exploit either the redox properties or the BDE of the radical precursors. Recently, our research group has developed a method to produce radicals solely harnessing the electrophilic properties of the substrate.²¹ This approach was developed by shifting the previously discussed Zard's

²⁰ Lalevée, J.; Blanchard, N.; El-Roz, M.; Allonas, X.; Fouassier, J. P. "New Photoiniferters: Respective Role of the Initiating and Persistent Radicals" *Macromolecules* **2008**, *41*, 2347-2352.

²¹ Schweitzer-Chaput, B.; Horwitz, M. A.; de Pedro Beato, E.; Melchiorre, P. "Photochemical generation of radicals from alkyl electrophiles using a nucleophilic organic catalyst" *Nat. Chem.* **2019**, *11*, 129-135.

xanthate chemistry¹⁹ to a catalytic regime. This shift was achieved by designing a nucleophilic dithiocarbonyl catalyst (DTC catalyst, Figure 3.7) that could activate alkyl electrophiles **6** through a bimolecular nucleophilic substitution (S_N2) pathway. The resulting intermediate **8** can absorb a photon to subsequently undergo C-S bond cleavage, producing the desired radical **I** and the sulfur centered radical **V**. In our strategy, we found a way to reduce the sulfur radical **V** via an SET mechanism, therefore turning over the DTC catalyst and making the overall process catalytic.

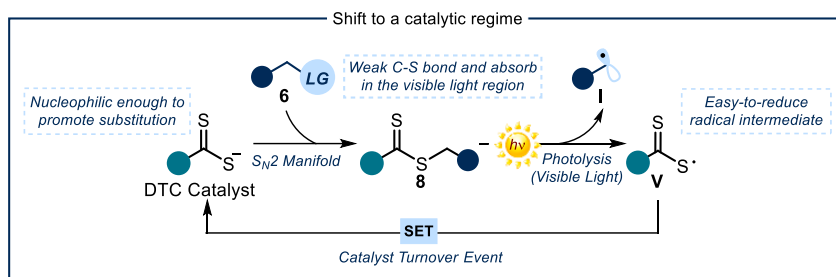


Figure 3.7: Thiocarbonyl compounds as catalysts to promote the formation of radicals via an S_N2 pathway.

Four aspects were crucial for the development of this photochemical catalytic strategy: i) the DTC catalyst has to be nucleophilic enough to efficiently displace the leaving group within substrate **6** and produce the intermediate **8**; ii) **8** has to productively absorb light, preferably within the visible range; iii) the BDE of the C-S bond within **8** has to be sufficiently low to promote its cleavage upon light absorption; iv) finally, the sulfur-centered radical **V**, emerging from the photolysis, should easily accept one electron to turnover the DTC catalyst. All these requirements were fulfilled by the dithiocarbamate salt **A** (Figure 3.8a), a derivative decorated with an indole unit as a chromophore. This catalyst was employed to promote a Giese-type addition of alkyl electrophiles **6**, which were unsuitable radical precursors in other radical generation strategies, to electron-poor olefins **9**. Mechanistically, the nucleophilic catalyst **A** (Figure 3.8b) reacts with the alkyl electrophile **6** to promote, after nucleophilic displacement,²² the visible light-absorbing intermediate **8a**. Photolysis of **8a** using 465 nm light irradiation produces the dithiocarbonyl radical **Va** and the alkyl radical **I**. The latter can react with electron-poor olefins **9** to forge a new C-C bond. The ensuing electrophilic radical **VIa** can abstract a hydrogen atom from an appropriate donor, such as γ -terpinene, to yield product **10** and the cyclohexadienyl radical **VII**. At this stage, an exergonic SET between the dithiocarbonyl radical **Va** ($E(A/Va) = +0.44$ V versus Ag/Ag^+ in CH_3CN)²³ and the cyclohexadienyl radical **VII** ($E_{red} = -0.05$ V versus Ag/Ag^+ in CH_3CN)²⁴ closes the catalytic cycle by regenerating catalyst **A**.

²² Duan, X.-H.; Maji, B.; Mayr, H. "Characterization of the Nucleophilic Reactivities of Thiocarboxylate, Dithiocarbonate and Dithiocarbamate Anions" *Org. Biomol. Chem.* **2011**, *9*, 8046-8050.

²³ Dag, Ö.; Yaman, S. Ö.; Önal, A. M.; İsci, H. "Spectroelectrochemistry of Potassium Ethylxanthate, Bis(ethylxanthato)nickel(II) and Tetraethylammonium Tris(ethylxanthato)nickel(II)" *J. Chem. Soc., Dalton Trans.*, **2001**. 2819-2824.

²⁴ Bahtia, K.; Schuler, R. H. Oxidation of Hydroxycyclohexadienyl Radical by Metal Ions. *J. Phys. Chem.* **1974**, *78*, 2335-2338.

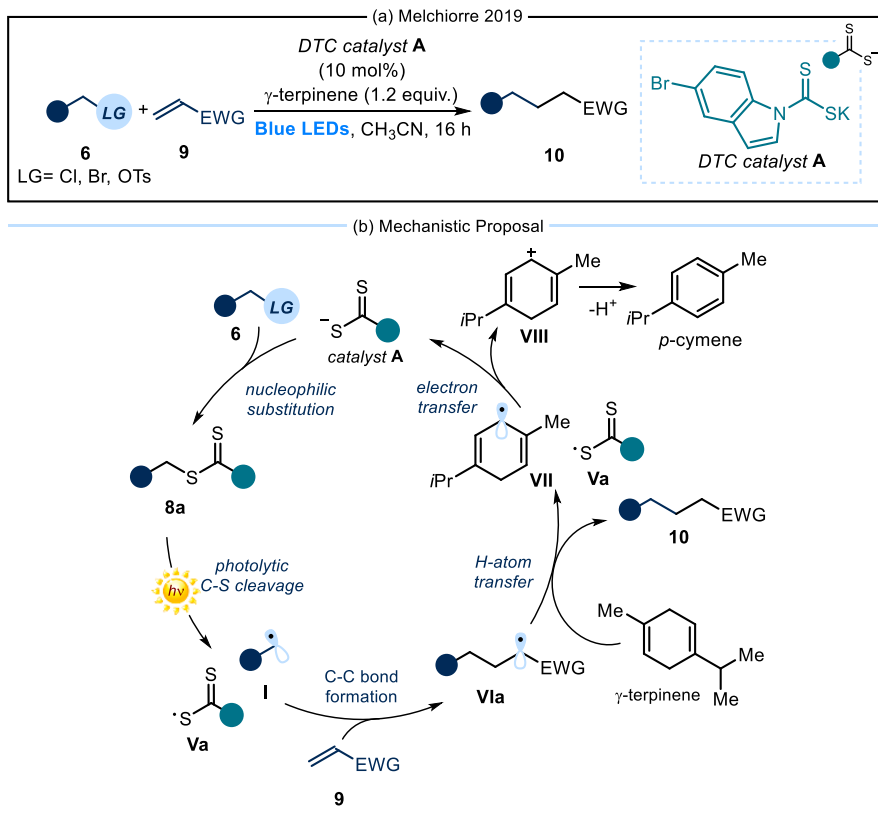


Figure 3.8: (a) Giese-type addition of alkyl electrophiles **6** on electron-poor olefins **9** developed by Melchiorre. (b) Proposed mechanism. EWG: Electron-withdrawing group. DTC: Dithiocarbamate. LEDs: Light emitting diodes.

3.4 Target of the Project

The aim of the project discussed in this chapter was to expand the synthetic applicability of the catalytic dithiocarbonyl strategy. Specifically, our target was to exploit this mild radical-generating strategy to develop a metal-free photochemical radical borylation of not activated alkyl halides, including chlorides.

3.4.1 Methods for the synthesis of alkyl boronic derivatives

A classical way to obtain alkyl boronic acid derivatives is through hydroboration of alkenes. Alternatively, these compounds can be readily synthesized from the corresponding organo-lithium and organo-magnesium reagents through transmetalation.²⁵ Both strategies suffer from functional group incompatibility and regioselectivity issues. Moreover, in the second strategy, super-stoichiometric quantities of magnesium or organolithium reagents are required. A more effective approach relies on transition-metal-catalyzed processes, where the metal catalyst

²⁵ Hall, D, G, "Boronic Acids: Preparation and Applications in Organic Synthesis, Medicine and Materials" 2011, Wiley-VCH.

activates alkyl halides and functionalizes them with a diboron reagent (Figure 3.9a).⁹ The majority of these strategies uses alkyl iodides and bromides,²⁶ while few processes, based on manganese and copper,²⁷ have been described for the borylation of unactivated alkyl chlorides.

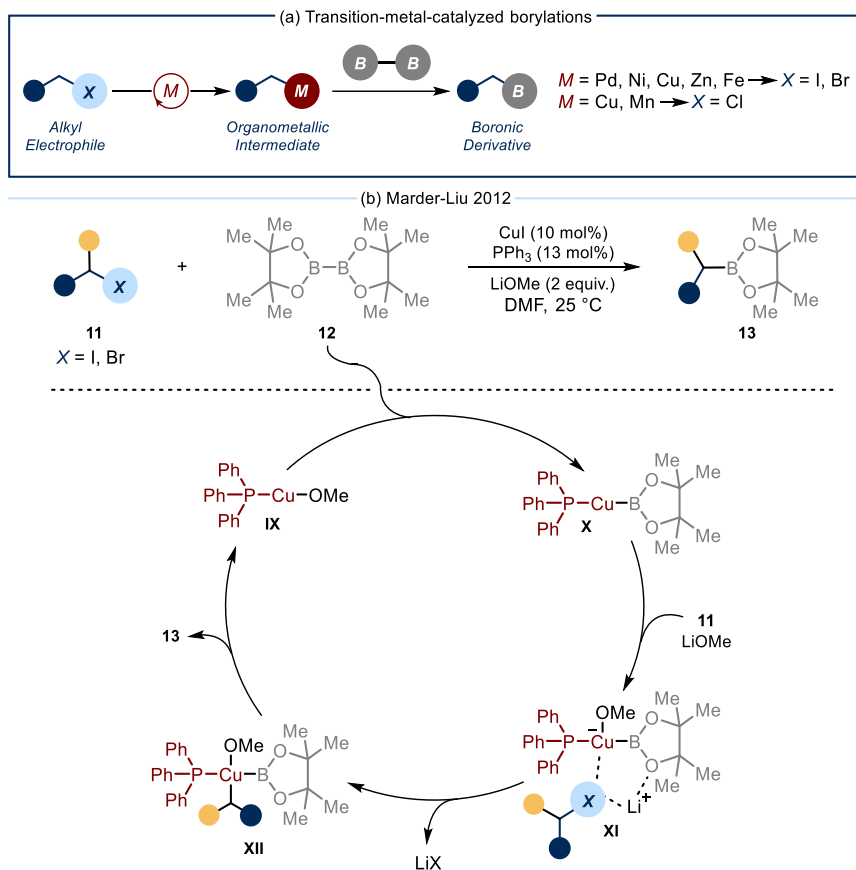


Figure 3.9: (a) General representation of transition-metal-catalyzed borylation processes. (b) Copper-catalyzed borylation developed by Marder and Liu. DMF: Dimethylformamide.

²⁶ Selected examples: (a) Yang, C.-T.; Zhang, Z.-Q.; Tajuddin, H.; Wu, C.-C.; Liang, J.; Liu, J.-H.; Fu, Y.; Czyzewska, M.; Steel, P. G.; Marder, T. B.; Liu, L. "Alkylboronic Esters from Copper-Catalyzed Borylation of Primary and Secondary Alkyl Halides and Pseudohalides" *Angew. Chem. Int. Ed.* **2012**, *51*, 528-532. (b) Dudnik, A. S.; Fu, G. C. "Nickel-Catalyzed Coupling Reactions of Alkyl Electrophiles, Including Unactivated Tertiary Halides, to Generate Carbon-Boron Bonds" *J. Am. Chem. Soc.* **2012**, *134*, 10693-10697. (c) Bose, S. K.; Fucke, K.; Liu, L.; Steel, P. G.; Marder, T. B. "Zinc-catalyzed Borylation of Primary, Secondary and Tertiary Alkyl Halides with Alkoxy Diboron Reagents at Room Temperature" *Angew. Chem., Int. Ed.* **2014**, *53*, 1799-1803.

²⁷ (a) Atack, T. C.; Cook, S. P. "Manganese-Catalyzed Borylation of Unactivated Alkyl Chlorides" *J. Am. Chem. Soc.* **2016**, *138*, 6139-6142. (b) Bose, S. K.; Brand, S.; Omeregic, H. O.; Haenel, M.; Maier, J.; Bringmann, G.; Marder, T. B. "Highly Efficient Synthesis of Alkylboronate Esters via Cu(II)-Catalyzed Borylation of Unactivated Alkyl Bromides and Chlorides in Air" *ACS Catal.* **2016**, *6*, 8332-8335.

One of the first examples was reported by Liu, Marder and co-workers (Figure 3.9b).^{26a} A simple copper/triphenylphosphine complex, in the presence of LiOMe as a base additive in dimethylformamide (DMF), enabled the borylation of primary and secondary alkyl bromides and iodides **11** with bis(pinacolato)diboron **12**. Mechanistically, this reaction proceeds through the base-promoted formation of the Cu(I)/boryl complex **X** that is responsible for the activation of the alkyl halides **11**. Experimental results suggest that this activation proceeds through an SET oxidative addition within **XI** thus generating complex **XII** that, upon reductive elimination, furnishes product **13** and restores catalyst **IX**.

These processes, although successful, require the use of transition metal catalysts, which might be incompatible with *N*-heterocycle-containing substrates because of deleterious heteroatom-catalyst binding effects. Indeed, *N*-heterocyclic moieties, which are common motifs in drug molecules, generally represent a significant tolerability challenge for transition-metal promoted synthetic methods.²⁸ As a result, few metal-based borylation methods compatible with heteroarenes containing multiple heteroatoms and high nitrogen content have been reported so far.²⁹

Borylation methods that do not require the use of a metal catalyst have also been developed. Among these, photochemically driven methodologies have attracted increasing interest for their mild reaction conditions and for the good functional group tolerance. These protocols take advantage of the ability of diboranes to intercept radical intermediates (Figure 3.10a).⁹ However, one of the main drawback is the requirement of tailored substrates, prefunctionalized with redox-active moieties, to facilitate the alkyl radical formation upon SET activation. As an example, the group of Aggarwal³⁰ used alkyl derivatives bearing different redox-active groups, such as *N*-(acyloxy)phthalimides **14a**,^{30a} Katritzky *N*-alkylpyridinium salts **14b**^{30b,d} and thionocarbonates **14c**,^{30c} in photochemical borylation processes using bis(catecholato)diboron (B_2cat_2) **15** (Figure 3.10b).

²⁸ (a) Blakemore, D. C.; Castro, L.; Churcher, I.; Rees, D. C.; Thomas, A. W.; Wilson, D. M.; Wood, A. "Organic Synthesis Provides Opportunities to Transform Drug Discovery" *Nat. Chem.* **2018**, *10*, 383-394. (b) Pitt, W. R.; Parry, D. M.; Perry, B. G.; Groom, C. R. "Heteroaromatic Rings of the Future" *J. Med. Chem.* **2009**, *52*, 2952-2963.

²⁹ For examples discussing catalyst poisoning in various metal-catalyzed reactions, see: (a) Kudo, N.; Perseghini, M.; Fu, G. C. "A Versatile Method for Suzuki Cross-Coupling Reactions of Nitrogen Heterocycles" *Angew. Chem., Int. Ed.* **2006**, *45*, 1282-1284. (b) Ge, S.; Hartwig, J. F. "Highly Reactive, Single-Component Nickel Catalyst Precursor for Suzuki-Miyaura Cross-Coupling of Heteroaryl Boronic Acids with Heteroaryl Halides" *Angew. Chem., Int. Ed.* **2012**, *51*, 12837-12841. (c) Düfert, M. A.; Billingsley, K. L.; Buchwald, S. L. "Suzuki-Miyaura Cross-Coupling of Unprotected, Nitrogen-Rich Heterocycles: Substrate Scope and Mechanistic Investigation" *J. Am. Chem. Soc.* **2013**, *135*, 12877-12885. (d) Shang, M.; Sun, S.-Z.; Dai, H.-X.; Yu, J.-Q. "Cu(II)-Mediated C-H Amidation and Amination of Arenes: Exceptional Compatibility with Heterocycles" *J. Am. Chem. Soc.* **2014**, *136*, 3354-3357. (e) Liu, Y.-J.; Xu, H.; Kong, W.-J.; Shang, M.; Dai, H.-X.; Yu, J.-Q. "Overcoming the limitations of directed C-H functionalizations of heterocycles" *Nature* **2014**, *515*, 389-393.

³⁰ (a) Fawcett, A.; Pradeilles, J.; Wang, Y.; Mutsuga, T.; Myers, E. L.; Aggarwal, V. K. "Photoinduced decarboxylative borylation of carboxylic acids" *Science* **2017**, *357*, 283-286. (b) Wu, J.; He, L.; Noble, A.; Aggarwal, V. K. "Photoinduced Deaminative Borylation of Alkylamines" *J. Am. Chem. Soc.* **2018**, *140*, 10700-10704. (c) Wu, J.; Bar, R. M.; Guo, L.; Noble, A.; Aggarwal, V. K. "Photoinduced Deoxygenative Borylations of Aliphatic Alcohols" *Angew. Chem., Int. Ed.* **2019**, *58*, 18830-18834. For a related study, see: (d) Sandfort, F.; Strieth-Kalthoff, F.; Klauk, F. J. R.; James, M. J.; Glorius, F. Deaminative "Borylation of Aliphatic Amines Enabled by Visible Light Excitation of an Electron Donor-Acceptor Complex" *Chem. - Eur. J.* **2018**, *24*, 17210-17214.

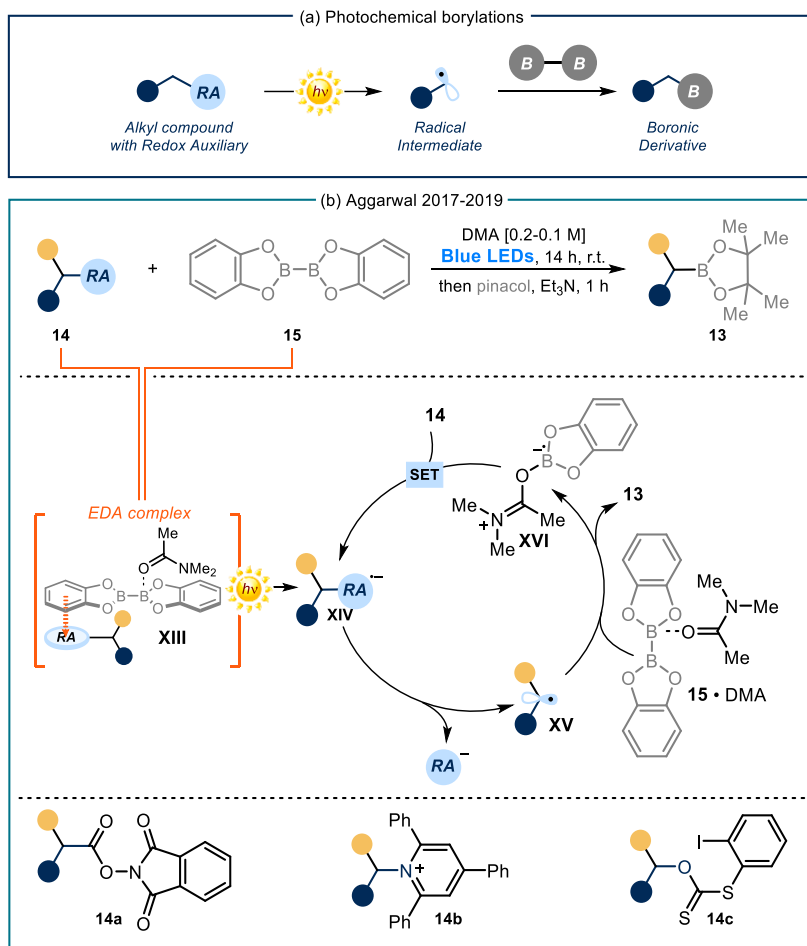


Figure 3.10: (a) General representation of photochemical borylation processes with diboron reagents. (b) Photochemistry of an electron-donor acceptor (EDA) complex XIII triggers the borylation of carboxylic acids, amines and alcohols derivatives. DMA: Dimethylacetamide. LEDs: Light emitting diodes

In these examples, the pendant redox-active groups have a dual function: first, these moieties trigger the formation of the photoactive intermediates. This is because the electron-poor redox active moiety within substrate **14** forms an EDA complex XIII upon charge-transfer interaction with an electron-rich adduct generated from $B_2\text{cat}_2$ and dimethylacetamide (15^\bulletDMA).³¹ The EDA complex XIII can absorb visible light. Irradiation promotes an intra-complex SET that affords the radical anion XIV. The redox auxiliary groups are then readily extruded, ultimately affording the radical XV which is trapped by a second molecule of 15^\bulletDMA . This radical trapping event produces the borylated product **13** while forming the boryl radical XVI which can reduce ($E_{1/2} = -1.53$ V vs SCE)^{30d} a second molecule of **14**, promoting the formation of radical anion

³¹ (a) Mulliken, R. S. "Molecular Compounds and their Spectra. II" *J. Am. Chem. Soc.* **1952**, *74*, 811-824. (b) Crisenza, G. E. M.; Mazzarella, D.; Melchiorre, P. "Synthetic Methods Driven by the Photoactivity of Electron Donor-Acceptor Complexes" *J. Am. Chem. Soc.* **2020**, *141*, 5461-5476.

XIV, thus feeding a radical chain propagation manifold. Despite the broad applications, these strategies, which are based on redox-active moieties on the substrates, suffer from poor atom-economy.

This limitation has been overcome by the group of Studer.³² They reported a strategy to readily convert alkyl iodides **16** into boronic derivatives **13** by simply shining visible light on the reaction mixture in the presence of B_2cat_2 **15** (Figure 3.11). Light radiation elicits the homolytic cleavage of the weak C-I bond within the substrate, producing the alkyl radical **XV**. This intermediate is rapidly trapped by B_2cat_2 , affording radical **XVII** which is subsequently intercepted by DMF, furnishing **XVIII**. This radical rapidly collapses to afford product **13** along with the boryl radical **XVI**. The latter can activate a second molecule of iodide **16** by either SET or iodine atom abstraction, regenerating radical **XV**, hence feeding a radical chain manifold. Primary, secondary and tertiary derivatives are all amenable to this photochemical borylation protocol, highlighting the generality of the reaction. However, despite the clear improvement in terms of atom economy, this methodology relies on the use of highly unstable alkyl iodides as radical precursors.

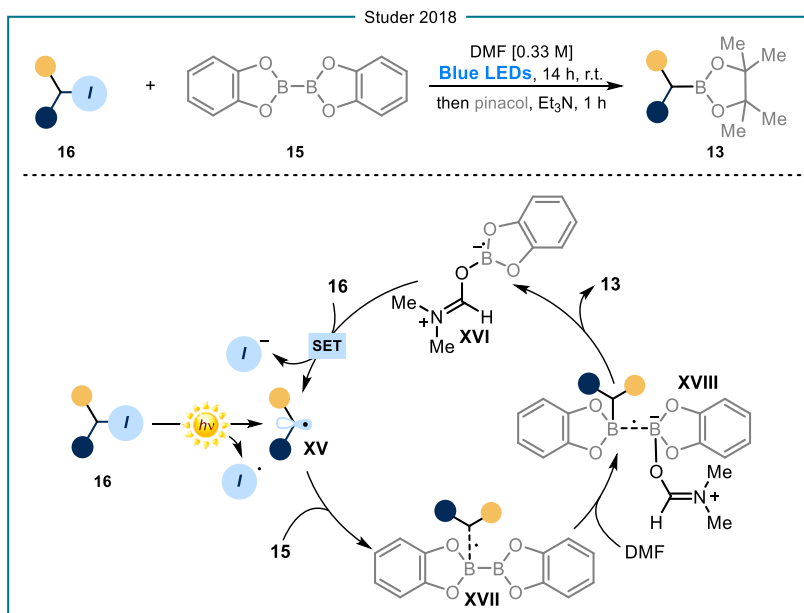


Figure 3.11: Photochemical borylation of alkyl iodides.

3.4.2 Design plan

We wondered whether the ability of B_2cat_2 **15** to intercept carbon radicals could be coupled with the photochemical S_N2 -based radical generation strategy for the activation of alkyl electrophiles previously developed in our laboratories (e.g. Figure 3.8). If successful, this approach would offer a metal-free radical borylation of readily

³² Cheng, Y., Mück-Lichtenfeld, C., Studer, A. "Metal-Free Radical Borylation of Alkyl and Aryl Iodides" *Angew. Chem. Int. Ed.* **2018**, *57*, 16832-16836.

available alkyl chlorides, bromides and sulfonates **6**. As detailed in Figure 3.12a, we envisioned that a S_N2 reaction of the organic catalyst **A** with substrate **6** would form the light-absorbing adduct **8a**. Photolysis of the latter would produce the alkyl radical **I**, which can be rapidly captured by the diboron reagent **15** to afford the borylated product **13**. In order to employ **A** in catalytic amounts, the boryl radical **XIX** (Figure 3.12b), formed after radical trap of **I** by **15**, should transfer one electron to the xanthyl radical **Va**, thus regenerating the catalyst **A** while producing cation **XX**.

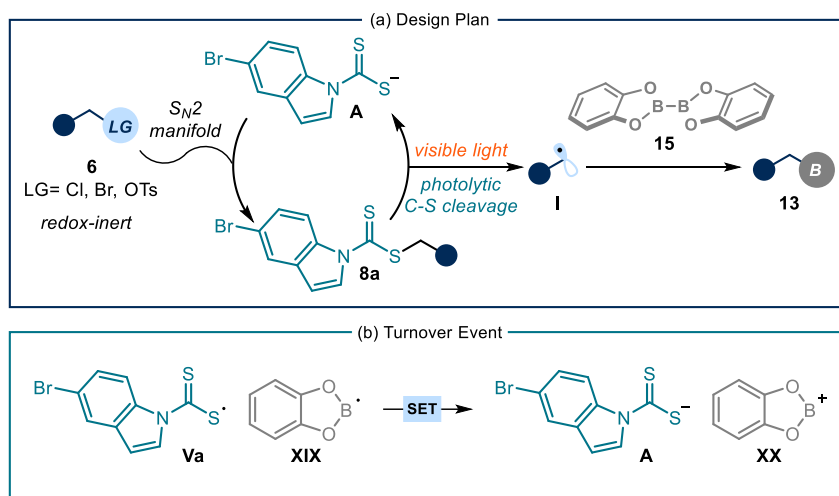


Figure 3.12: (a) Design plan for the photochemical organocatalytic borylation of alkyl electrophiles. (b) Turnover event to secure catalysis.

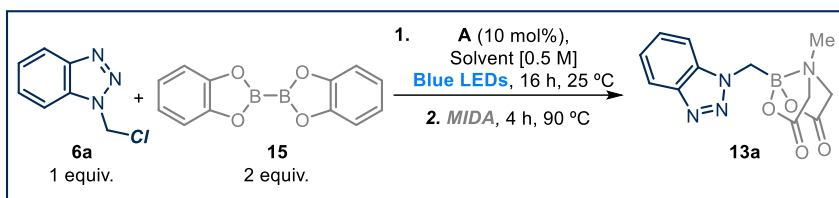
Overall, this strategy would enable the easy conversion of alkyl electrophiles **6** into value-added boronic derivatives **13** without the need of a metal catalyst, under mild conditions and with high atom-economy.

3.5 Results and Discussion

3.5.1 Reaction optimization

The feasibility of the plan was evaluated by exploring the reactivity of the commercially available 1-(chloromethyl)-1*H*-benzotriazole **6a** (Figure 3.13) as the radical precursor. The choice of this reagent was guided by our desire to develop a metal-free protocol that could activate difficult to reduce alkyl chlorides and, at the same time, tolerate sensitive functional moieties, such as *N*-heterocyclic ones. The reaction was conducted at ambient temperature using 2 equivalents of B_2cat_2 **15**. As catalyst, we selected the indole-containing dithiocarbamate **A**, which allowed the use of a light source centered at 465 nm to promote the photolysis of the corresponding intermediate **8a**.

We started our optimization by evaluating the influence of different (Table 3.1). After 16 hours, the crude mixture was treated with 4 equivalents of methyliminodiacetic acid (MIDA) at 90 °C to promote ligand exchange and generate the more stable MIDA boronate **13a**.

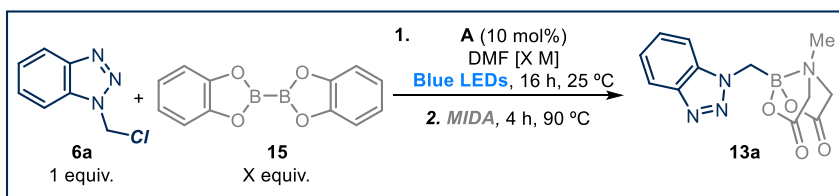
Table 3.1: Effect of the solvent on the photochemical organocatalytic borylation.^a

Entry	Solvent	Yield
1	DMF	83%
2	DMA	82%
3	ACN	-
4	DMSO	-

^aReaction performed on a 0.2 mmol scale. Yield refers to the isolated product **13a** after chromatographic purification on silica gel. DMF: Dimethylformamide. LEDs: Light Emitting Diodes. MIDA: Methyliminodiacetic acid.

In analogy to the reports of Aggarwal³⁰ and Studer,³² we reasoned that the use of a solvent that could coordinate the boron atom of B_2cat_2 **15** acting as a Lewis base, thus stabilizing the ensuing boryl radical **XIX**, could favor the borylation process. Indeed, the use of dimethylformamide (DMF, entry 1) or dimethylacetamide (DMA, entry 2) afforded **13a** in very good yields. Accordingly, the use of acetonitrile (ACN, entry 3), a solvent with diminished Lewis basic properties compared to DMF and DMA, completely inhibited the reaction. Surprisingly, the use of dimethylsulfoxide (DMSO, entry 4), a solvent characterized by enhanced Lewis basic properties compared to DMF and DMA, also inhibited the reaction.

Having identified DMF as the most suitable solvent, we tested the effects of a different stoichiometry of **6a** and **15** and different concentrations of the reaction (Table 3.2).

Table 3.2: Effect of stoichiometry and concentration on photochemical organocatalytic borylation.^a

Entry	6a : 15	Concentration	Yield
1	1 : 1.5	[0.5 M]	65%
2	1 : 1	[0.5 M]	36%
3	1 : 2	[1 M]	70%
4	1 : 2	[0.25 M]	68%

^aReaction performed on a 0.2 mmol scale. Yield refers to the isolated product **13a** after chromatographic purification on silica gel.

Lowering the amount of **15** to 1.5 or 1 equiv. (entries 1 and 2, respectively) resulted in a diminished reactivity. Increasing (entry 3) or decreasing (entry 4) the concentration of the reaction also proved detrimental for efficiency (compared with entry 1 in Table 3.1). We then demonstrated that this process is amenable to a preparative scale. Indeed, a 25-fold scale up of the model reaction (5 mmol) furnished product **13a** in 52% yield (750 mg) using the same experimental setup as for the 0.2 mmol process.

3.5.2 Scope of the reaction

Adopting the optimized conditions reported in entry 1, Table 3.1, we set to demonstrate the generality of the photochemical organocatalytic borylation of alkyl electrophiles **6**. We first demonstrated that not only MIDA (**13b**, Figure 3.13), but also pinacol in triethylamine could be used to provide the corresponding pinacol boronic esters of type **13c**. Due to the superior stability of the corresponding adducts, we preferentially used MIDA. However, we note that pinacol in triethylamine can be used in all cases to provide the corresponding pinacol boronic esters.

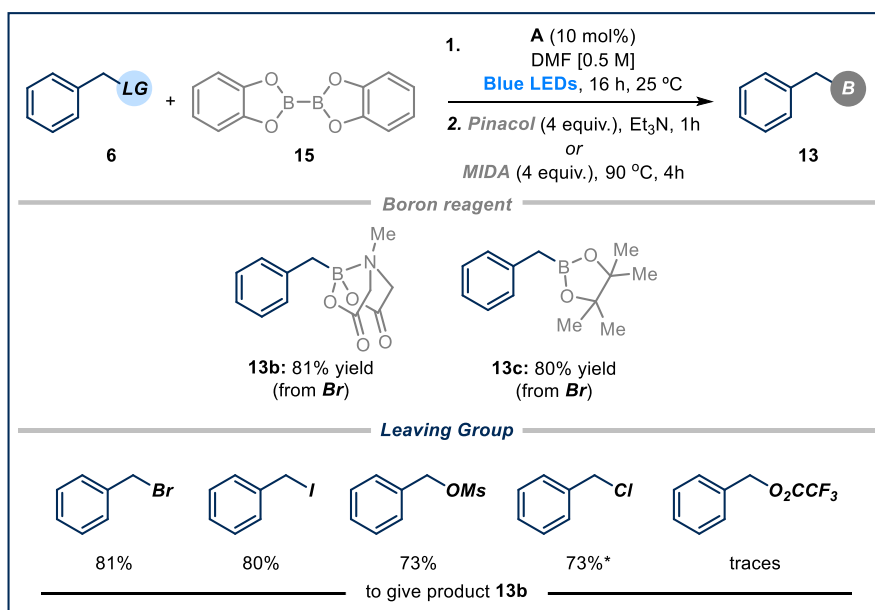


Figure 3.13: Survey of boron reagents and leaving groups amenable to the photochemical borylation of benzyl electrophiles. Reactions performed on a 0.2 mmol scale using 2 equiv. of bis(catecholato)diboron **15** in 0.4 mL of DMF. Yields of the isolated products **13** are indicated below each entry. *Reaction performed in the presence of 2 equiv. of NaBr.

As for the radical precursors, this photochemical strategy is suitable for substrates bearing different leaving groups, which can undergo S_N2 activation from the organic catalyst **A**. Apart from the bromide derivatives, also benzyl iodide and mesylate could be readily functionalized. In the case of benzyl chloride, the substrate is not activated enough to undergo the S_N2 reaction, thus requiring the addition of sodium bromide, which is necessary to generate the corresponding bromide in situ. Disappointingly, the use of benzyl trifluoroacetate completely suppressed the reactivity.

Next, we set to evaluate the generality of the reaction (Figure 3.14). Different heteroaromatic-containing substrates could be productively converted into the corresponding boronates, including thiazole (**13d**), oxazole (**13e**), pyrazole (**13f**), and furan (**13g**) derivatives. Moreover, because this method is not reliant on the redox properties of the radical precursor, both electron-rich (**13h**) and electron-poor (**13i**) benzyl derivatives could be efficiently borylated. Compounds bearing an aryl chloride (**13j**), an aryl iodide (**13k**), an ester (**13l**) and an unprotected alcohol (**13m**) all reacted to exclusively furnish the benzylic boronate, this showcasing the high functional group tolerability as well as the selectivity of the process. In addition to benzylic electrophiles, allyl substrates could be activated. For example, both farnesyl (**3n**) and prenyl (**3o**) derivatives could be successfully borylated.

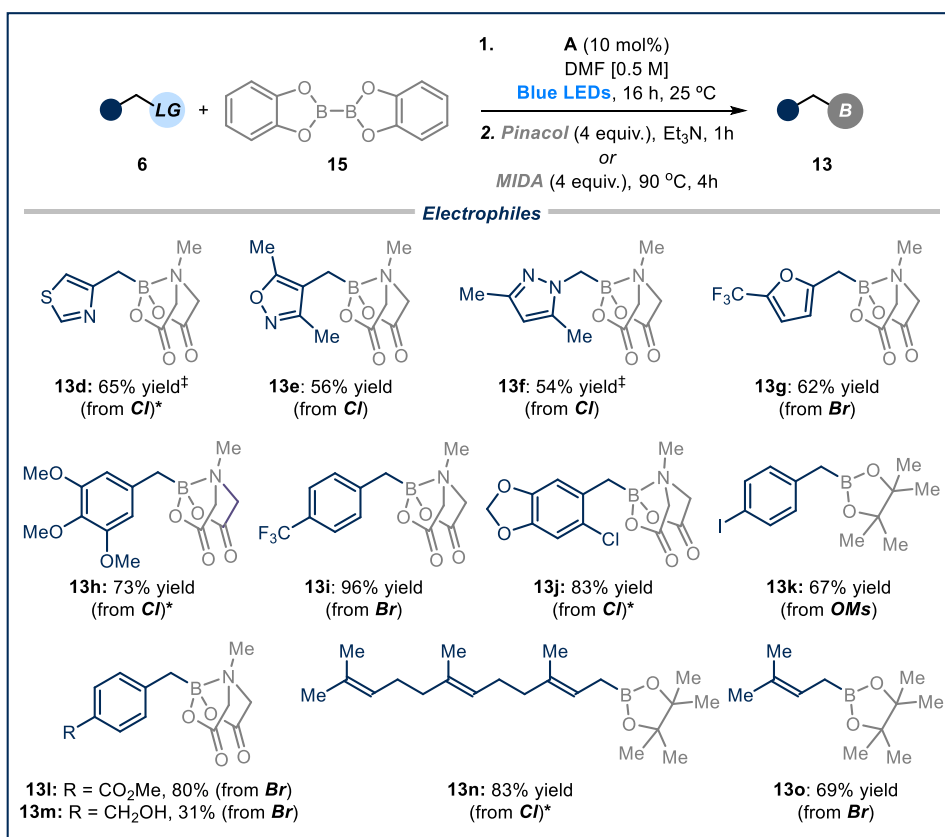


Figure 3.14: Survey of electrophiles amenable to the photochemical borylation reaction. Reactions performed on a 0.2 mmol scale using 2 equiv. of bis(catecholato)diboron **15** in 0.4 mL of DMF. Yields of the isolated products **13** are indicated below each entry. *Reaction performed in the presence of 2 equiv. of NaBr. ‡Reaction performed in the presence of 1 equiv. of 2,6-lutidine.

Overall these results highlight that commercially or readily available electrophiles can be easily converted into boronic derivatives **13a** under mild conditions through the use of the dithiocarbonyl catalyst **A** and under visible light irradiation.

3.5.3 Reaction limitations

Along with the successful examples highlighted in the previous section, we also defined the limitations of this borylation protocol (Figure 3.15).

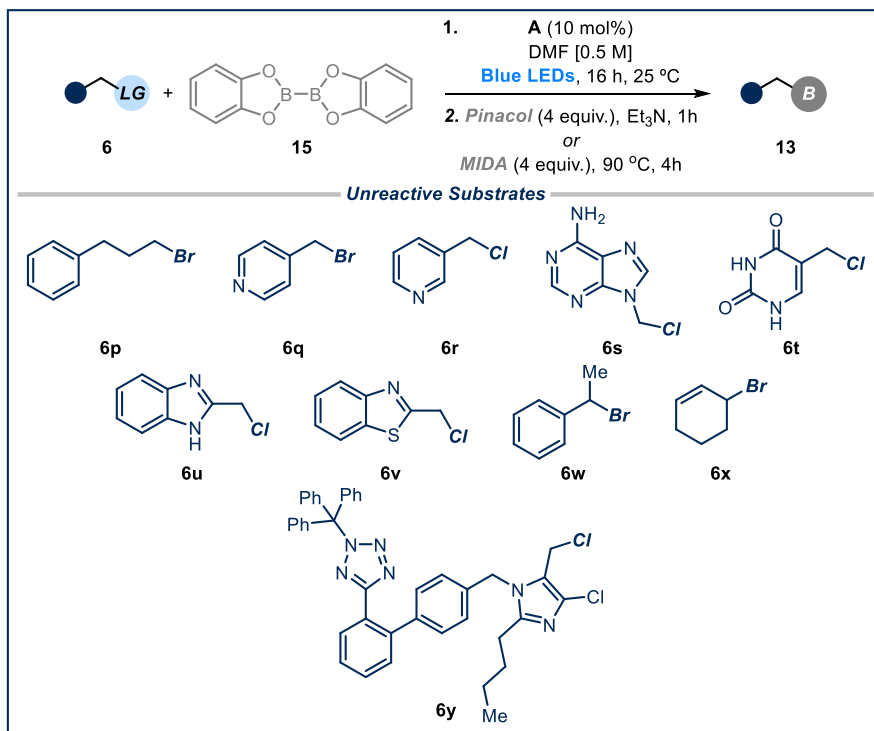


Figure 3.15: Survey of electrophiles which did not convert into products **13**. Reactions performed on a 0.2 mmol scale using 2 equiv. of bis(catecholato)diboron **15** in 0.4 mL of DMF.

When employing primary aliphatic bromides, such as **6p**, we did not obtain the corresponding boron-containing product. As expected, the S_N2 step is efficiently proceeding, generating the corresponding intermediate **8ap** (Figure 3.16), as observed by ¹H NMR analysis. If generated, the primary alkyl radical should rapidly react with B₂cat₂ to forge the C-B bond, as reported by Studer (rate constant estimated to be 3.8 × 10⁶ M⁻¹·s⁻¹).³¹ The lack of reactivity in our system suggests that our photolytic mechanism is not suitable to generate unactivated primary alkyl radicals.

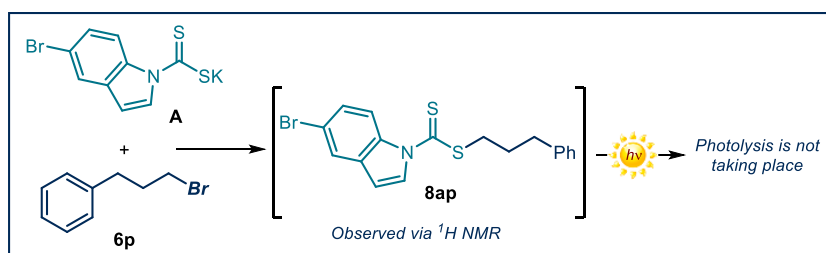


Figure 3.16: Formation of intermediate **8ap** and unsuccessful photolysis.

Pyridines **6q** and **6r** did not deliver the desired product. We mostly observed the formation of the corresponding reduced picoline products, suggesting that the radical prefers to abstract a hydrogen atom rather than reacting with B_2cat_2 . Similarly, when employing heterocyclic compounds such as **6s-v**, we observed the formation of the dehalogenated products. This lack of reactivity is not due to the radical-forming step, as our group already demonstrated that catalyst **A** can activate these substrates to promote radical C-C bond forming protocols.²¹ A plausible explanation to rationalize these findings is that the desired borylated products could be actually formed. However, a rapid protodeborylation, facilitated by the coordination of boron to the heteroatom within the products, could take place (Figure 3,17). This type of protodeborylation side reaction has been observed in the synthesis of similar heteroatom-containing boron compounds.³³

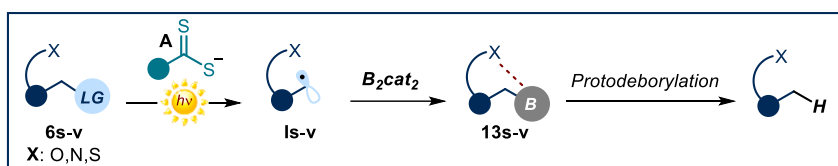


Figure 3.17: Formation of intermediate **8ap** and non-productive photolysis.

We also investigated whether secondary stabilized radicals could be used under this photochemical process. However, when **6w** and **6x** were submitted to the reaction conditions, no products were observed. This is in agreement with the lack of reactivity of secondary benzylic and allylic derivatives observed by Aggarwal³⁰ and Studer³² in other radical borylation protocols. Finally, employing a more complex molecule, such as the Losartan derivative **6y**, completely inhibited the reaction and the starting material was left untouched.

3.6 Reaction Mechanism

3.6.1 Proposed mechanism

Based on the previous reports from our group²¹ and from the group of Studer,³² we propose the mechanistic picture detailed in Figure 3.18. Catalyst **A** reacts with electrophile **6** in a S_N2 reaction, forming **8a**. Photolysis of this intermediate furnishes the S-centered radical **Va** and the C-centered radical **I**, which is intercepted by B_2cat_2 forging a C-B bond. The ensuing radical **XVII** is then intercepted by DMF to give the intermediate **XVIII**. The latter collapses to afford the desired alkyl boronic derivative **13**, along with the DMF-complexed boryl radical **XVI**. This intermediate is reducing enough ($E(XVI/XX) = -1.53$ V vs SCE, calculated redox potential in MeCN)^{30d} to transfer one electron to the dithiocarbonyl radical **Va** ($E(A/Va) = +0.44$ V versus Ag/Ag^+ in CH_3CN),²⁴ thus closing the catalytic cycle.

³³ (a) Diaz, D. B.; Scully, C. C. G.; Liew, S. K.; Shinya Adachi S.; Trinchera, P.; Denis, J. D.; Yudin A. K. "Synthesis of Aminoboronic Acid Derivatives from Amines and Amphoteric Boryl Carbonyl Compounds" *Angew. Chem. Int. Ed.* **2016**, *55*, 12659-12663. (b) Kaldas, S. J.; Rogova, T.; Nenajdenko, V. G.; Yudin, A. K. "Modular Synthesis of β -Amino Boronate Peptidomimetics" *J. Org. Chem.* **2018**, *83*, 7296-7302. (c) Ng, E. W. H.; Low, K.-H.; Chiu, P. "Synthesis and Applications of Unquaternized C-Bound Boron Enolates" *J. Am. Chem. Soc.* **2018**, *140*, 3537-3541.

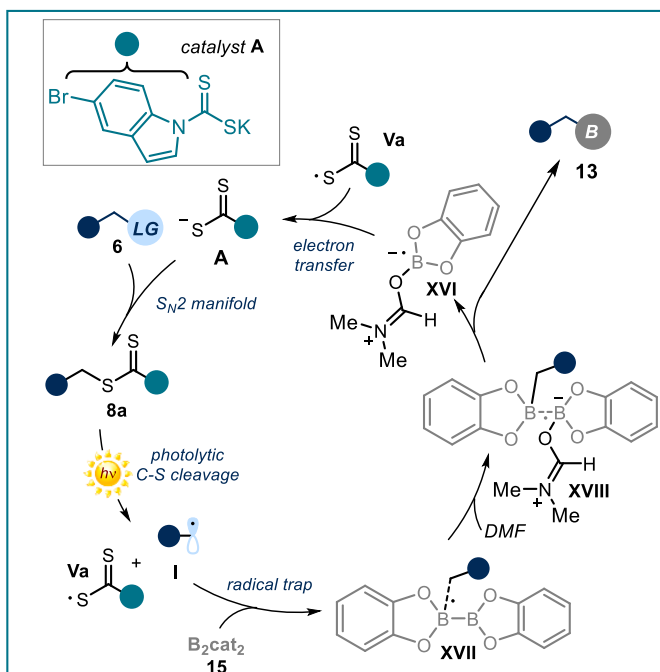


Figure 3.18: Proposed mechanism for the photochemical organocatalytic borylation of alkyl electrophiles.

3.6.2 Other mechanistic scenarios

We considered other possible mechanistic pathways in addition to the one proposed in Figure 3.16. In the first alternative mechanism (Figure 3.19), the photolysis of **8a** to form alkyl radical **I** would serve only as the initiation step of a radical chain process. After addition of **I** onto B_2cat_2 , the ensuing boryl radical **XVI** could reduce intermediate **8a** via SET. This event would feed a radical chain where the propagating radical **I** is generated and the organic catalyst **A** is turned over.

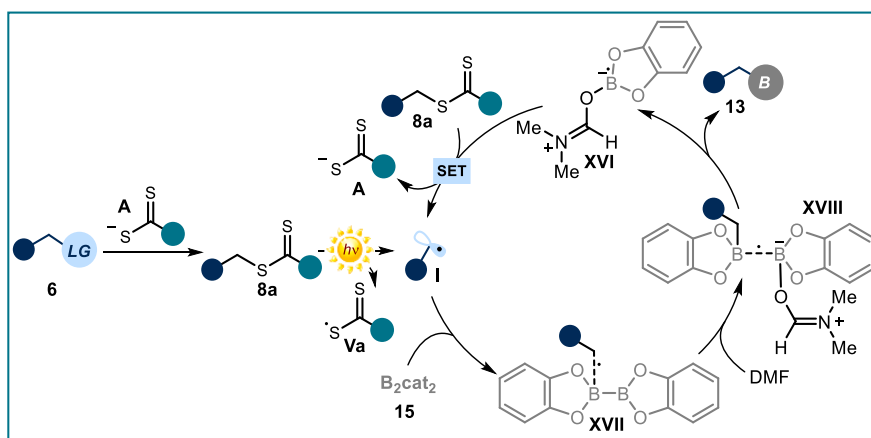


Figure 3.19: Possible alternative pathway based on a radical chain propagation mechanism. SET: Single electron transfer.

Based on the redox value reported in the literature for **XVI** ($E(\text{XVI}/\text{XX}) = -1.53 \text{ V vs SCE}$, calculated redox potential in MeCN)^{30d} and the data measured for the benzylic intermediate **8a** using cyclic voltammetry ($E(\mathbf{8a}/\mathbf{8a}^{\cdot-}) = -1.5 \text{ V vs Ag/AgCl}$ in MeCN, see section 3.9.5 for the cyclovoltammetric studies), this mechanistic possibility cannot be excluded.

In a second scenario depicted in Figure 3.20, the boryl radical **VI** could either perform SET reduction or halogen abstraction of the starting substrate **6**, which means that catalyst **A** would be only triggering the initiation of a radical chain process. While halogen abstraction from boryl radicals has been reported for iodides, bromides, and in rare cases for chlorides,³⁴ it has not been reported for mesylates, to the best of our knowledge. Since the present protocol tolerates the use of mesylates as radical precursors (**13k** in Figure 3.14), a halogen abstraction mechanism appears unlikely. On the other hand, an SET from the boryl radical **VI** to the substrates employed in this study would be highly endergonic, as indicated by the reduction potentials of representative substrates (see section 3.9.5 for the cyclovoltammetric studies).

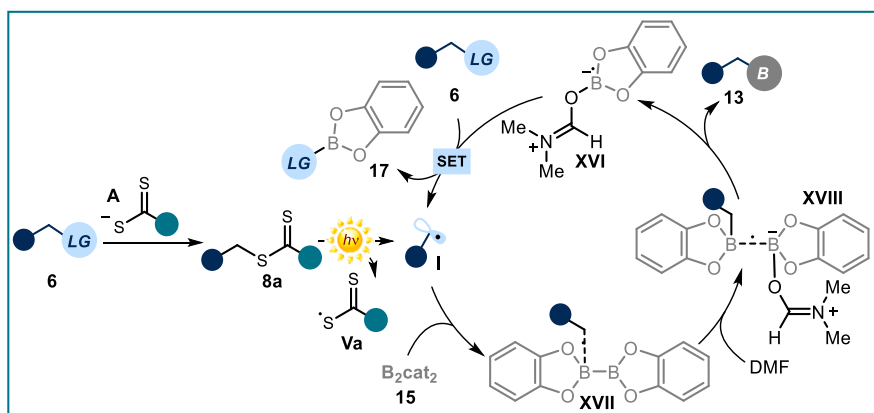


Figure 3.20: Alternative, albeit unlikely, mechanism reliant on a radical chain propagation mechanism.

Finally, we also considered the possibility of a mechanism involving the formation of an EDA complex **XXI** between the catalytically generated **8a** and **15**-DMF, in analogy to the proposal of Aggarwal³⁰ (Figure 3.21a). Excitation of this new intermediate would promote an intra-complex SET to ultimately furnish radical **I**. UV-Vis spectroscopic studies indicated that the addition of B_2cat_2 to a solution of **8a** did not result into the appearance of new absorption bands (Figure 3.21 b, perfect overlap between the red and the grey lines), which ruled out the formation of an EDA complex.

³⁴ (a) Curran, D. P.; Solovyev, A.; Makhlof Brahmi, M.; Fensterbank, L.; Malacria, M.; Lacote, E. "Synthesis and Reactions of N-Heterocyclic Carbene Boranes" *Angew. Chem., Int. Ed.* **2011**, *50*, 10294-10317. (b) Tehfe, M.-A.; Monot, J.; Makhlof Brahmi, M.; Bonin-Dubarle, H.; Curran, D. P.; Malacria, M.; Fensterbank, L.; Lacote, E.; Lalevee, J.; Fouassier, J.-P. "N-Heterocyclic carbene-borane radicals as efficient initiating species of photopolymerization reactions under air" *Polym. Chem.* **2011**, *2*, 625-631. (b) Pan, X.; Lacôte, E.; Lalevee, J.; Curran, D. P. "Polarity Reversal Catalysis in Radical Reductions of Halides by N-Heterocyclic Carbene Boranes" *J. Am. Chem. Soc.* **2012**, *134*, 5669-5674.

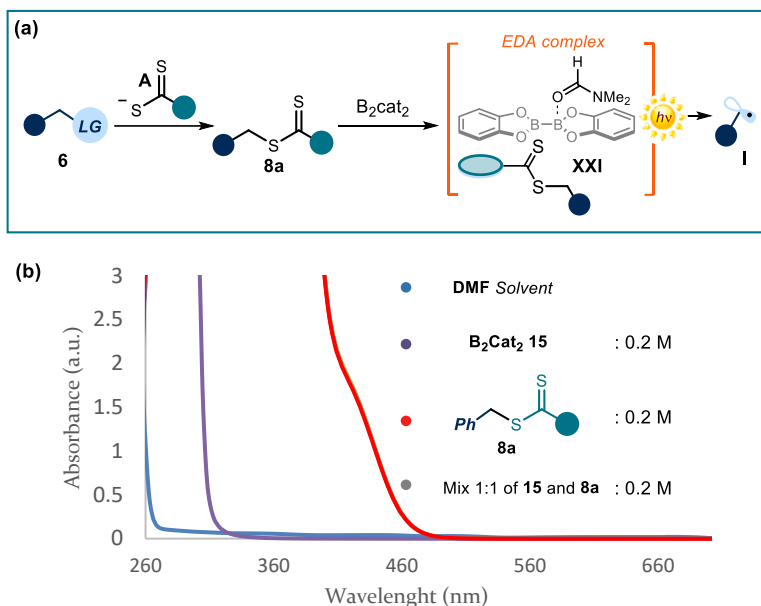


Figure 3.21: (a) Possible radical generation based on an EDA complex formation (b) Spectroscopic studies discard this pathway.

3.7 Three-component Variant

The vicinal difunctionalization of olefins is a powerful approach to increase molecular complexity in one step.³⁵ Difunctionalization methods that include a C-B bond forming process are interesting since the resulting functionalized alkylboranes can be employed as versatile building blocks in organic synthesis. As a result, transition-metal-catalyzed carboboration of alkenes has been widely explored as a reliable approach for the production of functionalized alkylboranes.³⁶ In contrast, only few reports on transition-metal free vicinal carboboration of olefins have been reported. Studer reported a general method for the 1,2-carboboration of alkenes.³⁷ This protocol uses electron-poor alkyl iodides **18**, olefins **19**, B_2cat_2 and blue light illumination to produce difunctionalized product **20** (Figure 3.22). Mechanistically, this photochemical procedure relies on a radical chain process where the initiation event is the light-promoted homolysis of the labile C-I bond of the substrate to furnish the carbon radical **XXII**. The latter, because of its electrophilic nature, preferentially reacts

³⁵ (a) McDonald, R. I.; Liu, G.; Stahl, S. S. "Palladium(II)-Catalyzed Alkene Functionalization via Nucleopalladation: Stereochemical Pathways and Enantioselective Catalytic Applications" *Chem. Rev.* **2011**, *111*, 2981-3019. (b) Zeng, X. "Recent Advances in Catalytic Sequential Reactions Involving Hydroelement Addition to Carbon-Carbon Multiple Bonds" *Chem. Rev.* **2013**, *113*, 6864-6900. (c) Greenhalgh, M. D.; Jones, A. S.; Thomas, S. P. "Iron-Catalysed Hydrofunctionalisation of Alkenes and Alkynes" *ChemCatChem* **2015**, *7*, 190-222.

³⁶ (a) Shimizu, Y.; Kanai, M. "Recent progress in copper-catalyzed difunctionalization of unactivated carbon-carbon multiple bonds" *Tetrahedron Lett.* **2014**, *55*, 3727-3737. (b) Neeve, E. C.; Geier, S. J.; Mkhaliid, I. A. I.; Westcott, S. A.; Marder, T. B. "Diboron(4) Compounds: From Structural Curiosity to Synthetic Workhorse" *Chem. Rev.* **2016**, *116*, 9091-9161.

³⁷ Cheng, Y., Mück-Lichtenfeld, C., Studer, A. "Transition Metal-Free 1,2-Carboboration of Unactivated Alkenes" *J. Am. Chem. Soc.* **2018**, *140*, 6221-6225.

with olefin **19** to produce the radical **XXIII**, which possesses the right polarity to interact with B_2cat_2 **15**. The ensuing radical **XXIV** is subsequently intercepted by DMF, furnishing **XXV**. This radical rapidly collapses to afford product **20** along with the boryl radical **XVI**. The latter can activate a second molecule of iodide **16** by either SET or iodine atom abstraction, regenerating radical **XXII**, hence feeding a radical chain manifold.

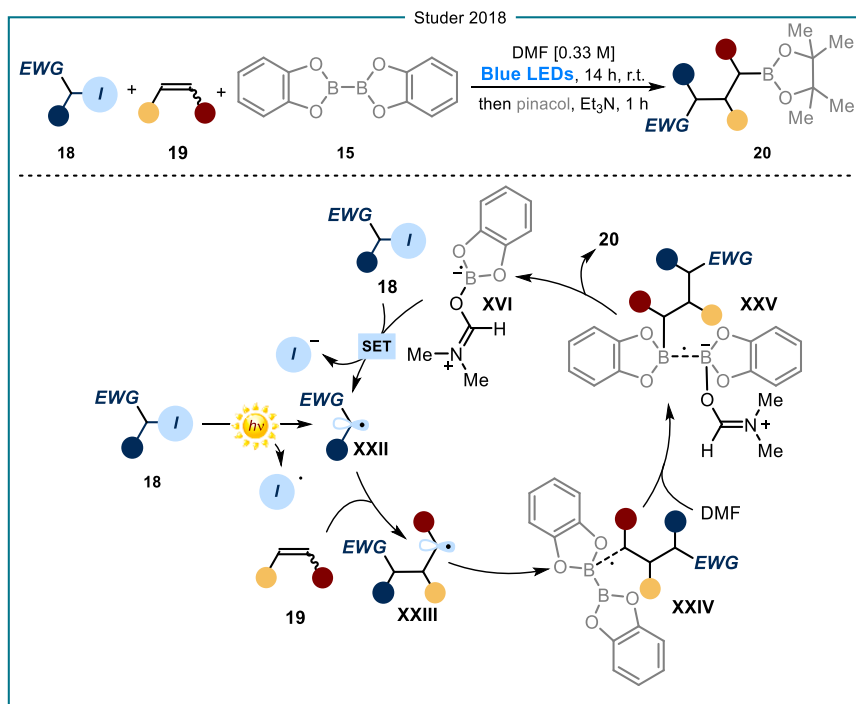


Figure 3.22: Transition-metal-free 1,2-carboration of unactivated alkenes.

Aware that our S_N2 -based radical-generation approach could produce electrophilic radicals, as previously reported in the original work,²¹ we explored the possibility of developing a three-component variant. In our mechanistic design (Figure 3.23), the generated electrophilic radical **XXII** would be intercepted by olefin **19**, generating a nucleophilic radical **XXIII**. The latter rapidly reacts with B_2cat_2 to produce the difunctionalized borylated product **20** and the boryl radical **XVI**. Transfer of one electron from **XVI** to xanthyl radical **Va** closes the catalytic cycle regenerating the DTC catalyst.

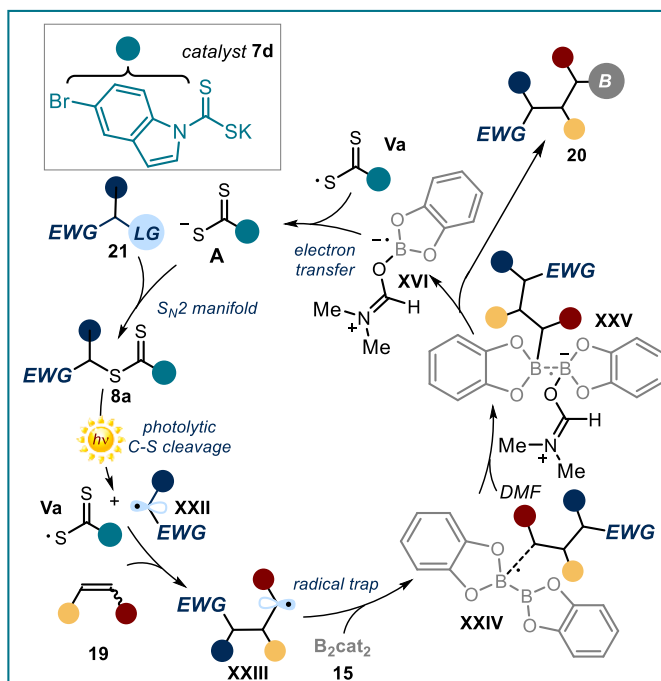
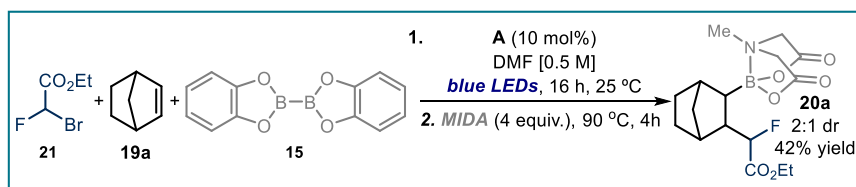


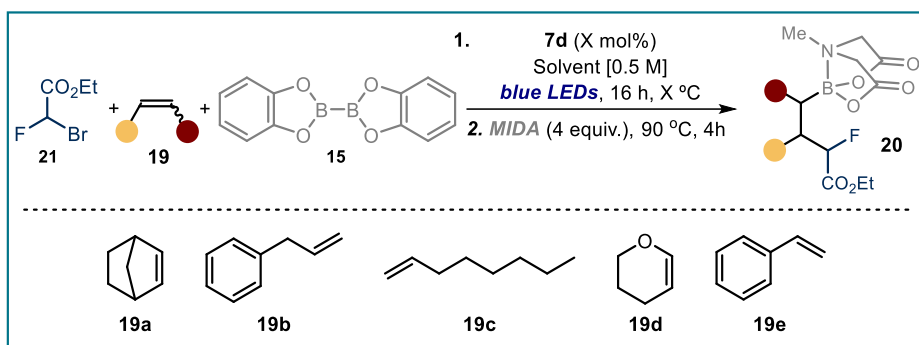
Figure 3.23: Proposed mechanism for the photochemical organocatalytic carboboration of olefins.

Applying the optimized conditions for the borylation of alkyl electrophiles (c.f. entry 1 table 3.1), we found that catalyst **A** could promote the difunctionalization of norbornene **19a** with fluorobromoacetate **21** and diborane **15**.



Scheme 3.1: First attempt to expand the photochemical organocatalytic borylation to a three-component reaction. Reaction performed on a 0.2 mmol scale. Yield refers to the isolated product **20a** after chromatographic purification on silica gel. DMF: Dimethylformamide. LEDs: Light Emitting Diodes. MIDA: Methyliminodiacetic acid.

With these results in hand, we started the optimization of the reaction conditions, focusing on different parameters, including catalyst loading, solvent, stoichiometry, nature of the olefin, and temperature.

Table 3.3: Optimization studies for the photochemical organocatalytic carboboration of olefins.^a

Entry	7d Loading	Solvent	XX : XX : 15	Olefin	Yield (%) ^b
1	10 mol%	DMF	1:3:2	19a	45
2	20 mol%	DMF	1:3:2	19a	56
3	20 mol%	DMA	1:3:2	19a	62 (54)
4	20 mol%	DMPU	1:3:2	19a	32
5 ^c	20 mol%	DMA	1:3:2	19a	54
6	20 mol%	DMA	3:1:2	19a	45
7	20 mol%	DMA	1:3:2	19b	20
8	20 mol%	DMA	1:3:2	19c	33
9	20 mol%	DMA	1:3:2	19d	-
10	20 mol%	DMA	1:3:2	19e	-

^aReaction performed on a 0.2 mmol scale. ^bYield of **20** determined by ¹H NMR analysis of the crude mixture using nitromethane as the internal standard; the value shown in parentheses refers to the yield of isolated **20** after chromatographic purification on silica gel. ^cReaction performed at 60 °C.

Increasing the catalyst loading to 20 mol% (entry 2) resulted in a higher chemical efficiency. Moreover, other Lewis basic solvents such as dimethylacetamide (entry 3) or *N,N'*-Dimethylpropyleneurea (DMPU, entry 4) proved effective, with DMA offering the best results. Increasing the temperature (entry 5), as well as changing the stoichiometry (entry 6), promoted the reaction with less efficiency. Finally, norbornene **19a** proved to be the best substrate, since the use of less strained olefins, such as vinyl benzene **19b** (entry 7) or 1-octene **19c** (entry 8), resulted in a substantial drop in chemical yield. No product was observed when substrates **19d** (entry 9) and **19e** (entry 10) were employed.

3.8 Conclusions

In conclusion, we have developed a photochemical organocatalytic approach which converts commercially available electrophiles into synthetically valuable boronic esters. This protocol uses a readily available organic catalyst and mild reaction conditions. Mechanistically, this process exploits an S_N2-based radical-generation

strategy, which does not rely on the redox properties or the BDE of the radical precursors. Hence, electrophiles which are difficult to be activated by other methods, such as SET reduction or atom abstraction, are amenable to this protocol. These electrophiles include benzylic and allylic bromides, chlorides and mesylates. In addition, the redox neutral conditions of this process make it tolerant of redox-sensitive substrates and allow the borylation of heterocyclic-containing substrates. This methodology was expanded to design a three-component variant, allowing the carboboration of alkenes.

3.9 Experimental Section

3.9.1 General information

The NMR spectra are available in the published manuscript¹ and are not reported in the present dissertation.

The NMR spectra were recorded at 400 MHz and 500 MHz for ¹H and 100 or 125 MHz for ¹³C. The chemical shift (δ) for ¹H and ¹³C are given in ppm relative to residual signals of the solvents (CHCl₃ @ 7.26 ppm ¹H NMR and 77.16 ppm ¹³C NMR, CD₃CN @ 1.94 ppm ¹H NMR and 118.26 ppm ¹³C NMR, (CD₃)₂CO @ 2.05 ppm ¹H NMR and 29.84 ppm ¹³C NMR and tetramethylsilane @ 0 ppm. Coupling constants are given in Hertz. The following abbreviations are used to indicate the multiplicity: s, singlet; d, doublet; q, quartet; m, multiplet; bs, broad signal; app, apparent.

High resolution mass spectra (HRMS) were obtained from the ICIQ HRMS unit on MicroTOF Focus and Maxis Impact (Bruker Daltonics) with electrospray ionization. (ESI). UV-vis measurements were carried out on a UV-Vis Agilent Cary60 spectrophotometer equipped with photomultiplier detector, double beam optics and D₂ and W light sources. Cyclic voltammetry studies were carried out on a Princeton Applied Research PARSTAT 2273 potentiostat offering compliance voltage up to ± 100 V (available at the counter electrode), ± 10 V scan range and ± 2 A current range. Isolated yields refer to materials of >95% purity as determined by ¹H NMR.

General Procedures. All reactions were set up under an argon atmosphere in oven-dried glassware using standard Schlenk techniques, unless otherwise stated. Synthesis grade solvents were used as purchased; anhydrous solvents were taken from a commercial SPS solvent dispenser. Chromatographic purification of products was accomplished using forced-flow chromatography (FC) on silica gel (35-70 mesh). For thin layer chromatography (TLC) analysis throughout this work, Merck pre-coated TLC plates (silica gel 60 GF₂₅₄, 0.25 mm) were employed, using UV light as the visualizing agent and an acidic mixture of vanillin or basic aqueous potassium permanganate (KMnO₄) stain solutions, and heat as developing agents. Organic solutions were concentrated under reduced pressure on a Büchi rotatory evaporator (in vacuo at 40 °C, ~5 mbar).

Determination of Diastereomeric Ratio. The diastereomeric ratio of product **6** was determined by ¹H NMR analysis of the crude reaction mixture through integration of diagnostic signals.

Materials. The majority of substrates used in this study are commercially available and they were purchased at the highest purity available from Sigma-Aldrich, Fluka, Alfa Aesar, Fluorochem, and used as received, without further purifications. The synthesis of the nucleophilic organic catalyst **A** and the benzyl intermediate **Bn8** are described in the literature.²¹ The substrates displayed in Figure 3.24 were synthesized according to procedures reported in the literature.³⁸

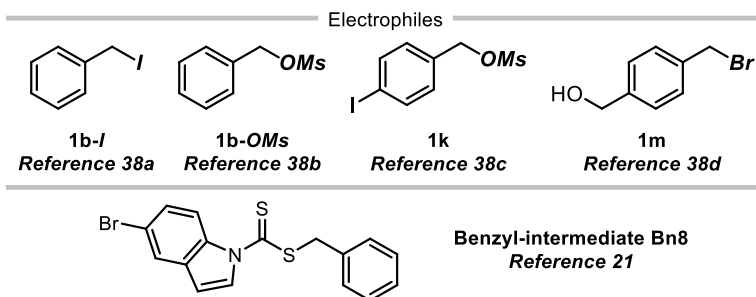


Figure 3.24: Starting materials synthesized according to literature precedents and corresponding references.

3.9.2 Experimental setup

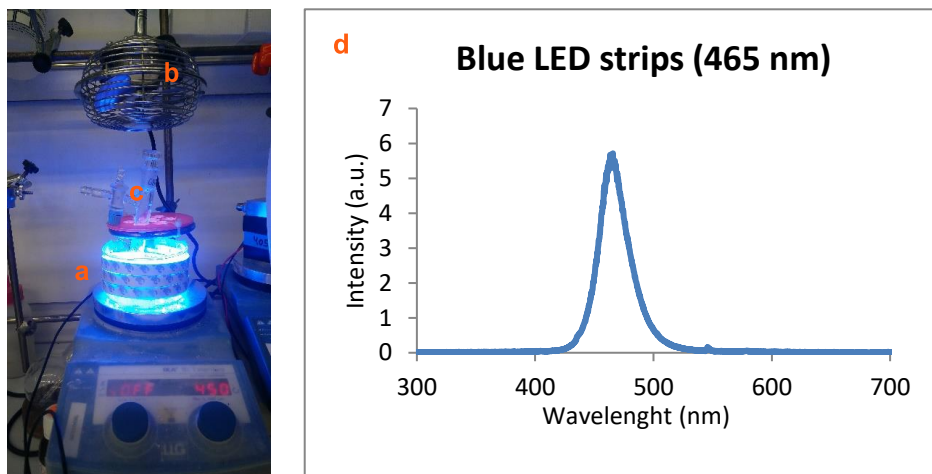
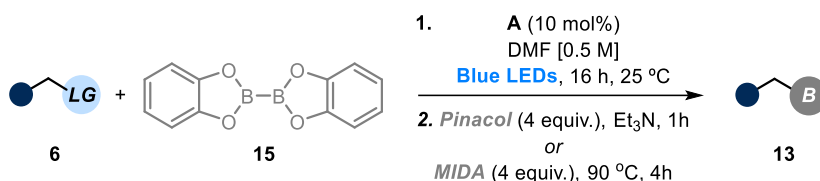


Figure 3.25: (a) The photoreactor and the experimental setup used in this study. (b) Fan to cool down the temperature. (c) Holder to accommodate Schlenk tubes in the photoreactor. (d) Emission spectrum of the 465 nm blue LED strips used in this study.

³⁸ a) Loim, N. M.; Kelbysheva, E. S. "Synthesis of dendrimers with terminal formyl groups" *Russ. Chem. Bull.* **2004**, *53*, 2080-2085. b) Chardin, C.; Rouden, J.; Livi, S.; Baudoux, J. "Dimethyldioxirane (DMDO) as a valuable oxidant for the synthesis of polyfunctional aromatic imidazolium monomers bearing epoxides" *J. Green Chem.* **2017**, *19*, 5054-5059. c) Yang, Z.; Zhou, J. "Palladium-Catalyzed, Asymmetric Mizoroki–Heck Reaction of Benzylic Electrophiles Using Phosphoramidites as Chiral Ligands" *J. Am. Chem. Soc.* **2012**, *134*, 11833-11835. d) Bridger, G. J.; Skerlj, R. T.; Hernandez-Abad, P. E.; Bogucki, D. E.; Wang, Z.; Zhou, Y.; Nan, S.; Boehringer, E. M.; Wilson, T.; Crawford, J.; Metz, M.; Hatse, S.; Princen, K.; De Clercq, E.; Schols, D. "Synthesis and Structure–Activity Relationships of Azamacrocyclic C-X-C Chemokine Receptor 4 Antagonists: Analogues Containing a Single Azamacrocyclic Ring are Potent Inhibitors of T-Cell Tropic (X4) HIV-1 Replication" *Med. Chem.* **2010**, *53*, 3, 1250-1260.

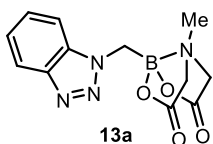
The photoreactor consisted of a 12.5 cm diameter crystallizing dish wrapped in a commercial 1 meter LED strip. A fan placed above the photoreactor was used in order to keep the temperature constant during the reaction time (about 30° C). The light source used in this study consisted of a 1 m strip, 14.4W “LEDXON MODULAR 9009083 LED, SINGLE 5050 purchased from Farnell, catalogue number 9009083. The emission spectrum of these LEDs was recorded (Figure 3.25).

3.9.3 General procedure for the photochemical organocatalytic borylation



General Procedure: An oven-dried 15 mL Schlenk tube was charged with a mixture of B₂Cat₂ **15** (95 mg, 0.4 mmol, 2 equiv.), the nucleophilic organic catalyst **A** (6 mg, 0.02 mmol, 0.1 equiv.), the alkyl electrophile **6** (0.2 mmol, 1 equiv.) in dimethylformamide (DMF 0.4 mL, 0.5 M). When necessary, NaBr (41 mg, 0.4 mmol, 2 equiv.) and 2,6-dimethylpyridine (23 μL, 0.2 mmol, 1 equiv.) were also added. The reaction mixture was placed under an atmosphere of argon, cooled to -78 °C, degassed *via* vacuum evacuation (5 minutes), backfilled with argon and, ultimately, warmed to ambient temperature. This freeze-pump-thaw cycle was repeated four times, and then the Schlenk tube was sealed with Parafilm and put under blue LEDs irradiation ($\lambda_{\max} = 465$ nm). The reaction was stirred at ambient temperature for 16 hours, using a fan to cool down the temperature (see Figure S2 for the setup and the photoreactor used). Then, methyliminodiacetic acid (118 mg, 0.8 mmol, 4 equiv.) was added and the reaction mixture heated to 90 °C for 4 hours, after which the solvent was removed *in vacuo*. Alternatively, a solution of pinacol (95 mg, 0.8 mmol, 4 equiv.) in triethylamine (500 μL) was added to the reaction vessel and the mixture was stirred for 1 hour at ambient temperature, after which water was added, the mixture was extracted with ethyl acetate (2x15 mL), and the combined layers were dried over magnesium sulfate, filtered, and concentrated. The resulting crude mixture was purified by column chromatography on silica gel to give the corresponding product **13** in the stated yield.

Characterization of products **13**



2-((1H-benzo[d][1,2,3]triazol-1-yl)methyl)-6-methyl-1,3,6,2-dioxaborocane-4,8-dione (13a). Prepared according to the general procedure using 1-(chloromethyl)-benzotriazole (33.5 mg, 0.2 mmol) and B₂Cat₂ (95 mg, 0.4 mmol, 2 equiv.) in dimethylformamide (0.4 mL). The crude mixture was purified by

flash column chromatography (isocratic ethyl acetate) to afford product **13a** (47.6 mg, 83% yield) as a white solid.

25-fold scale-up (5 mmol scale reaction) - The photochemical borylation reactions can be scaled-up up to 5 mmol scale by using the experimental setup described in Figure 3.23.

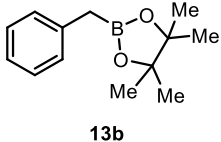
In an oven dried Schlenk tube (length x diameter = 15 x 2 cm), catalyst **A** (155 mg, 1 mmol, 0.1 equiv.), bis(catecholato)diboron **15** (2378 mg, 10 mmol, 2 equiv.) and 1-(chloromethyl)-1H-benzotriazole **6a** (838 mg, 5 mmol, 1 equiv.) were dissolved in DMF (10 mL, 0.5 M). The resulting mixture was degassed via three cycles of freeze-pump-thaw. The Schlenk tube was then placed in the irradiation setup (see Figure S2), maintained at a room temperature, and the reaction was stirred for 20 hours under continuous irradiation. Then, methyliminodiacetic acid (2943 mg, 20 mmol, 4 equiv.) was added and the reaction mixture heated to 90 °C for 4 hours, after which the solvent was removed *in vacuo*. The crude mixture was purified by flash column chromatography (isocratic ethyl acetate) to give the corresponding product **13a** (750 mg, 52 % yield) as a white solid.

¹H NMR (500 MHz, CD₃CN): δ 8.00 (dt, *J* = 8.4, 0.9 Hz, 1H), 7.77 (dt, *J* = 8.4, 1.0 Hz, 1H), 7.57 (ddd, *J* = 8.4, 6.9, 1.0 Hz, 1H), 7.42 (ddd, *J* = 8.4, 6.9, 1.0 Hz, 1H), 4.23 (s, 2H), 4.17 – 4.05 (m, 4H), 3.23 (s, 3H).

¹³C NMR (125.8 MHz, CD₃CN): δ 168.9 (2C), 146.3, 135.3, 128.0, 124.8, 120.0, 111.6, 64.0 (2C), 47.9. The signal of the α-B-carbon was not observed.

HRMS (ESI) Exact mass calculated for C₁₂H₁₄N₄O₄B [M+Na]⁺: 288.1139, found: 288.1128.

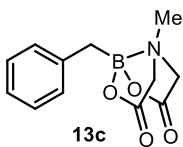
2-benzyl-4,4,5,5-tetramethyl-1,3,2-dioxaborolane (13b). Prepared according to the



general procedure using benzyl bromide (34 mg, 0.2 mmol) and B₂Cat₂ (95 mg, 0.4 mmol, 2 equiv.) in dimethylformamide (0.4 mL). The crude mixture was purified by flash column chromatography (hexane/ethyl acetate 95:5) to afford product **13b** (35 mg, 80% yield) as a colorless liquid. The spectroscopic properties of this compound were consistent with the data reported in the literature.³⁹

¹H NMR (400 MHz, CDCl₃): δ 7.30 – 7.19 (m, 4H), 7.12 (tt, *J* = 8.5, 1.5 Hz, 1H), 2.29 (s, 2H), 1.23 (s, 12H).

¹³C NMR (101 MHz, CDCl₃): δ 138.8, 129.1, 128.4, 124.9, 83.5, 24.9. The signal of the α-B-carbon was not observed.



2-benzyl-6-methyl-1,3,6,2-dioxazaborocane-4,8-dione (13c).

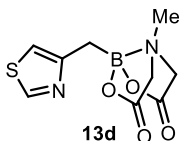
Prepared according to the general procedure using benzyl bromide (34 mg, 0.2 mmol) and B₂Cat₂ (95 mg, 0.4 mmol, 2 equiv.) in dimethylformamide (0.4 mL). The crude mixture was purified by flash column chromatography (isocratic ethyl acetate) to afford product **13c** (40 mg, 81% yield) as a white solid.

¹H NMR (400 MHz, CD₃CN): δ 7.26 – 7.17 (m, 4H), 7.14 – 7.09 (tt, *J* = 7.5, 1.5 Hz 1H), 3.93 (d, *J* = 17.0 Hz, 2H), 3.70 (d, *J* = 17.0 Hz, 2H), 2.90 (s, 3H), 2.18 (bs, 2H).

³⁹ Atack, T. C.; Lecker, R. M.; Cook, S. P. "Iron-Catalyzed Borylation of Alkyl Electrophiles" *J. Am. Chem. Soc.* **2014**, *136*, 9521–9523.

¹³C NMR (101 MHz, CD₃CN): δ 168.9 (2C), 141.4, 130.2 (2C), 129.0 (2C), 125.5, 62.9 (2C), 46.7. The signal of the α-B-carbon was not observed.

HRMS (ESI) Exact mass calculated for C₁₂H₁₄NNaO₄B [M+Na]⁺: 270.0908, found: 270.0907.

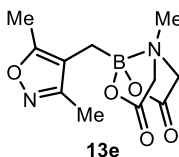


6-methyl-2-(thiazol-4-ylmethyl)-1,3,6,2-dioxazaborocane-4,8-dione (13d). Prepared according to the general procedure using 4-(chloromethyl)thiazole hydrochloride (34 mg, 0.2 mmol), B₂Cat₂ (95 mg, 0.4 mmol, 2 equiv.), NaBr (41 mg, 0.4 mmol, 2 equiv.) and 2,6-dimethylpyridine (23 μL, 0.2 mmol, 1 equiv.) in dimethylformamide (0.4 mL). The crude mixture was purified by flash column chromatography (isocratic ethyl acetate) to afford product **13d** (33 mg, 65% yield) as a white solid.

¹H NMR (400 MHz, CD₃CN): δ 8.76 (d, *J* = 2.0 Hz, 1H), 7.07 – 6.88 (m, 1H), 3.92 (d, *J* = 16.8 Hz, 2H), 3.83 (d, *J* = 16.8 Hz, 2H), 3.15 (s, 3H), 2.40 (s, 2H).

¹³C NMR (101 MHz, CD₃CN): δ 169.1 (2C), 156.7, 153.5, 114.2, 63.3 (2C), 47.0. The signal of the α-B-carbon was not observed.

HRMS (ESI) Exact mass calculated for C₉H₁₁N₂NaO₄SB [M+Na]⁺: 276.0461, found: 276.0449.

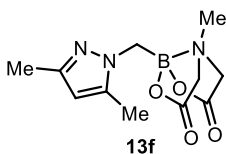


2-((3,5-dimethylisoxazol-4-yl)methyl)-6-methyl-1,3,6,2-dioxazaborocane-4,8-dione (13e). Prepared according to the general procedure using 4-(chloromethyl)-3,5-dimethylisoxazole (25 μL, 0.2 mmol) and B₂Cat₂ (95 mg, 0.4 mmol, 2 equiv.) in dimethylformamide (0.4 mL). The crude mixture was purified by flash column chromatography (isocratic ethyl acetate) to afford product **13e** (30 mg, 56% yield) as a white solid.

¹H NMR (400 MHz, CD₃CN): δ 3.98 (d, *J* = 17.0 Hz, 2H), 3.86 (d, *J* = 17.0 Hz, 2H), 2.94 (s, 3H), 2.26 (s, 3H), 2.15 (s, 3H), 1.66 (s, 2H).

¹³C NMR (101 MHz, CD₃CN): δ 168.7 (2C), 164.5, 160.9, 112.1, 62.9 (2C), 46.7, 27.6, 11.3, 10.6.

HRMS (ESI) Exact mass calculated for C₁₁H₁₅N₂NaO₅B [M+Na]⁺: 288.1003, found: 288.1005.



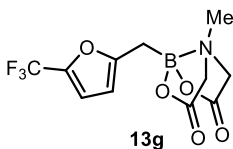
2-((3,5-dimethyl-1H-pyrazol-1-yl)methyl)-6-methyl-1,3,6,2-dioxazaborocane-4,8-dione (13f). Prepared according to the general procedure using 1-(chloromethyl)-3,5-dimethyl-1H-pyrazole hydrochloride (36 mg, 0.2 mmol), B₂Cat₂ (95 mg, 0.4 mmol, 2 equiv.) and 2,6-dimethylpyridine (23 μL, 0.2 mmol, 1 equiv.) in dimethylformamide (0.4 mL). The crude mixture was purified by flash

column chromatography (isocratic ethyl acetate) to afford product **13f** (29 mg, 54% yield) as a white solid.

$^1\text{H NMR}$ (400 MHz, CD_3CN): δ 5.88 – 5.65 (m, 1H), 4.08 (d, J = 16.5 Hz, 2H), 3.96 (d, J = 16.5 Hz, 2H), 3.51 (s, 2H), 3.20 (s, 3H), 2.18 (s, 3H), 2.07 (s, 3H).

$^{13}\text{C NMR}$ (101 MHz, CD_3CN): δ 169.3 (2C), 146.8, 141.1, 104.8, 64.0 (2C), 47.2, 13.4, 11.3. The signal of the α -B-carbon was not observed.

HRMS (ESI) Exact mass calculated for $\text{C}_{11}\text{H}_{17}\text{N}_3\text{O}_4\text{B}$ $[\text{M}+\text{H}]^+$: 265.1343, found: 265.1345.



6-methyl-2-((5-(trifluoromethyl)furan-2-yl)methyl)-1,3,6,2-dioxazaborocane-4,8-dione (13g). Prepared according to the general procedure using methyl 2-(bromomethyl)-5-(trifluoromethyl)furan (27.6 μL mg, 0.2 mmol) and B_2Cat_2 (95 mg, 0.4 mmol, 2 equiv.) in dimethylformamide (0.4 mL). The

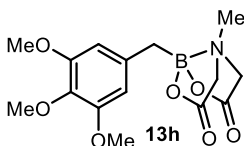
crude mixture was purified by flash column chromatography (isocratic ethyl acetate) to afford product **13g** (38.4 mg, 62% yield) as a white solid.

$^1\text{H NMR}$ (400 MHz, CD_3CN): δ 9.88 – 6.88 (m, 1H), 6.21 – 5.99 (m, 1H), 4.00 (d, J = 17.0 Hz, 2H), 3.77 (d, J = 17.0 Hz, 2H), 2.92 (s, 3H), 2.25 (s, 2H).

$^{13}\text{C NMR}$ (101 MHz, CD_3CN): δ 168.7 (2C), 159.6, 139.5 (q, J = 41.8 Hz), 120.5 (q, J = 265.5 Hz), 114.5 (q, J = 2.9 Hz), 107.7, 63.1 (2C), 47.0. The signal of the α -B-carbon was not observed.

$^{19}\text{F NMR}$ (376 MHz, CD_3CN): δ -59.0.

HRMS (ESI) Exact mass calculated for $\text{C}_{11}\text{H}_{11}\text{F}_3\text{NNaO}_5\text{B}$ $[\text{M}+\text{Na}]^+$: 327.0611, found: 327.0624.



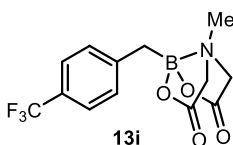
6-methyl-2-(3,4,5-trimethoxybenzyl)-1,3,6,2-dioxazaborocane-4,8-dione (13h). Prepared according to the general procedure using 5-(chloromethyl)-1,2,3-trimethoxybenzene (43 mg, 0.2 mmol), B_2Cat_2 (95 mg, 0.4 mmol, 2 equiv.) and NaBr (41 mg, 0.4 mmol, 2 equiv.) in

dimethylformamide (0.4 mL). The crude mixture was purified by flash column chromatography (isocratic ethyl acetate) to afford product **13h** (49 mg, 73% yield) as a yellow oil.

$^1\text{H NMR}$ (400 MHz, CD_3CN): δ 6.48 (s, 2H), 3.91 (d, J = 17.0 Hz, 2H), 3.76 (s, 6H), 3.67 (s, 3H), 3.60 (d, J = 17.0 Hz, 2H), 2.88 (s, 3H), 2.26 (s, 2H).

$^{13}\text{C NMR}$ (101 MHz, CD_3CN): δ 169.0 (2C), 153.9, 136.8, 136.3, 107.4, 63.0 (2C), 60.7, 56.5, 46.5. The signal of the α -B-carbon was not observed.

HRMS (ESI) Exact mass calculated for $\text{C}_{15}\text{H}_{21}\text{NO}_7\text{B}$ $[\text{M}+\text{H}]^+$: 337.1442, found: 337.1444.



6-methyl-2-(4-(trifluoromethyl)benzyl)-1,3,6,2-dioxazaborocane-4,8-dione (13i). Prepared according to the general procedure using 1-(bromomethyl)-4-(trifluoromethyl)benzene (47.8 mg, 0.2 mmol) and B_2Cat_2 (95 mg, 0.4 mmol, 2 equiv.) in dimethylformamide (0.4 mL). The

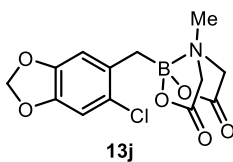
crude mixture was purified by flash column chromatography (isocratic ethyl acetate) to afford product **13i** (60.7 mg, 96% yield) as a white solid.

1H NMR (400 MHz, CD_3CN): δ 7.58 (d, J = 7.9 Hz, 2H), 7.39 (d, J = 7.9 Hz, 2H), 3.99 (d, J = 16.7 Hz, 2H), 3.81 (d, J = 16.9 Hz, 2H), 2.94 (s, 3H), 2.24 (s, 2H).

^{13}C NMR (101 MHz, CD_3CN): δ 168.8 (2C), 146.7, 130.5 (2C), 127.2 (q, J = 32.1 Hz), 125.9 (q, J = 270.7 Hz), 125.7 (q, J = 3.9 Hz, 2C), 62.9 (2C), 46.8. The signal of the α -B-carbon was not observed.

^{19}F NMR (376 MHz, CD_3CN): δ -62.67.

HRMS (ESI) Exact mass calculated for $C_{13}H_{13}F_3NNaNO_4B$ $[M+Na]^+$: 337.0818, found: 337.0823.



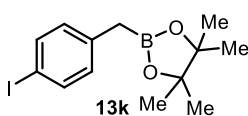
2-((6-chlorobenzo[d][1,3]dioxol-5-yl)methyl)-6-methyl-1,3,6,2-dioxazaborocane-4,8-dione (13j). Prepared according to the general procedure using 5-chloro-6-(chloromethyl)benzo[d][1,3]dioxole (41 mg, 0.2 mmol), B_2Cat_2 (95 mg, 0.4 mmol, 2 equiv.) and NaBr (41 mg, 0.4 mmol, 2

equiv.) in dimethylformamide (0.4 mL). The crude mixture was purified by flash column chromatography (isocratic ethyl acetate) to afford product **13j** (52 mg, 83% yield) as a white solid.

1H NMR (400 MHz, CD_3CN): δ 6.85 (s, 1H), 6.79 (s, 1H), 5.94 (s, 2H), 3.96 (d, J = 17.0 Hz, 2H), 3.82 (d, J = 17.0 Hz, 2H), 2.92 (s, 3H), 2.17 (s, 2H).

^{13}C NMR (101 MHz, CD_3CN): δ 168.8 (2C), 147.6, 146.7, 132.1, 125.1, 110.9, 110.0, 102.8, 62.8 (2C), 46.5. The signal of the α -B-carbon was not observed.

HRMS (ESI) Exact mass calculated for $C_{13}H_{13}NaO_6BCl$ $[M+Na]^+$: 347.0453, found: 347.0446.



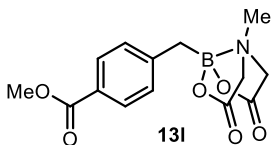
2-(4-iodobenzyl)-4,4,5,5-tetramethyl-1,3,2-dioxaborolane (13k). Prepared according to the general procedure using 4-iodobenzyl methanesulfonate (62 mg, 0.2 mmol) and B_2Cat_2 (95 mg, 0.4 mmol, 2 equiv.) in dimethylformamide (0.4 mL).

The crude mixture was purified by flash column chromatography (hexane/ethyl acetate 95:5) to afford product **13k** (46 mg, 67% yield) as a colorless liquid. The

spectroscopic properties of this compound were consistent with the data available in the literature.⁴⁰

¹H NMR (400 MHz, CDCl₃): δ 7.54 (d, *J* = 8.0 Hz, 2H), 6.93 (d, *J* = 8.0 Hz, 2H), 2.22 (s, 2H), 1.23 (s, 12H).

¹³C NMR (101 MHz, CDCl₃): δ 138.6, 137.4, 131.3, 89.9, 83.7, 24.9. The signal of the α-B-carbon was not observed.



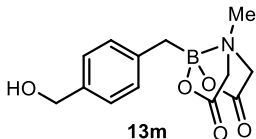
methyl-4-((6-methyl-4,8-dioxo-1,3,6,2-dioxazaborocane-2-yl)methyl)benzoate (13l). Prepared according to the general procedure using methyl 4-(bromomethyl)benzoate (46 mg, 0.2 mmol) and B₂Cat₂ (95 mg, 0.4 mmol, 2 equiv.) in dimethylformamide (0.4 mL). The crude mixture was

purified by flash column chromatography (isocratic ethyl acetate) to afford product **13l** (49 mg, 80% yield) as a white solid.

¹H NMR (400 MHz, CD₃CN): δ 7.87 (d, *J* = 8.5 Hz, 2H), 7.30 (d, *J* = 8.5 Hz, 2H), 3.95 (d, *J* = 17.0 Hz, 2H), 3.84 (s, 3H), 3.76 (d, *J* = 17.0 Hz, 2H), 2.90 (s, 3H), 2.21 (bs, 2H);

¹³C NMR (101 MHz, CD₃CN): δ 168.8 (2C), 167.8, 147.8, 130.2 (2C), 130.0 (2C), 127.6, 62.9 (2C), 52.4, 46.7. The signal of the α-B-carbon was not observed.

HRMS (ESI) Exact mass calculated for C₁₄H₁₆NNaO₆B [M+Na]⁺: 327.0999, found: 327.1001.



2-(4-(hydroxymethyl)benzyl)-6-methyl-1,3,6,2-dioxazaborocane-4,8-dione (13m). Prepared according to the general procedure using methyl (4-(bromomethyl)phenyl)methanol (40.2 mg, 0.2 mmol) and

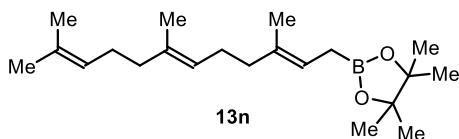
B₂Cat₂ (95 mg, 0.4 mmol, 2 equiv.) in dimethylformamide (0.4 mL). The crude mixture was purified by flash column chromatography (isocratic ethyl acetate) to afford product **13m** (17.2 mg, 31% yield) as a white solid.

¹H NMR (400 MHz, (CD₃)₂CO): δ 8.18 (s, 1H, OH), 7.25 – 7.19 (m, 4H), 5.11 (s, 2H), 4.17 (d, *J* = 16.8 Hz, 2H), 3.91 (d, *J* = 16.8 Hz, 2H), 3.10 (s, 3H), 2.18 (s, 2H).

¹³C NMR (101 MHz, (CD₃)₂CO): δ 168.7 (2C), 161.9, 141.8, 132.9, 130.3, 121.1, 65.9, 62.9 (2C), 45.9. The signal of the α-B-carbon was not observed.

HRMS (ESI) Exact mass calculated for C₁₃H₁₆NNaO₅B [M+Na]⁺: 300.1014, found: 300.1014.

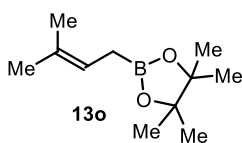
⁴⁰ Wu, C.; Wu, G.; Zhang, Y.; Wang, J. "One-carbon homologation of arylboronic acids: a convenient approach to the synthesis of pinacol benzylboronates" *Org. Chem. Front.* **2016**, *3*, 817-822.



4,4,5,5-tetramethyl-2-((2E,6E)-3,7,11-trimethyldodeca-2,6,10-trien-1-yl)-1,3,2-dioxaborolane (13n). Prepared according to the general procedure using (2E,6E)-1-chloro-3,7,11-trimethyldodeca-2,6,10-triene (48 mg, 0.2 mmol), B₂Cat₂ (95 mg, 0.4 mmol, 2 equiv.) and NaBr (41 mg, 0.4 mmol, 2 equiv.) in dimethylformamide (0.4 mL). The crude mixture was purified by flash column chromatography (hexane/ethyl acetate 95:5) to afford product **13n** (55 mg, 83% yield) as a colorless liquid. The spectroscopic properties of this compound were consistent with the data available in the literature.^{26c}

¹H NMR (400 MHz, CDCl₃): δ 5.32 – 5.23 (m, 1H), 5.17 – 5.08 (m, 2H), 2.15 – 1.91 (m, 8H), 1.70 (s, 3H), 1.61 (s, 11H), 1.26 (s, 12H).

¹³C NMR (101 MHz, CDCl₃): δ 135.31, 134.9, 131.3, 124.6, 124.5, 118.6, 83.2, 39.9, 39.9, 26.9, 26.9, 25.8, 24.9, 17.8, 16.1.

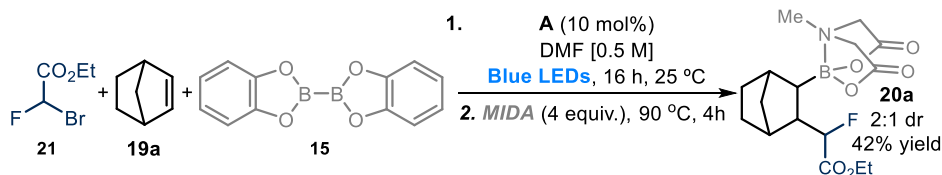


4,4,5,5-tetramethyl-2-(3-methylbut-2-en-1-yl)-1,3,2-dioxaborolane (13o). Prepared according to the general procedure using 1-bromo-3-methylbut-2-ene (23 μL, 0.2 mmol) and B₂Cat₂ (95 mg, 0.4 mmol, 2 equiv.) in dimethylformamide (0.4 mL). The crude mixture was purified by flash column chromatography (hexane/ethyl acetate 95:5) to afford product **13o** (27 mg, 69% yield) as a colorless liquid. The spectroscopic properties of this compound were consistent with the data available in the literature.⁴¹

¹H NMR (400 MHz, CDCl₃): δ 5.22 (tt, *J* = 6.5, 3.5 Hz, 1H), 1.69 (d, *J* = 1.4 Hz, 3H), 1.63 – 1.56 (m, 5H), 1.24 (s, 12H).

¹³C NMR (101 MHz, CDCl₃): δ 131.6, 118.6, 83.2, 25.8, 24.9, 17.8.

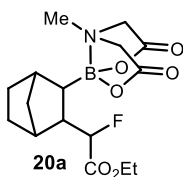
3.9.4 General procedure for the three-component borylation



An oven-dried 15 mL Schlenk tube was charged with a mixture of B₂Cat₂ **15** (95 mg, 0.4 mmol, 2 equiv.), catalyst **A** (12.4 mg, 0.02 mmol, 0.2 equiv.), norbornene **19a** (56.5 mg, 0.6 mmol, 3 equiv.), and ethyl 2-bromo-2-fluoroacetate **21** (0.2 mmol, 1 equiv.) in dimethylacetamide (DMA) (0.4 mL, 0.5 M). The mixture was placed under an atmosphere of argon, cooled to –78 °C, degassed *via* vacuum evacuation (5 minutes),

⁴¹ Lujia, M.; Bertermann, R.; Rachor, S. G.; Szabò, K. J.; Marder, T. B. "Palladium-Catalyzed Oxidative Borylation of Allylic C–H Bonds in Alkenes" *Org. Lett.* **2017**, *19*, 6590-6593.

backfilled with argon and, ultimately, warmed to room temperature. The freeze-pump-thaw cycle was repeated four times, and then the Schlenk tube was sealed with Parafilm and put under Blue LEDs irradiation ($\lambda_{\text{max}} = 465 \text{ nm}$). The reaction was stirred at room temperature for 16 hours. After this, methyliminodiacetic acid (118 mg, 0.8 mmol, 4 equiv.) was added to the reaction vessel and heated at 90 °C for 4 hours, after which the solvent was removed *in vacuo*. The resulting crude mixture was purified by column chromatography on silica gel to afford **20a**.



Ethyl 2-fluoro-2-(3-(6-methyl-4,8-dioxo-1,3,6,2-dioxazaborocan-2-yl)bicyclo[2.2.1]heptan-2-yl)acetate (20a). Prepared according to the general procedure for the three-component reaction, using B_2Cat_2 (95 mg, 0.4 mmol, 2 equiv.), catalyst A (12.4 mg, 0.02 mmol, 0.2 equiv.), norbornene (56.5 mg, 0.6 mmol, 3 equiv.) and the ethyl 2-bromo-2-fluoroacetate (0.2 mmol, 1 equiv.) in dimethylacetamide

(0.4 mL). The resulting crude mixture was purified by column chromatography (ethyl acetate) to afford product **20a** (40 mg, 56% yield) as a mixture of 2 diastereomers in a 2 to 1 ratio, as a colorless solid.

The signals relative to ^1H NMR, ^{13}C NMR and ^{19}F NMR analysis are reported as a mixture of 2 diastereomers in a 2 to 1 ratio:

^1H NMR (400 MHz, CDCl_3): δ 4.98 (dd, $J = 48.9, 4.8 \text{ Hz}$, 1H, *Major diastereomer*), 4.56 (dd, $J = 49.9, 9.6 \text{ Hz}$, 0.5H *Minor diastereomer*), 4.33 – 4.19 (m, 3H), 3.88 – 3.64 (m, 6.5 H), 3.07 (s, 3H), 2.99 (s, 1.5H), 2.47 (s, 0.5H), 2.45 (s, 1H), 2.30 – 2.22 (m, 1.5H), 2.04 (ddd, $J = 20.1, 7.2, 4.8 \text{ Hz}$, 1H), 1.86 – 1.73 (m, 1H), 1.69 – 1.50 (m, 3H), 1.50 – 1.37 (m, 2H), 1.37 – 1.18 (m, 11.5H),

^{13}C NMR (101 MHz, CDCl_3): δ 169.45 (d, $^2J_{\text{CF}} = 25.4 \text{ Hz}$, 1C, *Major diastereomer*), 169.12 (d, $^2J_{\text{CF}} = 24.9 \text{ Hz}$, 1C, *Minor diastereomer*), 167.9, 169.3, 169.2, 169.0, 94.4 (d, $^1J_{\text{CF}} = 178.8 \text{ Hz}$, 1C, *Minor diastereomer*), 92.1 (d, $^1J_{\text{CF}} = 179.6 \text{ Hz}$, 1C, *Major diastereomer*), 62.9, 62.8, 62.0, 61.9, 61.7, 61.6, 61.5, 46.9 (d, $^2J_{\text{CF}} = 18.2 \text{ Hz}$, 1C, *Minor diastereomer*), 46.8 (d, $J = 19.4 \text{ Hz}$, 1C, *Major diastereomer*), 45.9, 45.8, 44.9, 44.8, 40.9, 40.1, 40.0, 39.9, 39.56, 39.0, 38.9, 38.8, 30.4, 28.8, 26.1, 25.3, 14.1.

^{19}F NMR (376 MHz, CDCl_3): δ -185.62 (*Minor diastereomer*), -186.36 (*Major diastereomer*).

HRMS (ESI) Exact mass calculated for $\text{C}_{16}\text{H}_{23}\text{FNNaO}_6\text{B}$ $[\text{M}+\text{Na}]^+$: 378.1495, found: 378.1496.

3.9.5 Cyclic voltammometry measurements

Substrates **6a**, **6d**, **6e**, **6g**, **6h**, **6i**, **6j** were electrochemically characterized.

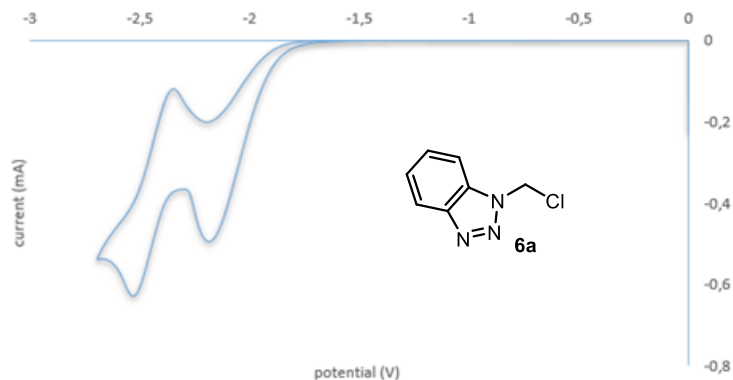


Figure 3.26: Cyclic voltammogram for 1-(chloromethyl)-1H-benzotriazole **6a** [0.02M] in [0.1 M] TBAPF₆ in CH₃CN. Sweep rate: 100 mV/s. Pt electrode working electrode, Ag/AgCl (KCl 3.5 M) reference electrode, Pt wire auxiliary electrode. First irreversible reduction, $E_p^c = E^{\text{red}}(\mathbf{6a}/\mathbf{6a}^{\cdot-}) = -2.2$ V, E_p^c refers to the cathodic peak potential, while the E^{red} value describes the electrochemical properties of **6a**.

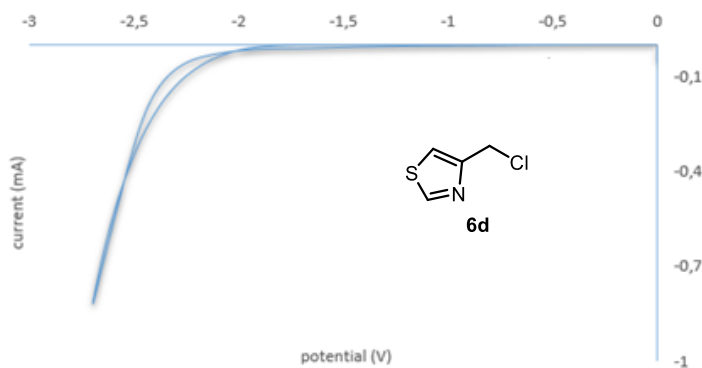


Figure 3.27: Cyclic voltammogram for 4-(chloromethyl)thiazole **6d** [0.02M] in [0.1 M] TBAPF₆ in CH₃CN. Sweep rate: 500 mV/s. Pt electrode working electrode, Ag/AgCl (KCl 3.5 M) reference electrode, Pt wire auxiliary electrode. Reduction of substrate **6d** was not observed in the registered potential window (from 0 to -2.7 V).

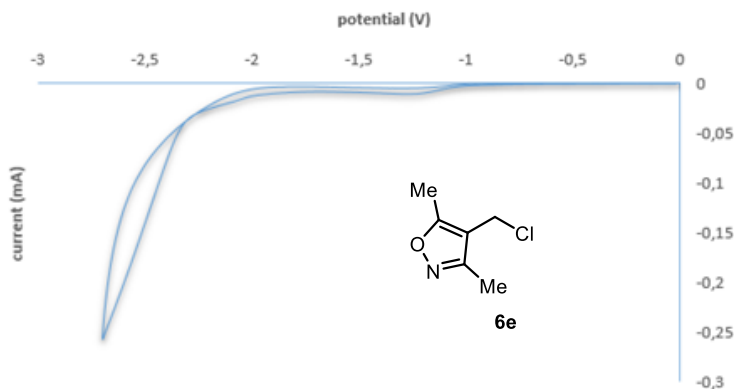


Figure 3.28: Cyclic voltammogram for 4-(chloromethyl)-3,5-dimethylisoxazole chloride **6e** [0.02M] in [0.1 M] TBAPF₆ in CH₃CN. Sweep rate: 50 mV/s. Glassy carbon electrode working electrode, Ag/AgCl (KCl 3.5 M) reference electrode, Pt wire auxiliary electrode. Reduction of substrate **6e** was not observed in the registered potential window (from 0 to -2.7 V).

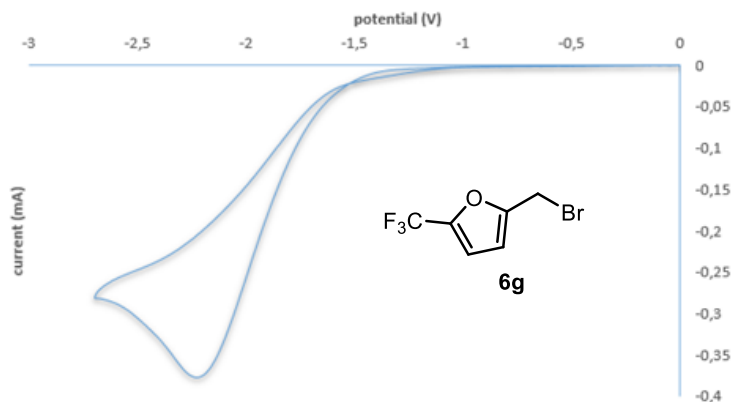


Figure 3.29: Cyclic voltammogram for 2-(bromomethyl)-5-(trifluoromethyl)furan bromide **6g** [0.02M] in [0.1 M] TBAPF₆ in CH₃CN. Sweep rate: 50 mV/s. Glassy carbon electrode working electrode, Ag/AgCl (KCl 3.5 M) reference electrode, Pt wire auxiliary electrode. Irreversible reduction, $E_p^c = E^{red}(\mathbf{6g}/\mathbf{6g}^-) = -2.25$ V, E_p^c refers to the cathodic peak potential, while the E^{red} value describes the electrochemical properties of **6g**.

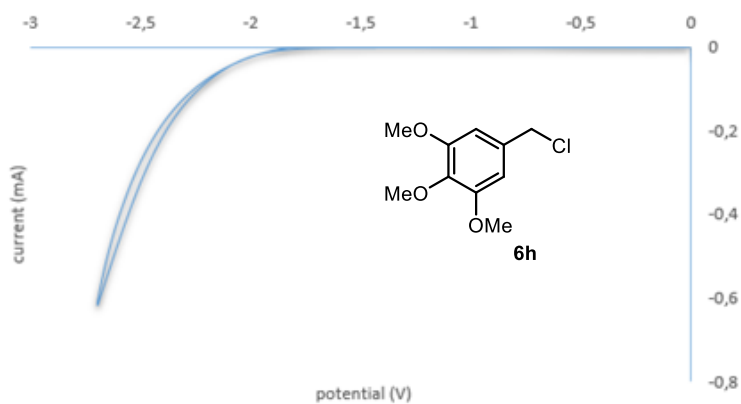


Figure 3.30: Cyclic voltammogram for 5-(chloromethyl)-1,2,3-trimethoxybenzene **6h** [0.02M] in [0.1 M] TBAPF₆ in CH₃CN. Sweep rate: 100 mV/s. Pt electrode working electrode, Ag/AgCl (KCl 3.5 M) reference electrode, Pt wire auxiliary electrode. Reduction of substrate **6h** was not observed in the registered potential window (from 0 to -2.7 V).

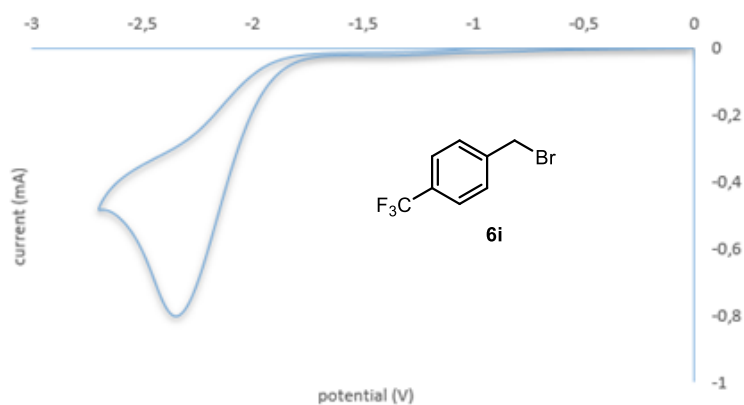


Figure 3.31: Cyclic voltammogram for 4-(trifluoromethyl)benzyl bromide **6i** [0.02M] in [0.1 M] TBAPF₆ in CH₃CN. Sweep rate: 500 mV/s. Pt electrode working electrode, Ag/AgCl (KCl 3.5 M) reference electrode, Pt wire auxiliary electrode. Irreversible reduction, $E_p^c = E^{\text{red}}(\mathbf{6i}/\mathbf{6i}^-) = -2.3 \text{ V}$, E_p^c refers to the cathodic peak potential, while the E^{red} value describes the electrochemical properties of **6i**.

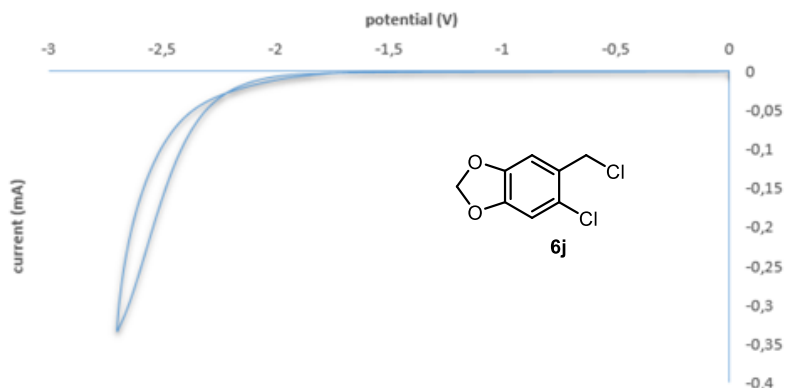


Figure 3.32: Cyclic voltammogram for 6-chloropiperonyl chloride **6j** [0.02M] in [0.1 M] TBAPF₆ in CH₃CN. Sweep rate: 50 mV/s. Glassy carbon electrode working electrode, Ag/AgCl (KCl 3.5 M) reference electrode, Pt wire auxiliary electrode. Reduction of substrate **6j** was not observed in the registered potential window (from 0 to -2.7 V).

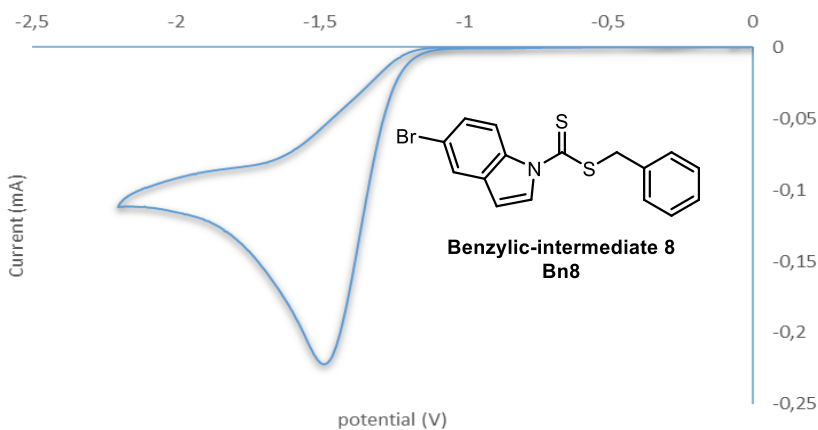


Figure 3.33: Cyclic voltammogram for Benzylic-intermediate I [0.02 M] in [0.1 M] TBAPF₆ in CH₃CN. Sweep rate: 50 mV/s. Pt electrode working electrode, Ag/AgCl (KCl 3.5 M) reference electrode, Pt wire auxiliary electrode. Irreversible reduction, $E_p^c = E^{\text{red}}(\text{Bn8}/\text{Bn8}^{\cdot-}) = -1.5 \text{ V}$, E_p^c refers to the cathodic peak potential, while the E^{red} value describes the electrochemical properties of the Benzylic-intermediate I.

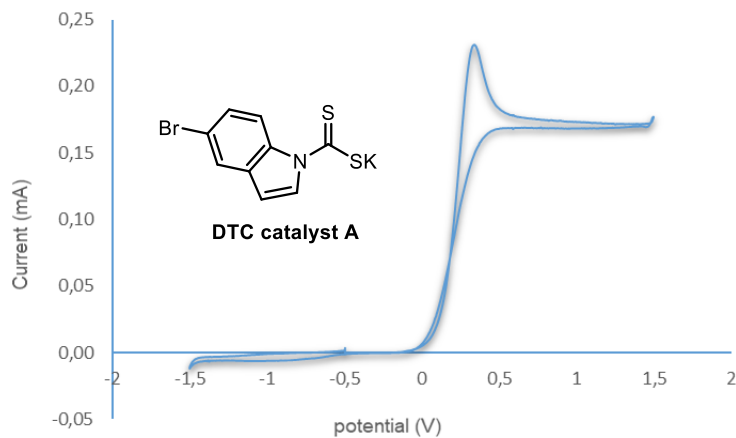


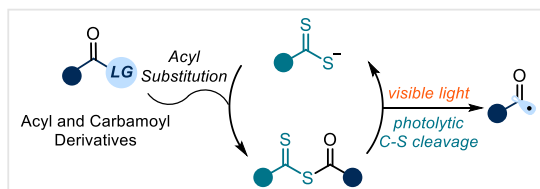
Figure 3.34: Cyclic voltammogram for DTC catalyst **A** [0.02 M] in [0.1 M] TBAPF₆ in CH₃CN. Sweep rate: 20 mV/s. Pt electrode working electrode, Ag/AgCl (KCl 3.5 M) reference electrode, Pt wire auxiliary electrode. Irreversible oxidation, $E_p^A = E^{ox}(A/Va) = +0.44$ V, E_p^A refers to the anodic peak potential, while the E^{ox} value describes the electrochemical properties of the DTC catalyst **A**.

Chapter IV

Photochemical generation of acyl and carbamoyl radicals using a nucleophilic organic catalyst

Target

Development of a photochemical organocatalytic method to generate acyl and carbamoyl radicals from readily available acyl chlorides, carbamoyl chlorides and anhydrides.



Tool

Exploit the nucleophilic properties of dithiocarbamate catalysts to displace suitable leaving groups within acyl and carbamoyl derivatives via a nucleophilic acyl substitution mechanism. The generated photo-absorbing intermediate, on excitation, produces the corresponding acyl and carbamoyl radicals.¹

4.1 Introduction

Acyl and carbamoyl radicals are nucleophilic intermediates of synthetic value² that can promote a variety of reactions, affording useful compounds including ketones, amides and lactams. Traditional strategies for their generation rely on the activation of preformed stoichiometric acyl³ and carbamoyl⁴ chalcogenes by means of radical

¹ The project discussed in this Chapter has been conducted in collaboration with Eduardo de Pedro Beato, who discovered the reaction with the acyl derivatives, performed the optimization, the scope of the acyl derivatives and part of the mechanistic studies, and Matteo Balletti, who performed part of the scope of the carbamoyl derivatives and part of the mechanistic studies. I was mainly involved in the development of the reaction concerning the carbamoyl chlorides, its optimization, the evaluation of the scope and part of the mechanistic studies. This work has been published, see: De Pedro Beato, E.; Mazzarella, D.; Balletti, M.; Melchiorre, P. "Photochemical generation of acyl and carbamoyl radicals using a nucleophilic organic catalyst: applications and mechanism thereof" *Chem. Sci.* **2020**, *11*, 6312-6324.

² Chatgililoglu, C.; Crich, D.; Komatsu, M.; Ryu, I. "Chemistry of Acyl Radicals" *Chem. Rev.* **1999**, *99*, 1991-2070.

³ (a) Barton, D. H. R.; George, M. V.; Tomoeda, M. "Photochemical Transformations. Part XIII. * A New Method for the Production of Acyl Radicals" *J. Chem. Soc.* **1962**, 1967-1974. (b) Delduc, P.; Tailhan, C.; Zard, S. Z. "A Convenient Source of Alkyl and Acyl Radicals" *J. Chem. Soc., Chem. Comm.* **1988**, 308-310. (c) Chen, C.; Crich, D.; Papadatos, A. "The chemistry of acyl tellurides: generation and trapping of acyl radicals, including aryltellurium group transfer" *J. Am. Chem. Soc.* **1992**, *114*, 8313-8314.

⁴ (a) Fujiwara, S.; Shimizu, Y.; Shinike, T.; Kambe, N. "Photoinduced Group Transfer Radical Addition of Carbamotelluroates to Acetylenes" *Org. Lett.* **2001**, *3*, 2085-2088. (b) Grainger, R. S.; Innocenti, P. "Dithiocarbamate Group Transfer Cyclization Reactions of Carbamoyl Radicals under "Tin-Free" Conditions" *Angew. Chem. Int. Ed.* **2004**, *43*, 3445-3448. (c) Millán-Ortiz, A.; López-Valdez, G.; Cortez-Guzmán, F.; Miranda, L. D. "A novel carbamoyl radical based dearomatizing spiroacylation process" *Chem. Commun.* **2015**, *51*, 8345-8348.

initiators or photolytic bond cleavage. With the advent of photoredox catalysis,^{5,6} methodologies based on hydrogen atom transfer (HAT)⁷ and single-electron transfer (SET)⁸ mechanisms have been developed. The HAT-based procedures employ commercially-available aldehydes and formamides. However, these methodologies suffer from regioselectivity issues when applied to complex molecules.⁷ On the other hand, the SET procedures require the use of purposely designed substrates adorned with redox-active auxiliaries.⁸ Thus the development of a strategy that can use commercially or readily-available substrates to produce acyl and carbamoyl radicals with good selectivity would be synthetically valuable.

Our research group has recently developed a photochemical strategy to produce alkyl radicals I via S_N2 activation of alkyl electrophiles (Figure 4.1).

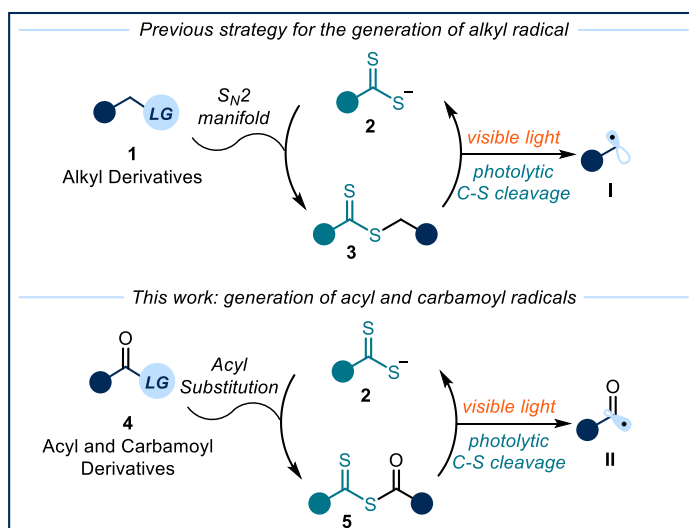


Figure 4.1: Formation of acyl and carbamoyl radicals II through dithiocarbonyl catalysis.

⁵ Shaw, M. H.; Twilton, J.; MacMillan, D. W. C. "Photoredox Catalysis in Organic Chemistry" *J. Org. Chem.* **2016**, *81*, 6898-6926.

⁶ For reviews on the generation of acyl and carbamoyl radicals via photoredox catalysis: (a) Raviola, C.; Protti, S.; Ravelli, D.; Fagnoni, M. "Photogenerated acyl/alkoxycarbonyl/carbamoyl radicals for sustainable synthesis" *Green Chem.* **2019**, *21*, 748-764. (b) Banerjee, A.; Lei, Z.; Ngai, M.-Y. "Acyl Radical Chemistry via Visible-Light Photoredox Catalysis" *Synthesis* **2019**, *51*, 303-333.

⁷ For a perspective on photocatalytic HAT procedures, see: Ravelli, D.; Fagnoni, M.; Fukuyama, T.; Nishikawa, T.; Ryu, I. "Site-Selective C-H Functionalization by Decatungstate Anion Photocatalysis: Synergistic Control by Polar and Steric Effects Expands the Reaction Scope" *ACS Catal.* **2018**, *8*, 701-713.

⁸ For selected examples see: (a) Wang, G.-Z.; Shang, R.; Cheng, W.-M.; Fu, Y. "Decarboxylative 1,4-Addition of α -Oxocarboxylic Acids with Michael Acceptors Enabled by Photoredox Catalysis" *Org. Lett.* **2015**, *17*, 4830-4833. (b) Capaldo, L.; Riccardi, R.; Ravelli, D.; Fagnoni, M. "Acyl Radicals from Acylsilanes: Photoredox-Catalyzed Synthesis of Unsymmetrical Ketones" *ACS Catal.* **2018**, *8*, 304-309. For selected examples on carbamoyl derivatives see: (c) Jouffroy, M.; Kong, J. "Direct C-H Carbamoylation of Nitrogen-Containing Heterocycles" *Chem. Eur. J.* **2019**, *25*, 2217-2221. (d) Petersen, W. F.; Taylor, R. J. K.; Donald, J. R. "Photoredox-Catalyzed Reductive Carbamoyl Radical Generation: "A Redox-Neutral Intermolecular Addition-Cyclization Approach to Functionalized 3,4-Dihydroquinolin-2-ones"" *Org. Lett.* **2017**, *19*, 874-877.

This radical generation strategy relied on the electrophilic properties of substrate **1**.⁹ We envisioned that this photochemical approach could be exploited to activate acyl and carbamoyl chlorides **4** via a nucleophilic acyl substitution pathway, ultimately affording the corresponding radicals **II**. Within this chapter, I discuss the successful implementation of this idea. Here, I will provide a general discussion on the formation of carbamoyl radicals, which will be useful to delineate the context of this project.

4.2 Generation of Carbamoyl Radicals

4.2.1 Use of stoichiometric oxidants

The generation of carbamoyl radicals under oxidative conditions has been demonstrated by the pioneering work of Francesco Minisci.¹⁰ Specifically, the authors used formamide **6** (Figure 4.2a) as the carbamoyl radical precursor and a combination of iron sulfate and hydrogen peroxide as source of hydroxyl radicals. HAT from hydroxyl radical onto **6** generates the carbamoyl radical **III**, which is subsequently trapped by the acid-activated quinoline **7** to yield product **8**. One of the main drawback of this method, which is a consequence of the harsh conditions, is the low selectivity for the generation of the carbamoyl radical. Indeed, when the substituents on the nitrogen atom of the formamide **6** are alkyl chains, alkyl radical intermediates are also formed. To address this issue, Minisci used oxalic acid monoamide derivatives **9** (Figure 4.2b) as radical precursors.¹¹ The use of sodium persulfate and silver nitrite as oxidizing agents led to the desired carbamoyl radicals with much better selectivity.

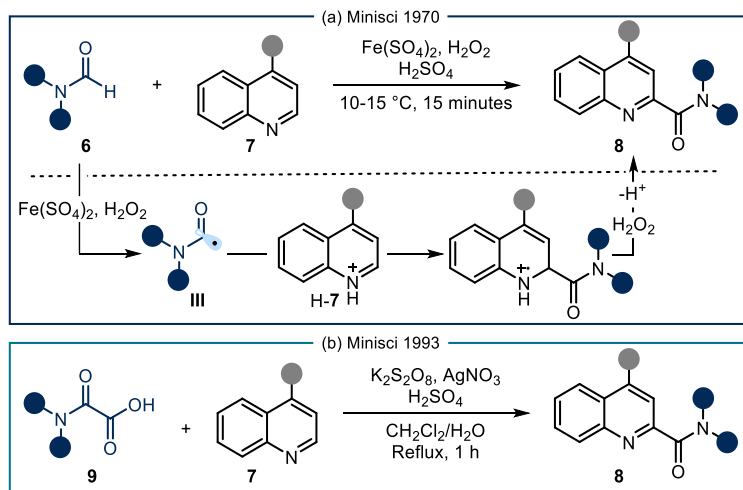


Figure 4.2: Use of stoichiometric oxidants to promote the formation of carbamoyl radicals and subsequent trap with electron-poor heteroaromatics.

⁹ Schweitzer-Chaput, B.; Horwitz, M. A.; de Pedro Beato, E.; Melchiorre, P. "Photochemical generation of radicals from alkyl electrophiles using a nucleophilic organic catalyst" *Nat. Chem.* **2019**, *11*, 129-135.

¹⁰ Minisci, F.; Gardini, G. P.; Galli, E.; Bertini, F. "A New Selective Type of Aromatic Substitution: Homolytic Amidation" *Tetrahedron Lett.* **1970**, *11*, 15-16.

¹¹ Minisci, F.; Citterio, A.; Vismara, E. "Polar Effects in Free-Radical Reactions. New Synthetic Developments in the Functionalization of Heteroaromatic Bases by Nucleophilic Radicals" *Tetrahedron* **1985**, *41*, 4157-4170.

Overall, these examples provided the first methods for generating carbamoyl radicals, although using rather harsh reaction conditions.

4.2.2 Use of carbamoyl cobalt salophens and chalcogenes

Cobalt salophens¹² and chalcogens derivatives¹³ have been widely used as radical precursors in concert with initiators, heat or light. One common feature of these derivatives is their tendency to operate through a group transfer mechanism, where both fragments of the radical precursor are incorporated into the structure of the final product. Because of their wide applicability, these strategies have been also applied for the generation of carbamoyl radicals. Early works from the group of Pattenden highlighted that readily synthesized carbamoyl cobalto-salophen derivatives **10** (Figure 4.3) could undergo photolytic or thermolytic cleavage of the C-Co bond, yielding carbamoyl radical **IV**.¹⁴ The latter intermediate cyclized on a pendant olefin to produce radical **V**, which subsequently propagates the radical chain reacting with a second molecule of cobalto-salophen **10**, delivering product **11** while regenerating radical **IV**.

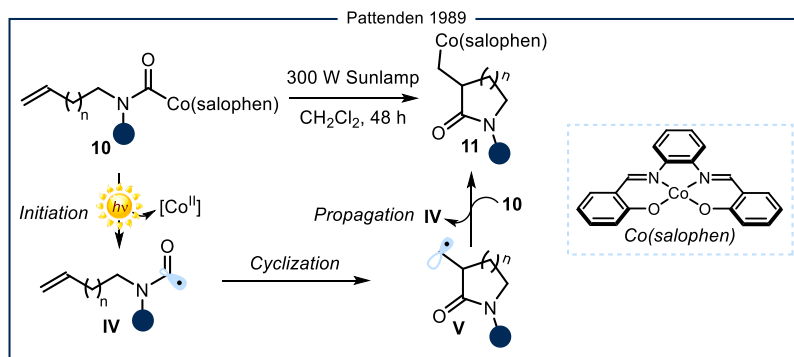


Figure 4.3: Carbamoyl cobaltosalophen derivatives as precursors of carbamoyl radicals and their use in group transfer reactivity.

Organotellurides **12** (Figure 4.4) have also been converted into α,β -unsaturated amides **14** through the intermediacy of carbamoyl radicals.^{4a} Specifically, irradiation with a tungsten lamp at 60 °C promoted the cleavage of the Te-C bond, furnishing the carbamoyl radical **III**. This fleeting intermediate was trapped by the terminal alkyne **13**, yielding the C(sp²)-centered radical **VI**. The latter was rapidly intercepted by a second molecule of organotelluride **12**, yielding tellurium-centered radical **VII** which collapsed to afford product **14** while regenerating radical **III**.

¹² Demarteau, J.; Debuigne, A.; Detrembleur, C. "Organocobalt Complexes as Sources of Carbon-Centered Radicals for Organic and Polymer Chemistries" *Chem. Rev.* **2019**, *119*, 6906-6955.

¹³ (a) Ogawa, A. "Selenium and Tellurium in Organic Synthesis". In *Main Group Metals in Organic Synthesis*, **2004**, Wiley-VCH. (b) Zard, S. Z. "On the Trail of Xanthates: Some New Chemistry from an Old Functional Group" *Angew. Chem. Int. Ed.* **1997**, *36*, 672-685. (c) Quiclet-Sire, B.; Zard, S. Z. "Powerful Carbon-Carbon Bond Forming Reactions Based on a Novel Radical Exchange Process" *Chem. Eur. J.* **2006**, *12*, 6002-6016.

¹⁴ Gill, G. B.; Pattenden, G.; Reynolds, S. J. "Cobalt-Mediated Reactions. A New Synthetic Approach to β -, γ - and δ -Lactams" *Tetrahedron Lett.* **1989**, *30*, 3229-3232.

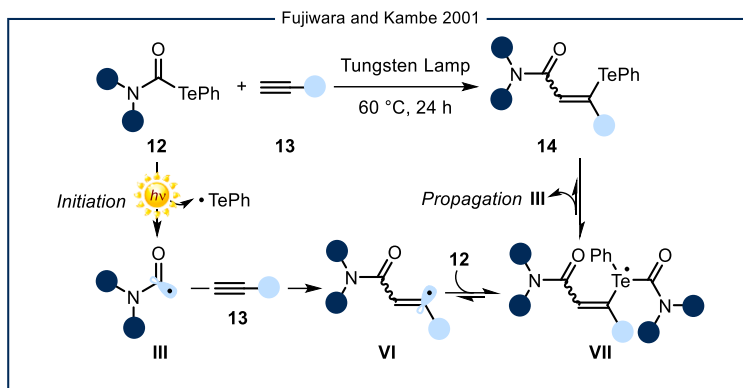


Figure 4.4: Carbamoyl telluride derivatives as precursors of carbamoyl radicals and their use in group transfer reactivity.

Also thiocarbonyl derivatives have been used to produce carbamoyl radicals. Grainger and Innocenti demonstrated how carbamoyl dithiocarbamates **15** (Figure 4.5) could generate carbamoyl radicals under either photolytic conditions or through the use of a radical initiator.^{4b} The ensuing C(sp²)-centered radical **IX** cyclized on a pendant olefin to produce the alkyl radical **X**. This intermediate was reversibly intercepted by a second molecule of dithiocarbamate **15** to produce radical **XI**, which subsequently collapsed to form product **16** while regenerating radical **IX**, thus feeding a radical chain mechanism. The reversibility of several steps within the group transfer manifold implies that a strict thermodynamic requirement must be fulfilled in order for the reaction to effectively proceed: specifically, radical **X** has to be less stable than the progenitor radical **IX**. This allows the preferential collapse of intermediate **XI** into **IX**, rather than into **X**, and the concomitant formation of **16**.

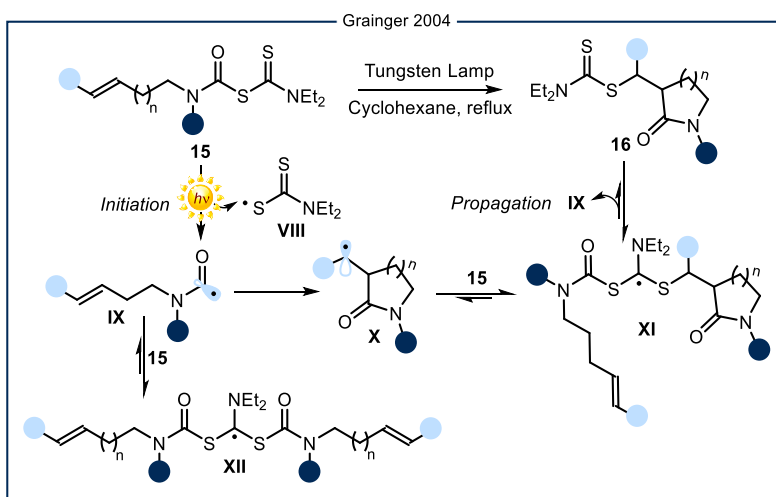


Figure 4.5: Carbamoyl dithiocarbamates as precursors of carbamoyl radicals and their use in group transfer reactivity.

One general interesting feature of xanthates and dithiocarbamates **15** is the intrinsic ability to increase the lifetime of the ensuing radicals through a degenerative mechanism.^{13c} As illustrated in Figure 4.5, after the initiation event, radical **IX** can be intercepted by a second molecule of **15**, furnishing the open-shell intermediate **XII**. This radical can then collapse through a β -scission of the *S*-alkyl bond, regenerating radical **IX** and dithiocarbamate **15**. This addition-fragmentation sequence provides a tool to stabilize radical **IX** increasing its lifetime. Because of this peculiar feature, the chemistry of xanthates and dithiocarbamates has enabled radical additions on unactivated alkenes and other kinetically slow radical transformations that are not feasible when a different radical-generating method is employed.^{13b} Overall, these methods provide access to carbamoyl radicals under milder conditions than the examples highlighted in section 4.2.1. However, preformed stoichiometric substrates are required.

4.2.3 Catalytic formation of carbamoyl radicals

Catalytic methods to produce carbamoyl radicals have also been recently developed.⁶ The renaissance of photoredox catalysis undoubtedly helped in developing new catalytic processes based on previous stoichiometric variants. As an example, the group of Feng,¹⁵ inspired by the seminal examples of Minisci,^{10,11} developed a photoredox procedure to catalytically convert oxalic acid monoamide derivatives **17** into carbamoyl radicals **XIII** (Figure 4.6).

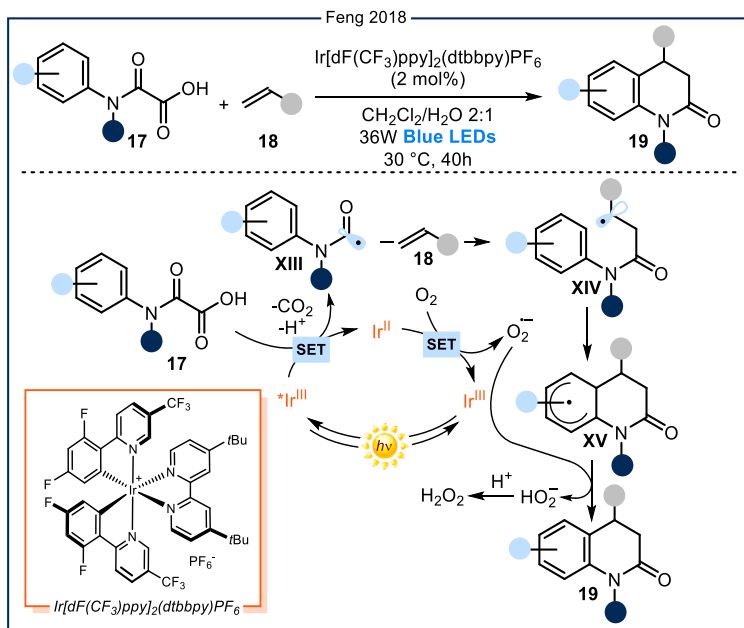


Figure 4.6: Oxalic acid monoamide derivatives as precursors of carbamoyl radicals under photoredox catalytic conditions. LEDs: Light-emitting diodes. SET: Single electron transfer.

¹⁵ Bai, Q.-F.; Jin, C.; He, J.-Y.; Feng, G. "Carbamoyl Radicals via Photoredox Decarboxylation of Oxamic Acids in Aqueous Media: Access to 3,4-Dihydroquinolin-2(1H)-ones" *Org. Lett.* **2018**, *20*, 2172-2175.

Specifically, light excitation of the $\text{Ir}[\text{dF}(\text{CF}_3)\text{ppy}]_2(\text{dtbbpy})\text{PF}_6$ catalyst promotes the SET oxidation of substrate **17** to produce, after extrusion of CO_2 , the desired carbamoyl radical **XIII**, which is intermolecularly trapped by olefin **18**, producing alkyl radical **XIV**. The latter intermediate undergoes an intramolecular homolytic aromatic substitution, furnishing cyclohexadienyl radical **XV**. In the meantime, the iridium catalyst is regenerated by molecular oxygen, thus producing the oxygen radical anion $\text{O}_2^{\cdot-}$. The latter performs hydrogen atom transfer (HAT) from **XV**, providing the desired product **19** and, after protonation, hydrogen peroxide.

Not only substrates amenable to oxidation, such as oxalic acid monoamide derivatives **17**, can be used to generate carbamoyl radicals under photocatalytic conditions. *N*-hydroxyphthalimido oxamides **20** (Figure 4.7) can produce carbamoyl radicals **XIII** upon SET reduction.^{8d} This reaction is triggered by the absorption of light from $\text{Ir}(\text{ppy})_3$, producing its highly reducing excited state, which transfers one electron to **20**, promoting the loss of the phthalimide anion and CO_2 to ultimately afford radical **XIII**. Analogously to the previous photocatalytic example, the radical **XIII** is trapped by olefin **18** to produce the alkyl radical **XIV**, which is intramolecularly trapped by the pendant aryl moiety. The ensuing intermediate **XV** is oxidized by the reduced form of the photocatalyst to yield, after deprotonation, the desired product **19**.

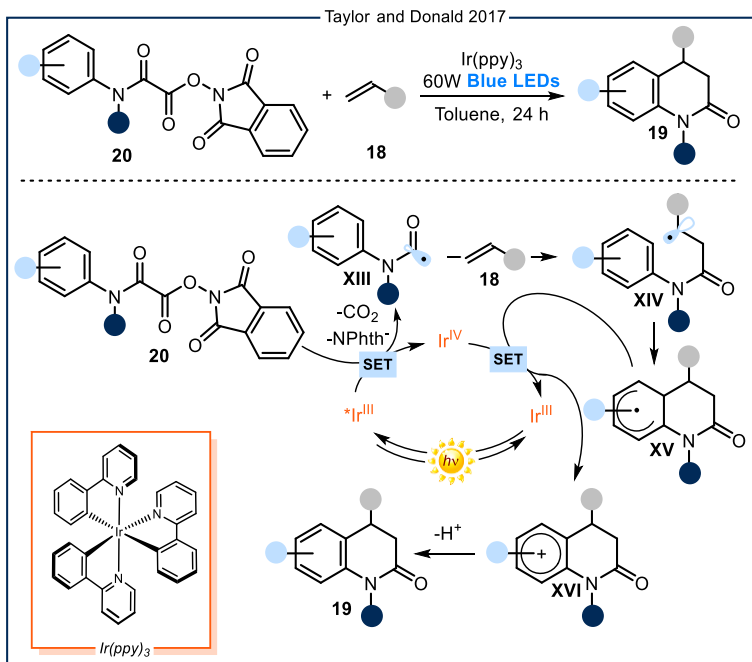


Figure 4.7: *N*-hydroxyphthalimido oxamides derivatives as precursors of carbamoyl radicals under photoredox conditions. LEDs: Light-emitting diodes. SET: Single electron transfer.

Both catalytic strategies, albeit effective for producing carbamoyl radicals under mild conditions, rely on the use of purposely designed substrates, such as **17** and **20**. This is because of the necessity to have a redox auxiliary group that can receive or donate

electrons to the photocatalyst. Besides facilitating the SET event, this moiety then fragments to produce the radical **XIII**.

An alternative strategy to promote the catalytic formation of carbamoyl radicals is based on the use of HAT reagents. A widely used catalyst is tetrabutylammonium decatungstate (TBADT), which after light absorption ($\lambda_{\text{max}} = 365 \text{ nm}$), acquires an outstanding activity towards SET oxidation and HAT.¹⁶ TBADT has been recently used to drive the C-H functionalization of relatively inert C-H bonds, such as in alkanes, cyclic ethers and carbonyl derivatives.⁷ Moreover, TBADT can also abstract a hydrogen atom from formamide derivatives **6** (Figure 4.8), furnishing carbamoyl radicals **III** and TBADTH.¹⁷ The latter intermediate is oxidized by the stoichiometric persulfate, restoring TBADT while producing the oxidizing $\text{SO}_4^{\cdot-}$. Meanwhile, radical **III** is trapped in a Minisci-type pathway by the acid-activated quinoline **21**, affording the radical cation **XVII**. Finally, **XVII** is oxidized and deprotonated to afford product **22**.

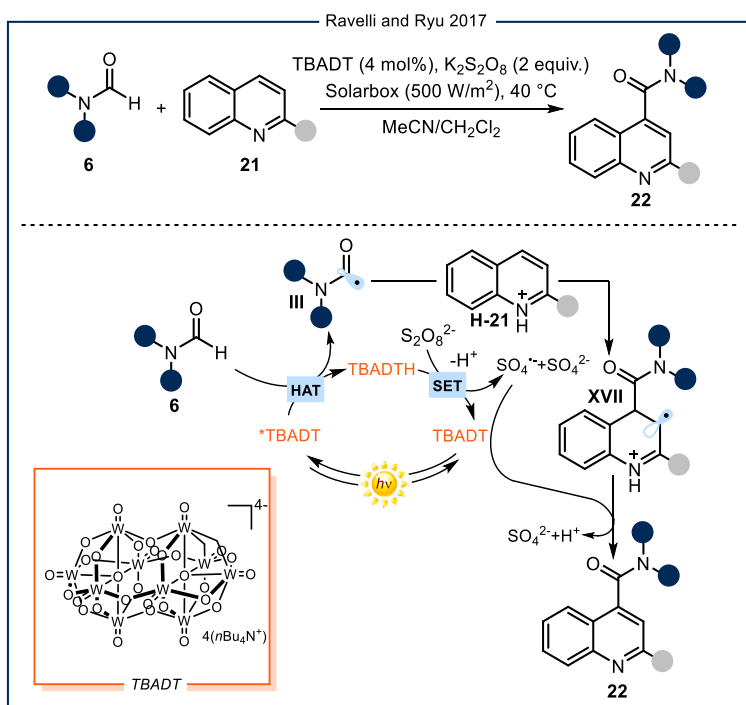


Figure 4.8: Formamide derivatives as precursors of carbamoyl radicals through the use of TBADT. TBADT: tetrabutylammonium decatungstate. HAT: Hydrogen atom transfer. SET: Single electron transfer.

Generally, these photochemical methods serve to produce carbamoyl radicals under a catalytic regime. However, they require substrates either adorned with purposely

¹⁶ Tzirakis, M. D.; Lykakis, I. N.; Orfanopoulos, M. "Decatungstate as an efficient photocatalyst in organic chemistry" *Chem. Soc. Rev.* **2009**, *38*, 2609-2621.

¹⁷ Quattrini, M.; Fujii, S.; Yamada, K.; Fukuyama, T.; Ravelli, D.; Fagnoni, M.; Ryu, I. "Versatile cross-dehydrogenative coupling of heteroaromatics and hydrogen donors via decatungstate photocatalysis" *Chem. Commun.* **2017**, *53*, 2335-2338.

tailored redox moieties for enabling the SET or possessing C-H bonds with sufficiently low bond dissociation energy (BDE) for promoting HAT.

4.3 Target of the Project

The aim of the project discussed in this chapter is to expand the range of electrophiles amenable to the photochemical radical generation strategy based on the use of nucleophilic DTC organic catalysts. To date, our strategy has been limited by the need for substrates amenable to an S_N2 displacement. Herein, we expand the potential of this photochemical catalytic approach to include *nucleophilic acyl substitution* as a suitable manifold for radical generation. We used this approach to generate acyl and carbamoyl radicals upon activation of the corresponding chlorides and anhydrides. These substrates, due to their high reduction potential, are not readily prone to redox-based activation mechanisms.

I will mainly focus on the generation and synthetic use of carbamoyl derivatives, since this is the research I was directly involved in.

4.3.1 Design plan

Figure 4.9 highlights the proposed mechanism for the photochemical catalytic generation of carbamoyl radicals from the corresponding chlorides. This initial mechanistic picture was based on our previous works dealing with the S_N2 activation of alkyl electrophiles (Figure 3.8 in Chapter III).^{9,18} By analogy, we envisioned a catalytic cycle where the nucleophilic dithiocarbonyl (DTC) catalyst would engage carbamoyl chlorides **23** in a nucleophilic acyl substitution reaction. The ensuing intermediate **24** possesses a weak C-S bond, which could be cleaved by low-energy photons to promote the formation of the carbamoyl radical **XVIII** and the dithiocarbonyl radical **XIX**. The feasibility of this crucial step finds support in the aforementioned studies by Grainger,^{4b} who demonstrated the tendency of stoichiometric carbamoyl dithiocarbamates to undergo photolysis affording carbamoyl radicals, which later reacted in a group transfer manifold (*e.g.* Figure 4.5). In our mechanistic picture (Figure 4.9), the carbamoyl radical would be generated under a catalytic regime and would not be limited within the constraints of a group transfer mechanism.

¹⁸ (a) Cuadros, S.; Horwitz, M. A.; Schweitzer-Chaput, B.; Melchiorre, P. "A visible-light mediated three-component radical process using dithiocarbamate anion catalysis" *Chem. Sci.* **2019**, *10*, 5484-5488. (b) Mazarella, D.; Magagnano, G.; Schweitzer-Chaput, B.; Melchiorre, P. "Photochemical Organocatalytic Borylation of Alkyl Chlorides, Bromides and Sulfonates" *ACS Catal.* **2019**, *9*, 5876-5880. (c) Spinnato, D.; Schweitzer-Chaput, B.; Goti, G.; Ošeka, M.; Melchiorre, P. "A Photochemical Organocatalytic Strategy for the α -Alkylation of Ketones by using Radicals" *Angew. Chem. Int. Ed.* **2020**, *59*, 9485-9490.

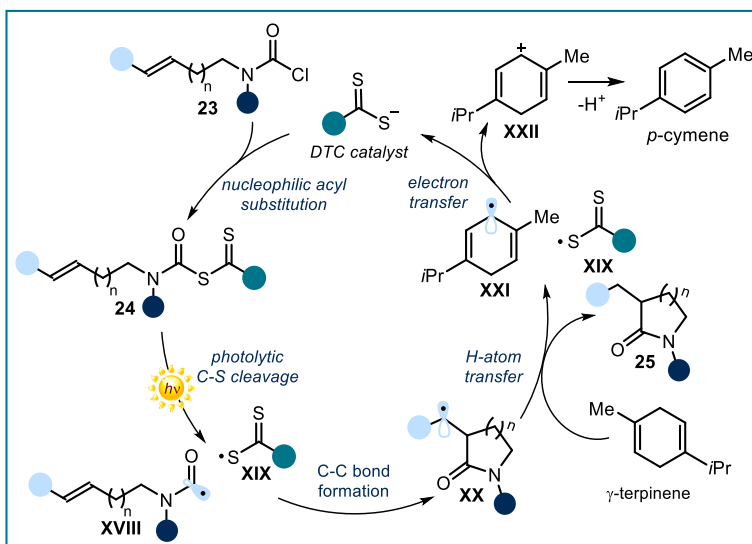


Figure 4.9: Design plan for the photochemical catalytic generation of carbamoyl radicals from carbamoyl chlorides and their intramolecular trapping. DTC: Dithiocarbonyl.

As such, we envisioned that the photogenerated carbamoyl radical **XVIII** would be intramolecularly intercepted by a pendant olefin, forging a new C-C bond. The ensuing alkyl radical **XX** would then perform HAT from γ -terpinene (an H donor), delivering the desired lactam product **24** while forming the cyclohexadienyl radical **XXI**. Crucial for catalyst turnover would be an SET reduction of the dithiocarbonyl radical **XIX** (for example ethyl xanthogenate anion has a reduction potential $E(\text{XIX}/\text{DTC}) = +0.04$ V vs SCE)¹⁹ from the cyclohexadienyl radical **XXI** ($E(\text{XXII}/\text{XXI}) = -0.1$ V vs SCE).²⁰ Moreover, we envisioned that this strategy could be further expanded to an intermolecular process (Figure 4.10), where the photogenerated carbamoyl radical **III** is trapped by an electro-poor olefin **18**, yielding the electrophilic radical **XXIII**. The latter abstracts a hydrogen atom from γ -terpinene, yielding the desired product **28**.

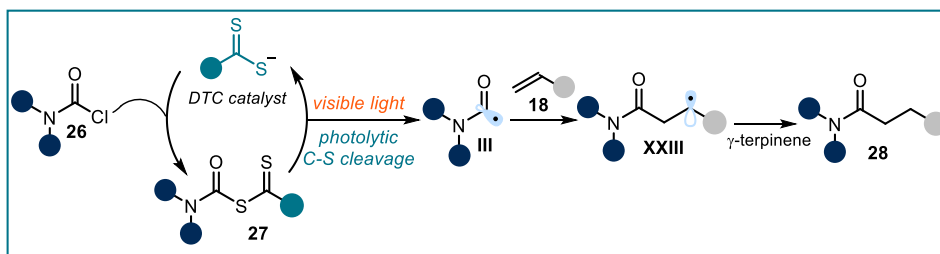


Figure 4.10: Design plan for the photochemical catalytic generation of carbamoyl radicals from carbamoyl chlorides and their intermolecular trapping. DTC: Dithiocarbonyl.

¹⁹ Dag, O.; Yaman, S. O.; Onal, A. M.; Isci, H. "Spectroelectrochemistry of potassium ethylxanthate, bis(ethylxanthato)nickel(II) and tetraethylammonium tris(ethylxanthato)nickelate(II)" *J. Chem. Soc. Dalton Trans.* **2001**, 2819-2824.

²⁰ Bahtia, K.; Schuler, R. H. "Oxidation of hydroxycyclohexadienyl radical by metal ions" *J. Phys. Chem.* **1974**, *78*, 2335-2338.

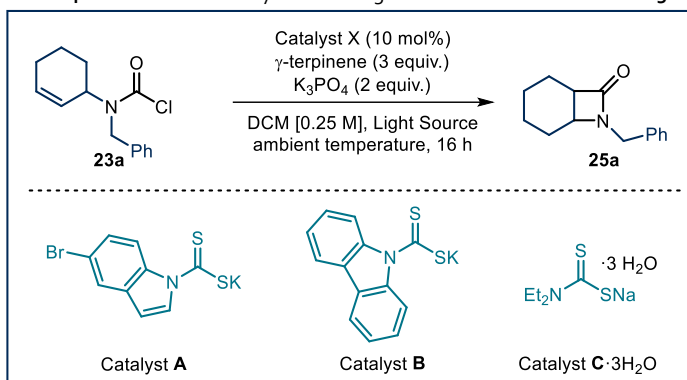
Overall, these strategies would enable the conversion of carbamoyl chlorides **23** and **26** into valuable lactams **24** and amides **28** without the need of a metal catalyst and under mild conditions.

4.4 Results and Discussion

4.4.1 Optimization and scope of the intramolecular reaction

The feasibility of the intramolecular reaction was evaluated using substrate **23a** as the carbamoyl radical precursor (Table 4.1). The reaction was conducted in dichloromethane at ambient temperature using three equivalents of γ -terpinene, two equivalents of K_3PO_4 as the basic additive to quench the *in situ* formed hydrochloric acid, and under irradiation of a blue LED (465 nm) to promote the photolysis of the corresponding dithiocarbamates intermediate **24**. We started the optimization by evaluating the influence of different dithiocarbonyl catalysts.

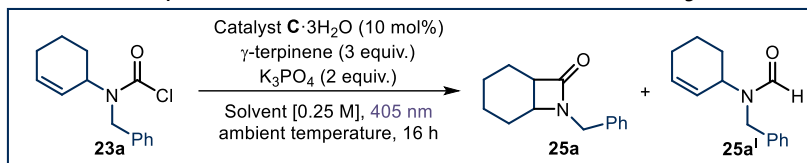
Table 4.1: Effect of the catalyst and the light source on the formation of **25a**.^a



Entry	Catalyst	Light	Yield ^b
1	A	465 nm	-
2	B	465 nm	-
3	C	405 nm	5%

^aReaction performed on a 0.2 mmol scale. ^bYield of **25a** determined by ¹H NMR analysis of the crude mixture using trichloroethane as the internal standard.

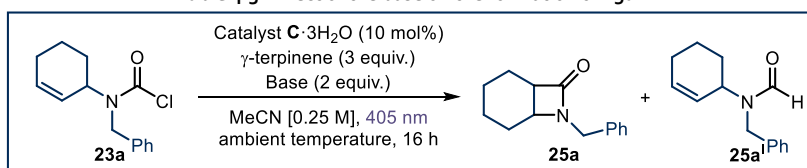
Surprisingly, the indole- and carbazole-containing dithiocarbonyl anions **A** and **B** (entries 1 and 2 respectively), which were the best performing catalysts in previous strategies,^{9,18} proved unsuitable to promote the formation of carbamoyl radicals. On the other hand, the commercially available diethylamino dithiocarbamate trihydrate (catalyst **C**, which required irradiation at 405 nm) provided the corresponding product **25a**, albeit in very low yields (entry 3). Catalyst **C** was selected for further optimization. We focused on the influence of the reaction solvent (Table 4.2).

Table 4.2: Effect of the nature of the solvent on the formation of **25a**.^a

Entry	Solvent	Yield ^b 25a / 25a^I
1	acetonitrile	28/19
2	acetone	26/19
3	AcOEt	7/traces
4	THF	27/24
5	toluene	18/13
6	DMF	10/10
7	DMA	-/-

^aReaction performed on a 0.2 mmol scale. ^bYields of **25a** and **25a^I** determined by ¹H NMR analysis of the crude mixture using trichloroethane as the internal standard.

The use of acetonitrile (entry 1) delivered product **25a** with better efficiency compared to CH₂Cl₂. We also noticed the formation of the by-product **25a^I**, arising from the H abstraction from carbamoyl radical **XVIII** (Figure 4.9). Acetone furnished the same product distribution with a similar ratio (entry 2). While ethyl acetate almost completely suppressed the reactivity (entry 3), tetrahydrofuran (THF) promoted the reaction with a poor ratio between **25a** and **25a^I** (entry 4). The use of either a less polar solvent, such as toluene (entry 5), or of highly polar solvents, such as DMF or DMA (entries 6 and 7), had a detrimental effect on the chemical yield. Acetonitrile was selected as the optimal solvent. We then investigated the effect of the base (Table 4.3).

Table 4.3: Effect of the base on the formation of **25a**.^a

Entry	Base	Yield ^b 25a / 25a^I
1	Na ₃ PO ₄	18/13
2	K ₂ CO ₃	23/13
3	DBU	14/11
4	TMG	11/9
5	Lutidine	7/traces

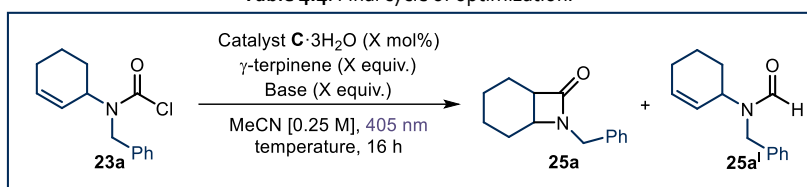
^aReaction performed on a 0.2 mmol scale. ^bYields of **25** and **25a^I** determined by ¹H NMR analysis of the crude mixture using trichloroethane as the internal standard.

Interestingly, the use of Na₃PO₄ and K₂CO₃ instead of K₃PO₄ had a negative effect on the overall yield of the process (entries 1 and 2). Apparently, for a productive process, the base should be poorly soluble in the reaction medium. Indeed, when employing

soluble organic bases, such as 1,8-diazabicyclo[5.4.0]undec-7-ene (DBU), 1,1,3,3-tetramethylguanidine (TMG) or lutidine (entries 3-5), both **25a** and **25a^I** were obtained in lower amounts.

In a final cycle of optimization, we evaluated the effect of catalyst loading, stoichiometry of both γ -terpinene and base, and the temperature (Table 4.4). When employing 20 mol% of catalyst **C**, the target product **25a** was obtained in 40% yield, together with 20% of by-product **25a^I**. However, a further catalyst increase to 40 mol% (entry 2) proved detrimental for the chemical yield. Trying to suppress the undesired HAT event, which forms by-product **25a^I**, we reduced the amount of γ -terpinene to 1.5 equivalents (entry 3). Although the product distribution remained unchanged, the chemical yield of product **25a** increased to 51%. The use of either 1 equivalent (entry 4) or 5 equivalents (entry 5) of γ -terpinene delivered the product with reduced efficiency. Changing the amount of the base (decrease to 1.5 equivalents (entry 6) or increase to 3 equivalents (entry 7)) afforded reduced yield.

Table 4.4: Final cycle of optimization.^a



Entry	C	H donor	Base	Temperature	Yield ^b 25a / 25a^I
1	20 mol%	2 equiv.	2 equiv.	Ambient	40/20
2	40 mol%	2 equiv.	2 equiv.	Ambient	30/12
3	20 mol%	1.5 equiv.	2 equiv.	Ambient	51/25
4	20 mol%	1 equiv.	2 equiv.	Ambient	45/20
5	20 mol%	5 equiv.	2 equiv.	Ambient	25/17
6	20 mol%	1.5 equiv.	1.5 equiv.	Ambient	35/20
7	20 mol%	1.5 equiv.	3 equiv.	Ambient	30/18
8	20 mol%	1.5 equiv.	2 equiv.	50 °C	65(65)/25

^aReaction performed on a 0.2 mmol scale. ^bYields of **25a** and **25a^I** determined by ¹H NMR analysis of the crude mixture using trichloroethane as the internal standard; the value shown in parentheses refers to the yield of isolated **25a** after chromatographic purification on silica gel.

Finally, we found that the temperature had a marked influence on the efficiency of the process, since increasing it from ambient (around 30 °C, as measured with a thermometer) to 50 °C delivered the desired product **25a** in 65% yield (entry 8). Further change of the temperature did not have any influence. Adopting the optimized conditions reported in Table 4.4, entry 8, we evaluated the generality of the intramolecular trap of carbamoyl radicals (Figure 4.11).

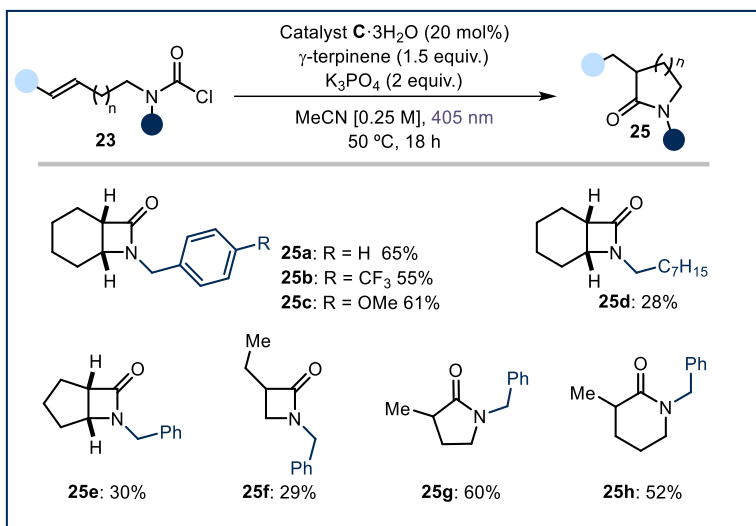
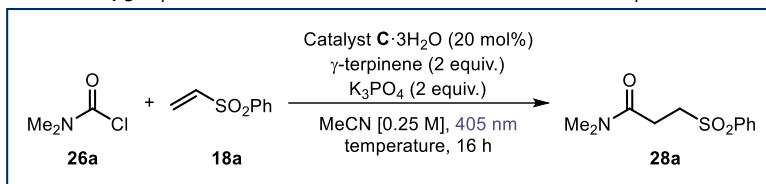


Figure 4.11 Survey of carbamoyl chlorides **23** amenable to the photochemical cyclization reaction. Reactions performed on a 0.2 mmol scale in 0.8 mL of MeCN. Yields of the isolated products **25** are indicated below each entry.

Because this photochemical radical generation strategy is not based on the redox potential of the substrates, both electron-withdrawing (**25b**) and electron-donating (**25c**) substituents were tolerated. The benzyl moiety on the nitrogen atom is not required, as the installment of a simple alkyl chain delivered the product, albeit with lower yields (**25d**). This approach enables the direct production of β -lactams fused with a 6 membered ring, a 5-membered ring (**25e**), or without any fused ring (**25f**). However, in these cases, the competitive HAT of the carbamoyl radical greatly influenced the overall efficiency of the product. Finally, both 5-membered (**25g**) and 6-membered ring lactams (**25h**) could be synthesized in good yields.

4.4.2 Optimization and scope of the intermolecular reaction

We then set to investigate the optimal conditions of the intermolecular process. We used the carbamoyl chloride **26a** as the radical precursor and vinyl sulfone **18a** as the electron-poor olefin (Table 4.5). Applying the previously optimized conditions (*c.f.* Table 4.4, entry 8), product **28a** was obtained in 40% yield (entry 1). Increasing the equivalents of the hydrogen atom donor proved beneficial for the chemical efficiency. Indeed, the use of 2 equivalents of γ -terpinene afforded **28a** in 60% yield (entry 2). Further increase to 3 equivalents afforded the product with similar results (entry 3). Finally, in analogy to the previous reaction, a high temperature (50 °C) was needed to secure good reactivity, as the process conducted at ambient temperature furnished the product with diminished yields (entry 4).

Table 4.5: Optimization of the intermolecular addition of carbamoyl radicals.^a

Entry	H donor	Temperature	Yield ^b
1	1.5 equiv.	50 °C	40
2	2 equiv.	50 °C	60(60)
3	3 equiv.	50 °C	60
4	2 equiv.	Ambient	38

^aReaction performed on a 0.2 mmol scale, using 2 equivalents of **26a**. ^bYield of **28a** determined by ¹H NMR analysis of the crude mixture using trichloroethane as the internal standard; the value shown in parentheses refers to the yield of isolated **28a** after chromatographic purification on silica gel.

Adopting the optimized conditions detailed in Table 4.5, entry 2, we evaluated the generality of the intermolecular trap of carbamoyl radicals (Figure 4.12).

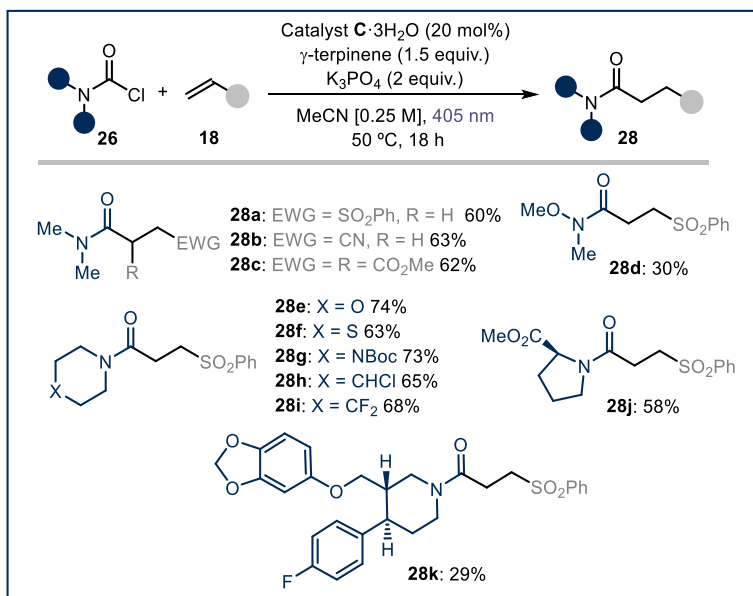


Figure 4.12 Survey of electron-poor olefins **18** and carbamoyl chlorides **26** amenable to the intermolecular addition of carbamoyl radicals. Reactions performed on a 0.2 mmol scale using 2 equiv. of **26** in 0.8 mL of MeCN. Yields of the isolated products **28** are indicated below each entry.

Three different electron-poor olefins smoothly reacted with dimethylcarbamoyl chloride **26a**, affording the corresponding amides **28a-c**. A variety of carbamoyl precursors were successfully employed in this photochemical process. Specifically, *N*-methoxy-*N*-methylcarbamoyl chloride afforded the Weinreb amide derivative **28d** through an alternative disconnection compared to the classical one. Oxygen-, sulfur-, nitrogen-, chlorine- and fluorine-containing carbamoyl chlorides (**28e-i**) smoothly

reacted with vinyl sulfone **18a** with good efficiency. Moreover, the chloride obtained from proline methyl ester was functionalized, affording product **28j**. Finally, the paroxetine-derived carbamoyl derivative delivered the addition product **28k**, albeit with lower efficiency than simpler substrates.

4.5 Acyl derivatives²¹

The photochemical method detailed in the previous section was also applied for the production of acyl radicals. In this case, the nucleophilic acyl substitution on acyl derivative **29** (Figure 4.13) from the dithiocarbonyl catalyst, followed by photolysis of the ensuing intermediate **30**, would produce the acyl radical **XXIV**. Analogously to carbamoyl radicals **III**, the acyl analogues **XXIV** would be intercepted by electron-poor olefins **18**, producing the electrophilic radical **XXV**. Abstraction of a hydrogen atom from γ -terpinene generates the product **31** and cyclohexadienyl radical **XXI**. SET reduction of the dithiocarbonyl radical **XIX** from **XXI** turns over the catalyst, closing the catalytic cycle.

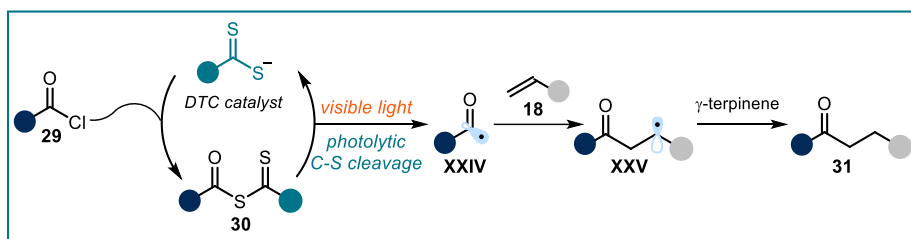


Figure 4.13: Design plan for the photochemical catalytic generation of acyl radicals from acyl chlorides and their intermolecular trapping. DTC: Dithiocarbonyl.

Optimization of the reaction conditions established dichloromethane as the best solvent and potassium ethyl xanthogenate catalyst **D** as the optimal dithiocarbonyl catalyst (Figure 4.14). The acyl intermediate **30**, transiently generated during the process, can absorb light at 465 nm, allowing the use of blue LEDs for the photolysis of the weak C-S bond. Under the optimized conditions, several electron-poor olefins reacted with 4-methoxybenzoyl chloride, affording the corresponding products in good yields (Figure 4.14). Terminal olefins bearing different electron-withdrawing moieties, such as a cyano, an ester, an aldehyde, a ketone, a phosphonate, a sulfone, and a sulfonamide group, afforded the corresponding products **31a-j** with good yields. Also internal olefins were amenable to this protocol (products **31k-m**).

²¹ The experimental work detailed in this section has been performed by Eduardo de Pedro Beato.

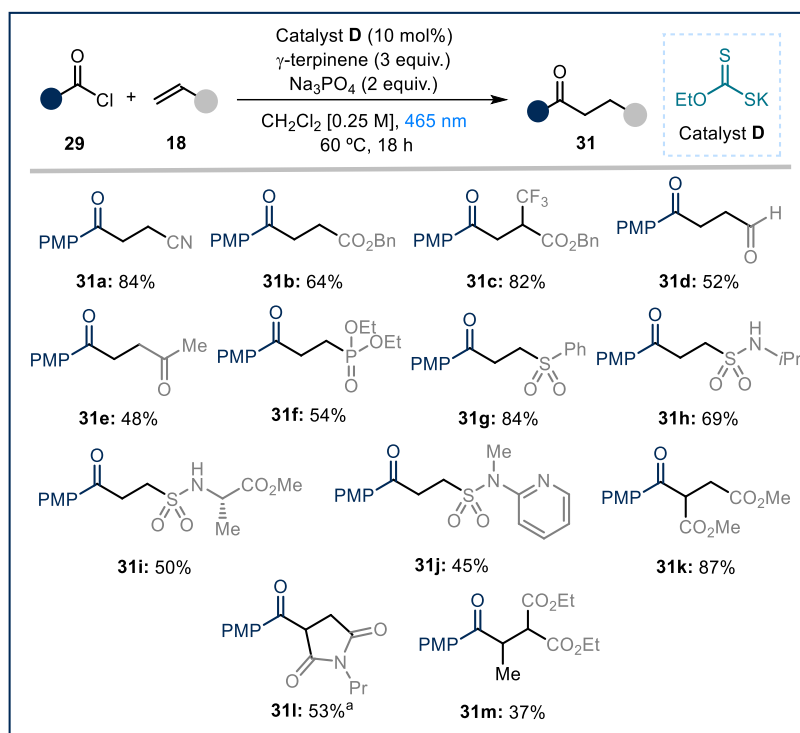


Figure 4.14: Survey of electron-poor olefins **18** amenable to the intermolecular addition of acyl radicals. Reactions performed on a 0.5 mmol scale using 1.5 equiv. of **29** in 2 mL of CH_2Cl_2 . Yields of the isolated products **31** are indicated below each entry. ^aYield measured by ^1H NMR analysis using trichloroethylene as the internal standard.

Next, we focused on the scope of the acyl radical precursor (Figure 4.15). Different aromatic acyl chlorides bearing either electron-poor or electron-rich substituents reacted with phenyl vinyl sulfone or acrylonitrile, affording products **31n-s**. Additionally, several aroyl chlorides adorned with heterocyclic scaffolds, such as benzofuran (**31u**), pyrazole (**31v**) and isoxazole (**31w**), smoothly participated in this process.

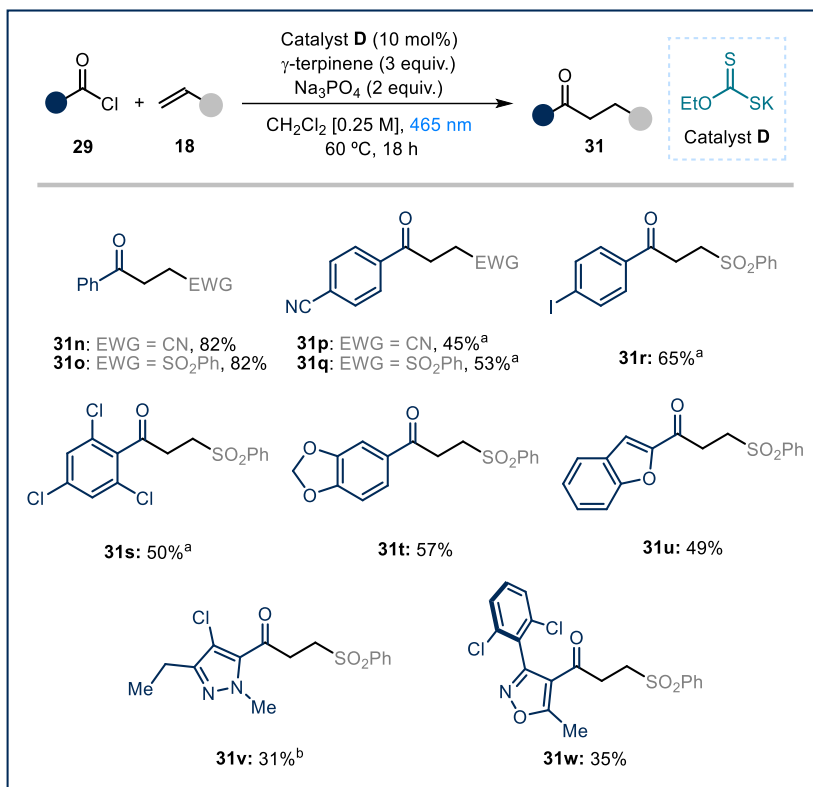


Figure 4.15: Survey of aromatic acyl chlorides **29** amenable to the intermolecular addition of acyl radicals. Reactions performed on a 0.5 mmol scale using 1.5 equiv. of **29** in 2 mL of CH_2Cl_2 . Yields of the isolated products **31** are indicated below each entry. ^aReaction time: 60 h. ^bAcid chloride prepared from the acid and used without further purification, 20 mol % catalyst.

Because of the mechanism of activation, which exploits the electrophilic properties of the substrates, difficult-to-reduce alkyl acyl chlorides could be employed in this photochemical procedure (Figure 4.16a). Primary (**31ix-ac**), secondary (**31iad-am**) and bridged tertiary (**31ian-ap**) derivatives successfully afforded the corresponding products in moderate to good yields. Interestingly, we could conveniently activate carboxylic acids through a two-step procedure (Figure 4.16b) in which the acyl chloride was formed in situ and used without any additional purification step (**31iv** Figure 4.15, **31aa**, **31ag-ai**, **31ak**, **31am-an** Figure 4.16).

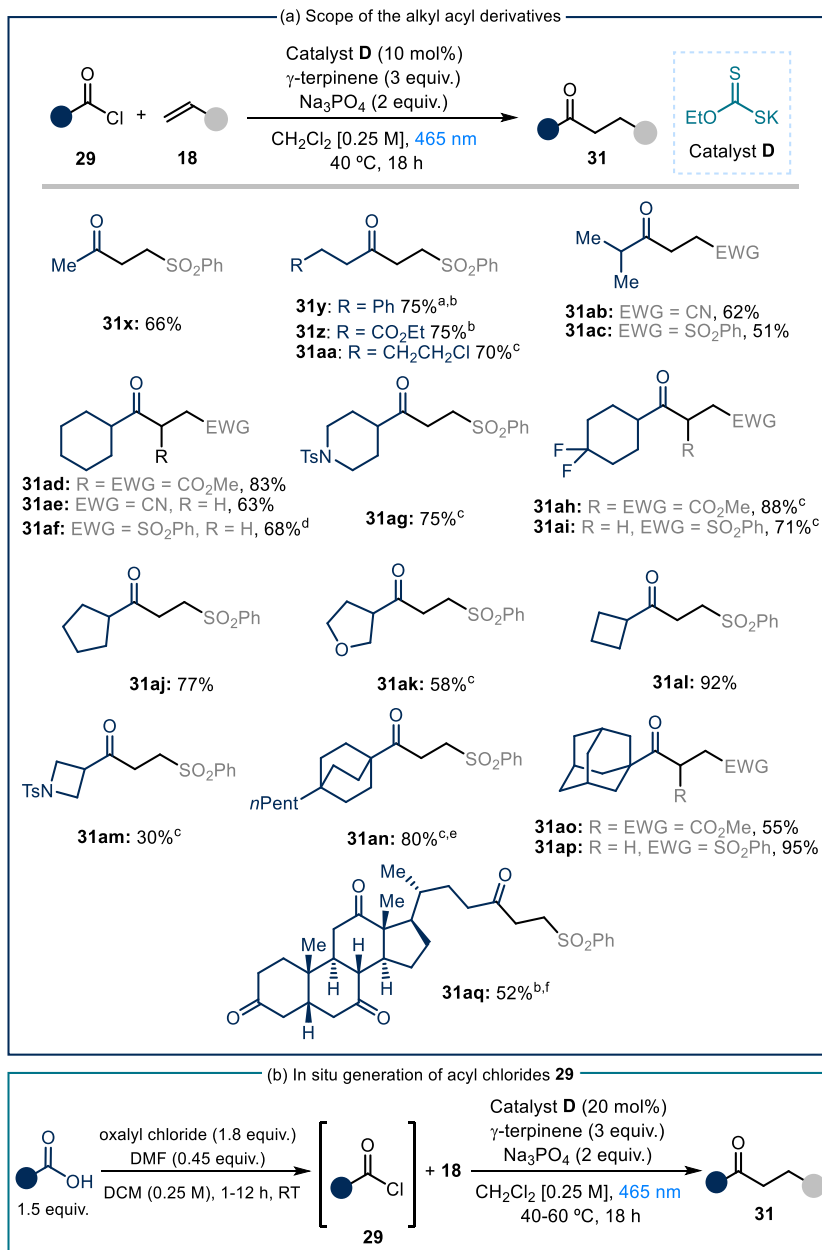


Figure 4.16: (a) Survey of alkyl acyl chlorides **29** amenable to the intermolecular addition of acyl radicals. Reactions performed on a 0.5 mL scale using 1.5 equiv. of **29** in 2 mL of CH_2Cl_2 . Yields of the isolated products **31** are indicated below each entry. ^aReaction time: 60 h. ^bReaction temperature: 60 °C. ^cAcid chloride prepared from the acid and used without further purification, 20 mol % catalyst. ^dProduct isolated as a 6 : 1 mixture with the olefin substrate, the corrected yield is reported. ^eYield measured by ¹H NMR analysis using trichloroethylene as the internal standard. ^fMixed anhydride prepared from the acid and used without further purification, 20 mol % catalyst. (b) Generation of acyl chlorides **29** from the corresponding carboxylic acids.

4.6 Mechanistic Studies

Our mechanistic picture for the photochemical catalytic formation of acyl and carbamoyl radicals (Figures 4.9, 4.10, 4.13 and 4.17) was based on previous works concerning the use of nucleophilic DTC catalysts.^{9,18} The key steps within the catalytic cycle are: *i*) the nucleophilic acyl substitution reaction between the acyl and carbamoyl electrophiles and the dithiocarbonyl catalyst, *ii*) the photoactivity of the ensuing intermediate **30** to form the corresponding radical **XXIV**, *iii*) the SET reduction of radical **XIX**, emerging from the photolysis of **30**, from the cyclohexadienyl radical **XXI**, to restore the original DTC catalyst, allowing its use in a catalytic fashion.

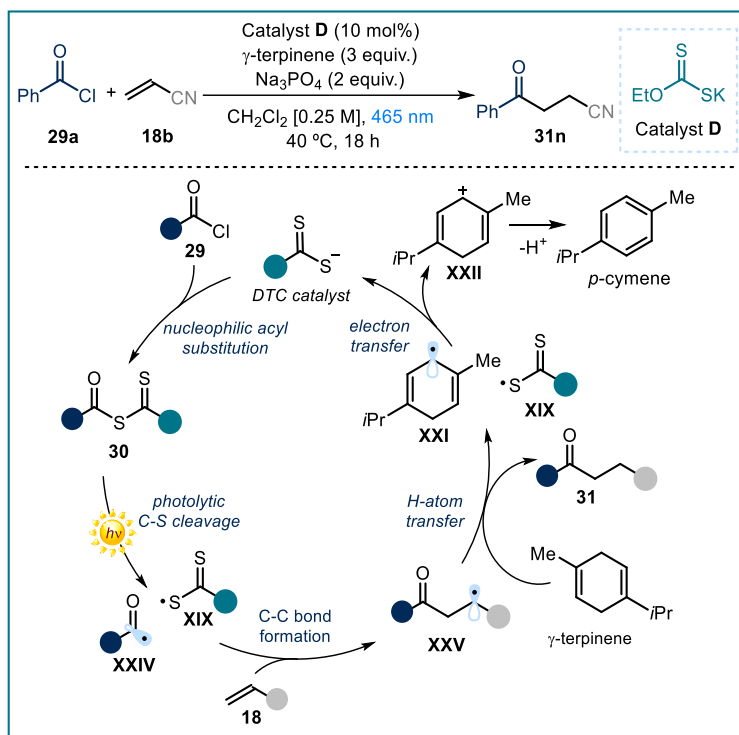
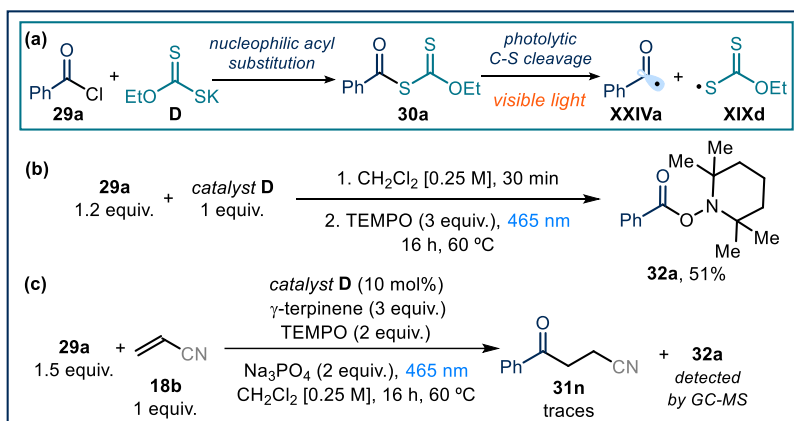


Figure 4.17: Proposed mechanistic picture for the formation of acyl and carbamoyl chlorides. DTC: Dithiocarbonyl.

As already discussed in section 4.2.2, xanthates and dithiocarbamates have been extensively used in reaction characterized by a group transfer mechanism,^{3,4b,13b,c} and it is not clear if this mechanistic path could play a role in our catalytic system too. To this end, we selected the reaction between benzoyl chloride **29a** (Figure 4.17) and acrylonitrile **18b** promoted by catalyst **D** to perform extensive mechanistic studies. Specifically, we deconstructed the catalytic cycle described in Figure 4.17 to focus on the most relevant steps, while characterizing the key intermediates responsible for the process.

4.6.1 Nucleophilic acyl substitution and photochemical behavior of **30a**

The first step of the catalytic cycle involves a nucleophilic acyl substitution between **29a** and catalyst **D** (Scheme 4.1a). According to the Mayr's scale of nucleophilicity,²² catalyst **D** is nucleophilic enough²³ to react with **29a** and produce **30a**. The second step involves the photolysis of **30a** to produce acyl radical **XXIVa**. To gain more information on this photolytic step, we prepared intermediate **30a** in situ (Scheme 4.1b) and we submitted it to blue light illumination in the presence of 2,2,6,6-tetramethylpiperidine 1-oxyl (TEMPO). This experiment afforded product **32a**, originated from the trapping of the photochemically generated acyl radical **XXIVa** by TEMPO. Moreover, when adding TEMPO to the catalytic model reaction (Scheme 4.1c), the reactivity was almost totally suppressed, while the adduct **32a** was detected via GC-MS analysis.



Scheme 4.1: (a) Production and photolytic cleavage of acylxanthate **30a**. (b) Trap of the acyl radical **XXIVa** with the radical scavenger TEMPO. (c) The model reaction is inhibited by addition of TEMPO. TEMPO: 2,2,6,6-tetramethylpiperidine 1-oxyl. LEDs: Light emitting diodes.

To further corroborate that the photolysis of **30a** was responsible for the generation of acyl radical **XXIVa**, we performed laser flash photolysis and electron paramagnetic resonance (EPR) studies. Previous laser flash photolysis investigations established that the xanthyl radical **XIXd** displays a characteristic absorption band with a maximum at 620 nm.²⁴ Accordingly, when a sample of **30a** was irradiated with a laser beam centered at 355 nm (Figure 4.18), we observed the formation of a transient species absorbing at 620 nm, consistent with radical **XIXd**, whose half lifetime was measured to be in the order of 0.1 ms. This transient was also detected when a laser beam centered at 460 nm was employed (Figure 4.44 in the Experimental Section), further indicating that photolysis is possible under the reaction conditions.

²² Mayr, H.; Ofial, A. R.; "Do general Nucleophilicity scales exist?" *J. Phys. Org. Chem.* **2008**, *21*, 584-595.

²³ Duan, X.-H.; Maji, B.; H. Mayr, "Characterization of the nucleophilic reactivities of thiocarboxylate, dithiocarbonate and dithiocarbamate anions" *Org. Biomol. Chem.* **2011**, *9*, 8046-8050.

²⁴ Kaga, A.; Wu, X.; Lim, J. Y. J.; Hayashi, H.; Lu, Y.; Yeow E. K. L.; Chiba, S. "Degenerative Xanthate Transfer to Olefins Under Visible-Light Photocatalysis" *Beilstein J. Org. Chem.* **2018**, *14*, 3047-3058.

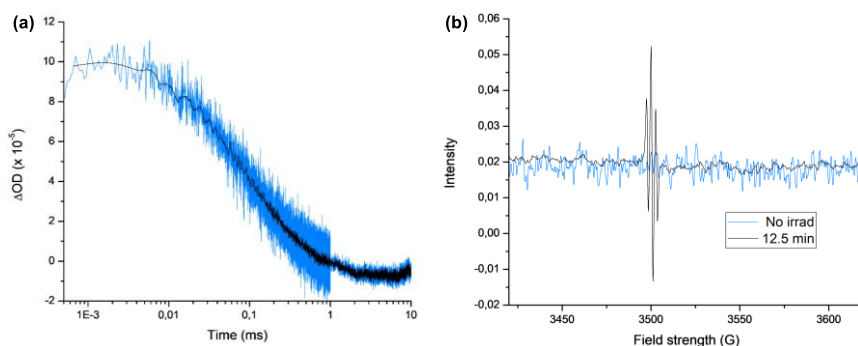


Figure 4.18: (a) Absorption at 620 nm of the transient xanthyl radical **XIXd** (blue line) generated upon 355 nm laser excitation of **30a** ($[30a]_0 = 3.00$ mM in MeCN). Note logarithmic scale for time. Absorption decay (black line) processed through Savinsky Golay filter to facilitate lifetime measurement. ΔOD : optical density variation. (b) EPR spectrum generated from **30a** ($[30a]_0 = 0.1$ M in toluene) at 298 K after 12.5 minutes (black line) of light irradiation by a 100 W mercury lamp.

We then used EPR spectroscopy to detect the formation of the acyl radical **XXIVa** (Figure 4.19a). When conducting the analysis on a solution of **30a** in toluene at 298K under light illumination by a mercury lamp, we observed a signal that was not consistent with that of **XXIVa**, which should be a singlet.²⁵ Instead, the EPR spectrum showed a pattern (sharp triplet centered at 3505 G, g -value = 2.00272, hyperfine splitting value = 2.6 G) that is consistent²⁶ with a more stabilized carbon radical of type **XXVI** (Figure 4.19), which lies in proximity of two sulfur atoms and an ethoxy moiety. Aware of the high tendency of xanthates of the type **30a** to trap radicals, we reasoned that **XXVI** could be generated from the reversible addition of radical **XXIVa** onto **30a**.

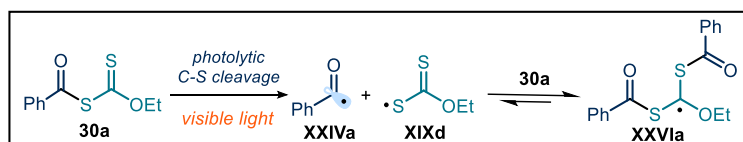
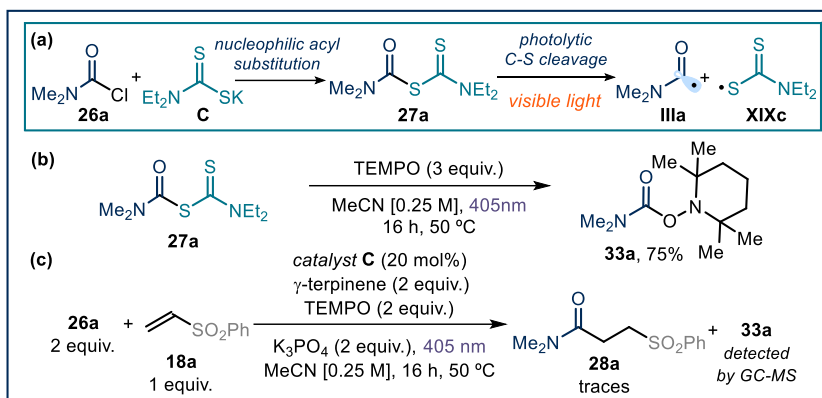


Figure 4.19: The reaction of the acyl radical **XXIVa** with its precursor **30a** is reversible and imparts an increased lifetime to **XXIVa**.

Additionally, we performed the TEMPO trapping experiment for the reaction involving dimethyl carbamoyl chloride **26a**, vinyl sulfone **18a** and catalyst **D** (Scheme 4.2a). Analogously to the acyl derivatives, when submitting **27a** (Scheme 4.2b) to 405 nm illumination in the presence of TEMPO, product **33a**, generated by the trapping of **IIIa** from TEMPO, was obtained. Finally, addition of TEMPO to the catalytic reaction inhibited the reactivity (Scheme 4.2c).

²⁵ Bieszczad, B.; Perego, L. A.; Melchiorre, P. "Photochemical C-H Hydroxyalkylation of Quinolines and Isoquinolines" *Angew. Chem. Int. Ed.* **2019**, *58*, 16878-16883.

²⁶ Hawthorne, D. G.; Moad, G.; Rizzardo, E.; Thang, S. H. "Living Radical Polymerization with Reversible Addition-Fragmentation Chain Transfer (RAFT): Direct ESR Observation of Intermediate Radicals" *Macromolecules* **1999**, *32*, 5457-5459.

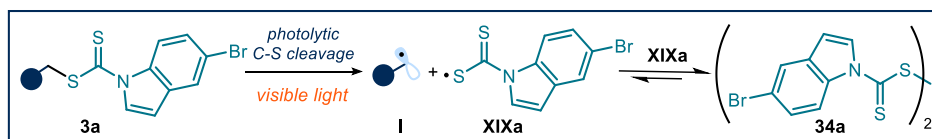


Scheme 4.2: (a) Production and photolytic cleavage of carbamoyldithiocarbamate **27a**. (b) Trapping of the carbamoyl radical **IIIa** with the radical scavenger TEMPO. (c) The model reaction is inhibited by addition of the radical scavenger TEMPO. TEMPO: 2,2,6,6-tetramethylpiperidine 1-oxyl.

Collectively these experiments indicate the radical nature of the process and the intermediacy of acylxanthate **30a**, carbamoyldithiocarbamate **27a**, as well as radicals **XXIVa** and **IIIa**. Moreover the EPR studies highlighted how, after its generation, radical **XXIVa** could engage a second molecule of **30a** in a reversible addition-fragmentation sequence, leading to intermediate **XXVI**.

4.6.2 Fate and behavior of the xanthyl radical **XIXd**

After the photolytic cleavage of the acylxanthate intermediate **30a**, the ensuing xanthyl radical **XIXd** has to be reduced to regenerate catalyst **D**, allowing its use in catalytic amounts. During a recent study on the use of indole-based DTC catalyst **A**, we observed the formation in small amounts of the dimer **34a** (Scheme 4.3), which originates from the self-reaction of the sulfur-centered radical **XIXa**.^{18c}



Scheme 4.3: Formation of dimer **34a** from the dimerization of radical **XIXa**.

We decided to test whether the dimers of catalyst **C** and **D** (adducts **34c** and **34d** respectively) could play a role in the photochemical production of acyl and carbamoyl radicals. Both these dimers, readily synthesized in one step from the catalysts **C** and **D**, could absorb in the visible region (Figure 4.20).

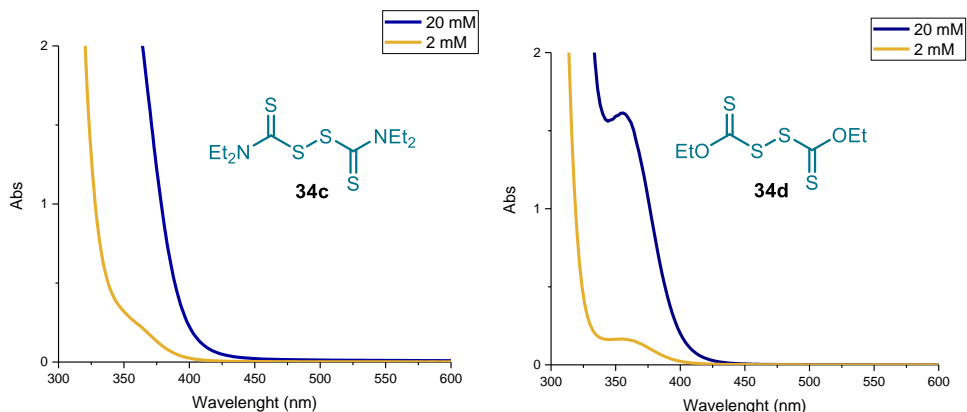
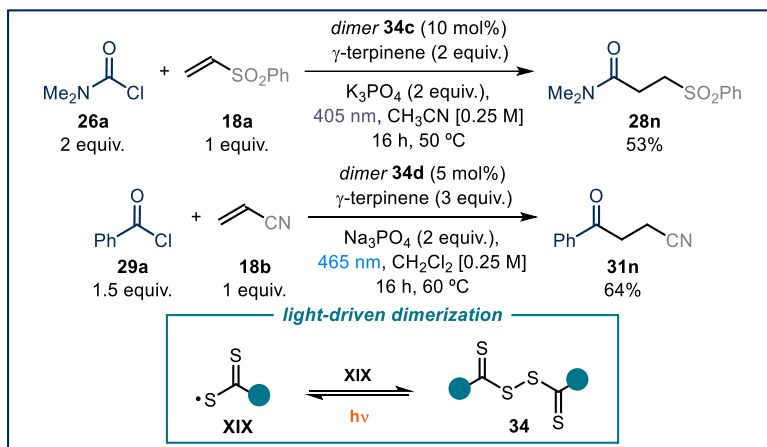


Figure 4.20: UV-vis spectra of dimers **34c** and **34d**.

We used the two dimers **34c** and **34d** to catalyze the model reactions with carbamoyl and acyl chlorides (Scheme 4.4).

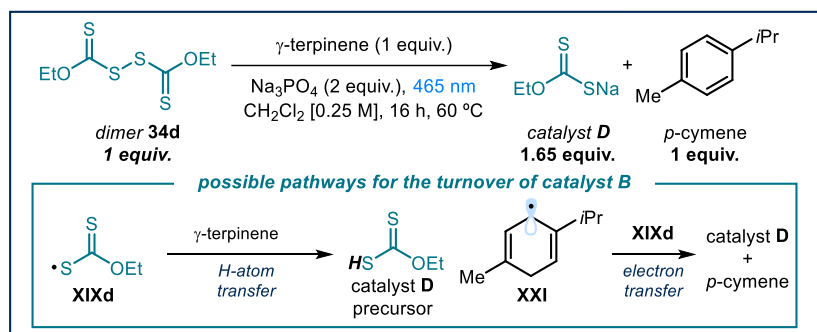


Scheme 4.4: Experiments highlighting that dimers **34c** and **34d** are catalytically active and the light-driven equilibrium between **XIX** and **34**.

Irradiation with a 405 nm lamp for the carbamoyl chlorides and 465 nm lamp for the acyl chloride afforded the corresponding products **28a** and **31a** in good yields. These results indicate that dimers **34c** and **34d** are photoactive species in equilibrium with the xanthyl radicals **XIX**. This dimerization path renders the xanthyl radical **XIX** more persistent,²⁷ thus facilitating its SET reduction from the cyclohexadienyl radical **XXI**. To gain further information on the light-driven equilibrium between the dimer **34d** and its xanthyl radical progenitor **XIXd**, we assessed the behavior of **34d** using 1 equivalent of γ -terpinene and under blue light illumination (Scheme 4.5). Dimer **34d** was completely converted into 1.65 equivalents of catalyst **D**, providing compelling evidence to rationalize the mechanism of turnover of the DTC catalyst. Crucially,

²⁷ Leifert, D.; Studer, A. "The Persistent Radical Effect in Organic Synthesis" *Angew. Chem. Int. Ed.* **2020**, *59*, 74-108.

because of the stoichiometry of the reaction in Scheme 4.5, it seems that γ -terpinene can provide two different pathways to turnover the xanthyl radical **XIXd**, namely an HAT process to turnover the first equivalent of **XIXd** while providing radical **XXI**, and an SET reduction from **XXI** to the second equivalent of **XIXd**.



Scheme 4.5: Experiment probing the ability of γ -terpinene to reduce the xanthyl radical **XIXd** via both an HAT and an SET manifold.

To gain further evidence into the production of the xanthyl radical **XIXd** from the dimer **34d** under light illumination, we performed laser flash photolysis studies. The same transient intermediate detected in the experiments with acylxanthate **30a** was observed (Figure 4.21a). This transient was also detected when a laser beam centered at 420 and 460 nm was used (Figures 4.46-47 in the Experimental Section). Additionally, the lifetime of **XIXd** decreased upon addition of γ -terpinene (orange, green and blue lines in Figure 4.21b), which corroborates the notion, discussed in Scheme 4.5, that these two species can readily react. Overall, these experiments indicate that dimer **34d** can produce the xanthyl radical **XIXd** under light irradiation through photolytic S-S bond cleavage.

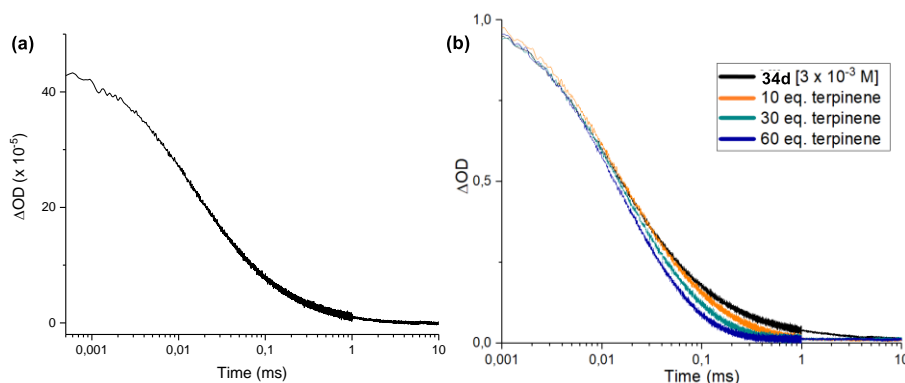


Figure 4.21: (a) Absorption at 620 nm of the transient xanthyl radical **XIXd** generated upon 355 nm laser excitation of dimer **34d** ($[\mathbf{34d}]_0 = 3 \times 10^{-3}$ M in MeCN). (b) Decrease of the lifetime of **XIXd** upon addition of γ -terpinene. Note logarithmic scale for time. ΔOD : optical density variation. Absorption decays (orange, green, and blue lines) observed in the presence of increasing amounts of γ -terpinene. Green line: ratio **34d**/ γ -terpinene mimics the reaction conditions. ΔOD : optical density variation.

Next, we studied the electrochemical behavior of catalyst **D** and dimer **34d** with the aim of gaining direct evidence of the dimerization tendency of the xanthyl radical **XIXd**. We first performed cyclic voltammetry studies on catalyst **D**, which was analyzed during the initial forward scan applying an increasingly reducing potential (0 to -2.0 V, Figure 4.22a). No reduction peaks were detected. However, during the reverse scan toward oxidation (from -2.0 V to +1.5 V), an irreversible peak ($E_p^A = E_{ox} = 0.73$ V in CH₃CN vs Ag/AgCl), due to the oxidation of catalyst **D** to **XIXd**, was observed. We then performed the analysis in the opposite order, first applying an increasingly oxidizing potential (0 to +1.5 V, Figure 4.22b). As expected, we observed the same peak as in the previous experiment, ascribable to the formation of **XIXd** from **D**. Interestingly, during the reverse scan towards reduction (from +1.5 V to -2.0 V), an additional peak was detected ($E_p^C = E_{red} = -1.40$ V in CH₃CN vs Ag/AgCl), which was not observed during the previous experiment. This result can be explained based on the already discussed dimerization of the xanthyl radical **XIXd**, generated during the oxidation scan, that produces dimer **34d**, a molecule prone to reduction (Figure 4.22c). This is in agreement with the following observations: *i*) the formation of the stable dimer makes the oxidation of catalyst **D** irreversible, as the xanthyl radical **XIXd** is rapidly sequestered in the form of its dimer **34d**; *ii*) it is only in the cyclic voltammetric analysis that starts with oxidation (Figure 4.22b) that a reduction peak appears, which is ascribable to the reduction of dimer **34d**: this is because the dimer first requires the oxidation of catalyst **D** to be generated (Figure 4.22c).

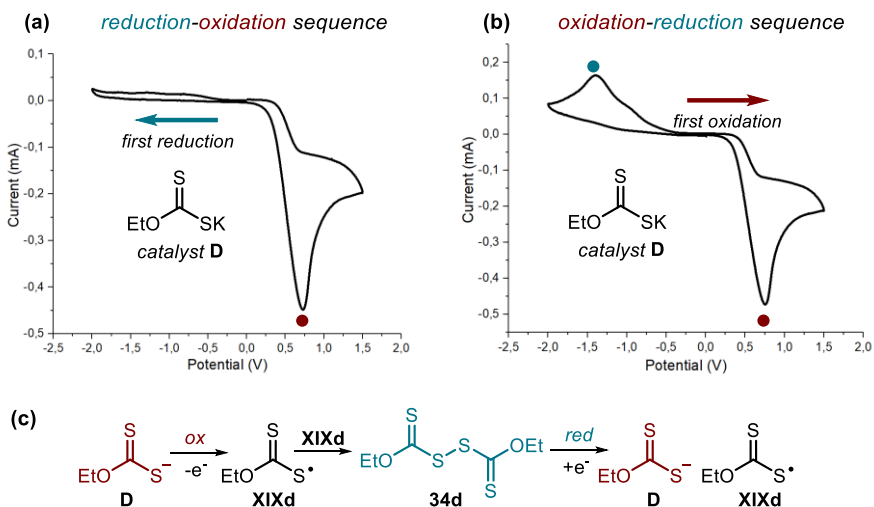


Figure 4.22: Cyclovoltammetric studies of catalyst **D** [0.02 M] in [0.1 M] TBAPF₆ in MeCN: (a) reduction-oxidation scan sequence. (b) Oxidation-reduction scan sequence. (c) The xanthyl radical **XIXd**, which can be formed by SET reduction of **34d** and oxidation of **D**, is the link between catalyst **D** and dimer **34d**. (e) Reduction-oxidation scan sequence. Sweep rate: 500 mV/s. Pt electrode working electrode, Ag/AgCl (KCl 3.5 M) reference electrode, Pt wire auxiliary electrode.

To further corroborate this proposal, we repeated the same analysis using dimer **34d**. Applying an initial forward scan towards an increasingly oxidizing potential (0 to +1.5, Figure 4.23a), no oxidation was detected. As observed before, during the reverse scan

(from +1.5 V to -2.0 V), the reduction peak of **34d** was detected ($E_p^C = E_{\text{red}} = -1.61$ V in CH_3CN vs Ag/AgCl).

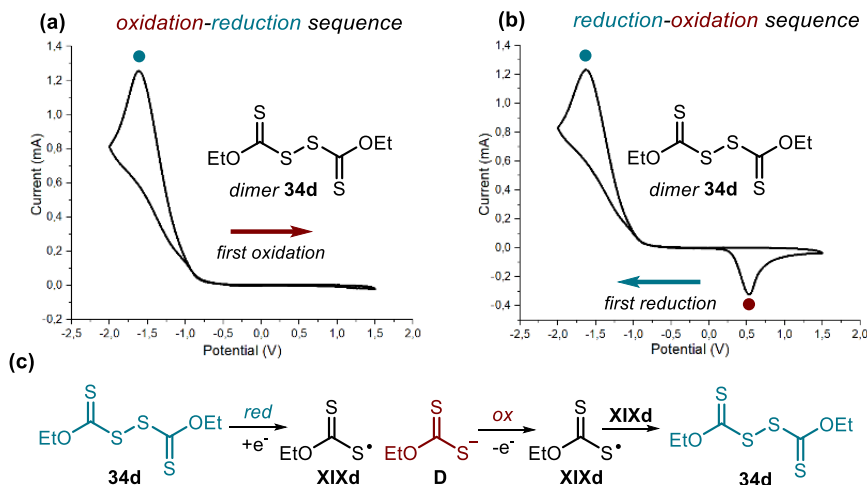


Figure 4.23: Cyclic voltammetric studies of dimer **34d** [0.02 M] in [0.1 M] TBAPF₆ in MeCN: (a) oxidation-reduction scan sequence. (b) reduction-oxidation scan sequence. (c) The xanthyl radical **XIXd**, which can be formed by SET reduction of **34d** and oxidation of **D**, is the link between catalyst **D** and dimer **34d**. Sweep rate: 500 mV/s. Pt electrode working electrode, Ag/AgCl (KCl 3.5 M) reference electrode, Pt wire auxiliary electrode.

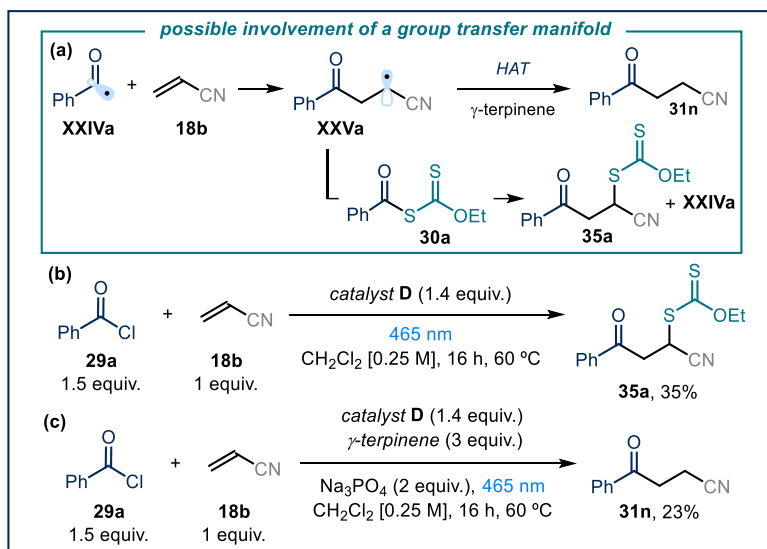
However, when we started the electrochemical analysis towards reduction (0 to -2.0 V and then to +1.5 V, Figure 4.23b), an additional oxidation peak was registered ($E_p^A = E_{\text{ox}} = 0.53$ V in CH_3CN vs Ag/AgCl). This is in agreement with the reduction of **34d** that produces xanthyl radical **XIXd** and catalyst **D**, which is subsequently oxidized during the oxidative step (red dot in the reverse scan phase), in agreement with the experiments depicted in Figures 4.22a,b.

The comparison of the cyclic voltammograms clearly highlights a correlation between the new reduction peak detected in the analysis of catalyst **D** with the peak observed for the reduction of dimer **34d**. A correlation exists also between the new oxidation peak in the analysis of dimer **34d** in Figure 4.23b and the oxidation of catalyst **D** (Figures 4.22a-b). Collectively, these studies indicate that the link between catalyst **D** and dimer **34d** is the xanthyl radical **XIXd** (Figures 4.22c and 4.23c). They also show the strong tendency of the xanthyl radical **XIXd** to dimerize and form **34d**.

4.6.3 Trap of the acyl radical and ensuing processes

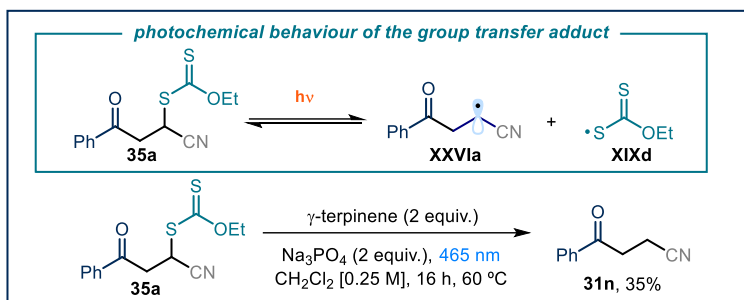
After having elucidated the role of the xanthyl radical **XIXd**, we focused on the fate of the other radical generated upon photolysis: the acyl radical **XXIVa**. This radical can either react with a second molecule of acyl xanthate **30a** generating **XXVIa**, as highlighted through EPR studies (Figure 4.18), or add on acrylonitrile **2a**, promoting the C-C bond formation (e.g. Figure 4.17). In the last case, the ensuing electrophilic radical **XXVa** would then perform HAT on γ -terpinene, producing the final product **31n** and the cyclohexadienyl radical **XXI**. Because of the already mentioned tendency of xanthates and dithiocarbamates to react in a group transfer mechanism (e.g. Figure 4.5),^{13c} we wondered whether this mechanistic path played a relevant role in the

present catalytic system. We therefore performed investigations to probe the possible intermediacy of the group transfer product of type **35a** (Scheme 4.6a). Product **35a** could be formed either through a xanthate transfer process between the electrophilic radical **XXVa** and acylxanthate **30a**, or through a cross-coupling process between radical **XXVa** and xanthyl radical **XIXd**. When performing the model reaction with a stoichiometric amount of catalyst **D** (1.4 equiv.) and in the absence of γ -terpinene, the group transfer product **35a** was isolated in 35% yield (Scheme 4.6b). At the same time, the Giese type product **31n** was not detected, highlighting the crucial role of γ -terpinene in enabling the radical conjugate addition manifold. By contrast, under identical conditions but in the presence of γ -terpinene, no traces of the group transfer product **35a** could be detected, while product **31n** was exclusively formed. Interestingly, the yield of **31n** was much lower with respect to the experiment conducted using catalytic amounts of catalyst **D** (10 mol%, 82% yield). We suppose that the lower efficiency of the Giese addition path under stoichiometric conditions could be a consequence of the equilibrium showed in Figure 4.19b, i.e. a higher amount of acylxanthate **30a** inhibits the radical addition onto electron-poor olefin **18a** since the acyl radicals **XXIVa** are sequestered by **30a**.



Scheme 4.6: (a) Focusing on the acyl radical addition step. The model reaction in the presence of a stoichiometric amount of **D** and (b) in the absence or (c) in the presence of γ -terpinene (group transfer conditions).

Next, we prepared an authentic sample of the group transfer product **35a** and submitted it to the optimized reaction conditions but in the absence of catalyst **D**: the Giese-type adduct **31n** was obtained in moderate yield (35% yield, Scheme 4.7). This experiment highlights the ability of the group transfer product **35a**, in the presence of γ -terpinene and under blue light irradiation, to afford product **31n**. This suggests that the group transfer product **35a**, upon irradiation, may regenerate the progenitor radicals **XXVa** and **XIXd**.



Scheme 4.7: Photolysis of the group transfer product **35a**.

This was corroborated by laser flash photolysis studies on **35a**, where the same transient, associated to xanthyl radical **XIXd**, observed also for acyl xanthate **30a** and dimer **34d**, was detected (Figure 4.24).

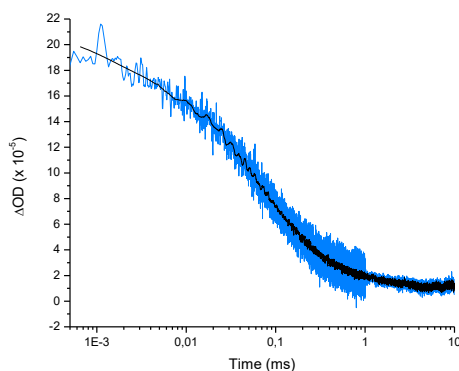
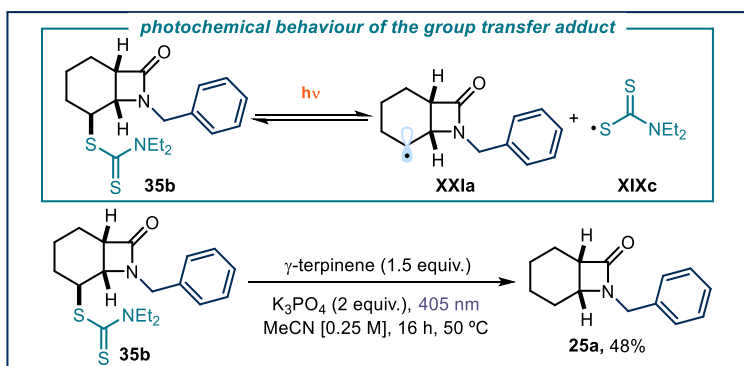


Figure 4.24: Absorption at 620 nm of the transient xanthyl radical **XIXd** (blue line) generated upon 355 nm laser excitation of the group transfer product **35a** ($[\mathbf{35a}]_0 = 3.00 \text{ mM}$ in MeCN). Note logarithmic scale for time. Absorption decay (black line) processed through Savinsky Golay filter to facilitate lifetime measurement. ΔOD : optical density variation.

We performed a similar analysis for the intramolecular addition of carbamoyl radicals (Scheme 4.8). The group transfer product **35b** was synthesized and submitted to the optimized reaction conditions for the intramolecular process, but in the absence of catalyst **C**. We detected the formation of product **25a** in 48% yield.



Scheme 4.8: Photolysis of the group transfer product **35b**.

Although we never detected the group transfer adducts **35a** and **35b** under catalytic conditions, we cannot exclude that this pathway is operative in our catalytic system. It is possible that the group transfer adducts **35a** and **35b** can function as another stabilizing, off-the-cycle intermediates, which can control the concentration of xanthyl radical **XIXd** and dithiocarbamyl radical **XIXc** in solution through an additional equilibrium.

4.6.4 Overall catalytic cycle

Based on the aforementioned experiments (Sections 4.6.1-4.6.3), we propose the mechanistic picture reported in Figure 4.25 for the photochemical Giese addition of acyl radicals.

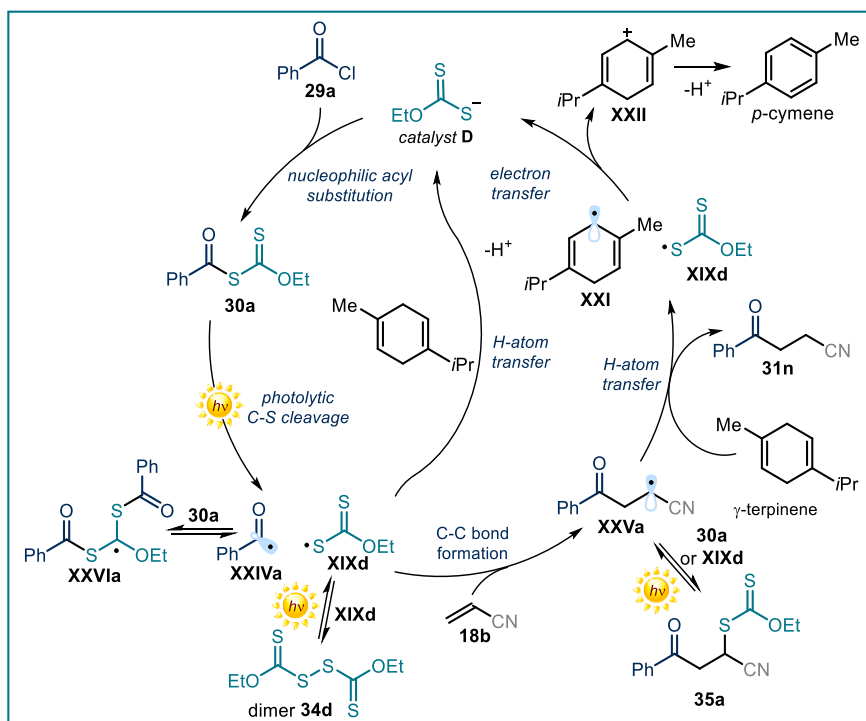


Figure 4.25: Detailed mechanistic picture, comprehensive of the off-the-cycle equilibria, based on the mechanistic investigations conducted on the model reaction of **29a** and **18b** catalyzed by **D**.

The catalytic machinery is regulated by different equilibria that serve as a tool to stabilize the radical intermediates and to control their overall concentration. For example, the amounts of acyl radical **XXIVa** are regulated by the reversible addition-fragmentation sequence on acyl xanthate **30a**, leading to intermediate **XXVIa**. Meanwhile, xanthyl radical **XIXd** can dimerize to form **34d** or interact with the electrophilic radical **XXVa** to produce the transfer product **35a**. All these equilibria are controlled by light and confer a persistent radical character to **XIXd**,²⁷ this facilitating the single electron reduction from the cyclohexadienyl radical **XXI** which restore catalyst **D**. Moreover, γ -terpinene provides an additional mean to reduce the xanthyl radical **XIXd** other than the SET reduction, the HAT process.

In our proposed mechanism, the photoactivity of acyl xanthate **30a** dictates the formation of any molecule of the product. This scenario differs from a possible radical chain propagation manifold where the photoactivity of **30a** would serve as an initiation event solely. To discriminate between the two possibilities, we measured the quantum yield of the reaction, which was found as low as 0.034 ($\lambda = 460$ nm, using potassium ferrioxalate as the actinometer, details about quantum yield determination in the Experimental Section). This fractional value is far lower than the typical ones of chain propagation mechanisms ($\Phi > 1$), indicating that a radical chain process, based on either the SET from intermediate **XXVa** to acyl xanthate **30a** or through a group transfer mechanism, is unlikely. Instead, the low quantum yield corroborates the proposed mechanism highlighted in Figure 4.23.

4.7 Conclusions

Our studies led to the development of a catalytic methodology for the formation of acyl and carbamoyl radicals through the use of a dithiocarbonyl catalyst that exploits solely the electrophilic properties of the substrate. This feature enables the use of readily-available acyl and carbamoyl chlorides as radical precursors, which are difficult to be activated by other strategies based on single-electron transfer or atom abstraction. The ensuing radicals are trapped with a variety of electron-poor olefins in a Giese addition manifold or by a pendant olefin in an intramolecular fashion. Extensive mechanistic investigations have been performed, including transient absorption spectroscopy investigations, electrochemical studies, quantum yield measurements, and the characterization of key intermediates. Collectively, these studies identified a variety of off-the-cycle intermediates that are in a light-regulated equilibrium with the reactive radicals. These regulated equilibria cooperate to control the overall concentrations of the radicals, contributing to the efficiency of the process.

4.8 Experimental Section

4.8.1 General information

The NMR spectra are available in the published manuscript¹ and are not reported in the present dissertation.

The NMR spectra were recorded at 400 MHz and 500 MHz for ¹H and 100 or 125 MHz for ¹³C. The chemical shift (δ) for ¹H and ¹³C are given in ppm relative to residual signals of the solvents (CHCl₃ @ 7.26 ppm ¹H NMR and 77.16 ppm ¹³C NMR, and tetramethylsilane @ 0 ppm). Coupling constants are given in Hz. The following abbreviations are used to indicate the multiplicity: s, singlet; d, doublet; q, quartet; m, multiplet; bs, broad signal; app, apparent. High resolution mass spectra (HRMS) were obtained from the ICIQ HRMS unit on MicroTOF Focus and Maxis Impact (Bruker Daltonics) with electrospray ionization. (ESI). UV-vis measurements were carried out on a Shimadzu UV-2401PC spectrophotometer equipped with photomultiplier detector, double beam optics and D₂ and W light sources or an Agilent Cary 60 spectrophotometer. Emission spectra of light sources were recorded on Ocean Optics

USB4000 fiber optic spectrometer. Isolated yields refer to materials of >95% purity as determined by ^1H NMR.

General Procedures. All reactions were set up under an argon atmosphere in oven-dried glassware. Synthesis grade solvents were used as purchased, anhydrous solvents were taken from a commercial SPS solvent dispenser. Chromatographic purification of products was accomplished using forced-flow chromatography (FC) on silica gel (35–70 mesh). For thin layer chromatography (TLC) analysis throughout this work, Merck pre-coated TLC plates (silica gel 60 GF₂₅₄, 0.25 mm) were employed, using UV light as the visualizing agent and an acidic mixture of vanillin or basic aqueous potassium permanganate (KMnO_4) stain solutions, and heat as developing agents. Organic solutions were concentrated under reduced pressure on a Büchi rotatory evaporator.

Materials. Most of the starting materials used in this study are commercial and were purchased in the highest purity available from Sigma-Aldrich, Fluka, Alfa Aesar, Fluorochem, and used as received, without further purifications. The following substrates were synthesized according to reported procedures (Figure 4.26).^{18c,28}

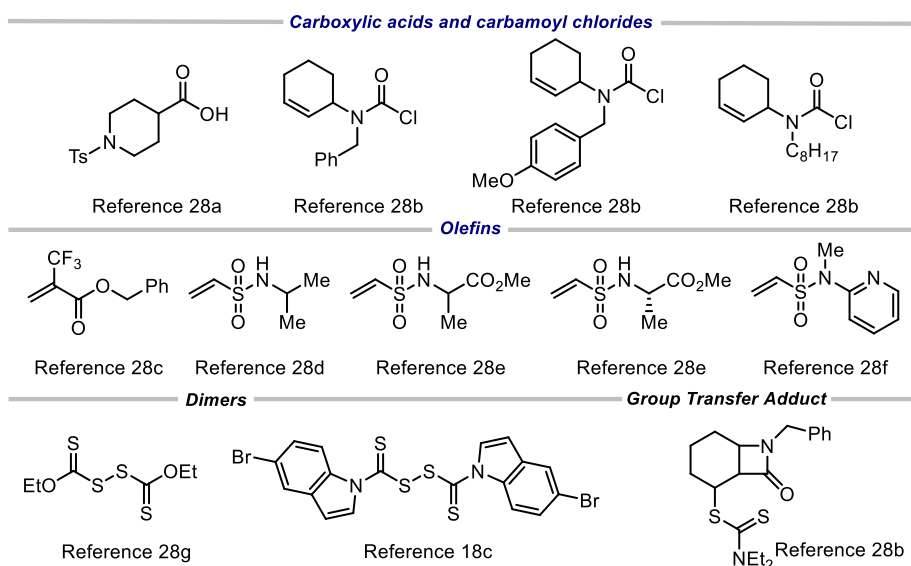
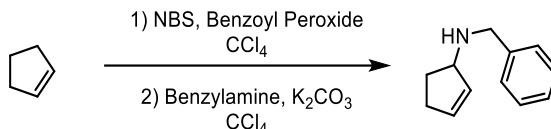


Figure 4.26: Starting materials synthesized according to literature precedents and corresponding references.

²⁸ (a) Nyfeler, E.; Renaud, P. "Decarboxylative Radical Azidation Using MPDOC and MMDOC Esters" *Org. Lett.* **2008**, *10*, 985–988. (b) Grainger, R. S.; Betou, M.; Male, L.; Pitak, M. B.; Coles, S. J. "Semipinacol Rearrangement of Cis-Fused β -Lactam Diols into Keto-Bridged Bicyclic Lactams" *Org. Lett.* **2012**, *14*, 2234–2237. (c) Avenoz, A.; Busto, J. H.; Jiménez-Osés, G.; Peregrina, J. M. "A Convenient Enantioselective Synthesis of (S)- α -Trifluoromethylisoserine" *J. Org. Chem.* **2005**, *70*, 5721–5724. (d) Wang, M.; Wang, Y.; Qi, X.; Xia, G.; Tong, K.; Tu, J.; Pittman, C. U.; Zhou, A. "Selective Synthesis of Seven- and Eight-Membered Ring Sultams via Two Tandem Reaction Protocols from One Starting Material" *Org. Lett.* **2012**, *14*, 3700–3703. (e) Fenster, E.; Long, T. R.; Zang, Q.; Hill, D.; Neuenswander, B.; Lushington, G. H.; Zhou, A.; Santini, C.; Hanson, P. R. "Automated Synthesis of a 184-Member Library of Thiazepan-1,1-dioxide-4-ones" *ACS Comb. Sci.* **2011**, *13*, 244–250. (f) Huang, R.; Li, Z.; Ren, P.; Chen, W.; Kuang, Y.; Chen, J.; Zhan, Y.; Chen, H.; Jiang, B. "N-Phenyl-N-aceto-vinylsulfonamides as Efficient and Chemoselective Handles for N-Terminal Modification of Peptides and Proteins" *Eur. J. Org. Chem.* **2018**, *2018*, 829–836. (g) Jiang, S.; Li, Y.; Luo, X.; Huang, G.; Shao, Y.; Li, D.; Li, B. "NH₄/EtOCS₂K promoted synthesis of substituted benzils from diphenylacetylene derivatives" *Tetrahedron Lett.* **2018**, *59*, 3249–3252.

4.8.2 Substrate synthesis

Synthesis of *N*-benzylcyclopent-2-en-1-amine:

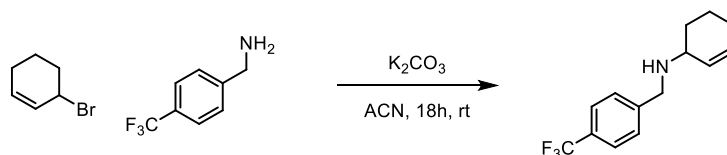


A 2 M solution of cyclopentene (0.973 mL, 11 mmol) in CCl_4 (5.4 mL) was prepared and then NBS (2.26 g, 10 mmol) and benzoic peroxyanhydride (36 mg, 0.15 mmol) were sequentially added. The solution was stirred at 40 °C for 4 hours, after which the reaction was left at ambient temperature without stirring. After 2 hours, the floating materials were filtered off and washed with CCl_4 . The organic phase was then placed in a separatory funnel and washed with distilled water. The organic phase was collected, treated with MgSO_4 and subsequently filtered. At this stage, benzylamine (3.28 mL, 30 mmol) and K_2CO_3 (1.38 g, 10 mmol) were directly added to the solution. The reaction was stirred overnight at r.t and the resulting crude mixture was purified by silica gel chromatography (eluent: 9:1 hexane/AcOEt) to afford 234 mg of *N*-benzylcyclopent-2-en-1-amine (14% yield over 2 steps) as a yellow-orange oil.

$^1\text{H NMR}$ (400 MHz, CDCl_3) δ 7.39 – 7.24 (m, 5H), 5.89 (m, 2H), 3.93 (m, 1H), 3.84 (dd, $J=16.6, 12.9$ Hz, 2H), 2.48 (m, 1H), 2.36 – 2.18 (m, 2H), 1.63 (m, 1H).

$^{13}\text{C NMR}$ (101 MHz, CDCl_3) δ 140.5, 133, 132.8, 128.4, 128.3, 126.9, 63.9, 51.8, 31.3, 30.8

Synthesis of *N*-(4-(trifluoromethyl)benzyl)cyclohex-2-en-1-amine:



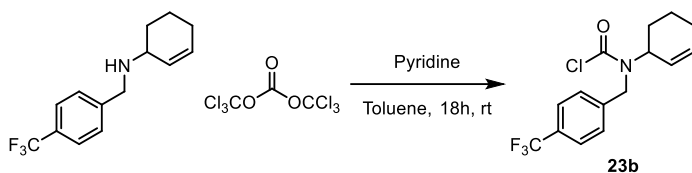
N-(4-(trifluoromethyl)benzyl)cyclohex-2-en-1-amine was prepared according to a reported procedure.^{28b} A solution of (4-(trifluoromethyl)phenyl)methanamine (1.314 g, 7.5 mmol) in CH_3CN (1.7 mL) was treated with 3-bromocyclohexene (0.288 mL, 2.5 mmol) and K_2CO_3 (346 mg, 2.5 mmol). After 2 hours at ambient temperature, the reaction mixture was quenched with H_2O (20 mL) and extracted with EtOAc (2 x 25 mL). The combined organic extracts were washed with brine (20 mL), dried over MgSO_4 , filtered, evaporated under reduced pressure, and purified by column chromatography (eluent: CH_2Cl_2 to $\text{CH}_2\text{Cl}_2/\text{EtOH}$ 9:1) to give the product (607 mg, 95 % yield) as a light-yellow oil.

$^1\text{H NMR}$ (400 MHz, CDCl_3) δ 7.57 (d, $J = 8.1$ Hz, 2H), 7.47 (d, $J = 8.0$ Hz, 2H) 5.82 – 5.76 (m, 1H), 5.75 – 5.62 (m, 1H) 3.90 (dd, $J = 13.6, 3.3$ Hz, 2H), 3.23 – 3.16 (m, 1H), 2.10 – 1.97 (m, 2H), 1.93 – 1.85 (m, 1H), 1.80 – 1.70 (m, 1H), 1.61 – 1.42 (m, 2H).

$^{13}\text{C NMR}$ (101 MHz, CDCl_3) δ 145.1, 129.8, 129.4, 129.3 (q, $J = 32.7$ Hz) 128.4, 125.4 (q, $J = 3.7$ Hz), 124.4 (q, $J = 271.9$ Hz), 52.6, 50.6, 29.6, 25.4, 20.3.

$^{19}\text{F NMR}$ (376 MHz, CDCl_3) δ -62.47.

Synthesis of compound **23b**:



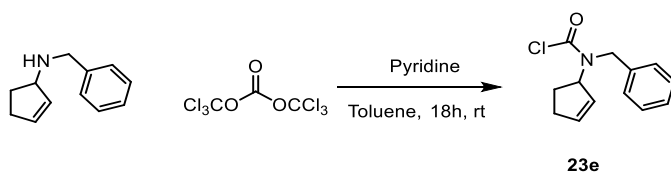
Compound **23b** was prepared according to a modification of a reported procedure.^{28b} To a solution of triphosgene (252 mg, 0.848 mmol) in toluene (15 mL) under N₂, pyridine (0.242 mL, 2.99 mmol) and subsequently a solution of *N*-(4-(trifluoromethyl)benzyl)cyclohex-2-en-1-amine (637 mg, 2.5 mmol) in toluene (4 mL), were added. The reaction mixture was stirred for 18 hours at ambient temperature, quenched with NH₄Cl (20 mL of a saturated aq. solution) and extracted with Et₂O (2 x 30 mL). The combined organic extracts were washed sequentially with HCl (40 mL of a 0.25 M aq. solution), H₂O (40 mL) and brine (40 mL), dried over MgSO₄, filtered and evaporated under reduced pressure to give carbamoyl chloride **23b** (722 mg, 91% yield) as a yellow oil.

¹H NMR (400 MHz, CDCl₃ mixture of rotamers) δ 7.60 (dd, *J* = 16.7, 8.1 Hz, 2H), 7.36 (d, *J* = 7.9 Hz, 2H), 5.85 – 6.00 (m, 1H), 5.55 – 5.41 (m, 1H), 5.10 – 4.90 (m, 1H), 4.82 – 4.49 (m, 2H), 2.08 – 1.94 (m, 3H), 1.85 – 1.40 (m, 3H).

¹³C NMR (101 MHz, CDCl₃ mixture of rotamers) δ 150.4, 150.3, 141.8, 141.4, 133.5, 133.4, 127.3, 126.5, 126.1, 126.1, 125.84 – 125.46 (m), 124.1 (q, *J* = 271.9 Hz) 58.7, 57.0, 50.4, 49.1, 28.5, 27.6, 24.5, 24.4, 21.2, 21.1.

¹⁹F NMR (376 MHz, CDCl₃ mixture of rotamers) δ -62.59, -62.63.

Synthesis of compound **23e**:



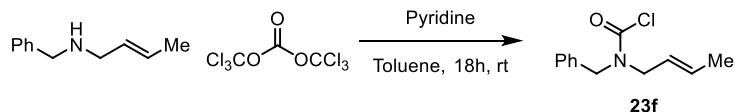
Compound **23e** was prepared according to a modification of a reported procedure.^{28b} To a solution of triphosgene (134 mg, 0.44 mmol) in toluene (8 mL) under N₂, pyridine (0.129 mL, 1.6 mmol) and subsequently a solution of *N*-benzylcyclopent-2-en-1-amine (231 mg, 1.33 mmol) in toluene (2 mL). The reaction mixture was stirred for 18 hours at ambient temperature, quenched with NH₄Cl (20 mL of a saturated aq. solution) and extracted with Et₂O (2 x 30 mL). The combined organic extracts were washed sequentially with HCl (40 mL of a 0.25 M aq. solution), H₂O (40 mL) and brine (40 mL), dried over MgSO₄, filtered and evaporated under reduced pressure to give carbamoyl chloride **23e** (106 mg, 34% yield) as a yellowish oil.

¹H NMR (400 MHz, CDCl₃, mixture of rotamers) δ. 7.40 – 7.20 (m, 5H), 6.02 – 5.95 (m, 1H), 5.58 – 5.46 (m, 2H), 4.66 – 4.37 (m, 1H), 2.44 – 2.20 (m, 3H), 1.75 – 1.59 (m, 1H).

$^{13}\text{C NMR}$ (101 MHz, CDCl_3 , mixture of rotamers) δ 150.1, 150, 137.3, 136.9, 136.4, 128.8, 128.7, 128.7, 128.6, 128.5, 127.3, 127.2, 126.2, 67.6, 66, 50.6, 48.9, 31.4, 31.3, 28.9, 28.4.

HRMS (ESI pos): calculated for $\text{C}_{13}\text{H}_{14}\text{ClNaNO}$ ($\text{M}+\text{Na}^+$) 258.07, found 258.0653.

Synthesis of compound 23f:

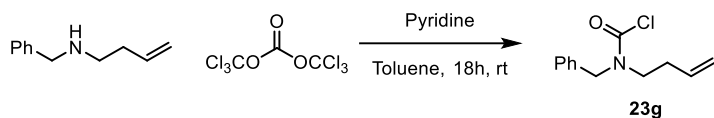


Compound **23f** was prepared according to a modification of a reported procedure.^{28b} To a solution of triphosgene (250 mg, 0.843 mmol) in toluene (15 mL) under N_2 , pyridine (0.241 mL, 2.98 mmol) and subsequently a solution of *N*-benzylbut-2-en-1-amine (400 mg, 2.48 mmol) in toluene (4 mL), were added. The reaction mixture was stirred for 18 hours at ambient temperature, quenched with NH_4Cl (20 mL of a saturated aq. solution) and extracted with Et_2O (2 x 30 mL). The combined organic extracts were washed sequentially with HCl (40 mL of a 0.25 M aq. solution), H_2O (40 mL) and brine (40 mL), dried over MgSO_4 , filtered and evaporated under reduced pressure to give carbamoyl chloride **23f** (508 mg, 92% yield) as a yellow oil.

$^1\text{H NMR}$ (400 MHz, CDCl_3 , 1:1 mixture of rotamers) 7.42 – 7.30 (m, 3H), 7.29 – 7.24 (m, 2H), 5.75 – 5.54 (m, 1H), 5.53 – 5.34 (m, 1H), 4.68 (s, 1H), 4.55 (s, 1H), 3.90 (dd, $J = 15.6$, 6.3 Hz, 2H), 1.78 – 1.66 (m, 3H).

$^{13}\text{C NMR}$ (101 MHz, CDCl_3 , 1:1 mixture of rotamers) δ 150.2, 149.6, 135.8, 135.6, 131.3, 130.7, 129.0, 128.9, 128.4, 128.3, 128.1, 128.1, 127.3, 124.3, 124.0, 53.2, 51.9, 51.5, 50.5, 17.8.

Synthesis of compound 23g:

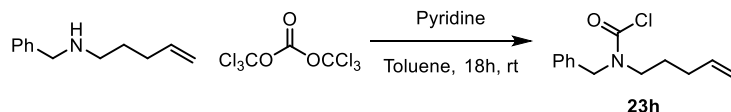


Compound **23g** was prepared according to a modification of a reported procedure.^{28b} To a solution of triphosgene (252 mg, 0.85 mmol) in toluene (15 mL) under N_2 , pyridine (0.243 mL, 3.0 mmol) and subsequently a solution of *N*-benzylbut-3-en-1-amine (403 mg, 2.5 mmol) in toluene (4 mL), were added. The reaction mixture was stirred for 18 hours at ambient temperature, quenched with NH_4Cl (20 mL of a saturated aq. solution) and extracted with Et_2O (2 x 30 mL). The combined organic extracts were washed sequentially with HCl (40 mL of a 0.25 M aq. solution), H_2O (40 mL) and brine (40 mL), dried over MgSO_4 , filtered and evaporated under reduced pressure to give carbamoyl chloride **23g** (475 mg, 85% yield) as a yellow oil.

$^1\text{H NMR}$ (400 MHz, CDCl_3 , 1:1 mixture of rotamers) δ 7.41 – 7.31 (m, 3H), 7.30 – 7.24 (m, 2H), 5.80 – 5.67 (m, 1H), 5.16 – 5.04 (m, 2H), 4.72 (s, 1H), 4.59 (s, 1H), 3.53 – 3.35 (m, 2H), 2.42 – 2.30 (m, 2H).

$^{13}\text{C NMR}$ (101 MHz, CDCl_3 , 1:1 mixture of rotamers) δ 150.3, 149.6, 135.8, 135.6, 134.3, 134.0, 129.1, 129.0, 128.3, 128.2, 128.2, 127.2, 118.0, 117.8, 54.7, 52.7, 49.8, 48.9, 32.6, 31.7.

Synthesis of compound 23h:

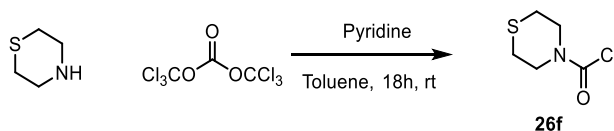


Compound **23h** was prepared according to a modification of a reported procedure.^{28b} To a solution of triphosgene (252 mg, 0.85 mmol) in toluene (15 mL) under N₂, pyridine (0.243 mL, 3.0 mmol) and subsequently a solution of *N*-benzylpent-4-en-1-amine (438 mg, 2.5 mmol) in toluene (4 mL), were added. The reaction mixture was stirred for 18 hours at ambient temperature, quenched with NH₄Cl (20 mL of a saturated aq. solution) and extracted with Et₂O (2 x 30 mL). The combined organic extracts were washed sequentially with HCl (40 mL of a 0.25 M aq. solution), H₂O (40 mL) and brine (40 mL), dried over MgSO₄, filtered and evaporated under reduced pressure to give carbamoyl chloride **23h** (553 mg, 93% yield) as a yellow oil.

¹H NMR (400 MHz, CDCl₃, 1:1 mixture of rotamers) δ 7.41 – 7.30 (m, 3H), 7.29 – 7.24 (m, 2H), 5.81 – 5.68 (m, 2H), 5.08 – 4.92 (m, 2H), 4.71 (s, 1H), 4.58 (s, 1H), 3.36 (dt, *J* = 13.6, 7.8 Hz, 2H), 2.05 (q, *J* = 7.5 Hz, 2H), 1.70 (app h, *J* = 7.6 Hz, 2H).

¹³C NMR (101 MHz, CDCl₃, 1:1 mixture of rotamers) δ 150.3, 149.6, 137.3, 137.1, 135.9, 135.7, 129.0, 129.0, 128.2, 127.2, 115.8, 115.6, 54.5, 52.6, 50.0, 49.1, 30.8, 30.8, 27.1, 26.3.

Synthesis of compound 26f:

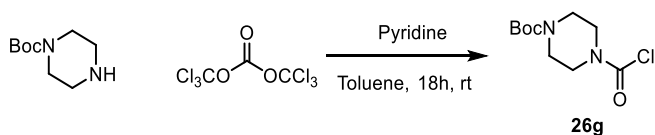


Compound **26f** was prepared according to a modification of a reported procedure.^{28b} To a solution of triphosgene (294 mg, 0.99 mmol) in toluene (15 mL) under N₂, pyridine (0.290 mL, 3.60 mmol) and subsequently a solution of thiomorpholine (310 mg, 3 mmol) in toluene (5 mL) were added. The reaction mixture was stirred for 18 hours at ambient temperature, quenched with NH₄Cl (20 mL of a saturated aq. solution) and extracted with Et₂O (2 x 30 mL). The combined organic extracts were washed sequentially with HCl (40 mL of a 0.25 M aq. solution), H₂O (40 mL) and brine (40 mL), dried over MgSO₄, filtered and evaporated under reduced pressure to afford carbamoyl chloride **26f** (310 mg, 75% yield) as a colorless oil.

¹H NMR (400 MHz, CDCl₃) δ 3.94 (dt, *J* = 38.9, 5.1 Hz, 1H), 2.72 – 2.64 (m, 1H).

¹³C NMR (101 MHz, CDCl₃) δ 148.5, 51.7, 49.3, 27.7, 27.3.

Synthesis of **26g**:



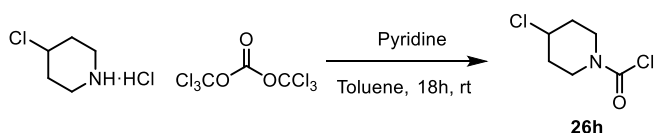
Compound **26g** was prepared according to a modification of a reported procedure.^{28b} To a solution of triphosgene (294 mg, 0.99 mmol) in toluene (15 mL) under N₂, pyridine (0.290 mL, 3.60 mmol) and subsequently a solution of *N*-Boc Piperazine (559 mg, 3 mmol) in toluene (5 mL) were sequentially added. The reaction mixture was stirred for 18 hours at ambient temperature, quenched with NH₄Cl (20 mL of a saturated aq. solution) and extracted with Et₂O (2 x 30 mL). The combined organic extracts were washed sequentially with HCl (40 mL of a 0.25 M aq. solution), H₂O (40 mL) and brine (40 mL), dried over MgSO₄, filtered and evaporated under reduced pressure to give carbamoyl chloride **26g** (597 mg, 82% yield) as a colorless oil.

¹H NMR (300 MHz, CDCl₃) δ 3.64 (m, 4H), 3.48 (d, *J* = 4.8 Hz, 4H), 1.46 (s, 9H).

¹³C NMR (101 MHz, CDCl₃) δ 154.3, 148.5, 80.7, 48.5, 46, 28.3.

HRMS (ESI pos): calculated for C₁₀H₁₇ClNaN₂O₃ (M+Na⁺): 271.0800, found: 271.0818.

Synthesis of compound **26h**:

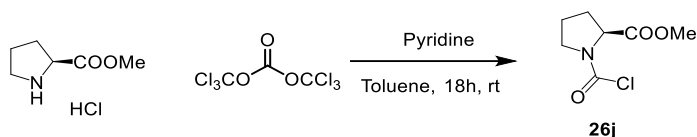


Compound **26h** was prepared according to a modification of a reported procedure.^{28b} To a solution of triphosgene (259 mg, 0.872 mmol) in toluene (15 mL) under N₂, pyridine (0.498 mL, 6.15 mmol) and subsequently a solution of 4-chloropiperidine hydrochloride (400 mg, 2.56 mmol) in toluene (5 mL) were sequentially added. The reaction mixture was stirred for 18 hours at ambient temperature, quenched with NH₄Cl (20 mL of a saturated aq. solution) and extracted with Et₂O (2 x 30 mL). The combined organic extracts were washed sequentially with HCl (40 mL of a 0.25 M aq. solution), H₂O (40 mL) and brine (40 mL), dried over MgSO₄, filtered and evaporated under reduced pressure to give carbamoyl chloride **26h** (420 mg, 90% yield) as a colorless oil.

¹H NMR (400 MHz, CDCl₃) δ 4.34 (tt, *J* = 6.5, 3.6 Hz, 1H), 4.01 – 3.64 (m, 4H), 2.18 – 2.03 (m, 2H), 2.00 – 1.86 (m, 2H).

¹³C NMR (101 MHz, CDCl₃) δ 148.4, 55.6, 45.6, 43.1, 34.7, 34.2.

Synthesis of compound 26j:

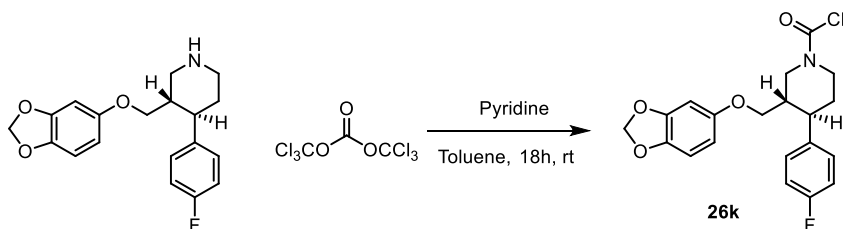


Compound **26j** was prepared according to a modification of a reported procedure.^{28b} To a solution of triphosgene (207 mg, 0.68 mmol) in toluene (15 mL) under N₂, pyridine (0.204 mL, 2.54 mmol) and subsequently a solution of L-methyl proline hydrochloride (350 mg, 2.13 mmol). The reaction mixture was stirred for 18 hours at ambient temperature, quenched with NH₄Cl (20 mL of a saturated aq. solution), and extracted with Et₂O (2 x 30 mL). The combined organic extracts were washed sequentially with HCl (40 mL of a 0.25 M aq. solution), H₂O (40 mL) and brine (40 mL), dried over MgSO₄, filtered and evaporated under reduced pressure to give carbamoyl chloride **26j** (275 mg, 68% yield) as a colorless oil.

¹H NMR (400 MHz, CDCl₃, 1:1 mixture of rotamers) δ: 4.57 – 4.46 (m, 1H), 3.85 – 3.55 (m, 2H), 3.77 (d, *J* = 12.4 Hz, 3H), 2.35 – 2.25 (m, 1H), 2.17 – 1.93 (m, 3H).

¹³C NMR (124 MHz, CDCl₃, 1:1 mixture of rotamers) δ: 171.8, 171.3, 147.8, 146.9, 62.4, 60.7, 52.9, 50.7, 49.2, 30.4, 30.3, 23.7, 23.6

Synthesis of compound 26k:



Compound **26k** was prepared according to a modification of a reported procedure.^{28b} To a solution of triphosgene (89 mg, 0.30 mmol) in toluene (3 mL) under N₂, pyridine (88 μL, 1 mmol) and subsequently a solution of Paroxetine (300 mg, 0.91 mmol) in toluene (6 mL), were added. The reaction mixture was stirred for 18 hours at ambient temperature, quenched with NH₄Cl (20 mL of a saturated aq. solution) and extracted with Et₂O (2 x 30 mL). The combined organic extracts were washed sequentially with HCl (40 mL of a 0.25 M aq. solution), H₂O (40 mL) and brine (40 mL), dried over MgSO₄, filtered and evaporated under reduced pressure to afford carbamoyl chloride **26k** (130 mg, 36% yield) as a white crystal.

¹H NMR (500 MHz, CDCl₃) δ 7.14 (m, 2H), 7.00 (m, 2H), 6.64 (m, 1H), 6.36 (s, 1H), 6.14 (m, 1H), 5.89 (s, 2H), 4.63 (m, 1H), 4.49 (m, 1H), 3.63 (t, *J* = 8.7 Hz, 1H), 3.48 (dd, *J* = 9.6, 6.0 Hz, 1H), 3.20 (t, *J* = 12.9 Hz, 1H), 3.02 (m, 1H), 2.82 (m, 1H), 2.10 (m, 1H), 1.93 (m, 1H), 1.82 (qd, *J* = 12.9, 4.4 Hz, 1H)

¹³C NMR (126 MHz, CDCl₃) δ 162.9, 160.9, 154.0, 148.4, 142.0, 128.9, 115.8, 108.0, 105.8, 101.3, 98.1, 68.4, 52.2, 49.6, 47.0, 43.8, 42.3, 33.7

^{19}F NMR (376 MHz, CDCl_3 , proton decoupled) δ -115.51

HRMS (ESI pos): calculated for $\text{C}_{20}\text{H}_{19}\text{ClFNaNO}_4$ ($\text{M}+\text{Na}^+$): 414.09, found 414.0884.

4.8.3 Reaction of carbamoyl chlorides

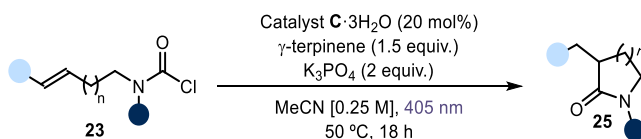
4.8.3.1 Experimental setup

For the generation of carbamoyl radicals, we used the Hepatochem PhotoRedOx Box equipped with an EvoluChem LED 18 W light source at 405 nm, supplied by Hepatochem. The reactor was connected to a Huber Minichiller 300 in order to perform reactions at 50 °C with accurate control of the reaction temperature ($\pm 1^\circ\text{C}$, Figure 4.27).



Figure 4.27: Photoreactor used for the reaction with the carbamoyl chlorides.

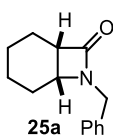
4.8.3.2 General procedure for the intramolecular Giese type addition (General Procedure A)



An oven-dried 15 mL Schlenk tube was charged with a mixture of carbamoyl chloride **23** (0.2 mmol, 1 equiv.), catalyst **C** trihydrate (9 mg, 0.04 mmol, 0.2 equiv.), γ -terpinene (48 μL , 0.3 mmol, 1.5 equiv.) and K_3PO_4 (85 mg, 0.4 mmol, 2 equiv.) in acetonitrile (0.8 mL, 0.25 M). The reaction mixture was placed under an atmosphere of argon, cooled to -78°C , degassed *via* vacuum evacuation (5 minutes), backfilled with argon and, ultimately, warmed to ambient temperature. This freeze-pump-thaw cycle was

repeated four times, and then the Schlenk tube was sealed with Parafilm and put into the Hepatochem PhotoRedOx Box equipped with a 405 nm EvoluChem LED 18 W light source at 50 °C (Figure 4.27). After 18 hours, the reaction vessel was cooled down to ambient temperature, water was added and the mixture was extracted with ethyl acetate (2x15 mL). The combined layers were dried over magnesium sulfate, filtered, and concentrated. The resulting crude mixture was purified by column chromatography on silica gel to give the corresponding product **25** in the stated yield.

Characterization of Products

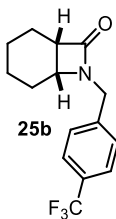


7-Benzyl-7-azabicyclo[4.2.0]octan-8-one (25a): Synthesized according to the general procedure A using benzyl(cyclohex-2-en-1-yl)carbamic chloride (50 mg, 0.2 mmol). The crude mixture was purified by flash column chromatography on silica gel (10% AcOEt in hexanes as eluent) to afford product **25a** (26 mg, 60% yield) as a pale-yellow oil.

¹H NMR (500 MHz, CDCl₃) δ 7.35 – 7.29 (m, 2H), 7.29 – 7.22 (m, 3H), 4.57 (d, *J* = 15.1 Hz, 1H), 4.08 (d, *J* = 15.1 Hz, 1H), 3.62 (ddd, *J* = 5.4, 4.2, 3.1 Hz, 1H), 3.20 – 3.15 (m, 1H), 1.89 – 1.80 (m, 1H), 1.74 – 1.49 (m, 5H), 1.49 – 1.33 (m, 2H).

¹³C NMR (126 MHz, CDCl₃) δ 171.1, 136.4, 128.9, 128.5, 127.8, 50.3, 47.1, 44.6, 23.0, 19.8, 19.1, 17.0.

HRMS (ESI pos): calculated for C₈H₁₈NaO₄ (M+H⁺): 216.1383, found: 216.1374.

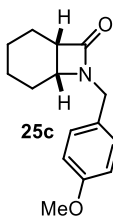


7-(4-(Trifluoromethyl)benzyl)-7-azabicyclo[4.2.0]octan-8-one (25b): Synthesized according to general procedure A using cyclohex-2-en-1-yl(4-(trifluoromethyl)benzyl)carbamic chloride (64 mg, 0.2 mmol). The crude mixture was purified by flash column chromatography on silica gel (5% AcOEt in hexanes as eluent) to afford product **25b** (31 mg, 55% yield) as a yellow oil.

¹H NMR (400 MHz, CDCl₃) δ 7.59 (d, *J* = 8.0 Hz, 2H), 7.39 (d, *J* = 8.0 Hz, 2H), 4.62 (d, *J* = 15.4 Hz, 1H), 4.16 (d, *J* = 15.4 Hz, 1H), 3.66 (dt, *J* = 5.1, 3.6 Hz, 1H), 3.23 (dt, *J* = 6.8, 4.6 Hz, 1H), 1.92 – 1.83 (m, 1H), 1.77 – 1.55 (m, 5H), 1.50 – 1.34 (m, 2H).

¹³C NMR (126 MHz, CDCl₃) δ 171.1, 140.5, 130.1 (q, *J* = 32.6 Hz), 128.6, 125.9 (q, *J* = 3.8 Hz), 124.2 (q, *J* = 272.1 Hz), 50.5, 47.3, 44.1, 23.0, 19.7, 19.0, 16.9.

HRMS (ESI pos): calculated for C₁₅H₁₇F₃NO (M+H⁺): 284.1257, found: 284.1258.

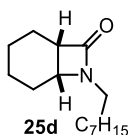


7-(4-Methoxybenzyl)-7-azabicyclo[4.2.0]octan-8-one (25c): Synthesized according to general procedure A using cyclohex-2-en-1-yl(4-methoxybenzyl)carbamic chloride (56 mg, 0.2 mmol). The crude mixture was purified by flash column chromatography on silica gel (15% AcOEt in hexanes as eluent) to afford product **25c** (30 mg, 61% yield) as a yellow oil.

¹H NMR (400 MHz, CDCl₃) δ 7.23 – 7.14 (m, 2H), 6.91 – 6.80 (m, 2H), 4.51 (d, *J* = 14.9 Hz, 1H), 4.04 (d, *J* = 14.9 Hz, 1H), 3.80 (s, 3H), 3.61 (ddd, *J* = 5.4, 4.1, 3.2 Hz, 1H), 3.17 (dt, *J* = 6.9, 4.6 Hz, 1H), 1.93 – 1.79 (m, 1H), 1.74 – 1.50 (m, 4H), 1.49 – 1.31 (m, 3H).

¹³C NMR (100 MHz, CDCl₃) δ 170.9, 159.2, 129.7, 128.4, 114.2, 55.4, 50.0, 46.9, 43.9, 23.0, 19.7, 19.0, 16.9.

HRMS (ESI pos): calculated for C₁₅H₁₉NnaO₂ (M+Na⁺): 268.1308, found: 268.1304.

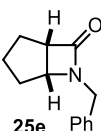


7-Octyl-7-azabicyclo[4.2.0]octan-8-one (25d): synthesized according to the general procedure A using cyclohex-1-en-1-yl(octyl)carbamic chloride **23d** (54 mg, 0.2 mmol). The crude mixture was purified by flash column chromatography on silica gel (5% AcOEt in Hexane) to afford **25d** (13 mg, 28% yield) as a colorless oil.

¹H NMR (400 MHz, CDCl₃) δ: 3.72 (ddd, *J* = 5.3, 4.2, 3.2 Hz, 1H), 3.33 (dt, *J* = 13.9, 7.6 Hz, 1H), 3.20 – 3.11 (m, 1H), 2.94 (ddd, *J* = 14.0, 7.9, 6.2 Hz, 1H), 1.94 – 1.39 (m, 10H), 1.35 – 1.20 (m, 9H), 1.00 – 0.81 (m, 3H).

¹³C NMR (101 MHz, CDCl₃) δ 171, 50.2, 46.6, 40.3, 31.9, 29.4, 29.3, 28.2, 27.3, 23.3, 22.8, 19.7, 19, 17.1, 14.2.

HRMS (ESI pos): calculated for C₁₅H₂₇NO (M+H⁺): 238,21 found: 238,2157

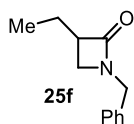


6-Benzyl-6-azabicyclo[3.2.0]heptan-7-one (25e): synthesized according to the general procedure A using benzyl(cyclopent-2-en-1-yl)carbamic chloride **23e** (47 mg, 0.2 mmol, 1 eq.). The crude mixture was purified by flash column chromatography on silica gel (5% AcOEt in hexane) to afford **25e** (11 mg, 30% yield) as a yellowish oil.

¹H NMR (400 MHz, CDCl₃) δ 7.54 – 7.08 (m, 5H), 4.50 (d, *J* = 15.1 Hz, 1H), 4.08 (d, *J* = 15.1 Hz, 1H), 3.91 (t, *J* = 4.1 Hz, 1H), 3.47 (dd, *J* = 8.0, 3.6 Hz, 1H), 2.05 (dd, *J* = 13.2, 6.3 Hz, 1H), 1.83 – 1.70 (m, 2H), 1.58 (m, 1H), 1.47 – 1.30 (m, 1H), 1.18 (m, 1H).

¹³C NMR (126 MHz, CDCl₃) δ 169.6, 136.3, 128.8, 128.4, 127.8, 57.6, 55.1, 44.2, 27, 25.1, 22.8.

HRMS (ESI pos): calculated for C₁₃H₁₅NaNO (M+Na⁺): 224.11 found: 224.1041

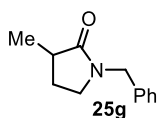


1-Benzyl-3-ethylazetid-2-one (25f): synthesized according to the general procedure A using benzyl(but-2-en-1-yl)carbamic chloride **23f** (47 mg, 0.2 mmol, 1 eq.). The crude mixture was purified by flash column chromatography on silica gel (5% AcOEt in hexane) to afford **25f** (11 mg, 29% yield) as a yellowish oil.

¹H NMR (500 MHz, CDCl₃) δ 7.37 – 7.26 (m, 5H), 4.46 (s, 2H), 3.60 – 3.52 (m, 2H), 3.18 – 3.10 (m, 1H), 1.72 – 1.65 (m, 2H), 0.93 (t, *J* = 7.3 Hz, 3H)

¹³C NMR (126 MHz, CDCl₃) δ: 171.9 (C), 136.3 (C), 128.9 (CH), 128.3 (CH), 127.9 (CH), 53.6 (CH₂), 48.7 (CH₂), 44 (CH), 29 (CH₂), 11.9 (CH₃).

Matching reported literature data.²⁹

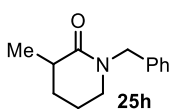


1-Benzyl-3-methylpyrrolidin-2-one (25g): Synthesized according to the general procedure A using benzyl(but-3-en-1-yl)carbamic chloride **23g** (48 mg, 0.2 mmol). The crude mixture was purified by flash column chromatography on silica gel (10% AcOEt in hexanes as eluent) to afford product **25g** (23 mg, 60% yield) as a yellow oil.

¹H NMR (500 MHz, CDCl₃) δ 7.37 – 7.30 (m, 2H), 7.29 – 7.24 (m, 1H), 7.24 – 7.20 (m, 2H), 4.49 – 4.40 (m, 2H), 3.22 – 3.09 (m, 2H), 2.51 (ddt, *J* = 15.8, 8.7, 7.2 Hz, 1H), 2.21 (dddd, *J* = 12.9, 8.7, 6.5, 4.4 Hz, 1H), 1.59 (dq, *J* = 12.6, 8.5 Hz, 1H), 1.24 (d, *J* = 7.1 Hz, 3H).

¹³C NMR (126 MHz, CDCl₃) δ 177.5, 136.8, 128.8, 128.2, 127.6, 46.9, 44.8, 36.9, 27.2, 16.5.

HRMS (ESI pos): calculated for C₁₂H₁₆NO (M+H⁺): 190.1226, found: 190.1228.



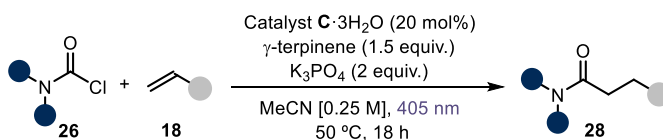
1-Benzyl-3-methylpiperidin-2-one (25h): Synthesized according to the general procedure A using benzyl(pent-4-en-1-yl)carbamic chloride **23h** (48 mg, 0.2 mmol). The crude mixture was purified by flash column chromatography on silica gel (10% AcOEt in hexanes as eluent) to afford product **25h** (21 mg, 52% yield) as a yellow oil.

¹H NMR (400 MHz, CDCl₃) δ 7.36 – 7.28 (m, 2H), 7.28 – 7.21 (m, 3H), 4.66 (d, *J* = 14.6 Hz, 1H), 4.50 (d, *J* = 14.6 Hz, 1H), 3.20 (dd, *J* = 7.2, 5.1 Hz, 2H), 2.56 – 2.42 (m, 1H), 1.96 (dtd, *J* = 12.8, 6.2, 3.4 Hz, 1H), 1.84 (ddtd, *J* = 13.5, 6.6, 5.0, 3.4 Hz, 1H), 1.78 – 1.66 (m, 1H), 1.53 (dddd, *J* = 12.8, 10.4, 9.1, 3.4 Hz, 1H), 1.30 (d, *J* = 7.2 Hz, 3H).

¹³C NMR (101 MHz, CDCl₃) δ 173.5, 137.7, 128.7, 128.1, 127.4, 50.4, 47.7, 36.8, 29.7, 21.8, 18.2.

HRMS (ESI pos): calculated for C₁₃H₁₈NO (M+H⁺): 204.1383, found: 204.1376.

4.8.3.3 General Procedure for the intermolecular Giese type addition (General Procedure B)

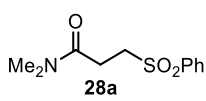


An oven-dried 15 mL Schlenk tube was charged with a mixture of carbamoyl chloride **26** (0.4 mmol, 2 equiv.), catalyst C trihydrate (9 mg, 0.04 mmol, 0.2 equiv.), alkene **18** (0.2 mmol, 1 equiv.), γ -terpinene (64 μ L, 0.4 mmol, 2 equiv.) and K₃PO₄ (85 mg, 0.4 mmol, 2 equiv.) in acetonitrile (0.8 mL, 0.25 M). The reaction mixture was placed under an atmosphere of argon, cooled to -78 °C, degassed *via* vacuum evacuation (5 minutes), backfilled with argon and, ultimately, warmed to ambient temperature. This

²⁹ Franco Bella, A.; Jackson, L. V.; Walton, J. C. "Preparation of β - and γ -lactams *via* ring closures of unsaturated carbamoyl radicals derived from 1-carbamoyl-1-methylcyclohexa-2,5-dienes" *Org. Biomol. Chem.* **2004**, *2*, 421-428.

freeze-pump-thaw cycle was repeated four times, and then the Schlenk tube was sealed with Parafilm and put into the Hepatochem PhotoRedOx Box equipped with a 405 nm EvoluChem LED 18 W light source at 50 °C (Figure 4.27). After 18 hours stirring, the reaction was cooled down to ambient temperature, water was added and the mixture was extracted with ethyl acetate (2x15 mL). The combined layers were dried over magnesium sulfate, filtered, and concentrated. The resulting crude mixture was purified by column chromatography on silica gel to give the corresponding product **9** in the stated yield.

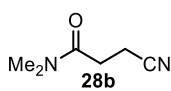
Characterization of Products

 ***N,N*-Dimethyl-3-(phenylsulfonyl)propanamide (28a):** Synthesized according to general procedure B using dimethylcarbamic chloride (37 μ L, 0.4 mmol, 2.0 equiv.) and phenyl vinyl sulfone (34 mg, 0.2 mmol). The crude mixture was purified by flash column chromatography on silica gel (gradient from hexane 100% to ethyl acetate 100%) to afford product **28a** (29 mg, 60% yield) as a pale-yellow oil.

$^1\text{H NMR}$ (400 MHz, CDCl_3) δ 7.95 – 7.88 (m, 2H), 7.69 – 7.62 (m, 1H), 7.61 – 7.52 (m, 2H), 3.53 – 3.33 (m, 2H), 2.99 (s, 3H), 2.89 (s, 3H), 2.85 – 2.73 (m, 2H).

$^{13}\text{C NMR}$ (100 MHz, CDCl_3) δ 168.8, 139.2, 134.0, 129.5, 128.1, 52.2, 37.2, 35.7, 26.2.

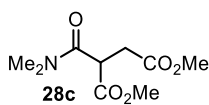
HRMS (ESI pos): calculated for $\text{C}_{11}\text{H}_{15}\text{N}_2\text{O}_3\text{S}$ ($\text{M}+\text{Na}^+$): 264.0665, found 264.0653.

 **3-Cyano-*N,N*-dimethylpropanamide (28b):** Synthesized according to general procedure B using dimethylcarbamic chloride (37 μ L, 0.4 mmol, 2.0 equiv.) and acrylonitrile (13 μ L, 0.2 mmol). The crude mixture was purified by flash column chromatography on silica gel (gradient from hexane 100% to ethyl acetate 100%) to afford product **28b** (16 mg, 63% yield) as a pale-yellow oil.

$^1\text{H NMR}$ (400 MHz, CDCl_3) δ 3.01 (s, 3H), 2.97 (s, 3H), 2.68 (s, 4H).

$^{13}\text{C NMR}$ (100 MHz, CDCl_3) δ 168.8, 119.6, 37.0, 35.7, 29.5, 13.1.

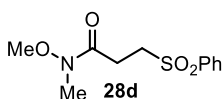
HRMS (ESI pos): calculated for $\text{C}_6\text{H}_{11}\text{N}_2\text{O}$ ($\text{M}+\text{H}^+$): 127.0866, found: 127.0869.

 **dimethyl 2-(dimethylcarbamoyl)succinate (28c):** Synthesized according to general procedure B using dimethylcarbamic chloride (37 μ L, 0.4 mmol, 2.0 equiv.) and dimethyl fumarate (29 mg, 0.2 mmol). The crude mixture was purified by flash column chromatography on silica gel (gradient from hexane 100% to ethyl acetate 100%) to afford product **28c** (27 mg, 62% yield) as a pale-yellow oil.

$^1\text{H NMR}$ (400 MHz, CDCl_3) δ 4.14 (dd, $J = 8.3, 6.0$ Hz, 1H), 3.72 (s, 3H), 3.67 (s, 3H), 3.16 (s, 3H), 3.11 – 2.80 (m, 6H).

$^{13}\text{C NMR}$ (100 MHz, CDCl_3) δ 172.4, 169.5, 167.9, 53.0, 52.2, 44.6, 38.0, 36.4, 33.6.

HRMS (ESI pos): calculated for $\text{C}_9\text{H}_{15}\text{N}_2\text{O}_5$ ($\text{M}+\text{Na}^+$): 240.0842, found: 240.0844.



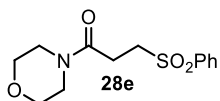
***N*-Methoxy-*N*-methyl-3-(phenylsulfonyl)propanamide** (**28d**):

Synthesized according to general procedure B using methoxy(methyl)carbamic chloride (41 μ L, 0.4 mmol, 2.0 equiv.) and phenyl vinyl sulfone (34 mg, 0.2 mmol). The crude mixture was purified by flash column chromatography on silica gel (gradient from hexane 100% to hexane 50% : 50% ethyl acetate) to afford product **28d** (16 mg, 30% yield) as a pale yellow oil.

$^1\text{H NMR}$ (400 MHz, CDCl_3) δ 7.97 – 7.90 (m, 2H), 7.75 – 7.63 (m, 1H), 7.63 – 7.54 (m, 2H), 3.69 (s, 3H), 3.52 – 3.37 (m, 2H), 3.14 (s, 3H), 2.97 – 2.92 (m, 2H).

$^{13}\text{C NMR}$ (101 MHz, CDCl_3) 170.4, 139.2, 134.0, 129.5, 128.2, 61.6, 51.5, 32.3, 25.4.

HRMS (ESI pos): calculated for $\text{C}_9\text{H}_{15}\text{NNaO}_5$ ($\text{M}+\text{Na}^+$): 240.0842, found: 240.0844.



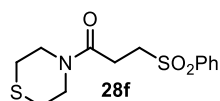
1-Morpholino-3-(phenylsulfonyl)propan-1-one (**28e**):

Synthesized according to general procedure B using morpholine-4-carbonyl chloride (47 μ L, 0.4 mmol, 2.0 equiv.) and phenyl vinyl sulfone (34 mg, 0.2 mmol). The crude mixture was purified by flash column chromatography on silica gel (gradient from hexane 100% to ethyl acetate 100%) to afford product **28e** (42 mg, 74% yield) as a pale-yellow oil.

$^1\text{H NMR}$ (400 MHz, CDCl_3) δ 8.00 – 7.85 (m, 2H), 7.71 – 7.62 (m, 1H), 7.62 – 7.51 (m, 1H), 3.76 – 3.58 (m, 5H), 3.55 – 3.49 (m, 2H), 3.47 – 3.42 (m, 3H), 2.94 – 2.74 (m, 2H).

$^{13}\text{C NMR}$ (100 MHz, CDCl_3) δ 167.5, 139.1, 134.0, 129.5, 128.0, 66.7, 66.5, 52.0, 45.8, 42.3, 25.9.

HRMS (ESI pos): calculated for $\text{C}_{13}\text{H}_{17}\text{NNaO}_4\text{S}$ ($\text{M}+\text{Na}^+$): 306.0770, found: 306.0762.



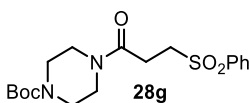
3-(Phenylsulfonyl)-1-thiomorpholinopropan-1-one (**28f**):

synthesized according the general procedure B using thiomorpholine-4-carbonyl chloride **26f** (99 mg, 0.4 mmol, 2 equiv.) and phenyl vinyl sulfone (34 mg, 0.2 mmol, 1 eq.). The crude mixture was purified by flash column chromatography on silica gel (5% AcOEt in hexane), followed by a second one (50% AcOEt in Hexane as eluent) to afford **28f** (37.8 mg, 63% yield) as a colorless oil.

$^1\text{H NMR}$ (400 MHz, CDCl_3) δ 7.96 (m, 2H) 7.70 (m, 1H) 7.61 (m, 2H) 3.85 (m, 2H), 3.76 (m, 1H), 3.65 (m, 1H), 3.50 (m, 1H), 2.86, (m, 2H), 2.64 (m, 6H).

$^{13}\text{C NMR}$ (126 MHz, CDCl_3) δ 167.3, 139.3, 134.1, 129.5, 128.1, 52.2, 48.3, 44.8, 27.9, 27.4, 26.2

HRMS (ESI pos): calculated for $\text{C}_{13}\text{H}_{17}\text{NaNO}_3\text{S}_2$ ($\text{M}+\text{Na}^+$): 322.05, found: 322.0533.



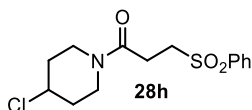
tert-Butyl 4-(3-(phenylsulfonyl)propanoyl)piperazine-1-carboxylate (28g): synthesized according general procedure B using tert-butyl 4-(chlorocarbonyl)piperazine-1-carboxylate

26g (99 mg, 0.4 mmol, 2 equiv.) and phenyl vinyl sulfone (34 mg, 0.2 mmol, 1 eq.). The crude mixture was purified by flash column chromatography on silica gel (5% AcOEt in hexane), followed by a second purification (50% AcOEt in hexane as eluent) to afford **28g** (55 mg, 73% yield) as a white solid.

¹H NMR (400 MHz, CDCl₃) δ 7.91 (m, 2H), 7.66 (m, 1H), 7.57 (m, 2H), 3.42 (m, 4H) 3.21 (m, 6H), 2.83 (t, *J* = 7.8 Hz, 2H), 1.45 (s, 9H)

¹³C NMR (126 MHz, CDCl₃) δ 167.6, 154.6, 139.3, 134.1, 129.6, 128.1, 80.7, 52.1, 45.4, 41.9, 28.5, 26.1

HRMS (ESI pos): calculated for C₁₈H₂₆NaN₂O₅S (M+Na⁺): 405.15, found 405.1455.



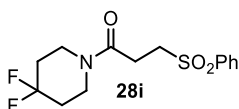
1-(4-Chloropiperidin-1-yl)-3-(phenylsulfonyl)propan-1-one (28h): Synthesized according to general procedure B using 4-chloropiperidine-1-carbonyl chloride (73 mg, 0.4 mmol, 2 equiv.) and phenyl vinyl sulfone (34 mg, 0.2 mmol).

The crude mixture was purified by flash column chromatography on silica gel (gradient from hexane 100% to ethyl acetate 100%) to afford product **28h** (41 mg, 65% yield) as a pale-yellow oil.

¹H NMR (400 MHz, CDCl₃) δ 7.96 – 7.87 (m, 2H), 7.72 – 7.62 (m, 1H), 7.60 – 7.53 (m, 2H), 4.27 (tt, *J* = 7.0, 3.6 Hz, 1H), 3.68 (tdt, *J* = 11.7, 8.2, 3.5 Hz, 2H), 3.58 (ddd, *J* = 13.6, 6.9, 4.0 Hz, 1H), 3.49 – 3.42 (m, 2H), 3.38 (ddd, *J* = 13.9, 7.0, 3.7 Hz, 1H), 2.83 (td, *J* = 7.1, 1.9 Hz, 2H), 2.16 – 1.93 (m, 2H), 1.90 – 1.72 (m, 2H).

¹³C NMR (100 MHz, CDCl₃) δ 167.2, 139.2, 134.0, 129.5, 128.0, 56.1, 52.1, 42.5, 39.1, 35.1, 34.4, 25.9.

HRMS (ESI pos): calculated for C₁₄H₁₉ClNO₃S (M+H⁺): 316.0769, found: 316.0773.



1-(4,4-Difluoropiperidin-1-yl)-3-(phenylsulfonyl)propan-1-one (28i): Synthesized according to general procedure B using 4,4-difluoropiperidine-1-carbonyl chloride (73 mg, 0.4 mmol, 2 equiv.) and phenyl vinyl sulfone (34 mg, 0.2 mmol). The crude

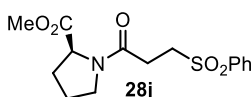
mixture was purified by flash column chromatography on silica gel (gradient from hexane 100% to 1:1 hexane/ethyl acetate) to afford product **28i** (43 mg, 68% yield) as an off-white solid.

¹H NMR (400 MHz, CDCl₃) δ 7.96 – 7.88 (m, 2H), 7.71 – 7.63 (m, 1H), 7.61 – 7.54 (m, 2H), 3.61 (dt, *J* = 43.9, 6.0 Hz, 4H), 3.51 – 3.43 (m, 2H), 2.92 – 2.83 (m, 2H), 2.13 – 1.84 (m, 4H).

¹³C NMR (100 MHz, CDCl₃) δ 167.4, 139.2, 134.1, 129.5, 128.0, 121.3 (t, *J* = 242.4 Hz), 52.1, 40.7 (dt, *J* = 330.8, 5.4 Hz), 34.1 (dt, *J* = 78.0, 23.6 Hz), 25.9.

¹⁹F NMR (376 MHz, CDCl₃) δ -98.22 (p, *J* = 13.5 Hz).

HRMS (ESI pos): calculated for C₁₈H₁₈NaO₄ (M+Na⁺): 340.0789, found: 340.0785.



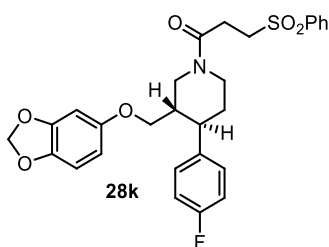
Methyl (3-(phenylsulfonyl)propanoyl)-L-prolinate (28j): synthesized according the general procedure B using methyl (chlorocarbonyl)-L-prolinate (77 mg, 0.4 mmol, 2 equiv.) and phenyl vinyl sulfone (34 mg, 0.2 mmol, 1 eq.). The crude

mixture was purified by flash column chromatography on silica gel (5% AcOEt in hexane) to afford **28j** (46 mg, 58% yield) as a yellowish oil.

$^1\text{H NMR}$ (400 MHz, CDCl_3) δ 7.95 – 7.89 (m, 2H), 7.69 – 7.64 (m, 1H), 7.61 – 7.53 (m, 2H), 4.42 (dd, $J = 8.4, 3.5$ Hz, 1H), 3.70 (s, 3H), 3.68 – 3.59 (m, 1H), 3.56 – 3.38 (m, 3H), 2.83 (dt, $J = 9.7, 5.6$ Hz, 2H), 2.11 – 1.94 (m, 4H).

$^{13}\text{C NMR}$ (126 MHz, CDCl_3) δ 172.6, 167.8, 139.2, 134, 129.5, 128.1, 58.9, 52.4, 51.7, 47.1, 29.3, 27.4, 24.8.

HRMS (ESI pos): calculated for $\text{C}_{15}\text{H}_{19}\text{NaNO}_5\text{S}$ ($\text{M}+\text{Na}^+$): 326.10, found: 326.1063.



1-(3-((Benzo[d][1,3]dioxol-5-yloxy)methyl)-4-(4-fluorophenyl)piperidin-1-yl)-3-(phenylsulfonyl)propan-1-one (28k): synthesized according the general procedure B using 3-((benzo[d][1,3]dioxol-5-yloxy)methyl)-4-(4-fluorophenyl)piperidine-1-carbonyl chloride **26k** (157 mg, 0.4 mmol, 2 eq.) and phenyl vinyl sulfone (34 mg, 0.2 mmol, 1 eq.). The crude mixture was purified by

flash column chromatography on silica gel (gradient from hexane 100% to hexane 50% : 50% ethyl acetate) to afford product **28k** (46 mg, 29% yield) as a yellowish oil.

$^1\text{H NMR}$ (400 MHz, CDCl_3) δ 7.98 (m, 2H), 7.71 (m, 1H), 7.65 – 7.58 (m, 2H), 7.17 – 7.11 (m, 2H), 7.01 (m, 2H), 6.66 (dd, $J = 17.8, 8.4$ Hz, 1H), 6.38 (dd, $J = 11.9, 2.5$ Hz, 1H), 6.17 (ddd, $J = 15.1, 8.5, 2.5$ Hz, 1H), 5.92 (d, $J = 13.5$ Hz, 2H), 4.79 (dd, $J = 55.2, 13.1$ Hz, 1H), 4.07 (dd, $J = 69.6, 13.5$ Hz, 1H), 3.68 – 3.60 (m, 1H), 3.59 – 3.45 (m, 3H), 3.17 (m, 1H), 3.03 – 2.80 (m, 2H), 2.80 – 2.62 (m, 1H), 1.92 (m, 1H), 1.81 – 1.53 (m, 3H).

$^{13}\text{C NMR}$ (126 MHz, CDCl_3) δ 167.5, 154.5, 148.7, 142.3, 139.6, 138.4, 134.3, 129.7, 129.1, 128.3, 115.7, 115.8, 108.2, 106.0, 101.5, 98.4, 68.9, 52.5, 49.2, 46.4, 44.5, 42.2, 34.6, 33.8, 30.1, 26.3.

$^{19}\text{F NMR}$ (376 MHz, CDCl_3 , proton decoupled) δ – 115.58

HRMS (ESI pos): calculated for $\text{C}_{28}\text{H}_{29}\text{FNO}_6\text{S}$ ($\text{M}+\text{H}^+$): 526.16, found: 526.1702.

4.8.4 Reaction of aromatic acyl chlorides

4.8.4.1 Experimental setup

Our photoreactor consisted of a 12.5 cm diameter jar, fitted with 4 standard 29 sized ground glass joints arranged in a square and a central 29 sized joint. A commercial 1-meter LED strip was wrapped around the jar, followed by a layer of aluminium foil and cotton for insulation (Figure 4.28).

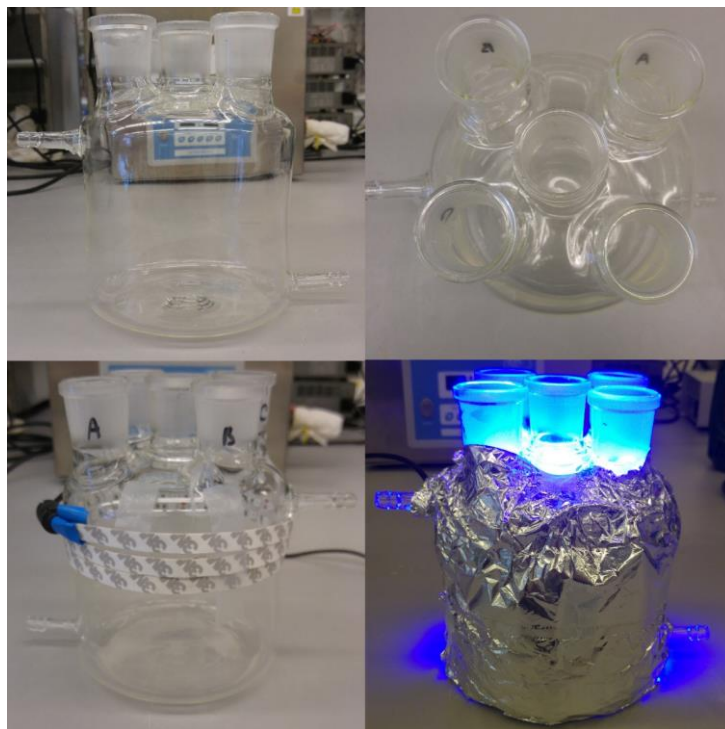


Figure 4.28: Photoreactor used for temperature-controlled reactions - pictures taken at different stages of the set-up assembly.

Each of the joints could be used to fit a standard 16 mm or 25 mm diameter Schlenk tube with a Teflon adaptor (Figure 4.29).



Figure 4.29: Teflon adaptors to use Schlenk tubes in the photoreactor.

An inlet and an outlet allow the circulation of liquid from a Huber Minichiller 300 inside the jar. This setup allows to perform reactions at temperatures ranging from -20 °C to 80 °C with accurate control of the reaction temperature ($\pm 1^\circ\text{C}$, Figure 4.30).

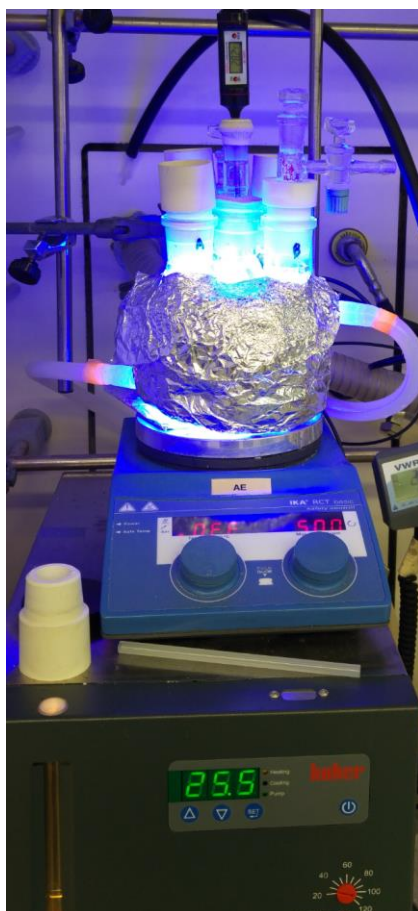
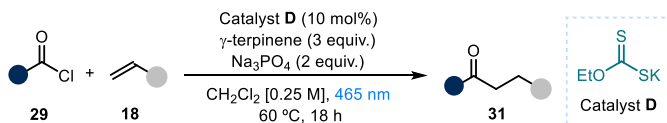


Figure 4.30: Fully assembled controlled temperature photoreactor in operation.

In order to maintain consistent illumination between different experiments, only the four external positions were used to perform reactions. The central position was used to monitor the temperature inside a Schlenk tube identical to those used to perform reactions, ensuring that the reaction mixtures are at the desired temperature.

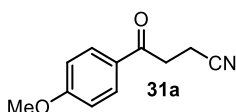
4.8.4.2 General Procedure C



In an oven dried tube of 15 mL (16 mm × 125 mm) with a Teflon septum screw cap, potassium ethyl xanthogenate **D** (8 mg, 0.05 mmol, 0.1 equiv.), sodium phosphate (164 mg, 1.00 mmol, 2 equiv.), acyl chloride **29** (0.75 mmol, 1.5 equiv.) and the electron-poor olefin **18** (0.5 mmol, 1 equiv., *if solid*), were dissolved in DCM (2 mL, HPLC grade). Then, γ -terpinene (240 μ L, 1.5 mmol, 3 equiv.) was added. The resulting yellow mixture

was degassed with argon sparging for 60 seconds. When the electron-poor olefin **18** is liquid, it was added via syringe after the argon sparging. The reaction vessel was then placed in the temperature-controlled photoreactor (Figures 4.28-4.30) set at 60 °C (60–61 °C measured in the central well) and irradiated for 16 hours upon stirring, if not otherwise specified. Then, the solvent was evaporated and the residue purified by column chromatography to afford the corresponding product in the stated yield with >95% purity according to ¹H NMR analysis.

Characterization of Products



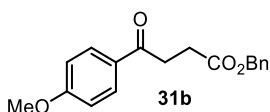
4-(4-methoxyphenyl)-4-oxobutanenitrile (31a):

Synthesized according to the general procedure C using 4-methoxybenzoyl chloride (102 μ L, 0.75 mmol, 1.5 equiv.) and acrylonitrile (33 μ L, 0.5 mmol, 1 equiv.). The crude mixture was purified by flash column chromatography on silica gel (15% AcOEt in hexanes as eluent) to afford **31a** (80 mg, 84% yield) as a white solid.

¹H NMR (500 MHz, CDCl₃) δ 7.92 (app d, J = 8.9 Hz, 2H), 6.95 (app d, J = 9.0 Hz, 2H), 3.87 (s, 3H), 3.32 (t, J = 7.3 Hz, 2H), 2.75 (t, J = 7.3 Hz, 2H).

¹³C NMR (126 MHz, CDCl₃) δ 193.9, 164.2, 130.4, 128.8, 119.5, 114.1, 55.7, 34.0, 12.0

Matching reported literature data.³⁰



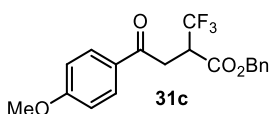
Benzyl 4-(4-methoxyphenyl)-4-oxobutanoate (31b):

Synthesized according to the general procedure A using 4-methoxybenzoyl chloride (102 μ L, 0.75 mmol, 1.5 equiv.) and benzyl acrylate (77 μ L, 0.5 mmol, 1 equiv.). The crude mixture was purified by flash column chromatography on silica gel (15% AcOEt in hexanes as eluent), followed by a second purification (AcOEt/hexanes/toluene 1:6:6 as eluent) to afford **31b** (96 mg, 64% yield) as a yellow solid.

¹H NMR (500 MHz, CDCl₃) δ 7.99 – 7.94 (m, 2H), 7.38–7.29 (m, 5H), 6.96 – 6.91 (m, 2H), 5.15 (s, 2H), 3.87 (s, 3H), 3.28 (t, J = 6.7 Hz, 2H), 2.81 (t, J = 6.7 Hz, 2H).

¹³C NMR (126 MHz, CDCl₃) δ 196.6, 173.0, 163.7, 136.1, 130.4, 129.8, 128.6, 128.3 (2C overlapping), 113.9, 66.6, 55.6, 33.1, 28.5.

HRMS (ESI pos): calculated for C₁₈H₁₈NaO₄ (M+Na⁺): 321.1097, found: 321.1091.



Benzyl 4-(4-methoxyphenyl)-4-oxo-2-(trifluoromethyl)butanoate (31c):

Synthesized according to the general procedure C using 4-methoxybenzoyl chloride (102 μ L, 0.75 mmol, 1.5 equiv.) and benzyl 2-(trifluoromethyl)acrylate (115 mg, 0.5 mmol, 1 equiv.). The crude mixture was purified

³⁰ Li, Y.; Shang, J.-Q.; Wang, X.-X.; Xia, W.-J.; Yang, T.; Xin, Y.; Li, Y.-M. "Copper-Catalyzed Decarboxylative Oxyalkylation of Alkynyl Carboxylic Acids: Synthesis of γ -Diketones and γ -Ketonitriles" *Org. Lett.* **2019**, *21*, 2227–2230

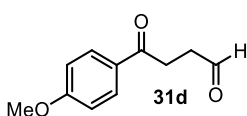
by flash column chromatography on silica gel (10% AcOEt in hexanes as eluent). In order to remove traces of *p*-anisaldehyde formed as a byproduct during the reaction, after the chromatographic purification and solvent removal, the mixture was dissolved in 1.5 mL of MeOH, and 7.5 mL of saturated NaHSO₃ (aq) were added. Subsequently, the mixture was stirred for 30 s, diluted with 7.5 mL of H₂O, and extracted with 7.5 mL of 10% AcOEt in hexanes. The organic layer was dried with MgSO₄, filtered, and concentrated in vacuo³¹ to afford **31c** (150 mg, 82% yield) as a colorless oil.

¹H NMR (400 MHz, CDCl₃) δ 7.99 – 7.91 (m, 2H), 7.42 – 7.29 (m, 5H), 6.99 – 6.91 (m, 2H), 5.24 (dd, *J* = 18.3; 12.3 Hz, 2H), 4.01 – 3.89 (m, 1H), 3.87 (s, 3H), 3.78 (dd, *J* = 17.7, 10.8 Hz, 1H), 3.32 (dd, *J* = 17.7, 3.1 Hz, 1H).

¹³C NMR (100 MHz, CDCl₃) δ 193.8, 166.9 (q, *J* = 2.9 Hz), 164.2, 135.2, 130.6 (2CH overlapping), 128.9, 128.7, 128.5, 128.1, 125.0 (q, *J* = 280.4 Hz), 114.0, 67.9, 55.6, 45.9 (q, *J* = 27.9 Hz), 34.9 (d, *J* = 1.4 Hz).

¹⁹F NMR (376 MHz, CDCl₃, proton decoupled) δ -67.51 (s, 3F).

HRMS (ESI pos): calculated for C₁₉H₁₇F₃NaO₄ (M+Na⁺): 389.0971, found: 389.0978.

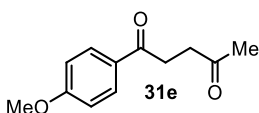


4-(4-Methoxyphenyl)-4-oxobutanal (31d): Synthesized according to the general procedure C using 4-methoxybenzoyl chloride (102 μL, 0.75 mmol, 1.5 equiv.) and acrolein (33 μL, 0.5 mmol, 1 equiv.). The crude mixture was purified by flash column chromatography on silica gel (20% AcOEt in hexanes as eluent), followed by a second purification (5:47:48 of Et₂O/DCM/hexanes as eluent) to afford **31d** (50 mg, 52% yield) as a yellow oil.

¹H NMR (400 MHz, CDCl₃) δ 9.89 (s, 1H), 7.99 – 7.91 (m, 2H), 6.96 – 6.89 (m, 2H), 3.85 (s, 3H), 3.27 (app t, *J* = 6.4 Hz, 2H), 2.89 (app t, *J* = 6.5 Hz, 2H).

¹³C NMR (100 MHz, CDCl₃) δ 201.0, 196.4, 163.7, 130.4, 129.6, 113.9, 55.6, 37.8, 30.8

Matching reported literature data.³²



1-(4-Methoxyphenyl)pentane-1,4-dione (31e): Synthesized according to the general procedure C using 4-methoxybenzoyl chloride (102 μL, 0.75 mmol, 1.5 equiv.) and methyl vinyl ketone (41 μL, 0.5 mmol, 1 equiv.). The crude mixture was purified by flash column chromatography on silica gel (20% AcOEt in hexanes as eluent), followed by a second one (10:45:45 of Et₂O/DCM/Hexanes as eluent) to afford **31e** (49 mg, 48% yield) white solid.

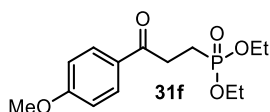
¹H NMR (400 MHz, CDCl₃) δ 7.98 – 7.91 (m, 2H), 6.95–6.89 (m, 2H), 3.85 (s, 3H), 3.25 – 3.18 (m, 2H), 2.88 – 2.82 (m, 2H), 2.24 (s, 3H).

³¹ Boucher, M. M.; Furigay, M. H.; Quach, P. K.; Brindle, C. S. "Liquid-Liquid Extraction Protocol for the Removal of Aldehydes and Highly Reactive Ketones from Mixtures" *Org. Process Res. Dev.* **2017**, *21*, 1394–1403.

³² Wang, J.; Huang, B.; Shi, C.; Yang, C.; Xia, W. "Visible-Light-Mediated Ring-Opening Strategy for the Regiospecific Allylation/Formylation of Cycloalkanols" *J. Org. Chem.* **2018**, *83*, 9696–9706.

$^{13}\text{C NMR}$ (100 MHz, CDCl_3) δ 207.6, 197.1, 164.6, 130.4, 129.9, 113.8, 55.6, 37.2, 32.2, 30.2.

Matching reported literature data.³⁰



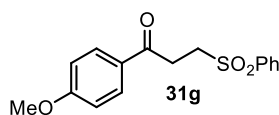
Diethyl

(3-(4-methoxyphenyl)-3-oxopropyl)phosphonate (31f): Synthesized according to the general procedure C using 4-methoxybenzoyl chloride (102 μL , 0.75 mmol, 1.5 equiv.) and diethyl vinylphosphonate (77 μL , 0.5 mmol, 1 equiv.). Irradiations time: 24 hours. The crude mixture was purified by flash column chromatography on silica gel (20% AcOEt in hexanes as eluent) to afford **31f** (81 mg, 54% yield) as a white solid.

$^1\text{H NMR}$ (400 MHz, CDCl_3) δ 7.91 (app d, $J = 8.8$ Hz, 2H), 6.89 (app d, $J = 8.9$ Hz, 2H), 4.20 – 3.96 (m, 4H), 3.82 (s, 3H), 3.28 – 3.12 (m, 2H), 2.22 – 2.04 (m, 2H), 1.28 (t, $J = 7.0$ Hz, 6H).

$^{13}\text{C NMR}$ (100 MHz, CDCl_3) δ 196.0 (d, $J = 16.2$ Hz), 163.7, 130.3, 129.4, 113.8, 61.7 (d, $J = 6.6$ Hz), 55.5, 31.3 (d, $J = 2.9$ Hz), 19.9 (d, $J = 144.3$ Hz), 6.5 (d, $J = 6.5$ Hz).

Matching reported literature data.³³



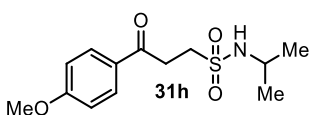
1-(4-Methoxyphenyl)-3-(phenylsulfonyl)propan-1-one (31g): Synthesized according to the general procedure C using 4-methoxybenzoyl chloride (102 μL , 0.75 mmol, 1.5 equiv.) and phenyl vinyl sulfone (84 mg, 0.5 mmol, 1 equiv.).

Reaction time: 24 hours. The crude mixture was purified by flash column chromatography on silica gel (25% AcOEt in hexanes as eluent), followed by a second one (20% AcOEt in hexanes as eluent) to afford **31g** (128 mg, 84% yield) as a white solid.

$^1\text{H NMR}$ (500 MHz, CDCl_3) δ 7.96 – 7.93 (m, 2H), 7.91 – 7.87 (m, 2H), 7.69 – 7.63 (m, 1H), 7.60 – 7.54 (m, 2H), 6.95 – 6.90 (m, 2H), 3.86 (s, 3H), 3.57 – 3.51 (m, 2H), 3.46 – 3.40 (m, 2H).

$^{13}\text{C NMR}$ (126 MHz, CDCl_3) δ 193.9, 164.1, 139.3, 134.0, 130.5, 129.5, 129.0, 128.1, 114.1, 55.7, 51.3, 31.0.

Matching reported literature data.³⁴



N-Isopropyl-3-(4-methoxyphenyl)-3-oxopropane-1-

sulfonamide (31h): Synthesized according to the general procedure C using 4-methoxybenzoyl chloride (102 μL , 0.75 mmol, 1.5 equiv.) and *N*-isopropylethanesulfonamide (75 mg, 0.5 mmol, 1 equiv.).

Reaction time: 24 hours. The

³³ Yu, J.-W.; Huang, S. K. "Synthesis of diethyl 3-aryl-3-oxopropylphosphonates" *Org. Prep. Proced. Int.* **1997**, *29*, 214-218.

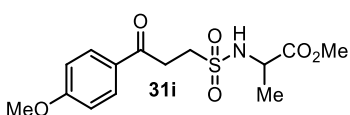
³⁴ Bhunia, A.; Yetra, S. R.; Bhojgude, S. S.; Biju, A. T. "Efficient Synthesis of γ -Keto Sulfones by NHC-Catalyzed Intermolecular Stetter Reaction" *Org. Lett.* **2012**, *14*, 2830-2833.

crude mixture was purified by flash column chromatography on silica gel (20% AcOEt in hexanes as eluent) to afford **31h** (98 mg, 69% yield) as a white solid.

¹H NMR (400 MHz, CDCl₃) δ 7.98 – 7.91 (m, 2H), 6.97 – 6.90 (m, 2H), 4.35 (bs, 1H, NH), 3.87 (s, 3H), 3.74 – 3.58 (m, 1H), 3.54 – 3.38 (m, 4H), 1.24 (d, *J* = 6.4 Hz, 6H).

¹³C NMR (100 MHz, CDCl₃) δ 194.7, 164.1, 130.6, 129.2, 114.1, 55.7, 48.7, 46.5, 32.7, 24.4.

HRMS (ESI neg): calculated for C₁₃H₁₈NO₄S (M⁻): 284.0962, found 284.0974.



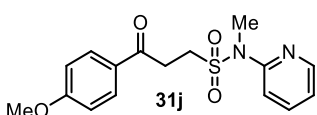
Methyl ((3-(4-methoxyphenyl)-3-oxopropyl)sulfonyl)alaninate (31i): Synthesized according to the general procedure C using 4-methoxybenzoyl chloride (102 μL, 0.75 mmol, 1.5 equiv.) and methyl (vinylsulfonyl)alaninate (97 mg, 0.5 mmol, 1 equiv.). Reaction time:

24 hours. The crude mixture was purified by flash column chromatography on silica gel (35% AcOEt in hexanes as eluent), followed by a second one (20:40:40 of AcOEt/DCM/Hexanes as eluent) to afford **31i** (83 mg, 50% yield) as a colorless oil.

¹H NMR (400 MHz, CDCl₃) δ 7.97 – 7.89 (m, 2H), 6.96 – 6.89 (m, 2H), 5.29 (d, *J* = 8.4 Hz, 2H), 4.25 – 4.14 (m, 1H), 3.85 (s, 3H), 3.73 (s, 3H), 3.53 – 3.40 (m, 4H), 1.45 (d, *J* = 7.15 Hz, 3H).

¹³C NMR (100 MHz, CDCl₃) δ 194.5, 173.2, 164.0, 130.5, 129.1, 114.0, 55.6, 52.9, 51.7, 48.4, 32.2, 19.9.

HRMS (ESI pos): calculated for C₁₄H₁₉NNaO₆S (M+Na⁺): 352.0825, found 352.0814.



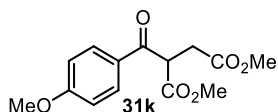
3-(4-Methoxyphenyl)-N-methyl-3-oxo-N-(pyridin-2-yl)propane-1-sulfonamide (31j): Synthesized according to the general procedure C using 4-methoxybenzoyl chloride (102 μL, 0.75 mmol, 1.5 equiv.) and *N*-methyl-*N*-(pyridin-2-yl)ethanesulfonamide (99 mg, 0.5 mmol, 1 equiv.).

Reaction time: 24 hours. The crude mixture was purified by flash column chromatography on silica gel (20:20:60 of AcOEt/DCM/Hexanes as eluent), followed by a second one (20:20:60 of Et₂O/DCM/Hexanes as eluent) to afford **31j** (75 mg, 45% yield) as a yellowish oil.

¹H NMR (400 MHz, CDCl₃) δ 8.41 – 8.34 (m, 1H), 7.92 – 7.84 (m, 2H), 7.72 – 7.65 (m, 1H), 7.42 (app d, *J* = 8.3 Hz, 1H), 7.15 – 7.08 (m, 1H), 6.95 – 6.87 (m, 2H), 3.85 (s, 3H), 3.72 – 3.64 (m, 2H), 3.45 (s, 3H), 3.46 – 3.39 (m, 2H).

¹³C NMR (100 MHz, CDCl₃) δ 194.2, 164.0, 154.0, 148.3, 138.2, 130.5, 129.1, 121.0, 118.6, 114.0, 55.6, 46.3, 35.9, 31.8.

HRMS (ESI pos): calculated for C₁₆H₁₉N₂O₄S (M+H⁺): 335.1060, found 335.1043.



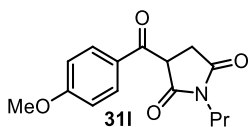
Dimethyl 2-(4-methoxybenzoyl)succinate (31k): Synthesized according to the general procedure C using 4-methoxybenzoyl chloride (102 μL, 0.75 mmol, 1.5 equiv.) and

dimethyl fumarate (72 mg, 0.5 mmol, 1 equiv.). The crude mixture was purified by flash column chromatography on silica gel (20% AcOEt in hexanes as eluent) to afford **31k** (122 mg, 87% yield) as a colorless oil.

¹H NMR (500 MHz, CDCl₃) δ 8.03 – 7.98 (m, 2H), 6.96 – 6.92 (m, 2H), 4.82 (t, *J* = 7.1 Hz, 1H), 3.85 (s, 3H), 3.66 (s, 3H), 3.65 (s, 3H), 3.09 – 2.97 (m, 2H).

¹³C NMR (126 MHz, CDCl₃) δ 192.3, 171.9, 169.5, 164.2, 131.4, 128.8, 114.0, 129.0, 128.1, 114.1, 55.6, 52.8, 52.1, 33.2.

Matching reported literature data.³⁵



3-(4-Methoxybenzoyl)-1-propylpyrrolidine-2,5-dione

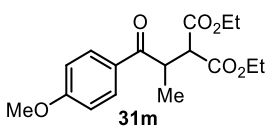
(31l): Synthesized according to the general procedure C using 4-methoxybenzoyl chloride (102 μL, 0.75 mmol, 1.5 equiv.) and 1-propyl-1H-pyrrole-2,5-dione (69.6 μL, 0.5 mmol, 1 equiv.).

Chromatography on silica gel (20% AcOEt in hexanes as eluent) could not remove byproduct completely. Therefore, a further purification by semipreparative HPLC (Column SunFire C18, 60:40 Methanol/Water 6 min, up to 100% Methanol 1 min, 100% Methanol 4 min, 1 mL/min) was performed to obtain an analytical amount of the isolated product as a white solid. NMR yield (Trichloroethylene was used as internal standard): 53%.

¹H NMR (500 MHz, CDCl₃) δ 8.12–8.07 (m, 2H), 7.02 – 6.97 (m, 2H), 4.78 (dd, *J* = 8.3, 3.9 Hz, 1H), 3.90 (s, 3H), 3.47 (t, *J* = 7.3 Hz, 2H), 3.37 (dd, *J* = 18.1, 3.8 Hz, 1H), 2.82 (dd, *J* = 18.1, 8.8 Hz, 1H), 1.64 – 1.54 (m, 2H, overlapping with water peak), 0.87 (t, *J* = 7.4 Hz, 3H).

¹³C NMR (126 MHz, CDCl₃) δ 190.9, 176.1, 173.4, 164.7, 132.4, 128.6, 114.2, 55.7, 48.2, 41.0, 31.8, 21.0, 11.3

HRMS (ESI pos): calculated for C₁₅H₁₇NNaO₄ (M+Na⁺): 298.1050, found 298.1056.



Diethyl 2-(1-(4-methoxyphenyl)-1-oxopropan-2-yl)malonate

(31m): Synthesized according to the general procedure C using 4-methoxybenzoyl chloride (102 μL, 0.75 mmol, 1.5 equiv.) and diethyl 2-ethylidenemalonate (93 μL, 0.5 mmol, 1 equiv.).

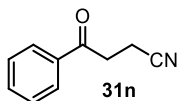
The crude mixture was purified by flash column chromatography on silica gel (10% AcOEt in hexanes as eluent) to afford **31m** (60 mg, 37% yield) as a colorless oil.

¹H NMR (400 MHz, CDCl₃) δ 8.03 – 7.96 (m, 2H), 6.98 – 6.93 (m, 2H), 4.31 – 4.21 (m, 2H), 4.20 – 4.02 (m, 3H), 3.97 (d, *J* = 10.8 Hz, 1H), 3.87 (s, 3H), 1.31 (t, *J* = 7.0 Hz, 3H), 1.19 (d, *J* = 7.0 Hz, 3H), 1.16 (t, *J* = 7.1 Hz, 3H).

¹³C NMR (100 MHz, CDCl₃) δ 200.2, 169.0, 168.5, 163.8, 131.0, 128.6, 114.0, 61.7, 55.6, 55.1, 40.3, 16.25, 14.3, 14.0.

³⁵ Bonassi, F.; Ravelli, D.; Protti, S.; Fagnoni, M. "Decatungstate Photocatalyzed Acylations and Alkylations in Flow via Hydrogen Atom Transfer" *Adv. Synth. Catal.* **2015**, *357*, 3687–3695.

HRMS (ESI pos): calculated for $C_{17}H_{22}NaO_6$ ($M+Na^+$): 345.1309, found 345.1306.

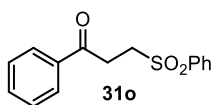


4-Oxo-4-phenylbutanenitrile (31n): Synthesized according to the general procedure C using benzoyl chloride (87 μ L, 0.75 mmol, 1.5 equiv.) and acrylonitrile (33 μ L, 0.5 mmol, 1 equiv.). The crude mixture was purified by flash column chromatography on silica gel (20% AcOEt in hexanes as eluent) to afford **31n** (65 mg, 82% yield) as a white solid.

1H NMR (500 MHz, $CDCl_3$) δ 7.98 – 7.93 (m, 2H), 7.64 – 7.59 (m, 1H), 7.53 – 7.47 (m, 2H), 3.41 – 3.35 (m, 2H), 2.80 – 2.75 (m, 2H).

^{13}C NMR (126 MHz, $CDCl_3$) δ 195.4, 135.7, 134.0, 129.0, 128.1, 119.3, 34.4, 11.9

Matching reported literature data.³⁰



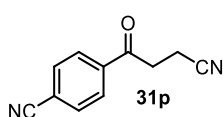
1-Phenyl-3-(phenylsulfonyl)propan-1-one (31o): Synthesized according to the general procedure C using benzoyl chloride (87 μ L, 0.75 mmol, 1.5 equiv.) and phenyl vinyl sulfone (84 mg, 0.5 mmol, 1 equiv.). The crude mixture was purified by flash column

chromatography on silica gel (20% AcOEt in hexanes as eluent) to afford **31o** (112 mg, 82% yield) as a white solid.

1H NMR (400 MHz, $CDCl_3$) δ 7.99 – 7.88 (m, 4H), 7.70 – 7.63 (m, 1H), 7.63 – 7.54 (m, 3H), 7.51 – 7.43 (m, 2H), 3.60 – 3.53 (m, 2H), 3.53 – 3.46 (m, 2H).

^{13}C NMR (100 MHz, $CDCl_3$) δ 195.5, 139.2, 135.9, 134.1, 133.9, 129.6, 128.9, 128.2, 128.1, 51.1, 31.5.

Matching reported literature data.³⁴



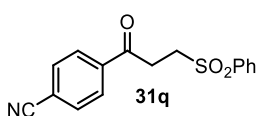
4-(3-Cyanopropanoyl)benzonitrile (31p): Synthesized according to the general procedure C using using 4-cyanobenzoyl chloride (124 mg, 0.75 mmol, 1.5 equiv.) and acrylonitrile (33 μ L, 0.5 mmol, 1 equiv.). In this case the reaction

was irradiated for 60 hours. The crude mixture was purified by flash column chromatography on silica gel (15% AcOEt in hexanes as eluent) to afford **31p** (92 mg, 45% yield) as a white solid.

1H NMR (500 MHz, $CDCl_3$) δ 8.04 (app d, $J = 8.2$ Hz, 2H), 7.80 (app d, $J = 8.2$ Hz, 2H), 3.39 (t, $J = 6.9$ Hz, 2H), 2.79 (t, $J = 7.0$ Hz, 2H).

^{13}C NMR (126 MHz, $CDCl_3$) δ 194.3, 138.5, 132.8, 128.6, 118.8, 117.7, 117.3, 34.7, 11.8.

Matching reported literature data.³⁰



4-(3-(Phenylsulfonyl)propanoyl)benzonitrile (31q): Synthesized according to the general procedure C using 4-cyanobenzoyl chloride (124 mg, 0.75 mmol, 1.5 equiv.) and phenyl vinyl sulfone (84 mg, 0.5 mmol, 1 equiv.). In this case

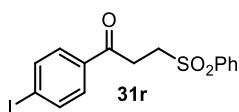
the reaction was irradiated for 60 hours. The crude mixture was purified by flash

column chromatography on silica gel (25% AcOEt in hexanes as eluent) to afford **31q** (79 mg, 53% yield) as a white solid.

¹H NMR (400 MHz, CDCl₃) δ 8.02 (app d, *J* = 8.5 Hz, 2H), 7.95 (app d, *J* = 7.3 Hz, 2H), 7.78 (app d, *J* = 8.4 Hz, 2H), 7.69 (app t, *J* = 7.4 Hz, 1H), 7.59 (app t, *J* = 7.7 Hz, 2H), 3.60 – 3.48 (m, 4H).

¹³C NMR (100 MHz, CDCl₃) δ 194.4, 139.1, 138.8, 134.2, 132.8, 129.6, 128.6, 128.1, 117.8, 117.2, 50.9, 31.8.

HRMS (ESI pos): calculated for C₁₆H₁₃NNaO₃S (M+Na⁺): 322.0508, found 322.0505.



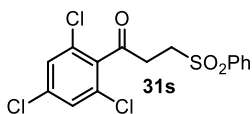
1-(4-Iodophenyl)-3-(phenylsulfonyl)propan-1-one (31r):

Synthesized according to the general procedure C using 4-iodobenzoyl chloride (200 mg, 0.75 mmol, 1.5 equiv.) and phenyl vinyl sulfone (84 mg, 0.5 mmol, 1 equiv.). In this case the reaction was irradiated for 60 hours. The crude mixture was purified by flash column chromatography on silica gel (20% AcOEt in hexanes as eluent) to afford **31r** (130 mg, 65% yield) as a white solid.

¹H NMR (500 MHz, CDCl₃) δ 7.99 – 7.92 (m, 2H), 7.87 – 7.82 (m, 2H), 7.70 – 7.65 (m, 1H), 7.65 – 7.61 (m, 2H), 7.61 – 7.56 (m, 2H), 3.58 – 3.51 (m, 2H), 3.49 – 3.42 (m, 2H).

¹³C NMR (126 MHz, CDCl₃) δ 194.9, 139.2, 138.3, 135.2, 134.1, 129.6, 129.5, 128.1, 102.1, 51.0, 31.4

HRMS (ESI pos): calculated for C₁₅H₁₃INaO₃S (M+Na⁺): 422.9522, found 422.9519.



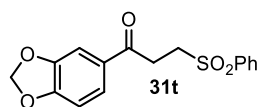
3-(Phenylsulfonyl)-1-(2,4,6-trichlorophenyl)propan-1-one (31s):

Synthesized according to the general procedure C using 2,4,6-trichlorobenzoyl chloride (183 mg, 0.75 mmol, 1.5 equiv.) and phenyl vinyl sulfone (84 mg, 0.5 mmol, 1 equiv.). In this case the reaction was irradiated for 60 hours. The crude mixture was purified by flash column chromatography on silica gel (25% AcOEt in hexanes as eluent) followed by a second one (5:25:70 of AcOEt/DCM/Hexanes as eluent) to afford **31s** (95 mg, 50% yield) as a white solid.

¹H NMR (400 MHz, CDCl₃) δ 7.98 – 7.92 (m, 2H), 7.72 – 7.65 (m, 1H), 7.63 – 7.56 (m, 2H), 7.36 (s, 2H), 3.58 – 3.50 (m, 2H), 3.33 – 3.25 (m, 2H).

¹³C NMR (100 MHz, CDCl₃) δ 197.2, 138.9, 137.0, 136.6, 134.2, 131.2, 129.6, 128.5, 128.1, 50.1, 36.5

HRMS (ESI pos): calculated for C₁₅H₁₁Cl₃NaO₃S (M+Na⁺): 398.9387, found 398.9390.



1-(Benzo[d][1,3]dioxol-5-yl)-3-(phenylsulfonyl)propan-1-one (31t):

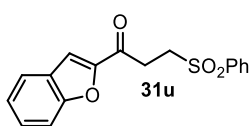
Synthesized according to the general procedure C using benzo[d][1,3]dioxole-5-carbonyl chloride (138 mg, 0.75 mmol, 1.5 equiv.) and phenyl vinyl sulfone (84 mg, 0.5 mmol, 1 equiv.). Reaction time: 24 hours. The crude mixture was purified by flash

column chromatography on silica gel (25% AcOEt in hexanes as eluent) to afford **31t** (90 mg, 57% yield) as a white solid.

$^1\text{H NMR}$ (500 MHz, CDCl_3) δ 7.96 – 7.92 (m, 2H), 7.67 (tt, J = 7.3, 1.8 Hz, 1H), 7.60 – 7.55 (m, 2H), 7.52 (dd, J = 8.1, 1.8 Hz, 1H), 7.36 (d, J = 1.7 Hz, 1H), 6.84 (d, J = 8.1 Hz, 1H), 6.04 (s, 2H), 3.57 – 3.50 (m, 2H), 3.44 – 3.37 (m, 2H).

$^{13}\text{C NMR}$ (126 MHz, CDCl_3) δ 193.5, 152.5, 148.5, 139.2, 134.0, 130.8, 129.5, 128.1, 124.7, 108.2, 107.8, 102.2, 51.3, 31.2.

HRMS (ESI pos): calculated for $\text{C}_{16}\text{H}_{14}\text{NaO}_5\text{S}$ ($\text{M}+\text{Na}^+$): 341.0454, found 341.0452.



1-(Benzofuran-2-yl)-3-(phenylsulfonyl)propan-1-one

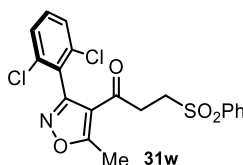
(31u): Synthesized according to the general procedure C using benzofuran-2-carbonyl chloride (135 mg, 0.75 mmol, 1.5 equiv.) and phenyl vinyl sulfone (84 mg, 0.5 mmol, 1 equiv.).

Reaction time: 24 hours. The crude mixture was purified by flash column chromatography on silica gel (25% AcOEt in hexanes as eluent) followed by a second one (20% AcOEt in hexanes as eluent) to afford **31u** (77 mg, 49% yield) as a yellowish solid.

$^1\text{H NMR}$ (500 MHz, CDCl_3) δ 7.99 – 7.94 (m, 2H), 7.71 (app d, J = 7.8 Hz, 1H), 7.70 – 7.65 (m, 1H), 7.61 – 7.55 (app t, J = 8.0 Hz, 3H), 7.55 (s, 1H), 7.53 – 7.48 (m, 1H), 7.35 – 7.30 (m, 1H), 3.61 – 3.55 (m, 2H), 3.53 – 3.47 (m, 2H).

$^{13}\text{C NMR}$ (126 MHz, CDCl_3) δ 186.6, 155.9, 151.6, 139.0, 134.2, 129.6, 128.9, 128.2, 126.9, 124.3, 123.6, 113.7, 112.6, 50.6, 31.8

HRMS (ESI pos): calculated for $\text{C}_{17}\text{H}_{14}\text{NaO}_4\text{S}$ ($\text{M}+\text{Na}^+$): 337.0505, found 337.0504.



1-(3-(2,6-Dichlorophenyl)-5-methylisoxazol-4-yl)-3-(phenylsulfonyl)propan-1-one

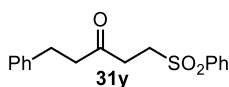
(31w): Synthesized according to the general procedure C using 3-(2,6-dichlorophenyl)-5-methylisoxazole-4-carbonyl chloride (218 mg, 0.75 mmol, 1.5 equiv.) and phenyl vinyl sulfone (84 mg,

0.5 mmol, 1 equiv.). Reaction time: 24 hours. The crude mixture was purified by flash column chromatography on silica gel (20% AcOEt in hexanes as eluent) to afford **31w** (75 mg, 35% yield) as a white solid.

$^1\text{H NMR}$ (400 MHz, CDCl_3) δ 7.75 – 7.67 (m, 2H), 7.67 – 7.60 (m, 1H), 7.57 – 7.43 (m, 5H), 3.41 – 3.34 (m, 2H), 2.74 (s, 3H), 3.68 – 3.60 (m, 2H).

$^{13}\text{C NMR}$ (126 MHz, CDCl_3) δ 189.0, 176.5, 157.2, 138.6, 135.6, 134.0, 132.2, 129.5, 128.6, 128.0, 127.9, 116.1, 50.1, 34.3, 14.2.

HRMS (ESI pos): calculated for $\text{C}_{19}\text{H}_{15}\text{Cl}_2\text{NNaO}_4\text{S}$ ($\text{M}+\text{Na}^+$): 445.9991, found 445.9992.



1-Phenyl-5-(phenylsulfonyl)pentan-3-one

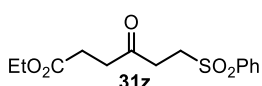
(31y): Synthesized according to the general procedure C using hydrocinnamoyl chloride (111 μL , 0.75 mmol, 1.5 equiv.) and

phenyl vinyl sulfone (84 mg, 0.5 mmol, 1 equiv.). In this case the reaction was irradiated for 60 hours. The crude mixture was purified by two rounds of flash column chromatography on silica gel (25% AcOEt in hexanes as eluent): to afford **31y** (113 mg, 75% yield) as a white solid.

$^1\text{H NMR}$ (400 MHz, CDCl_3) δ 7.92 – 7.87 (m, 2H), 7.71 – 7.63 (m, 1H), 7.61 – 7.53 (m, 2H), 7.31 – 7.23 (m, 2H), 7.22 – 7.16 (m, 1H), 7.16 – 7.10 (m, 2H), 3.42 – 3.33 (m, 2H), 2.92 – 2.82 (m, 4H), 2.81 – 2.72 (m, 2H).

$^{13}\text{C NMR}$ (100MHz, CDCl_3) δ 205.3, 140.5, 139.1, 134.1, 129.5, 128.7, 128.4, 128.1, 126.5, 50.6, 44.4, 35.3, 29.7.

Matching reported literature data.³⁶



Ethyl 4-oxo-6-(phenylsulfonyl)hexanoate (31z):

Synthesized according to the general procedure C using ethyl 4-chloro-4-oxobutanoate (107 μL , 0.75 mmol, 1.5 equiv.) and phenyl vinyl sulfone (84 mg, 0.5 mmol, 1 equiv.). Reaction time: 24 hours. The crude mixture was purified by flash column chromatography on silica gel (33% AcOEt in hexanes as eluent). Product was then dissolved in DCM, washed 3 times with a solution of CuSO_4 (5% in water), dried with MgSO_4 and evaporated under reduced pressure to afford **31z** (112 mg, 75% yield) as a white solid.

$^1\text{H NMR}$ (400 MHz, CDCl_3) δ 7.92 – 7.87 (m, 2H), 7.69 – 7.63 (m, 1H), 7.61 – 7.53 (m, 2H), 4.09 (q, $J = 7.1$ Hz, 2H), 3.42 – 3.35 (m, 2H), 2.98 – 2.91 (m, 2H), 2.75 – 2.69 (m, 2H), 2.59 – 2.52 (m, 2H), 1.22 (t, $J = 7.1$ Hz, 3H).

$^{13}\text{C NMR}$ (126 MHz, CDCl_3) δ 204.5, 172.5, 139.1, 134.1, 129.5, 128.1, 60.9, 50.6, 37.2, 35.3, 28.0, 14.2

HRMS (ESI pos): calculated for $\text{C}_{14}\text{H}_{18}\text{NaO}_5\text{S}$ ($\text{M}+\text{H}^+$): 321.0767, found 321.0765.

4.8.5 Reaction of aliphatic acyl chlorides

4.8.5.1 Experimental setup

Our 3D printed photoreactor consisted of a 9 cm diameter crystallizing dish with a 3D printed support of 6 positions, and a hole of 22 mm in the middle to allow ventilation. A commercial 1-meter LED strip was wrapped around the crystallizing dish. In order to control the temperature, a fan was used to cool down the reactor. Reaction temperature was measured, through a vial containing a thermometer, and it stayed between 35-40 $^\circ\text{C}$ (Figure 4.31). Each of the positions could be used to fit a standard 16 mm diameter vial with a Teflon screw cap.

³⁶ Ravelli, D.; Montanaro, S.; Zema, M.; Fagnoni, M.; Albini, A. "A Tin-Free, Radical Photocatalyzed Addition to Vinyl Sulfones" *Adv. Synth. Catal.* **2011**, *353*, 3295-3300.



Figure 4.31: Photoreactor used for the reactions of aliphatic acyl chlorides.

Experiments at 465 nm were conducted using a 1m strip, 14.4W “LEDXON MODULAR 9009083 LED, SINGLE 5050” purchased from Farnell, catalog number 9009083. The emission spectrum of these LEDs was recorded (Figure 4.32).

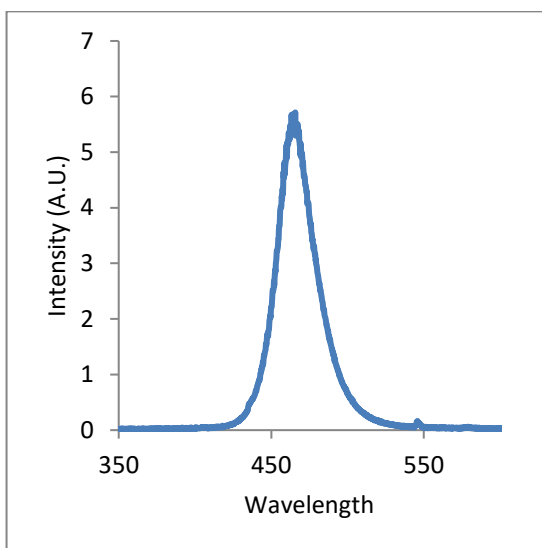
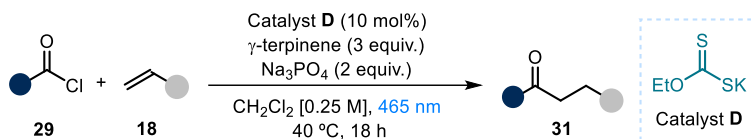


Figure 4.32: Emission spectrum of the 465 nm LED strip used in this study.

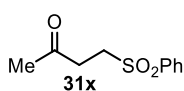
The emission maximum was determined as 465 nm with a spectral width of 30 nm (450-480 nm) at half peak intensity and a total spectral width of 120 nm (420-540 nm).

4.8.5.2 General Procedure D



In an oven dried tube of 15 mL (16 mm × 125 mm) with a Teflon septum screw cap, potassium ethyl xanthogenate **D** (8 mg, 0.05 mmol, 0.1 equiv.), sodium phosphate (164 mg, 1.00 mmol, 2 equiv.), acyl chloride **29** (0.75 mmol, 1.5 equiv.) and the electron-poor olefin **18** (0.5 mmol, 1 equiv., *if solid*), were dissolved in DCM (2 mL, HPLC grade). Then, γ -terpinene (240 μ L, 1.5 mmol, 3 equiv.) was added. The resulting yellow mixture was degassed with argon sparging for 60 seconds. When the electron-poor olefin **18** is *liquid*, it was added via syringe after the argon sparging. The vial was then placed in the 3D printed support photoreactor (Figure 4.31) and irradiated under stirring for 24 hours, if not otherwise specified. After this, the solvent was evaporated and the residue purified by column chromatography to afford the corresponding product in the stated yield with >95% purity according to ^1H NMR analysis.

C2.3 Characterization of Products

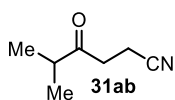


4-(Phenylsulfonyl)butan-2-one (31x): Synthesized according to the general procedure D using acetyl chloride (53 μ L, 0.75 mmol, 1.5 equiv.) and phenyl vinyl sulfone (84 mg, 0.5 mmol, 1 equiv.). The crude mixture was purified by flash column chromatography on silica gel (gradient from 25% to 100% AcOEt in hexanes as eluent): to afford product **31x** (70 mg 66% yield) as a colorless oil.

^1H NMR (400 MHz, CDCl_3) δ 7.94 – 7.86 (m, 2H), 7.70 – 7.62 (m, 1H), 7.61 – 7.53 (m, 2H), 3.40 – 3.33 (m, 2H), 2.96 – 2.88 (m, 2H), 2.17 (s, 3H).

^{13}C NMR (100 MHz, CDCl_3) δ 203.8, 139.1, 134.0, 129.6, 128.1, 50.6, 36.0, 30.0

Matching reported literature data.³⁷



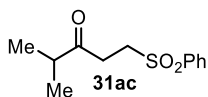
4-Cyclohexyl-4-oxobutanenitrile (31ab): Synthesized according to the general procedure D using isobutanoyl chloride (100 μ L, 0.75 mmol, 1.5 equiv.) and acrylonitrile (33 μ L, 0.5 mmol, 1 equiv.). The crude mixture was purified by flash column chromatography on silica gel (20% Et_2O in pentane as eluent) to afford **31ab** (39 mg, 62% yield) as a colorless oil.

^1H NMR (500 MHz, CDCl_3) δ 2.83 (t, J = 7.1 Hz, 2H), 2.66 – 2.56 (m, 1H), 2.57 (t, J = 7.2 Hz, 2H), 1.12 (d, J = 7.0 Hz, 6H).

^{13}C NMR (126 MHz, CDCl_3) δ 210.0, 119.2, 40.7, 35.6, 18.2, 11.6

³⁷ Capaldo, L.; Riccardi, R.; Ravelli, D.; Fagnoni, M. "Acyl Radicals from Acylsilanes: Photoredox-Catalyzed Synthesis of Unsymmetrical Ketones" *ACS Catal.* **2018**, *8*, 304-309.

Matching reported literature data.³⁸



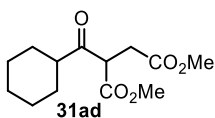
4-Methyl-1-(phenylsulfonyl)pentan-3-one (31ac): Synthesized according to the general procedure D using isobutanoyl chloride (100 μ L, 0.75 mmol, 1.5 equiv.) and phenyl vinyl sulfone (84 mg, 0.5 mmol, 1 equiv.). The crude mixture was purified by flash

column chromatography on silica gel (20% AcOEt in hexanes as eluent), followed by a second one (15% AcOEt in hexanes as eluent) to afford **31ac** (61 mg, 51% yield) as a colorless oil.

¹H NMR (500 MHz, CDCl₃) δ 7.94 – 7.88 (m, 2H), 7.69 – 7.64 (m, 1H), 7.61 – 7.54 (m, 2H), 3.40 – 3.35 (m, 2H), 3.00 – 2.93 (m, 2H), 2.66 – 2.55 (m, 1H), 1.08 (d, J = 7.0 Hz, 6H).

¹³C NMR (126 MHz, CDCl₃) δ 210.0, 139.2, 134.0, 129.5, 128.1, 50.8, 41.1, 32.7, 18.3.

HRMS (ESI pos): calculated for C₁₂H₁₆NaO₃S (M+Na⁺): 263.0712, found 263.0714.



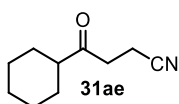
Dimethyl 2-(cyclohexanecarbonyl)succinate (31ad): Synthesized according to general procedure D using cyclohexanecarbonyl chloride (100 μ L, 0.75 mmol, 1.5 equiv.) and dimethyl fumarate (72 mg, 0.5 mmol, 1 equiv.). The crude mixture

was purified by flash column chromatography on silica gel (10% AcOEt in hexanes as eluent) to afford **31ad** (107 mg, 83% yield) as a white solid.

¹H NMR (500 MHz, CDCl₃) δ 4.14 (dd, J = 8.1, 6.2 Hz, 1H), 3.72 (s, 3H), 3.66 (s, 3H), 3.82 (s, 3H), 2.93 (dd, J = 17.5, 8.1 Hz, 1H), 2.81 (dd, J = 17.6, 6.5 Hz, 1H), 2.69 – 2.61 (m, 1H), 2.00 – 1.93 (m, 1H), 1.84 – 1.74 (m, 3H), 1.70 – 1.62 (m, 1H), 1.46 – 1.36 (m, 1H), 1.33 – 1.13 (m, 4H).

¹³C NMR (126 MHz, CDCl₃) δ 206.7, 171.9, 169.2, 52.8, 52.2, 52.1, 50.72, 32.4, 29.0, 28.1, 25.9, 25.8, 25.5.

Matching reported literature data.³⁹



4-Cyclohexyl-4-oxobutanenitrile (31ae): Synthesized according to the general procedure D using cyclohexanecarbonyl chloride (100 μ L, 0.75 mmol, 1.5 equiv.) and acrylonitrile (33 μ L, 0.5 mmol, 1 equiv.). The crude mixture was purified by flash column

chromatography on silica gel (20% Et₂O in pentane as eluent) to afford **31ae** (52 mg, 63% yield) as a colorless oil.

(For the gram scale procedure see paragraph C5, general procedure E)

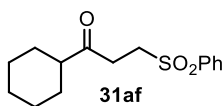
³⁸ Lee, W. Y.; Jang, S. Y.; Chae, W. K.; Park, O. S. "A Total Synthesis of Isosolanone" *Synth. Commun.* **1993**, *23*, 3037-3046.

³⁹ Cartier, A.; Levernier, E.; Corcé, V.; Fukuyama, T.; Dhimane, A.-L.; Ollivier, C.; Ryu, I.; Fensterbank, L. "Carbonylation of Alkyl Radicals Derived from Organosilicates through Visible-Light Photoredox Catalysis" *Angew. Chem. Int. Ed.* **2019**, *58*, 1789-1793.

¹H NMR (500 MHz, CDCl₃) δ 2.85-2.80 (m, 2H); 2.60-2.54 (m, 2H); 2.36 (tt, *J* = 11.3, 3.5 Hz, 1H); 1.89-1.82 (m, 2H); 1.82-1.75 (m, 2H); 1.71-1.64 (m, 1H); 1.40-1.15 (m, 5H).

¹³C NMR (126 MHz, CDCl₃) δ 209.4, 119.3, 50.6, 35.9, 28.5, 25.8, 25.6, 11.6.

Matching reported literature data.³⁹



1-Cyclohexyl-3-(phenylsulfonyl)propan-1-one (31af):

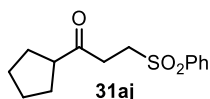
Synthesized according to the general procedure D using cyclohexanecarbonyl chloride (100 μL, 0.75 mmol, 1.5 equiv.) and phenyl vinyl sulfone (84 mg, 0.5 mmol, 1 equiv.). The crude mixture was purified by flash column chromatography on silica gel (20% AcOEt in hexanes as eluent) to afford **31af** (112 mg, 76% yield) as colorless oil.

A purity of 85% weight was determined ¹H NMR analysis (mixture with phenyl vinyl sulfone, see Figure below). Corrected yield: 68%.

¹H NMR (400 MHz, CDCl₃) δ 7.93 – 7.86 (m, 2H), 7.69 – 7.62 (m, 1H), 7.62 – 7.50 (m, 2H), 3.39 – 3.32 (m, 2H), 2.97 – 2.89 (m, 2H), 2.39 – 2.25 (m, 1H), 1.88 – 1.58 (m, 5H), 1.38 – 1.08 (m, 5H).

¹³C NMR (100 MHz, CDCl₃) δ 193.9, 164.2, 130.4, 128.8, 119.5, 114.1, 55.7, 34.0, 12.0.

Matching reported literature data.⁴⁰



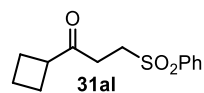
1-Cyclopentyl-3-(phenylsulfonyl)propan-1-one (31aj):

Synthesized according to the general procedure D using cyclopentanecarbonyl chloride (91 μL, 0.75 mmol, 1.5 equiv.) and phenyl vinyl sulfone (84 mg, 0.5 mmol, 1 equiv.). The crude mixture was purified by flash column chromatography on silica gel (20% AcOEt in hexanes as eluent) to afford **31aj** (102 mg, 77% yield) colorless oil.

¹H NMR (500 MHz, CDCl₃) δ 7.93 – 7.87 (m, 2H), 7.69 – 7.62 (m, 1H), 7.60 – 7.53 (m, 2H), 3.42 – 3.34 (m, 2H), 2.99 – 2.91 (m, 2H), 2.90 – 2.79 (m, 1H), 1.88 – 1.73 (m, 2H), 1.73 – 1.49 (m, 6H).

¹³C NMR (126 MHz, CDCl₃) δ 208.5, 139.2, 134.0, 129.5, 128.1, 51.5, 50.8, 34.0, 29.0, 26.0.

HRMS (ESI pos): calculated for C₁₄H₁₈NaO₃S (M+Na⁺): 289.0869, found 289.0873.



1-Cyclobutyl-3-(phenylsulfonyl)propan-1-one (31al):

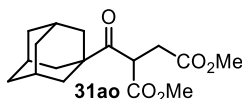
Synthesized according to the general procedure D using cyclobutanecarbonyl chloride (86 μL, 0.75 mmol, 1.5 equiv.) and phenyl vinyl sulfone (84 mg, 0.5 mmol, 1 equiv.). The crude mixture was purified by flash column chromatography on silica gel (20% AcOEt in hexanes as eluent) to afford **31al** (116 mg, 92% yield) as a colorless oil.

⁴⁰ Vu, M. D.; Das, M.; Liu, X.-W. "Direct Aldehyde Csp²-H Functionalization through Visible-Light-Mediated Photoredox Catalysis" *Chem. Eur. J.* **2017**, *23*, 15899-15902.

$^1\text{H NMR}$ (500 MHz, CDCl_3) δ 7.92 – 7.88 (m, 2H), 7.68 – 7.63 (m, 1H), 7.60 – 7.54 (m, 2H), 3.40 – 3.35 (m, 2H), 3.29 – 3.20 (m, 1H), 2.87 – 2.81 (m, 2H), 2.24 – 2.08 (m, 4H), 2.02 – 1.90 (m, 1H), 1.84 – 1.75 (m, 1H).

$^{13}\text{C NMR}$ (126 MHz, CDCl_3) δ 207.1, 139.2, 134.1, 129.5, 128.1, 50.6, 45.4, 32.3, 24.5, 17.9

HRMS (ESI pos): calculated for $\text{C}_{13}\text{H}_{15}\text{NaO}_6$ ($\text{M}+\text{Na}^+$): 275.0712, found 275.0716.

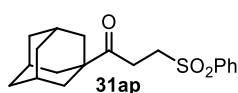


Dimethyl 2-((3r,5r,7r)-adamantane-1-carbonyl)succinate (31ao): Synthesized according to the general procedure D using 1-adamantanecarbonyl chloride (149 mg, 0.75 mmol, 1.5 equiv.) and dimethyl fumarate (72 mg, 0.5 mmol, 1 equiv.). The crude mixture was purified by flash column chromatography on silica gel (5% AcOEt in hexanes as eluent) to afford **31ao** (85 mg, 55% yield) as a colorless oil.

$^1\text{H NMR}$ (500 MHz, CDCl_3) δ 4.37 (app t, $J = 7.2$ Hz, 1H), 3.67 (s, 3H), 3.64 (s, 3H), 2.79 (app d, $J = 7.2$ Hz, 2H), 2.03 (bs, 3H), 1.89 – 1.79 (m, 6H), 1.76 – 1.63 (m, 6H).

$^{13}\text{C NMR}$ (126 MHz, CDCl_3) δ 208.8, 171.7, 169.5, 52.7, 52.1, 47.7, 47.4, 38.0, 36.4, 33.5, 27.9

HRMS (ESI pos): calculated for $\text{C}_{17}\text{H}_{24}\text{NaO}_5$ ($\text{M}+\text{Na}^+$): 331.1516, found 331.1523.



1-((3r,5r,7r)-Adamantan-1-yl)-3-(phenylsulfonyl)propan-1-one (31ap): Synthesized according to the general procedure D using 1-adamantanecarbonyl chloride (149 mg, 0.75 mmol, 1.5 equiv.) and phenyl vinyl sulfone (84 mg, 0.5 mmol, 1 equiv.). The crude mixture was purified by flash column chromatography on silica gel (15% AcOEt in hexanes as eluent) to afford **31ap** (165 mg, 95% yield) as a colorless oil.

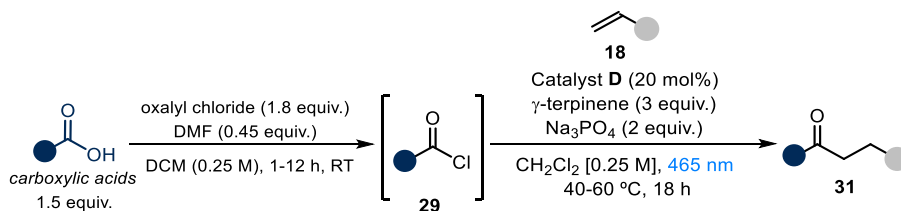
$^1\text{H NMR}$ (500 MHz, CDCl_3) δ 7.93 – 7.88 (m, 2H), 7.68 – 7.63 (m, 1H), 7.60 – 7.54 (m, 2H), 3.37 – 3.29 (m, 2H), 3.00–2.93 (m, 2H), 2.03 (bs, 3H), 1.79 – 1.70 (m, 9H), 1.66 (app d, $J = 12.2$ Hz, 3H).

$^{13}\text{C NMR}$ (126 MHz, CDCl_3) δ 211.2, 139.3, 133.9, 129.4, 128.0, 50.9, 46.5, 38.3, 36.5, 29.1, 27.9.

HRMS (ESI pos): calculated for $\text{C}_{19}\text{H}_{25}\text{O}_3\text{S}$ ($\text{M}+\text{H}^+$): 333.1519, found 333.1519.

4.8.6 Reaction of carboxylic acids through acyl chloride formation

4.8.6.1 General Procedure E

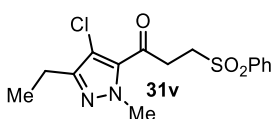


In a round bottom flask, the carboxylic acid (0.75 mmol, 1.5 equiv) was dissolved in DCM (3 mL, HPLC grade). Then, oxalyl chloride (0.79 μL , 0.90 mmol, 1.8 equiv.) and

DMF (17 μ L, 0.22 mmol, 0.45 equiv.) were added at ambient temperature. The reaction was stirred at ambient temperature until complete consumption of the carboxylic acid was observed by TLC. After that, the solvent was evaporated to dryness under vacuum at ambient temperature to obtain the crude acyl chloride, which was used without further purification in the next step.

In an oven dried vial, with a Teflon septum screw cap, potassium ethyl xanthogenate **D** (16 mg, 0.10 mmol, 0.2 equiv.), sodium phosphate (164 mg, 1.00 mmol, 2 equiv.), and the electron-poor olefin **18** (0.5 mmol, 1 equiv.), were added. The crude acyl chloride was dissolved in DCM (2 mL, HPLC grade) and the solution was added to the vial, followed by γ -terpinene (240 μ L, 1.5 mmol, 3 equiv.). The resulting yellow mixture was degassed via argon sparging for 60 seconds. If the electron-poor olefin **18** was *liquid*, it was added via syringe after the argon sparging. The vial was then placed in the correspondent reactor (depending on the temperature used for the reaction) and irradiated for 24 hours. The solvent was evaporated and the residue purified by column chromatography to afford the corresponding product in the stated yield with >95% purity according to ^1H NMR analysis.

Characterization of Products

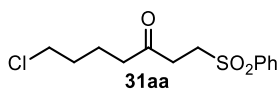


1-(4-Chloro-3-ethyl-1-methyl-1H-pyrazol-5-yl)-3-(phenylsulfonyl)propan-1-one (31v): Synthesized according to the general procedure E using 4-chloro-3-ethyl-1-methyl-1H-pyrazole-5-carboxylic acid (141 mg, 0.75 mmol, 1.5 equiv.) and phenyl vinyl sulfone (84 mg, 0.5 mmol, 1 equiv.). Acyl chloride formation was complete after 2 hours. The crude mixture was purified by flash column chromatography on silica gel (20% AcOEt in hexanes as eluent) to afford **31v** (52 mg, 31% yield) as a white solid.

^1H NMR (500 MHz, CDCl_3) δ 7.98 – 7.92 (m, 2H), 7.71 – 7.64 (m, 1H), 7.62 – 7.54 (m, 2H), 3.98 (s, 3H), 3.57 – 3.51 (m, 2H), 3.49 – 3.42 (m, 2H), 2.63 (q, J = 7.6, 2H), 1.23 (t, J = 7.5, 2H).

^{13}C NMR (126 MHz, CDCl_3) δ 186.6, 150.4, 139.0, 134.6, 134.1, 129.5, 128.3, 112.7, 50.6, 41.6, 35.5, 19.2, 12.9.

HRMS (ESI pos): calculated for $\text{C}_{15}\text{H}_{18}\text{ClN}_2\text{O}_3\text{S}$ ($\text{M}+\text{H}^+$): 341.0721, found 341.0709.

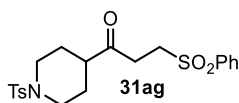


7-chloro-1-(phenylsulfonyl)heptan-3-one (31aa): Synthesized according to the general procedure E using 5-chloropentanoic acid (72 μ L, 0.75 mmol, 1.5 equiv.) and dimethyl fumarate (72 mg, 0.5 mmol, 1 equiv.). Acyl chloride formation was complete after 3 hours. The crude mixture was purified by flash column chromatography on silica gel (20% AcOEt in hexanes as eluent). The product was then dissolved in DCM, washed 3 times with a solution of CuSO_4 (5% in water), dried with MgSO_4 and evaporated under reduced pressure to afford **31aa** (108 mg, 70% yield) as a white solid.

¹H NMR (400 MHz, CDCl₃) δ 7.92 – 7.87 (m, 2H), 7.69 – 7.63 (m, 1H), 7.60 – 7.54 (m, 2H), 3.53 – 3.47 (m, 2H), 3.41 – 3.35 (m, 2H), 2.92 – 2.86 (m, 2H), 2.50 – 2.44 (m, 2H), 1.78 – 1.64 (m, 4H).

¹³C NMR (100 MHz, CDCl₃) δ 205.5, 139.1, 134.1, 129.5, 128.1, 50.6, 44.6, 41.9, 35.0, 31.8, 20.9.

HRMS (ESI pos): calculated for C₁₃H₁₇ClNaO₃S (M+Na⁺): 311.0479, found 311.0477.



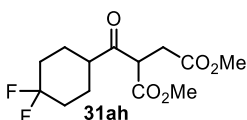
3-(Phenylsulfonyl)-1-(1-tosylpiperidin-4-yl)propan-1-one

(31ag): Synthesized according to the general procedure E using 1-tosylpiperidine-4-carboxylic acid (213 mg, 0.75 mmol, 1.5 equiv.) and dimethyl fumarate (72 mg, 0.5 mmol, 1 equiv.). Acyl chloride formation was complete after 3 hours. In this case the reaction was irradiated for 36 hours. The crude mixture was purified by flash column chromatography on silica gel (40% AcOEt in hexanes as eluent) to afford **31ag** (164 mg, 75% yield) as a white solid.

¹H NMR (500 MHz, CDCl₃) δ 7.90 – 7.85 (m, 2H), 7.69 – 7.64 (m, 1H), 7.64 – 7.60 (m, 2H), 7.60 – 7.54 (m, 2H), 7.32 (app d, *J* = 7.9 Hz, 2H), 3.71 (dt, *J* = 12.2, 3.5 Hz, 2H), 3.35 (app t, *J* = 7.4 Hz, 2H), 2.91 (app t, *J* = 7.4 Hz, 2H), 2.43 (s, 3H), 2.38 (td, *J* = 11.7, 2.5 Hz, 2H), 2.33 – 2.24 (m, 1H), 1.93 – 1.84 (m, 2H), 1.75 – 1.63 (m, 2H).

¹³C NMR (126 MHz, CDCl₃) δ 206.9, 143.8, 139.1, 134.2, 133.2, 129.9, 129.6, 128.0, 127.8, 50.6, 47.6, 45.5, 33.0, 27.0, 21.7.

HRMS (ESI pos): calculated for C₂₁H₂₆NO₅S₂ (M+H⁺): 436.1247, found 436.1251.



dimethyl 2-(4,4-difluorocyclohexane-1-carbonyl)succinate

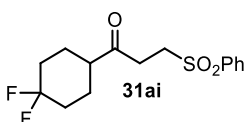
(31ah): Synthesized according to the general procedure E using 4,4-difluorocyclohexane-1-carboxylic acid (123 mg, 0.75 mmol, 1.5 equiv.) and dimethyl fumarate (72 mg, 0.5 mmol, 1 equiv.). Acyl chloride formation was complete after 1 hour. The crude mixture was purified by flash column chromatography on silica gel (20% Et₂O in hexanes as eluent) to afford **31ah** (128 mg, 88% yield) as a white solid.

¹H NMR (400 MHz, CDCl₃) δ 4.16 (dd, *J* = 9.1, 5.3 Hz, 1H), 3.73 (s, 3H), 3.67 (s, 3H), 3.03 (dd, *J* = 17.6, 9.3 Hz, 1H), 2.82 (dd, *J* = 17.5, 5.3 Hz, 1H), 2.83 – 2.74 (m, 1H), 2.22 – 2.02 (m, 3H), 1.98 – 1.65 (m, 5H).

¹³C NMR (100 MHz, CDCl₃) δ 205.6, 171.9, 168.8, 122.7 (dd, *J* = 241.6, 240.9 Hz), 53.0, 52.2, 52.1, 48.0, 32.7 (dd, *J* = 25.0 Hz), 25.2 (d, *J* = 9.0 Hz), 24.4 (d, *J* = 8.6 Hz)

¹⁹F NMR (376 MHz, CDCl₃, proton decoupled) δ -93.75 (d, *J* = 237.2 Hz, 1F); -100.48 (d, *J* = 238.2 Hz, 1F).

HRMS (ESI pos): calculated for C₁₃H₁₈F₂NaO₅ (M+Na⁺): 315.1015, found 315.1017.



1-(4,4-Difluorocyclohexyl)-3-(phenylsulfonyl)propan-1-one

(31ai): Synthesized according to the general procedure E using 4,4-difluorocyclohexane-1-carboxylic acid (123 mg, 0.75

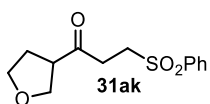
mmol, 1.5 equiv.) and dimethyl fumarate (72 mg, 0.5 mmol, 1 equiv.). Acyl chloride formation was complete after 1 hour. The crude mixture was purified by flash column chromatography on silica gel (30% AcOEt in hexanes as eluent) to afford **31ai** (112 mg, 71% yield) as a white solid.

$^1\text{H NMR}$ (400 MHz, CDCl_3) δ 7.93 – 7.88 (m, 2H), 7.70 – 7.64 (m, 1H), 7.61 – 7.55 (m, 2H), 3.41 – 3.35 (m, 2H), 3.01 – 2.94 (m, 2H), 2.52 – 2.39 (m, 1H), 2.18 – 2.04 (m, 2H), 1.99 – 1.86 (m, 2H), 1.85 – 1.64 (m, 4H).

$^{13}\text{C NMR}$ (100 MHz, CDCl_3) δ 207.4, 139.2, 134.1, 129.6, 128.0, 122.5 (dd, $J = 241.6, 240.7$ Hz) 50.6, 48.1, 33.2, 32.7 (dd, $J = 24.4, 24.2$ Hz), 24.7 (d, $J = 9.5$ Hz).

$^{19}\text{F NMR}$ (376 MHz, CDCl_3 , proton decoupled) δ -93.72 (dd, $J = 237.6$ Hz); -100.82 (d, $J = 237.7$ Hz).

HRMS (ESI pos): calculated for $\text{C}_{15}\text{H}_{18}\text{F}_2\text{NaO}_3\text{S}$ ($\text{M}+\text{Na}^+$): 339.0837, found 339.0840.



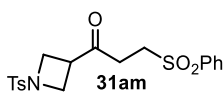
3-(Phenylsulfonyl)-1-(tetrahydrofuran-3-yl)propan-1-one (31ak): Synthesized according to the general procedure E using tetrahydrofuran-3-carboxylic acid (72 μL , 0.75 mmol, 1.5 equiv.) and dimethyl fumarate (72 mg, 0.5 mmol, 1 equiv.). Acyl chloride

formation was complete after 1 hour. The crude mixture was purified by flash column chromatography on silica gel (50% AcOEt in hexanes as eluent). The product was then dissolved in DCM, washed 3 times with a solution of CuSO_4 (5% in water), dried with MgSO_4 and evaporated under reduced pressure to afford **31ak** (78 mg, 58% yield) as a colorless oil.

$^1\text{H NMR}$ (500 MHz, CDCl_3) δ 7.94 – 7.87 (m, 2H), 7.71 – 7.64 (m, 1H), 7.62 – 7.54 (m, 2H), 3.94 – 3.73 (m, 4H), 3.47 – 3.34 (m, 2H), 3.26 – 3.17 (m, 1H), 3.07 – 2.89 (m, 2H), 3.16 – 2.01 (m, 2H).

$^{13}\text{C NMR}$ (126 MHz, CDCl_3) δ 205.6, 139.1, 134.1, 129.6, 128.1, 69.3, 68.4, 51.1, 50.6, 34.4, 29.1.

HRMS (ESI pos): calculated for $\text{C}_{13}\text{H}_{16}\text{NaO}_4\text{S}$ ($\text{M}+\text{Na}^+$): 291.0662, found 291.0665.



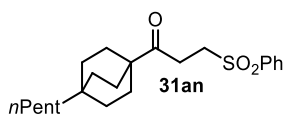
3-(Phenylsulfonyl)-1-(1-tosylazetididin-3-yl)propan-1-one (31am): Synthesized according to the general procedure E using 1-tosylazetididine-3-carboxylic acid (191 mg, 0.75 mmol, 1.5 equiv.)

and dimethyl fumarate (72 mg, 0.5 mmol, 1 equiv.). Acyl chloride formation was complete after 2 hours. In this case the reaction was irradiated for 36 hours. The crude mixture was purified by flash column chromatography on silica gel (40% AcOEt in hexanes as eluent) to afford **31am** (63 mg, 31% yield) as a white solid.

$^1\text{H NMR}$ (400 MHz, CDCl_3) δ 7.88 – 7.82 (m, 2H), 7.74 – 7.63 (m, 3H), 7.60 – 7.53 (m, 2H), 7.40 – 7.33 (m, 2H), 3.92 – 3.88 (m, 2H), 3.88 – 3.81 (m, 2H), 3.41 – 3.28 (m, 3H), 2.79 (app t, $J = 7.3$ Hz, 2H), 2.44 (s, 3H).

$^{13}\text{C NMR}$ (100 MHz, CDCl_3) δ 202.1, 144.6, 138.9, 134.2, 131.3, 130.0, 129.6, 128.5, 128.0, 51.8, 50.3, 38.1, 33.1, 21.7.

HRMS (ESI pos): calculated for $\text{C}_{19}\text{H}_{21}\text{NNaO}_5\text{S}_2$ ($\text{M}+\text{Na}^+$): 430.0753, found 430.0748.



1-(4-Pentylbicyclo[2.2.2]octan-1-yl)-3-(phenylsulfonyl)propan-1-one (31an): Synthesized according to the general procedure E using 4-pentylbicyclo[2.2.2]octane-1-carboxylic acid (168 mg, 0.75 mmol, 1.5 equiv.) and phenyl vinyl sulfone (84 mg, 0.5 mmol, 1 equiv.). Acyl chloride formation was complete after 2 hours. Chromatography on silica gel (10% AcOEt in hexanes as eluent) could not remove byproducts completely. Purification by semipreparative HPLC (IC column, 60:40 Hexane/Ethanol, 1 mL/min) was performed to obtain an analytical amount of product **31an** as a white solid. NMR yield (Trichloroethylene was used as internal standard): 80%.

¹H NMR (500 MHz, CDCl₃) δ 7.93 – 7.87 (m, 2H), 7.69 – 7.63 (m, 1H), 7.61 – 7.54 (m, 2H), 3.36 – 3.29 (m, 2H), 2.97 – 2.90 (m, 2H), 1.69 – 1.61 (m, 6H), 1.43 – 1.34 (m, 6H), 1.31 – 1.24 (m, 2H), 1.24 – 1.12 (m, 4H), 1.11 – 1.04 (m, 2H), 0.87 (t, *J* = 7.3 Hz, 3H).

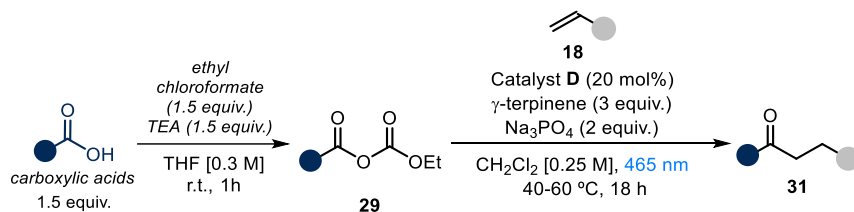
¹³C NMR (126 MHz, CDCl₃) δ 211.6, 139.4, 134.0, 129.5, 128.1, 51.0, 45.3, 41.3, 32.9, 30.8, 30.5, 30.1, 28.2, 23.5, 22.8, 14.2.

HRMS (ESI pos): calculated for C₂₂H₃₂NaO₃S (M+Na⁺): 399.1964, found 399.1951.

HRMS (ESI pos): calculated for C₂₂H₃₂NaO₃S (M+Na⁺): 399.1964, found 399.1951.

4.8.7 Reaction of carboxylic acids through anhydride formation

4.8.7.1 General Procedure F

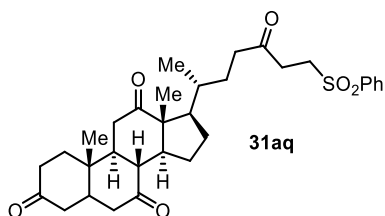


In a round bottom flask or vial, the carboxylic acid (0.75 mmol, 1.5 equiv.) was dissolved in THF (10 mL, HPLC grade). Then, triethylamine (105 μ L, 0.75 mmol, 1.5 equiv.) and ethyl chloroformate (72 μ L, 0.75 mmol, 1.5 equiv.) were added at ambient temperature. The reaction was stirred for 1 hour. The reaction crude was washed with water and NaHCO₃ saturated solution, dried over MgSO₄, filtered and the organic layers concentrated to dryness under vacuum. The crude carbonate was used without further purification in the next step.

In an oven dried tube of 15 mL (16 mm \times 12.5 mm) or a vial, with a Teflon septum screw cap, potassium ethyl xanthogenate (16.02 mg, 0.10 mmol, 0.2 equiv.) and the electron-poor olefin **2** (0.5 mmol, 1 equiv. *if solid*), were added. The crude carbonate was dissolved in DCM (2 mL, HPLC grade) and the solution was added to the vial, followed by γ -terpinene (240 μ L, 1.5 mmol, 3 equiv.). The resulting yellow mixture was degassed with argon sparging for 60 seconds. If the electron-poor olefin **2** was *liquid*, it was added via syringe after the argon sparging. The vial was then placed in the correspondent photoreactor (depending on the temperature used for the reaction) and irradiated for 24 hours. After cooling to ambient temperature, the solvent was

evaporated and the residue purified by column chromatography to afford the corresponding product in the stated yield with >95% purity according to ^1H NMR analysis.

Characterization of Products



(8R,9S,10S,13R,14S,17R)-10,13-dimethyl-17-((R)-5-oxo-7-(phenylsulfonyl)heptan-2-yl)dodecahydro-3H-cyclopenta[a]phenanthrene-3,7,12(2H,4H)-trione (31aq): Synthesized according to the general procedure F using dehydrocholic acid (302 μL , 0.75 mmol, 1.5 equiv.) and phenyl vinyl sulfone

(84 mg, 0.5 mmol, 1 equiv.). The crude mixture was purified by flash column chromatography on silica gel (33% acetone in hexanes as eluent), followed by a second purification (20% AcOEt in DCM as eluent) to afford **31aq** (145 mg, 52% yield) as a colorless oil.

^1H NMR (500 MHz, CDCl_3) δ 7.93 – 7.88 (m, 2H), 7.70 – 7.64 (m, 1H), 7.61 – 7.55 (m, 2H), 3.44 – 3.32 (m, 2H), 2.95 – 2.79 (m, 5H), 2.54 – 2.44 (m, 1H), 2.44 – 2.10 (m, 9H), 2.07 – 1.90 (m, 4H), 1.89 – 1.80 (m, 1H), 1.80 – 1.70 (m, 1H), 1.67 – 1.56 (m, 1H), 1.39 (s, 3H), 1.36 – 1.20 (m, 4H), 1.05 (s, 3H), 0.81 (d, $J = 6.5$ Hz, 3H).

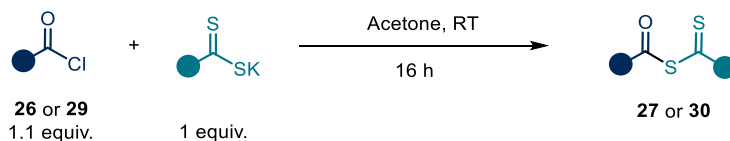
^{13}C NMR (126 MHz, CDCl_3) δ 212.0, 209.1, 208.8, 206.5, 139.2, 134.1, 129.6, 128.1, 57.0, 51.9, 50.6, 49.1, 47.0, 45.7, 45.7, 45.1, 42.9, 40.0, 38.8, 36.6, 36.1, 35.4, 35.4, 35.1, 29.1, 27.8, 25.2, 22.0, 18.9, 12.0.

HRMS (ESI pos): calculated for $\text{C}_{32}\text{H}_{42}\text{NaO}_6\text{S}$ ($\text{M}+\text{Na}^+$): 577.2594, found 577.2607.

4.8.8 Mechanistic studies

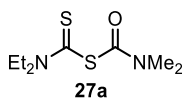
4.8.8.1 Characterisation of acylxanthate and carbamoyldithiocarbamate intermediates:

General procedure for the synthesis of acyl xanthate intermediates (general procedure G)



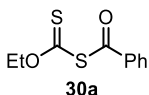
In a round bottom flask, carbamoyl chloride **26** or acyl chloride **29** (1.1 equiv.) was dissolved in acetone (0.1 M) and cooled to 0 $^\circ\text{C}$. The dithiocarbamate anion or the xanthate salt **C** or **D** (1 equiv.) was then added and the resulting reaction mixture was stirred for 1 hour at 0 $^\circ\text{C}$. The solvent was removed under reduced pressure at ambient temperature. The residue was then dissolved in DCM and washed with distilled water, NaHCO_3 solution and brine. The combined organic fractions were dried over MgSO_4 and concentrated to dryness to obtain the desired product.

Characterization of the Intermediates



N-Diethyl, N'-Dimethyl-Thiodicarbamic diamide (27a).

Prepared according to the general procedure G using potassium diethylcarbamodithioate trihydrate **C** (3 mmol, 724 mg) and dimethylcarbonyl chloride (1.1 mmol, 128 μ L) in 10 mL of acetone. After work-up and chromatography on silica gel (8:2 hexane/AcOEt), the product **27a** was obtained as a yellow oil (177 mg, 80% yield).



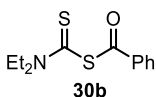
Benzoic (O-ethyl carbonothioic) thioanhydride (30a).

Prepared according to the general procedure G using potassium ethyl xanthogenate **D** (1 mmol, 160 mg) and benzoyl chloride (1.1 mmol, 128 μ L) in 10 mL of acetone. After work-up, the product **30a** (226 mg, 99% yield) was obtained as a yellow oil.

$^1\text{H NMR}$ (300 MHz, CDCl_3) δ 7.87 (app d, $J = 7.7$ Hz, 2 H); 7.64-7.54 (m, 1H); 7.49-7.39 (m, 2H); 4.69 (q, $J = 7.1$ Hz, 2H); 1.45 (t, $J = 7.1$ Hz, 3H).

$^{13}\text{C NMR}$ (75 MHz, CDCl_3) δ 203.4, 185.0, 135.7, 134.4, 129.0, 127.9, 71.1, 13.5.

Matching reported literature data.⁴¹

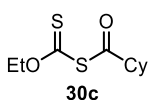


Benzoic diethylcarbamothioic thioanhydride (30b).

Prepared according to the general procedure G using sodium diethylcarbamodithioate trihydrate **C** (1.05 mmol, 237 mg) and benzoyl chloride (1 mmol, 116 μ L) in 10 mL of acetone. After work-up, the product **30b** was obtained as a yellow oil (220 mg, 87% yield).

$^1\text{H NMR}$ (300 MHz, CDCl_3) δ 7.95-7.88 (m, 2 H); 7.64-7.56 (m, 1H); 7.52-7.42 (m, 2H); 4.07-3.86 (m, 2H); 1.36 (t, $J = 7.1$ Hz, 3H).

Matching reported literature data.⁴²



cyclohexanecarboxylic (O-ethyl carbonothioic) thioanhydride (30c).

Prepared according to the general procedure G using potassium ethyl xanthogenate **D** (1 mmol, 160 mg) and cyclohexanecarbonyl chloride (1.1 mmol, 128 μ L) in 10 mL of acetone. After work-up, the product **30c** was obtained as a yellow oil (207 mg, 89% yield).

$^1\text{H NMR}$ (300 MHz, CDCl_3) δ 4.65 (q, $J = 7.1$ Hz, 2H); 2.53-2.39 (m, 1H); 1.98-1.85 (m, 2H); 1.83-1.70 (m, 2H); 1.68-1.53 (m, 1H); 1.55-1.35 (m, 5H); 1.34-1.10 (m, 3 H).

⁴¹ Ajayaghosh, A.; Das, S.; George, M. V. "S-benzoyl O-ethyl xanthate as a new photoinitiator: Photopolymerization and laser flash photolysis studies" *J. Polym. Sci., Part A: Polym. Chem.* **1993**, *31*, 653-659.

⁴² Azizi, N.; Alipour, M. "Synthesis of carboxylic dithiocarbamic anhydride and substituted thiourea derivatives in water" *Environ. Chem. Lett.* **2018**, *16*, 1415-1421.

^{13}C NMR (75 MHz, CDCl_3) δ 204.6 (C); 194.9 (C); 70.8 (CH_2); 52.8 (CH); 29.1 (CH_2); 25.5 (CH_2); 25.32 (CH_2); 13.6 (CH_3).

HRMS (ESI pos): calculated for $\text{C}_{10}\text{H}_{16}\text{NaO}_2\text{S}_2$ ($\text{M}+\text{Na}^+$): 255.0484, found: 255.0482.

^1H NMR (400 MHz, CDCl_3) δ 4.02 (q, $J = 7.1$ Hz, 1H), 3.79 (q, $J = 7.2$ Hz, 1H), 3.06 (s, 3H), 1.32 (dt, $J = 9.7, 7.1$ Hz, 3H)

^{13}C NMR (126 MHz, CDCl_3) δ 185.2 (C), 162 (C), 50.1 (CH_3), 49 (CH_3), 38.5 (CH_2), 37.3 (CH_2), 13.5 (CH_3), 11.3 (CH_3).

UV-Vis Characterization of the Intermediates.

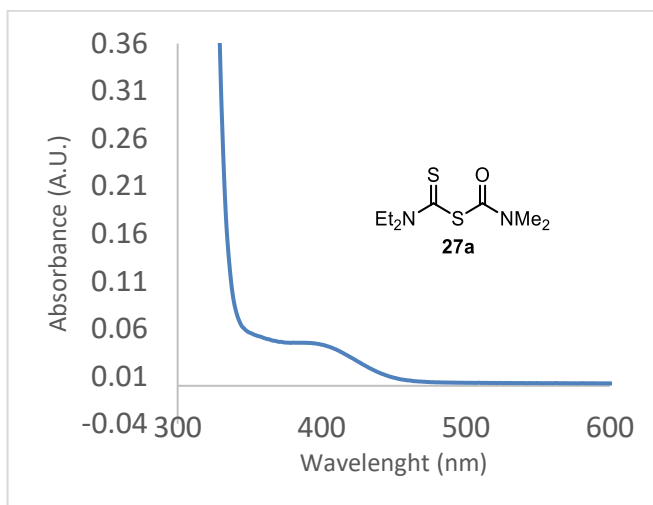


Figure 4.33: UV-Vis absorption spectrum of intermediate **27a** recorded at $2 \cdot 10^{-3}$ M concentration in acetonitrile.

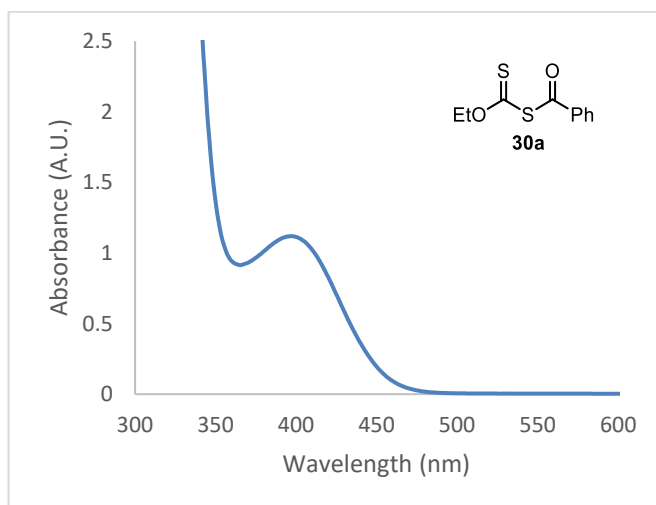


Figure 4.34: UV-Vis absorption spectrum of **30a** recorded at $1 \cdot 10^{-2}$ M concentration in acetonitrile.

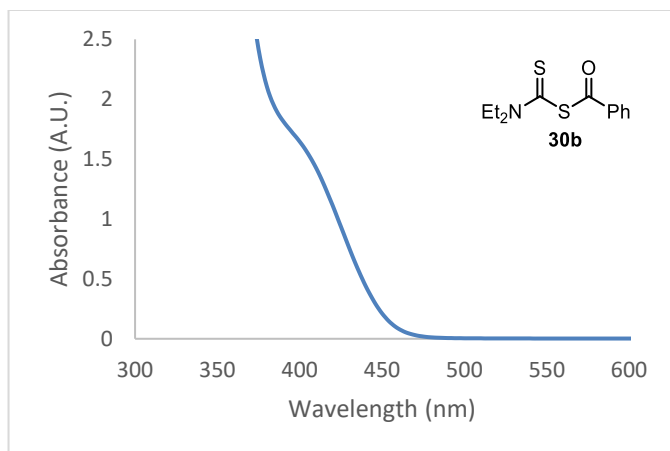


Figure 4.35: UV-Vis absorption spectrum of **30b** recorded at $1 \cdot 10^{-2}$ M concentration in acetonitrile.

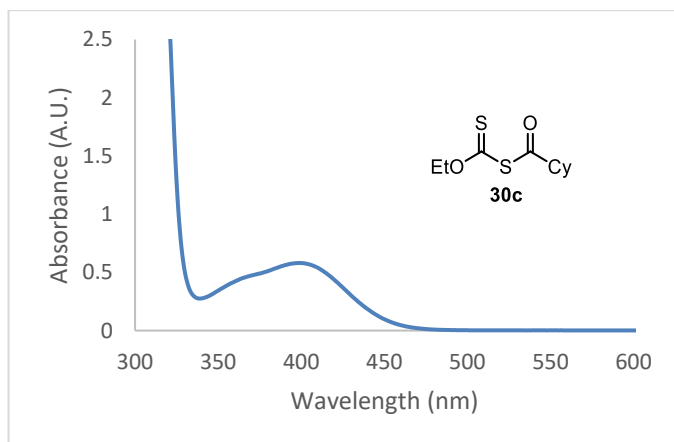


Figure 4.36: UV-Vis absorption spectrum of **30c** recorded at $2 \cdot 10^{-2}$ M concentration in acetonitrile.

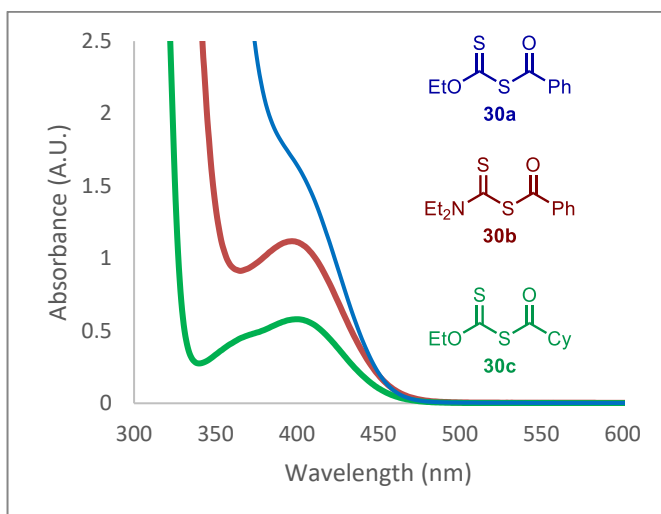


Figure 4.37: Superposition of the absorption spectra of the different acyl xanthates and acyl dithiocarbamate intermediates at the same concentration ($2 \cdot 10^{-2}$ M in acetonitrile).

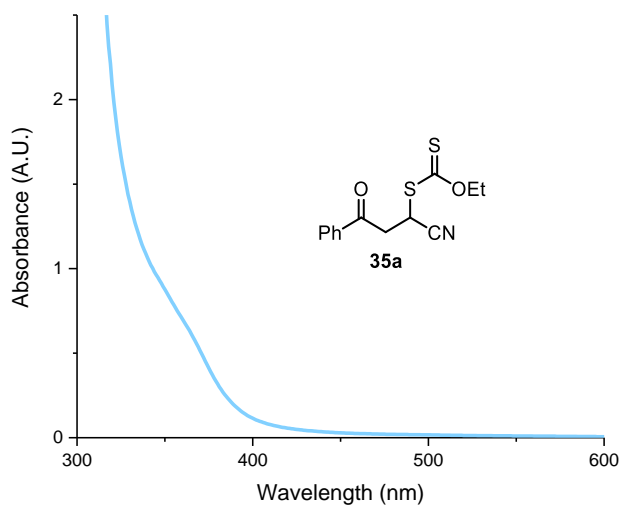
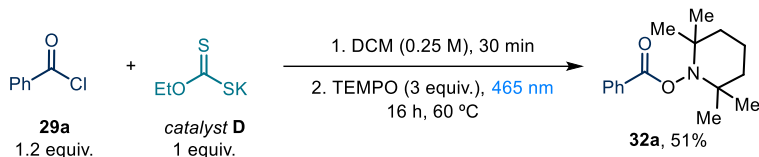


Figure 4.38: UV-Vis absorption spectrum of 35a recorded at $1 \cdot 10^{-2}$ M in acetonitrile.

4.8.8.2 TEMPO trapping experiments.

Stoichiometric reaction between TEMPO and in-situ acyl xanthate intermediate



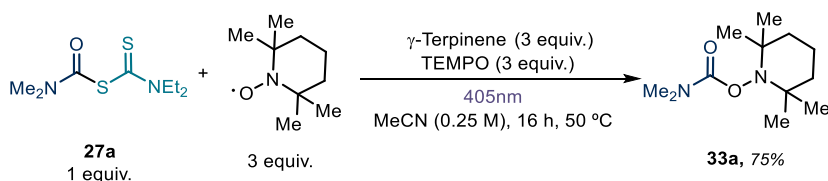
In an oven dried tube of 15 mL (16 mm × 125 mm) with a Teflon septum screw cap, potassium ethyl xanthogenate **D** (80.1 mg, 0.5 mmol, 1 equiv.) was suspended in DCM (2 mL, HPLC grade). Then, benzoyl chloride **29a** (69.6 μ L, 0.6 mmol, 1.2 equiv.) was added and the mixture was stirred at ambient temperature for 30 minutes. Then, TEMPO (234.4 mg, 1.5 mmol, 3 equiv.) was added and the resulting yellow solution was degassed with argon sparging for 60 seconds. The tube was then placed in the temperature controlled photoreactor (Figure 4.30) set at a temperature of 60 °C (60–61°C measured in the central well) and irradiated for 16 hours. Chromatography on silica gel (5% AcOEt in hexanes as eluent) afforded adduct **32a** (66 mg, yellow oil, 51% yield).

$^1\text{H NMR}$ (500 MHz, CDCl_3) δ 8.35 (d, $J = 6.9$ Hz, 2H), 7.83 (m, 1H), 7.74 (m, 2H), 2.12 – 1.70 (m, 6H), 1.55 (s, 6H), 1.40 (s, 6H).

$^{13}\text{C NMR}$ (126 MHz, CDCl_3) δ 161.45, 128.17, 124.89, 124.74, 123.78, 55.52, 34.28, 27.19, 16.09, 12.26.

Matching reported literature data.⁴³

Stoichiometric reaction between TEMPO and dithiocarbamate intermediate **27a**



In an oven-dried 15 mL Schlenk tube was added a 0.25 M solution of the dithiocarbamate intermediate **27a** (28 mg, 127 μ mol, 1 equiv.) and TEMPO (60 mg, 0.38 mmol, 3 equiv.) in acetonitrile (0.5 mL). The reaction mixture was placed under an atmosphere of argon, cooled to $-78\text{ }^\circ\text{C}$, degassed *via* vacuum evacuation (5 minutes), backfilled with argon and, ultimately, warmed to ambient temperature. This freeze-pump-thaw cycle was repeated four times, and then the Schlenk tube was sealed with Parafilm and put into the Hepatochem PhotoRedOx Box (Figure 4.27) equipped with a 405 nm EvoluChem LED 18 W light source at 50 °C. After 18 hours, the reaction vessel was cooled down to ambient temperature, water was added and the mixture was

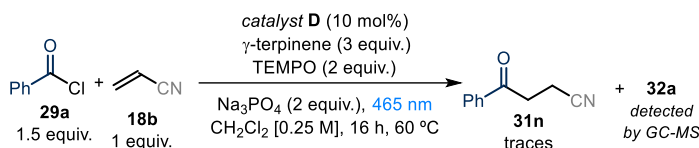
⁴³ He, X.-K.; Cai, B.-G.; Yang, Q.-Q.; Wang, L.; Xuan, J. "Visible-Light-Promoted Cascade Radical Cyclization: Synthesis of 1,4-Diketones Containing Chroman-4-One Skeletons" *Chem. Asian J.* **2019**, *14*, 3269–3273.

extracted with ethyl acetate (2x15 mL). The combined layers were dried over MgSO_4 , filtered, and concentrated. The resulting crude mixture was purified by column chromatography on silica gel (5% to 30% AcOEt in hexane) to give the corresponding product **33a** (21 mg, 75% yield).

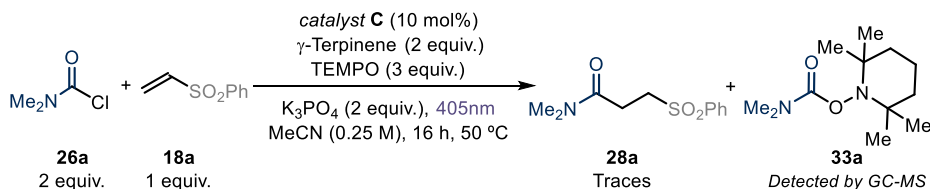
$^1\text{H NMR}$ (400 MHz, CDCl_3) δ 2.96 (s, 6H), 1.73 – 1.48 (m, 6H), 3.06 (s, 3H), 1.13 (d, J = 17.6 Hz, 1H)

$^{13}\text{C NMR}$ (101 MHz, CDCl_3) δ 157.8, 60.2, 50.1, 39.1, 31.9, 21.1, 17.2.

TEMPO inhibition of the model reactions



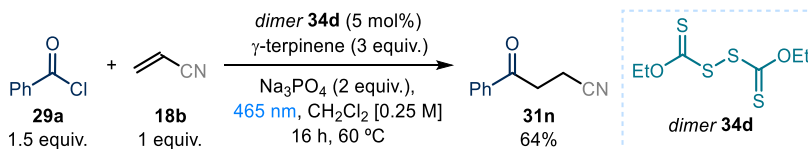
Reaction performed according to the general procedure C using benzoyl chloride (87 μL , 0.75 mmol, 1.5 equiv.) and acrylonitrile (33 μL , 0.5 mmol, 1 equiv.) and adding TEMPO (156.3 mg, 1 mmol, 2 equiv.) before the degassing step. The crude mixture was analyzed by $^1\text{H NMR}$ analysis after 16 hours using trichloroethylene (45 μL , 0.5 mmol, 1 equiv.) as internal standard, and by GC-MS. NMR yield: 5%. Traces of the TEMPO adduct **12** were detected by GC-MS analysis.



Reaction performed according to the general procedure B using dimethylcarbamyl chloride (37 μL , 0.4 mmol, 2 equiv.) and phenyl vinyl sulfone (34 mg, 0.2 mmol, 1 equiv.) and adding TEMPO (62 mg, 0.4 mmol, 2 equiv.) before the degassing step.

4.8.7.3 Experiments with the dimeric catalysts

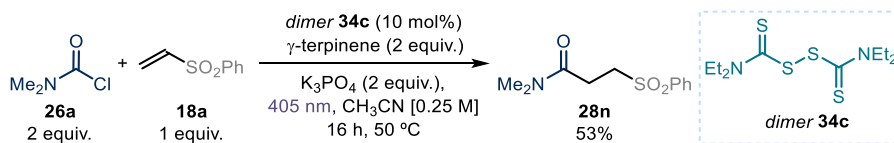
Model reaction with catalyst dimer **34d** – Acylation



Reaction performed according to the general procedure C using benzoyl chloride (87 μL , 0.75 mmol, 1.5 equiv.) and acrylonitrile (33 μL , 0.5 mmol, 1 equiv.) while replacing catalyst **D** with dimer **34d** (6 mg, 0.025 mmol, 0.05 equiv.). The crude reaction mixture

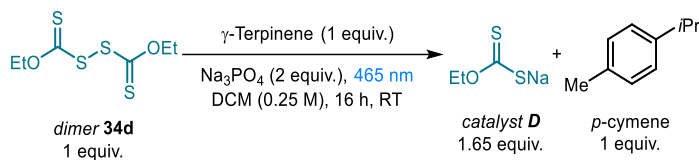
was analyzed by ^1H NMR analysis using trichloroethylene as internal standard. NMR yield: 64%.

Model reaction with dimer **34c** - Carbamoylation



Reaction performed according to general procedure B using dimethylcarbamoyl chloride (37 μL , 0.4 mmol, 2.0 equiv.) and phenyl vinyl sulfone (34 mg, 0.2 mmol, 1 equiv.) while replacing catalyst **C** with **34c** (6 mg, 0.02 mmol, 0.1 equiv.). The crude reaction mixture was analyzed by ^1H NMR analysis using trichloroethylene as internal standard. NMR yield: 53%.

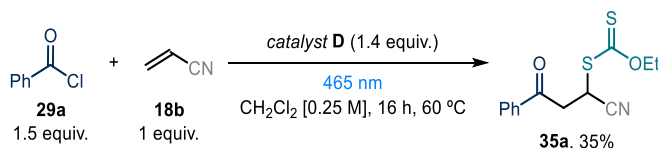
Turn-over experiment with dimer **34d** and terpinene



In an oven dried vial (16 mm \times 50 mm) with a Teflon septum screw cap, dimer **34d** (60.6 mg, 0.25 mmol, 1 equiv.) and sodium phosphate (82 mg, 0.5 mmol, 2 equiv.) were dissolved in DCM (2 mL, HPLC grade). Then, γ -terpinene (40 μL , 0.25 mmol, 1 equiv.) was added. The resulting yellow mixture was degassed with argon, sparging for 60 seconds. The vial was then placed in the 3D-printed support photoreactor (Figure 4.31) and irradiated for 24 hours. Trichloroethylene was added as internal standard and a sample of the crude mixture was diluted in d_6 -DMSO to record the NMR yield.

4.8.7.4 Group Transfer Experiments.

Stoichiometric group transfer reaction with in-situ acyl xanthate intermediate



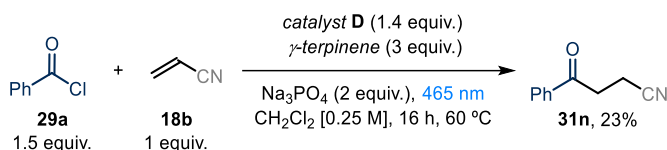
In an oven dried tube of 15 mL (16 mm \times 125 mm) with a Teflon septum screw cap, potassium ethyl xanthogenate **D** (112 mg, 0.7 mmol, 1.4 equiv.) was suspended in DCM (2 mL, HPLC grade). Then, benzoyl chloride (87 μL , 0.75 mmol, 1.5 equiv.) was added and the mixture was stirred at ambient temperature for 30 min. The reaction mixture was then degassed with argon, sparging for 60 seconds. Finally, acrylonitrile (33 μL , 0.5 mmol, 1 equiv.) was added via syringe. The tube was then placed in the temperature

controlled photoreactor (Figure 4.30) set at a temperature of 60 °C (60–61 °C measured in the central well) and irradiated for 16 hours. The crude mixture was purified by flash column chromatography on silica gel (5% to 10% AcOEt in hexanes as eluent) to afford **35a** (50 mg, 35% yield) as a yellow oil.

¹H NMR (400 MHz, CDCl₃) δ 7.97 – 7.89 (m, 2H), 7.69 – 7.58 (m, 1H), 7.50 (app t, *J* = 7.5 Hz, 2H), 5.08 (t, *J* = 6.2 Hz, 1H), 4.72 (q, *J* = 7.1 Hz, 2H), 3.70 (d, *J* = 6.3 Hz, 2H), 1.47 (t, *J* = 7.1 Hz, 3H).

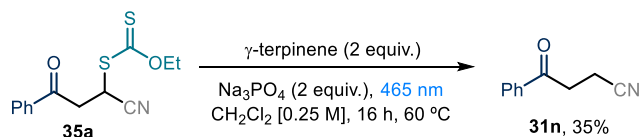
¹³C NMR (101 MHz, CDCl₃) δ 209.05, 193.54, 135.35, 134.39, 129.09, 128.30, 117.96, 71.54, 40.67, 32.49, 13.84.

Stoichiometric group transfer reaction with in-situ acyl xanthate intermediate in the presence of γ -terpinene



In an oven dried tube of 15 mL (16 mm × 125 mm) with a Teflon septum screw cap, potassium ethyl xanthogenate (112 mg, 0.7 mmol, 1.4 equiv.) and sodium phosphate (164 mg, 1.0 mmol, 2 equiv.) were dissolved in DCM (2 mL, HPLC grade). Benzoyl chloride (87 μ L, 0.75 mmol, 1.5 equiv.) was added and the mixture was stirred at ambient temperature for 30 min. Then, γ -terpinene (240 μ L, 1.5 mmol, 3 equiv.) was added. The mixture was degassed via argon sparging for 60 seconds. Finally, acrylonitrile (33 μ L, 0.5 mmol, 1 equiv.) was added via syringe. The tube was then placed in the temperature controlled photoreactor (Figure 4.30) set at a temperature of 60 °C (60–61 °C measured in the central well) and irradiated for 16 hours. Trichloroethylene was added as internal standard, and a sample of the crude mixture was diluted in CDCl₃ to record the NMR yield. *No group transfer product 35a was observed.*

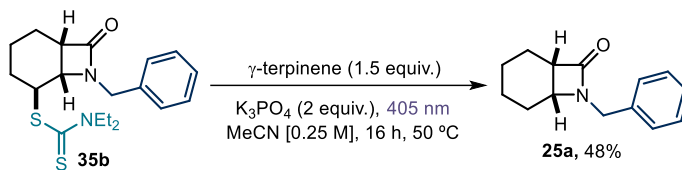
Direct photolysis of the group transfer product under reaction conditions



In an oven dried tube of 15 mL (16 mm × 125 mm) with a Teflon septum screw cap, the group transfer product **35a** (28.01 mg, 0.1 mmol, 1 equiv.) and sodium phosphate (33 mg, 0.2 mmol, 2 equiv.) were dissolved in DCM (2 mL, HPLC grade). Then, γ -terpinene (33 μ L, 0.2 mmol, 2 equiv.) was added. The reaction mixture was degassed with Argon sparging for 60 seconds. The tube was then placed in the temperature controlled photoreactor (Figure 4.30) set at a temperature of 60 °C (60–61 °C measured in the central well) and irradiated for 16 hours.

Trichloroethylene was added as internal standard and a sample of the crude mixture was diluted in CDCl_3 to record the NMR yield – product **31n** was formed in 35%.

Direct photolysis of the group transfer product for the intramolecular reaction



An oven-dried 15 mL Schlenk tube was charged with an authentic sample of the group transfer adduct **35b**, γ -terpinene (48 μL , 0.3 mmol, 1.5 equiv.) and K_3PO_4 (85 mg, 0.4 mmol, 2 equiv.) in acetonitrile (0.8 mL, 0.25 M). The reaction mixture was placed under an atmosphere of argon, cooled to -78°C , degassed *via* vacuum evacuation (5 minutes), backfilled with argon and, ultimately, warmed to ambient temperature. This freeze-pump-thaw cycle was repeated four times, and then the Schlenk tube was sealed with Parafilm and put into the Hepatochem PhotoRedOx Box equipped with a 405 nm EvoluChem LED 18 W light source at 50°C (Figure 4.27). After 18 hours stirring, the reaction was cooled down to ambient temperature, trichloroethylene was added as internal standard and a sample of the crude mixture was diluted in CDCl_3 to record the NMR of the crude - product **25a** was formed in 48%.

4.8.8.5 Cyclic voltammetry measurements

For the cyclic voltammetry (CV) measurements, a glassy carbon disk electrode (diameter: 3 mm) was used as a working electrode. A silver wire coated with AgCl immersed in a 3.5 M aqueous solution of KCl and separated from the analyte by a fritted glass disk was employed as the reference electrode. A Pt wire counter-electrode completed the electrochemical setup. The scan rate of used in each CV experiment is indicated case by case.

Potentials are quoted with the following notation: E_p^{C} refers to the cathodic peak potential, E_p^{A} refers to the anodic peak potential, while the E^{red} value describes the electrochemical properties of the referred compound.

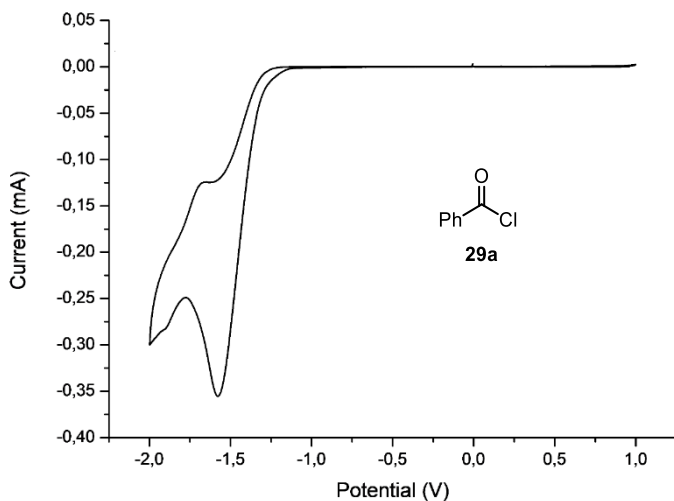


Figure 4.39: Cyclic voltammogram of benzoyl chloride **29a** [0.02 M] in [0.1 M] TBAPF₆ in CH₃CN. Sweep rate: 100 mV/s. Glassy carbon electrode working electrode, Ag/AgCl (KCl 3.5 M) reference electrode, Pt wire auxiliary electrode. Irreversible reduction, $E_p^C = E^{\text{red}}(29a/29a^-) = -1.57$ V.

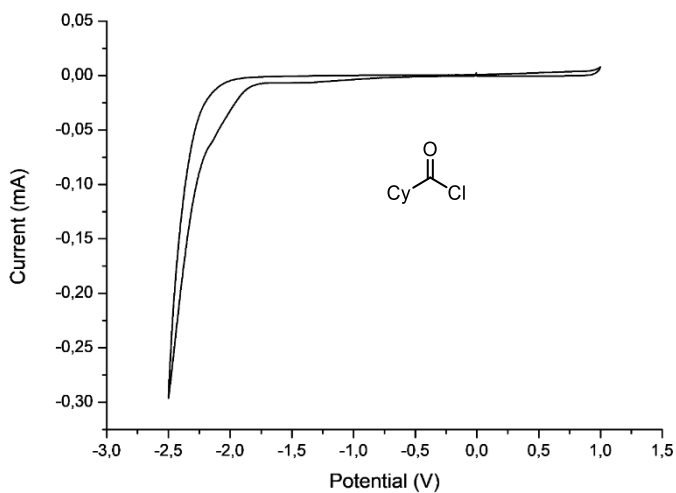


Figure 4.40: Cyclic voltammogram of cyclohexanecarbonyl chloride [0.02 M] in [0.1 M] TBAPF₆ in CH₃CN. Sweep rate: 100 mV/s. Glassy carbon electrode working electrode, Ag/AgCl (KCl 3.5 M) reference electrode, Pt wire auxiliary electrode. Reduction of cyclohexanecarbonyl chloride was not observed in the registered potential window (from 0 to -2.50 V).

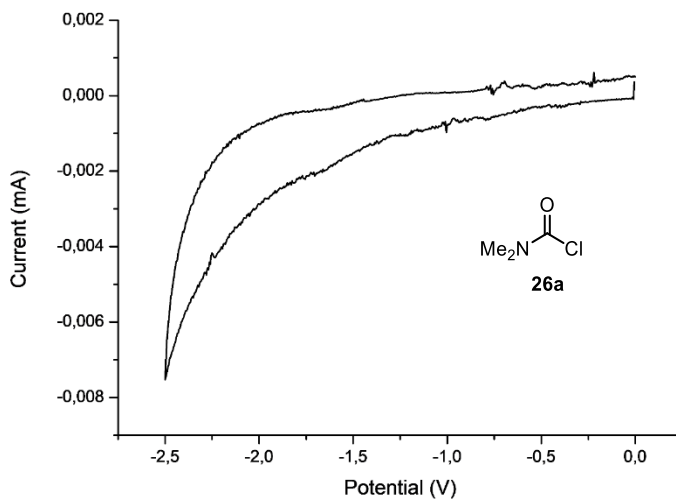


Figure 4.41: Cyclic voltammogram for **26a** [0.02M] in [0.1 M] TBAPF₆ in CH₃CN. Sweep rate: 50 mV/s. Glassy carbon electrode working electrode, Ag/AgCl (KCl 3.5 M) reference electrode, Pt wire auxiliary electrode. Reduction of **26a** was not observed in the registered potential window (from 0 to -2.50 V).

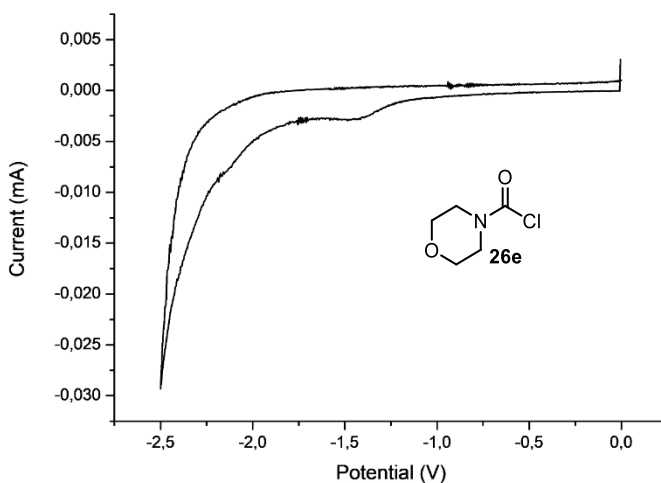


Figure 4.42: Cyclic voltammogram for **26e** [0.02M] in [0.1 M] TBAPF₆ in CH₃CN. Sweep rate: 100 mV/s. Glassy carbon electrode working electrode, Ag/AgCl (KCl 3.5 M) reference electrode, Pt wire auxiliary electrode. Reduction of **26e** was not observed in the registered potential window (from 0 to -2.50 V).

4.8.8.6 Transient absorption spectroscopy (TAS)

Studies with microsecond transient absorption spectroscopy (TAS) were performed using an excitation source of NdYAG (neodymium-doped yttrium aluminium garnet) Opolette laser with an optical parametric oscillator (OPO) system that allows variable wavelength excitation from 400 -1800 nm, pulse width of 6 ns, up to 2 mJ of energy from OPO output with fiber optic coupled, and high energy output from direct NdYAG

harmonics 355 (20 mJ, 5 ns) and 532 (45 mJ, 6 ns). The system is completed with 150 W tungsten lamp as probe; 2 monochromators Minuteman MM151; Si amplified photodetector module for VIS; DSPDAU high speed data rate recorder and interface software from RAMDSP. Laser intensities for each wavelength were the following: 355 nm – 1.30 mJ; 420 nm – 1.20 mJ; 460 nm – 1.95 mJ.

Several studies with different wavelengths and laser intensities were carried out, each of the conditions are indicated in a case by case bases. We selected a logarithmic time scale suitable for clearly showing the decay of the transient species in the samples. The characteristics of the detected transient species match literature data.²⁴

In a typical transient absorption spectroscopy experiment, solutions in acetonitrile of each of the substrates were prepared under an argon atmosphere and transferred into a screw-top 3.0 mL quartz cuvette for measurement. Upon irradiation with the appropriated wavelength, the decay of absorption at 620 nm of the transient xanthyl radical **XIXd** was recorded.

Acylxanthate **30a**

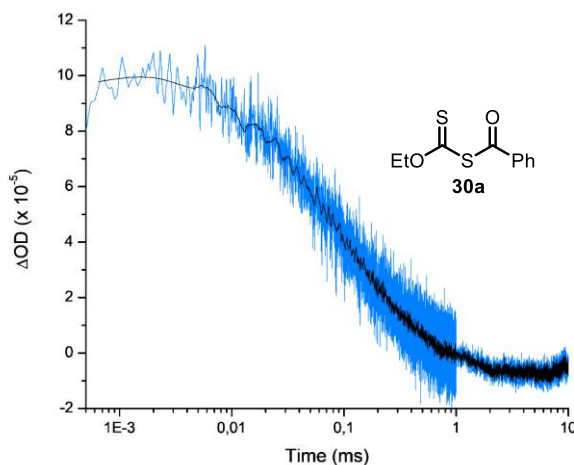


Figure 4.43: Absorption at 620 nm of the transient xanthyl radical **XIXd** (blue line) generated upon 355 nm laser excitation of Acylxanthate **30a** ($[30a]_0 = 3.00$ mM in acetonitrile). Note logarithmic scale for time. Absorption decay (black line) processed through Savitsky Golay filter to facilitate lifetime measurement. ΔOD : optical density variation.

Compound **30a** was also measured upon 460 nm excitation in order to mimic the conditions of photolysis under catalytic conditions. Since photolysis of **30a** is less efficient at longer wavelengths, a higher concentration of **30a** was needed to obtain a comparable scale signal. Note that changes in concentration of both **30a** and transient **XIXd** generated upon photolytic cleavage directly affects the lifetime of the detected species.

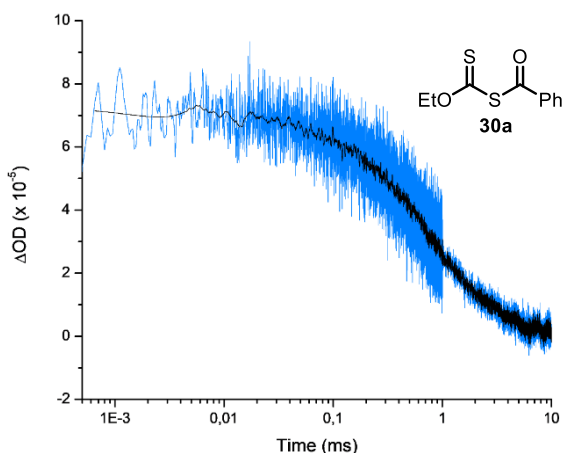


Figure 4.44: Absorption at 620 nm of the transient xanthyl radical XIXd (blue line) generated upon 460 nm laser excitation of acylxanthate **30a** ($[30a]_0 = 300$ mM in acetonitrile). Note logarithmic scale for time. Absorption decay (black line) processed through Savinsky Golay filter to facilitate lifetime measurement. ΔOD : optical density variation.

Dimer **34d**

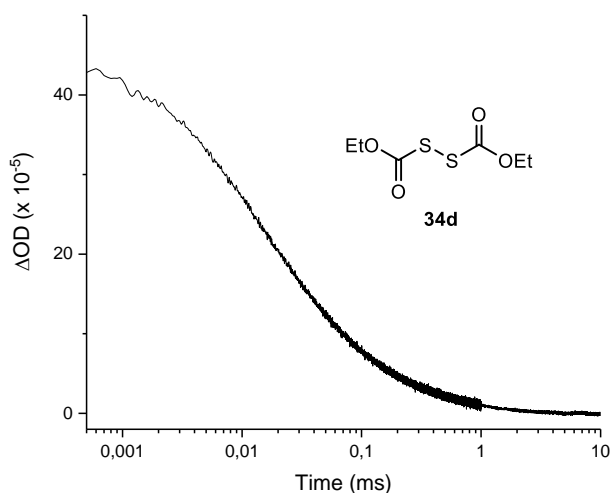


Figure 4.45: Absorption at 620 nm of the transient xanthyl radical XIXd (black line) generated upon 355 nm laser excitation of dimer **34d** ($[34d]_0 = 3.00$ mM in acetonitrile). Note logarithmic scale for time. ΔOD : optical density variation.

Dimer **34d** was also measured upon 420 nm and 460 nm irradiation in order to support photolysis under the reaction conditions. A higher concentration of **34d** was used to ensure comparable scale signal.

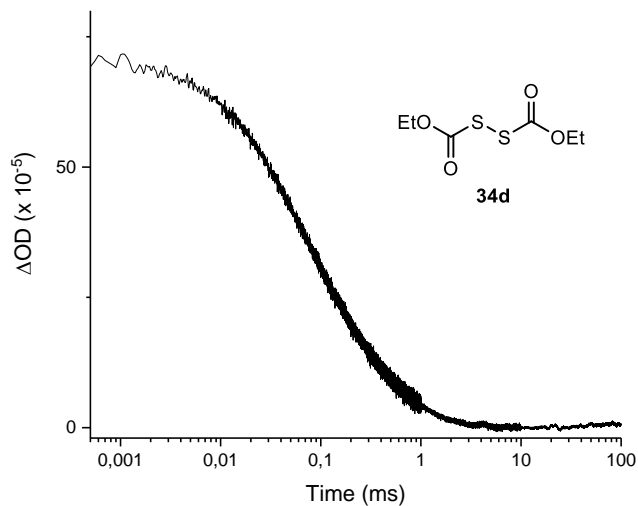


Figure 4.46: Absorption at 620 nm of the transient xanthy radical **XIXd** (black line) generated upon 420 nm laser excitation of dimer **34d** ($[34d]_0 = 300$ mM in acetonitrile). Note logarithmic scale for time. ΔOD : optical density variation.

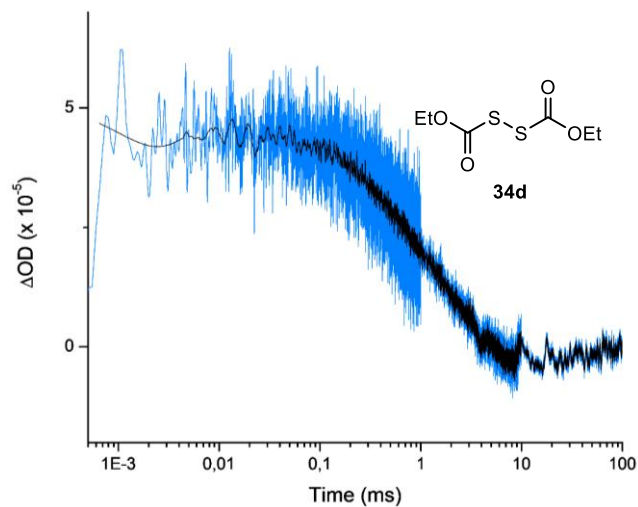


Figure 4.47: Absorption at 620 nm of the transient xanthy radical **XIXd** (blue line) generated upon 460 nm laser excitation of dimer **34d** ($[34d]_0 = 300$ mM in acetonitrile). Note logarithmic scale for time. Absorption decay (black line) processed through Savinsky Golay filter to facilitate lifetime measurement. ΔOD : optical density variation.

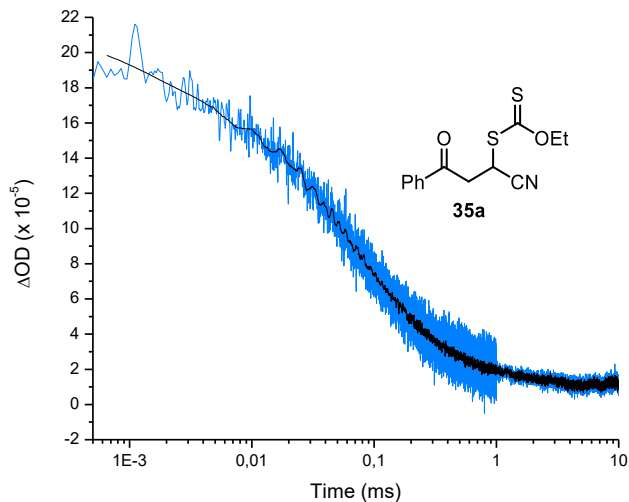
Group transfer product **35a**

Figure 4.48: Absorption at 620 nm of the transient xanthyl radical **XIXd** (blue line) generated upon 355 nm laser excitation of **35a** ($[35a]_0 = 3$ mM in acetonitrile). Note logarithmic scale for time. Absorption decay (black line) processed through Savinsky Golay filter to facilitate lifetime measurement. ΔOD : optical density variation.

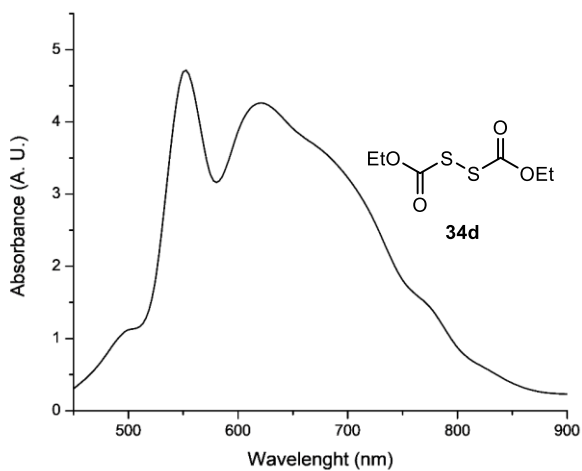
Absorption spectra of xanthyl radical **XIXd**

Figure 4.49: Absorption spectra of the transient xanthyl radical **XIXd** generated upon 355 nm laser excitation of Dimer **34d** ($[34d]_0 = 3$ mM in acetonitrile) at $1 \mu s$ time of irradiation. Maximum characteristic from xanthyl radical can be observed around 625 nm.

4.8.8.7 Electron paramagnetic resonance (EPR)

EPR spectra were acquired on a Bruker EMX X-band EPR spectrometer with an ER 4116 HS cavity (9.86 GHz at room temperature) using 100 kHz field modulation (modulation amplitude: 1 G). Individual EPR tubes were filled with ~0.7 mL of the solution and were placed at the same position of the resonant cavity for EPR spectral acquisition. The spectral data were collected at 298 K with the following spectrometer settings: microwave power = 2.020 mW; center field = 3518 G, sweep width = 200 G, sweep time = 30 s, modulation frequency = 100 KHz, modulation amplitude = 1 G, power attenuation = 20 dB, time constant = 0.01 ms.

A fresh solution of acylxanthate **30a** 0.10 M in Toluene was prepared under air and measured without further precautions to remove oxygen from the solution. As expected, no signal was observed before of irradiation (note that **30a** decomposes rapidly, and a sample older than one day did show signals appearing before irradiation, due to decomposition); on the other hand, upon irradiation of the sample, appearance of a triplet at 3505 G was observed with a g -value of 2.00272 and a hyperfine splitting value α_{H} (2.6, 2H, γ -H). This signal reaches a maximum of intensity after 12.5 minutes of irradiation. The calculated EPR spectrum for the carbon radical of type **XXVIa**, which lies in proximity of two sulfur atoms and an ethoxy moiety, is shown in the right panel of Figure 4.50.

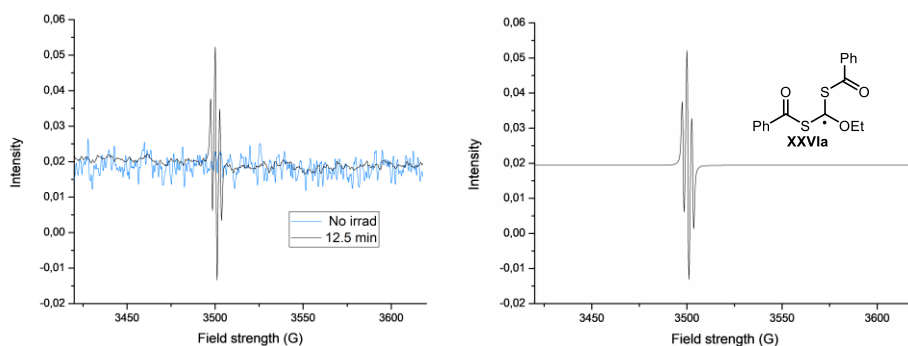


Figure 4.50: Comparison between (left) EPR spectra of acylxanthate **30a** (0.1 M in toluene) before irradiation (blue line) and after irradiation with a LSB610 100W mercury lamp during 12.5 min (black line). Open-shell specie was detected by appearance of a new signal centered at 3505 G (triplet); and (right) calculated EPR spectrum for intermediate **XXVIa** for a hyperfine coupling with two equivalent nuclei of spin $\frac{1}{2}$.

4.8.8.8 Quantum Yield Determination

A ferrioxalate actinometer solution was prepared by following the Hammond variation of the Hatchard and Parker procedure⁴⁴ outlined in the Handbook of Photochemistry.⁴⁵ The ferrioxalate actinometer solution measures the decomposition of ferric ions to ferrous ions, which are complexed by 1,10-phenanthroline and monitored by UV/Vis absorbance at 510 nm. The moles of iron-phenanthroline

⁴⁴ Hatchard, C. G.; Parker, C. A. "A new sensitive chemical actinometer II. Potassium ferrioxalate as a standard chemical actinometer" *Proc. R. Soc. Lond. A* **1956**, 518-536.

⁴⁵ Murov, S. L. *Handbook of Photochemistry* **1973**, Marcel Dekker Inc..

complex formed are related to moles of photons absorbed. The following solutions were prepared and stored in a dark laboratory (red light):

1. Potassium ferrioxalate solution: 294.8 mg of potassium ferrioxalate (commercially available from Alfa Aesar) and 139 μL of sulfuric acid (96%) were added to a 50 mL volumetric flask, and filled to the mark with water (HPLC grade).
2. Phenanthroline solution: 0.2% by weight of 1,10-phenanthroline in water (100 mg in 50 mL volumetric flask).
3. Buffer solution: 2.47 g of NaOAc and 0.5 mL of sulfuric acid (96%) were added to a 50 mL volumetric flask, and filled to the mark with water (HPLC grade).

The actinometry measurements were done as follows:

1. 1 mL of the actinometer solution was added to a screw-cap vial and placed on a single HP LED 1.5 cm away from the light source. The solution was irradiated at 460 nm (irradiance 40 mW/cm²). This procedure was repeated 4 times, quenching the solutions after different time intervals: 10 sec, 15 sec, 20 sec, and 25 sec.
2. After irradiation, the actinometer solutions were removed and placed in a 10 mL volumetric flask containing 0.5 mL of 1,10-phenanthroline solution and 2 mL of buffer solution. These flasks were filled to the mark with water (HPLC grade).
3. The UV-Vis spectra of the complexed actinometer samples were recorded for each time interval. The absorbance of the complexed actinometer solution was monitored at 510 nm.

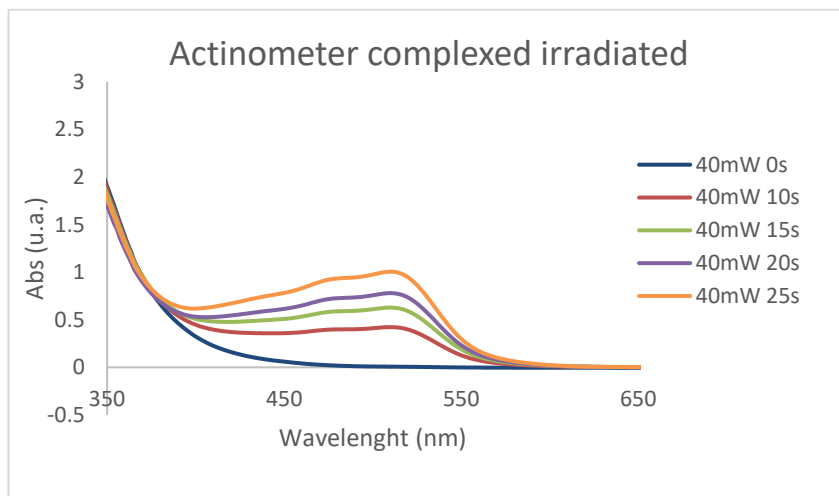


Figure 4.51: Absorbance of the complexed actinometer solutions.

The moles of Fe^{2+} formed for each sample is determined using Beers' Law (Eq. 1) :

$$\text{Mols of Fe(II)} = V_1 \times V_3 \times \Delta A(510 \text{ nm}) / 10^3 \times V_2 \times l \times \epsilon(510 \text{ nm}) \quad (\text{Eq. 1})$$

where V_1 is the irradiated volume (1 mL), V_2 is the aliquot of the irradiated solution taken for the determination of the ferrous ions (1 mL), V_3 is the final volume after complexation with phenanthroline (10 mL), l is the optical path-length of the irradiation cell (1 cm), $\Delta A(510 \text{ nm})$ is the optical difference in absorbance between the

irradiated solution and the one stored in the dark, $\epsilon(510 \text{ nm})$ is the extinction coefficient the complex $\text{Fe}(\text{phen})_3^{2+}$ at 510 nm ($11100 \text{ L mol}^{-1} \text{ cm}^{-1}$). The moles of Fe^{2+} formed (x) are plotted as a function of time (t). The slope of this line was correlated to the moles of incident photons by unit of time ($q_{n,0}$) by the use of the following Equation 2:

$$\Phi(\lambda) = dx/dt q_{n,0} [1-10^{-A(\lambda)}] \quad (\text{Eq. 2})$$

where dx/dt is the rate of change of a measurable quantity (spectral or any other property), the quantum yield (Φ) for Fe^{2+} at 458 nm is 1.1,⁴⁶ $[1-10^{-A(\lambda)}]$ is the ratio of absorbed photons by the solution, and $A(\lambda)$ is the absorbance of the actinometer at the wavelength used to carry out the experiments (460 nm). The absorbance at 460 nm $A(460)$ was measured using a Shimadzu 2401PC UV-Vis spectrophotometer in a 1 cm path quartz cuvette, obtaining an absorbance of 0.158.

$q_{n,0}$, which is the photon flux, was determined to be $1.048 \times 10^{-7} \text{ einstein s}^{-1}$.

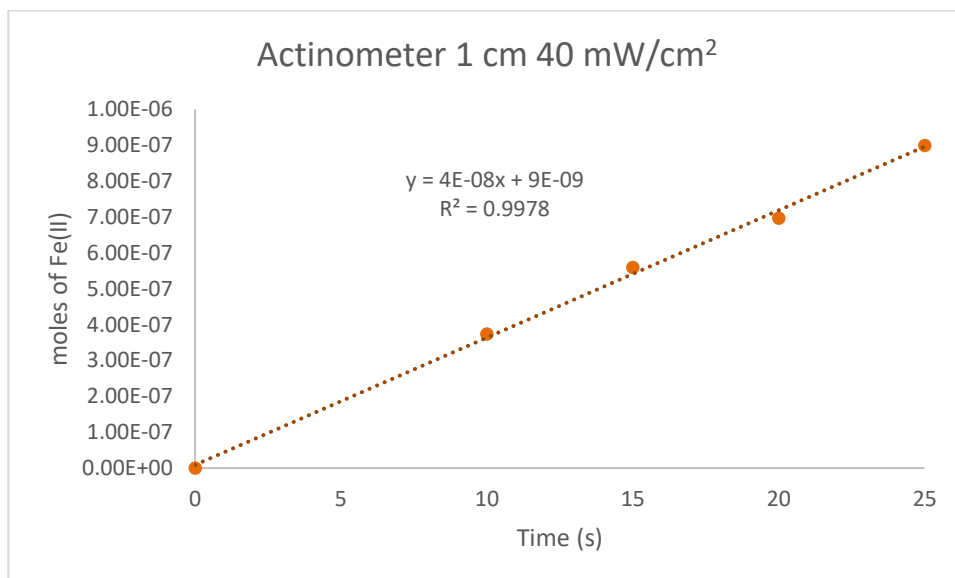


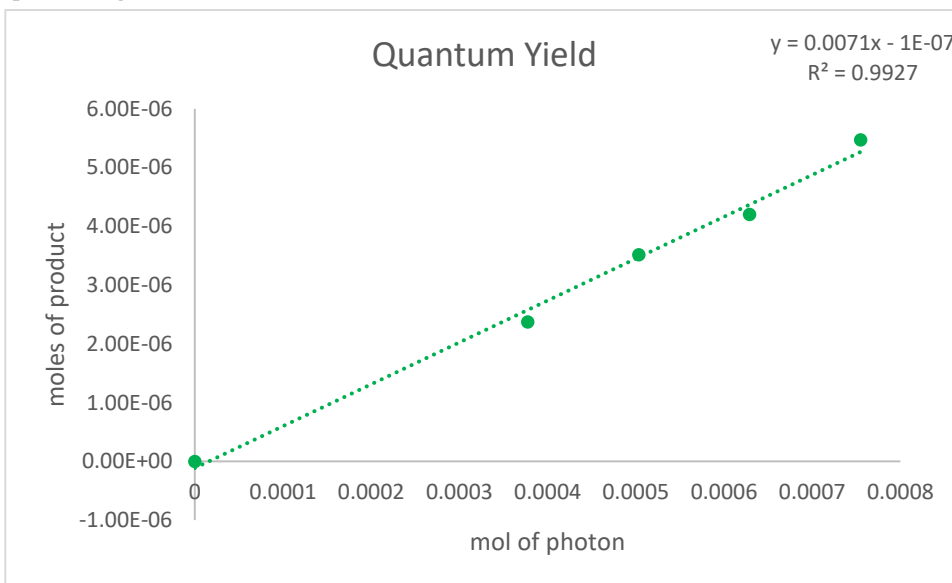
Figure 4.52: Plot of the moles of Fe^{2+} generated from the irradiation of the actinometer solutions against time.

Consequently, the model reactions were performed.

The reactions were prepared on a screw-cap vial with stir bar. cyclohexanecarbonyl chloride (50 μL , 0.375 mmol, 1.5 equiv.), γ -terpinene (120 μL , 0.75 mmol, 3 equiv.), and lutidine (58 μL , 0.5 mmol, 2 equiv.), were added to a solution of catalyst **D** (4 mg, 0.1 equiv.) in acetonitrile (1 mL). After degassing by bubbling Argon for 30 s, acrylonitrile (16 μL , 0.25 mmol) was added and the tube was sealed with parafilm and put in the HP-LED 460 nm at 1 cm distance at ambient temperature (reaction reaches around 35 $^{\circ}\text{C}$) with irradiance of 40 mW/cm^2 . Four different reactions were setup and irradiated for different times: 60 min, 80 min, 100 min and 120 min.

⁴⁶ Holubov, C. A.; Langford, C. H. "Wavelength and Temperature Dependence in the Photolysis of the Chemical Actinometer, Potassium trioxalatoferate(III), at Longer Wavelengths" *Inorganica Chim. Acta* **1981**, *53*, 59-60.

The moles of product **31ae** formed for the model reaction were determined by GC measurement (FID detector) using 1,3,5-trimethoxybenzene as internal standard. The moles of product per unit of time are related to the number of photons absorbed. The photons absorbed are correlated to the number of incident photons by the use of Equation 1. According to this, plotting the moles of product (x) versus the moles of incident photons ($q_n, \text{ }^\circ\text{dt}$), the slope is equal to: $\Phi \cdot (1 - 10^{-A(\lambda)(460 \text{ nm})})$, where Φ is the quantum yield to be determined and $A(460 \text{ nm})$ is the absorption of the reaction under study. $A(460 \text{ nm})$ was measured using a Shimadzu 2401PC UV-Vis spectrophotometer in 10 mm path quartz. An absorbance of 0.103 was determined for the model reaction mixture. The quantum yield (Φ) of the photochemical transformation was measured to be 0.0338. The procedure was repeated a second time to provide a similar value: quantum yield (Φ) at 460 nm of 0.0332.



Chapter V

General Conclusion

Over the past 20 years, organocatalysis has become an established tool for modern organic synthesis alongside biocatalysis and metal-based catalysis. Advances in the field of organocatalysis have been mainly dictated by new processes designed applying classical ground-state polar reactivity. Our research group has recently demonstrated that some organocatalytic intermediates can directly absorb light in the visible region and unlock new reactivity in the excited state. Capitalizing upon the new organocatalytic functions enabled by photoexcitation, I developed novel C-C and C-B bond forming strategies not achievable using ground-state organocatalytic reactivity. In the first project, detailed in Chapter II, the high oxidizing ability of excited chiral iminium ions was exploited, in combination with the basic character of their counteranions, to trigger a multisite proton coupled electron transfer. This radical generation mechanism served to promote the enantioselective organocatalytic C-H functionalization of toluene derivatives selectively at the benzylic position. This process is operationally simple, conducted at ambient temperature with commercially available substrates, and using a 420 nm high power LED as the light source.

In the second part of my doctoral studies, I focused on the catalytic generation of photolabile thiocarbonyl-based compounds to promote the formation of C-B and C-C bonds. In Chapter III, I detail how a nucleophilic dithiocarbonyl anion organocatalyst could activate alkyl electrophiles, such as benzylic and allylic bromides, chlorides and mesylates, through an S_N2 pathway. The ensuing photon-absorbing intermediate, upon visible light absorption, generates radicals through homolytic cleavage of the weak C-S bond. The generated radical is then intercepted by bis(catecholato)diboron to afford alkyl boronic ester products. This methodology was further expanded to include a three-component variant, allowing the carboboration of alkenes. In Chapter IV, this photolytic approach was expanded to the activation of acyl and carbamoyl chlorides through a nucleophilic acyl substitution pathway. The photochemically generated acyl and carbamoyl radicals have been trapped by a variety of electron-poor olefins in Giese-type addition manifolds, or by a pendant olefin in an intramolecular fashion, to form new C-C bonds. A detailed mechanistic investigation, based on spectroscopic and electrochemical analyses along with the characterization of key intermediates, identified a variety of off-the-cycle equilibria which cooperate to control the overall concentrations of the radicals, contributing to the efficiency of the process.

Overall, the excited-state reactivity of organocatalytic intermediates was used to develop novel catalytic radical reactions, not possible through classical thermal pathways.



UNIVERSITAT
ROVIRA i VIRGILI



Institut
Català
d'Investigació
Química